DINUCLEAR DINITROGEN AND MONONUCLEAR PARAMAGNETIC COMPLEXES OF ZIRCONIUM

by

MURUGESAPILLAI MYLVAGANAM

B.Sc. (Hons.), University of Jaffna, Sri Lanka, 1985
M. Sc., University of British Columbia, 1989

A THESIS SUBMITTED IN PARTIAL FULFILLMENT OF
THE REQUIREMENTS FOR THE DEGREE OF
DOCTOR OF PHILOSOPHY

in
THE FACULTY OF GRADUATE STUDIES
(Department of Chemistry)

We accept this thesis as conforming
to the required standard

.....

THE UNIVERSITY OF BRITISH COLUMBIA
June 1994

In presenting this thesis in partial fulfilment of the requirements for an advanced degree at the University of British Columbia, I agree that the Library shall make it freely available for reference and study. I further agree that permission for extensive copying of this thesis for scholarly purposes may be granted by the head of my department or by his or her representatives. It is understood that copying or publication of this thesis for financial gain shall not be allowed without my written permission.

(Signature)

Department of CHEMISTRY

The University of British Columbia
Vancouver, Canada

Date 20th July 94

DE-6 (2/88)

ABSTRACT

The basic focus of this work is the use of the tridentate, mixed donor ligand, $[N(SiMe_2CH_2PR_2)_2]^-$ abbreviated as PNP, to generate zirconium compounds that contain dinitrogen ligands in unusual bonding modes, or to allow the stabilization of the very rare zirconium(III) oxidation state. The approach that is used is to combine synthetic methods in organometallic chemistry with semi-empirical molecular orbital calculations as a means of designing new complexes and to rationalize bonding.

Reduction of $ZrCpCl_2[N(SiMe_2CH_2PPr^i_2)_2]$ **2.6**, or $ZrCl_2(OAr^*)[N(SiMe_2CH_2PPr^i_2)_2]$ (Ar^* = $(C_6H_3Me_2$-2,6)) **2.11**, under a dinitrogen atmosphere gave complexes $\{[(PPr^i_2CH_2SiMe_2)_2N]ZrCp\}_2(\mu\text{-}N_2)$ **2.9**, and $\{[(PPr^i_2CH_2SiMe_2)_2N]Zr(OAr^*)\}_2(\mu\text{-}N_2)$ **2.12**, respectively. The X-ray structure determination of these complexes confirmed the presence of an end-on bridging (μ-η^1:η^1-N_2) dinitrogen ligand in **2.9** whereas, **2.12** has a side-on bridging (μ-η^2:η^2-N_2) dinitrogen ligand. The observed nitrogen-nitrogen bond distances in **2.9** was 1.301 (3) Å and in **2.12**, it was 1.528 (7) Å.

The resonance Raman spectra of the solid and the solution state samples of **2.9** and **2.2** showed isotope sensitive peaks around 1200 and 730 cm^{-1} respectively, assigned to the nitrogen-nitrogen stretching of these complexes. Also, the fact that these resonance Raman features are the same in the solid and in the solution states strongly suggest that the mode of bonding of the dinitrogen ligand are same for the respective complexes.

The semi-empirical molecular orbital studies performed on the end-on derivative **2.9** and on the side-on derivatives **2.2** and **2.12** show that the π-acceptor interactions involving the π^*-orbitals of the dinitrogen ligand are significantly different. In the end-on case these interactions give rise to two π-MOs, whereas the side-on cases give rise to one δ-MO and one π-MO where the π-MO was found to be much lower in energy than the δ-MO. Mulliken population and Wiberg indices were calculated to show that in the side-on mode there is greater electron donation into the dinitrogen ligand than in the end-on cases and also the side-on bound

N_2 ligand has a very weak nitrogen-nitrogen bond, which is corroborated by the bond length parameters and the resonance Raman data. An analysis of the frontier orbitals of the fragment $[(H_3P)_2(H_2N)ZrX]$, where X = Cl, Cp or OH, shows that the metal-ligand d_π-p_π interactions influence the mode of dinitrogen coordination, i.e., end-on vs. side-on.

The paramagnetic zirconium(III) complex, $Zr(\eta^5\text{-}C_5H_5)Cl[N(SiMe_2CH_2PPr^i_2)_2]$ **4.1**, and the corresponding hafnium(III) derivative, $Hf(\eta^5\text{-}C_5H_5)Cl[N(SiMe_2CH_2PPr^i_2)_2]$ **4.1**, were synthesized by the reduction of the respective dichloro precursors $M(\eta^5\text{-}C_5H_5)Cl_2\text{-}[N(SiMe_2\text{-}CH_2PPr^i_2)_2]$, where M = Zr or Hf. The results of this study show that complex **4.1** is a viable precursor to the synthesis of a variety of derivatives such as the first stable examples of alkyl, aryl and borohydride complexes of zirconium(III). X-ray structure elucidation has been carried out for an alkyl **4.8**, phenyl **4.4** and borohydride complex, **4.17**. Spectroscopic studies (IR and ESR) indicate that in the case of the alkyl derivatives a weak agostic type interaction may be present between one of the α-hydrogens and the metal.

Hydrogenolysis of certain alkyl complexes shows a clean conversion to the mononuclear zirconium(III) hydride complex **4.14**. This hydride complex has been shown to undergo an insertion reaction with ethylene. The hydride complex also undergoes hydrogen exchange reactions with H–C(sp^2) and H–C(sp^3) bonds, presumably by way of σ-bond metathesis. Complexes **4.1** and the zirconium(III) borohydride complex undergo reversible disproportionation reactions under a CO atmosphere to give zirconium(IV) and zirconium(II) derivatives. It was also shown that CH_3CN reacts in a similar fashion with **4.1**, however the reversibility of this reaction was not established. In the case of the borohydride complex the reaction with CO proceeds further to give a complex containing a "formyl-ylid" type ligand.

TABLE OF CONTENTS

Chapter 2

Dinitrogen Complexes of Zirconium

List of Tables

List of Figures

LIST OF ABBREVIATIONS

The following abbreviations, most of which are commonly found in the literature, are used in this thesis.

Å	angström (10^{-10} m)
Anal.	analysis
atm	atmosphere
avg	average
br	broad
Bu^n	*n*-butyl group, $-CH_2CH_2CH_2CH_3$
Bu^i	*iso*-butyl group, $-CH_2CH(CH_3)_2$
Bu^tO	tertiary butoxy group, $-OC(CH_3)_3$
$^{11}B\{^1H\}$	observe boron while decoupling proton
°C	degrees Celsius
$^{13}C\{^1H\}$	observe carbon while decoupling proton
Calcd	calculated
Chem 3D®	molecular modelling program for the Macintosch
cm^{-1}	wave number
Cp	cyclopentadienyl group, $[C_5H_5]^-$
Cp^*	pentamethylcyclopentadienyl group, $\{C_5(CH_3)_5\}^-$
Cp'	substituted Cp ligand, e.g., $[C_5H_4Me]^-$
x.y-d_n	Complex **x.y** has n number of ^1H atoms replaced by ^2H atoms
d	doublet
d sept	doublet of septets
d of d	doublet of doublets
deg (or °)	degrees

Δ	heat
G	gauss
$\Delta G^{\ddagger}$	free energy of activation
ΔH°	enthalpy of reaction
EI	electron ionization
equiv	equivalent(s)
ESR	electron spin resonance
eV	electron Volt
$^{1}H\{^{11}B\}$	observe proton while decoupling boron
$^{1}H\{^{31}P\}$	observe proton while decoupling phosphorus
^{2}H	deuterium
m-Ph	*meta*-hydrogen or *meta*-carbon
o-Ph	*ortho*-hydrogen or *ortho*-carbon
p-Ph	*para*-hydrogen or *para*-carbon
h	Planck's constant (or hour)
HOMO	highest occupied molecular orbital
Hz	Hertz, seconds^{-1}
INDO	intermediate neglect differential overlap
IR	infrared
$^{n}J_{A-B}$	n-bond scalar coupling constant between A and B nuclei
K	Kelvin
kcal	kilocalories
K_{eq}	equilibrium constant
LUMO	lowest occupied molecular orbital
M	central metal atom (or "molar", when referring to concentration)
m	multiplet (or "medium", for infrared data)
M^{+}	parent ion

MS	mass spectrometry
Me	methyl group, $-CH_3$
mg	milligram(s)
MHz	megaHertz
mL	millilitre
mm	millimetre
mmol	millimole(s)
MO	molecular orbital
mol	mole
NMR	nuclear magnetic resonance
ORTEP	Oakridge Thermal Ellipsoid Plotting Program
OTf	triflate group, $-OSO_2CF_3$
$^{31}P\{^1H\}$	observe phosphorus while decoupling proton
Ph	phenyl group, $-C_6H_5$
ppm	parts per million
Pr^i	isopropyl group, $-CH(CH_3)_2$
ppm	parts per million
RT	room temperature
s	singlet (or "strong", for infrared data)
sept	septet
T	temperature
t	triplet
THF	tetrahydrofuran
TMS	tetramethylsilane
THT	tetrahydrothiophine
TMS	tetramethylsilane
VT	variable temperature

ACKNOWLEDGMENTS

I would like to thank my supervisor, Professor Mike Fryzuk, for sharing his inspired mind and for his meticulous guidance and patience (i.e., whenever I failed to make him famous) throughout this project. I enjoyed working with past and present members of Fryzuk's team; Dave, Guy, Patric, Lisa, Pauline, Tim, D. Berg, Kiran, Cam, Neil, Chas, Randy, Jesse, Craig, Cindy, Brian, Bobbi, Warren, Graham, Jonker, Danny, Garth, Laleh, Martin, Paul and Gao; I am thankful to all of them.

I extend my thanks to Professor Zaworotko, Department of Chemistry, St. Mary's University, for solving the zirconium(III) structures which were vital to this thesis; also, Dr. Steve Rettig for solving the dinitrogen structures. I greatly appreciate Mr. Jonathan Cohen and Professor Tom Loehr, Department of Chemistry, Oregon Graduate Institute of Science and Technology, for their contribution towards the resonance Raman studies. Dr. Peter Wassell is greatly appreciated for allowing (tolerating) me to use the IR and UV-Vis spectrometers; also, it is a pleasure working with Peter.

Many thanks go to Richard Schutte, Ken MacFarlane, Veranja Karunaratne, Danny Leznoff, Garth Giesbrecht and Guy Clentsmith, for proof reading my thesis, hopefully I will spell plan*er* correctly in future.

I would also like to acknowledge the assistance provided by the support staff of the chemistry department.

I greatly appreciate Yoga's family for their support during the course of my writing; if not for their help I would have been writing Chapter 2 forever.

I still admire and appreciate the professors and other support staff from the University of Jaffna for providing an excellent curriculum amidst the turbulent atmosphere.

TO MY PARENTS

with love and respect

Chapter 1

Introduction to Transition Metal Dinitrogen Chemistry

1.1 General

In the primitive atmosphere of the earth, the gaseous ammonia and dinitrogen molecules played a crucial role in the formation of more complex nitrogen containing derivatives, such as amino acids and other nitrogen-containing bases.[1-3] Formation of such biomonomers led to the chemical evolution of complex polymers such as proteins and nucleic acids, which eventually led to the origin of life on our planet.[4] After a few billion years of complex evolution, all living organisms rely on these essential building blocks for their survival. Presently, mankind consumes an enormous amount of nitrogen-containing fertilizers, which indirectly supplies their nutritional needs. In this respect, the synthesis of ammonia from dinitrogen and dihydrogen, the Haber process, could be ranked as one of the most important discoveries. This event led to the cheaper manufacture of fertilizers and thereby has helped to sustain the population explosion of this century and to some extent social and political stability.

Towards the end of nineteenth century, there was serious concern that the world's nitrate reserves would be exhausted due to the increased consumption by the explosives industry. This issue was certainly appreciated by the scientific community of the time. In 1898 William Crookes, in his presidential address to the British association for the advancement of science, said, "it is through the laboratory that starvation may ultimately be turned into plenty", and added that, "the fixation of atmospheric nitrogen is one of the great discoveries awaiting the ingenuity of chemists".[5]

Rayleigh and Crookes developed a method to fix atmospheric dinitrogen by electric discharge of hot air to give nitrous and nitric acids. This so-called arc process consumed such an enormous amount of energy that it was only feasible in countries where cheap hydroelectric power was available. In 1895 Frank and Caro discovered that the reaction of calcium carbide, CaC_2, with atmospheric nitrogen at very high temperatures gave calcium cyanamide $CaCN_2$.

references on page 18

This led to the development of cyanamide process in which the cyanamide produced was then hydrolyzed to give ammonia.[6]

In 1905 Fritz Haber[7] studied the equilibrium reaction of dinitrogen with dihydrogen over an iron catalyst, and determined the thermodynamic data associated with this reaction. Although his findings were disputed by Nernst, Haber within a few years not only confirmed his experimental data but also developed a reactor which utilized the heat evolved during the exothermic reaction to heat the reaction gas.[8] This convincing demonstration attracted the interest of the mighty, ambitious BASF company. An engineer from BASF, Carl Bosch, developed the high pressure technology, leading to the opening of a commercial plant in 1911.[6] At present, most Haber processes operate at pressures between 100 and 350 bar and at temperatures around 530 °C using a $Fe\text{-}Al_2O_3\text{-}K_2O$ catalyst. Dihydrogen used in the process is obtained by steam reforming or by partial oxidation of hydrocarbons and dinitrogen from air.[6]

1.2 Biological Nitrogen Fixation

Photosynthesis and nitrogen fixation are the two basic life processes that enable the survival of the plant and animal kingdoms. Unlike photosynthesis, nitrogen fixation is only carried out by some primitive prokaryotic micro-organisms. Bortels, in 1930, discovered that the trace element molybdenum is essential for dinitrogen metabolism.[9] It is now known that nitrogen fixation is carried out by enzymes known as nitrogenases which contain different combinations of transition metal elements: Fe-Mo, Fe-V and Fe-Fe.[10] The enzymatic reduction of one mole of dinitrogen requires the break-down of 16 MgATPs, equivalent to the loss of 488kJ, and suggests that the process is energy intensive (equation **1.1**).[11]

$$N_2 + 8\,H^+ + 8\,e^- + 16\,\text{MgATP} \xrightarrow{N_2\text{-ase}} 2\,NH_3 + H_2 + 16\,\text{MgADP} + 16\,PO_4^{3-} \qquad \textbf{1.1}$$

The nitrogenase enzyme consists of two proteins, the Fe protein and the MoFe protein. The Fe protein is a dimer of two identical subunits bridged by a Fe_4S_4 cluster which has a

references on page 18

cubane type geometry with alike atoms occupying the opposite corners of the cube. The MoFe protein has four subunits and contains two MoFe cofactors and two P clusters as illustrated in Figure **1.1**.[12,13] The Fe protein pumps the electrons into the cofactor consuming two moles of MgATP per electron. The reduction of the nitrogen proceeds in the cofactor. For a long time molybdenum was thought to be directly involved in the binding and the reduction of dinitrogen. On the basis of spectroscopic and modeling studies many structural models have been proposed for the cofactor.[14-16] Recently Rees *et al.* unveiled a crystallographic structure of MoFe protein from *Azotobacter vinelandii* at 2.7 Å resolution. The structure of the cofactor consists of two cuboidal units bridged by two sulfur atoms and another unidentified atom "Y".[17-19] The coordination geometry around the iron atoms is approximately trigonal planar. The location and the coordinative saturation of molybdenum seems to diminish the role played by molybdenum in the cofactor.

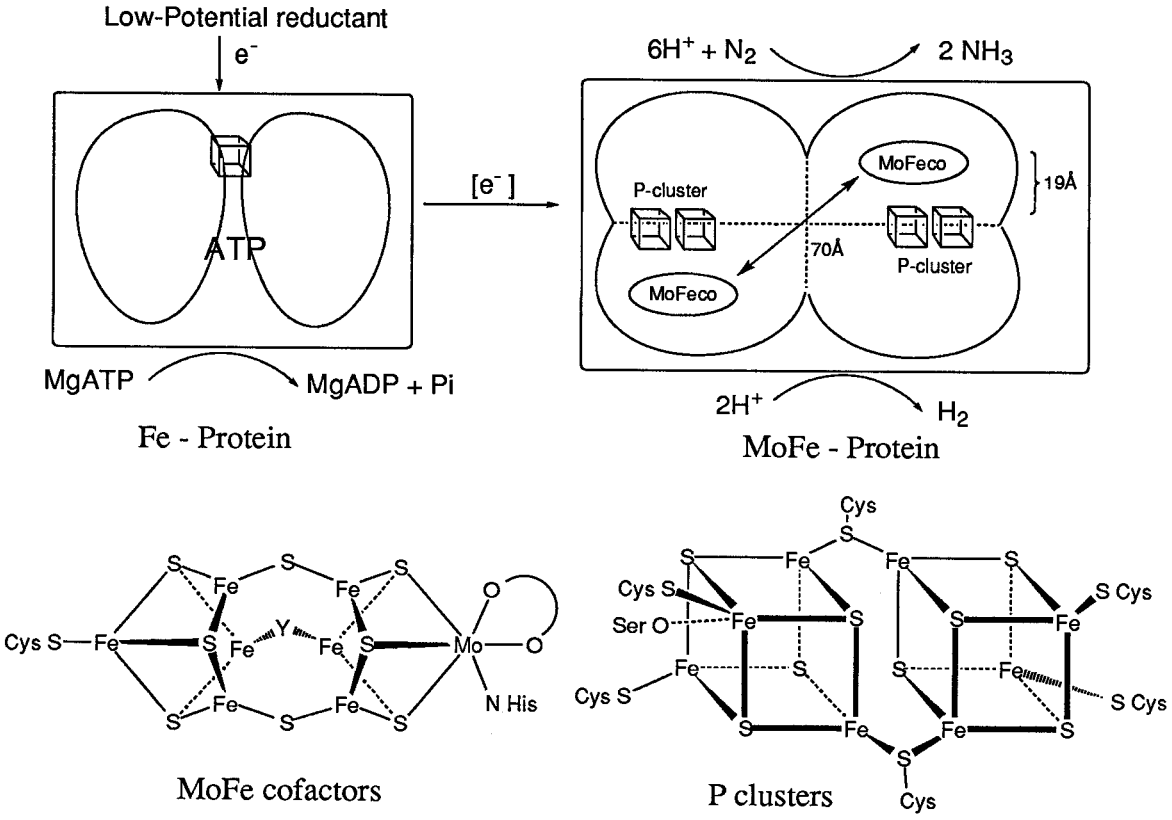

Figure 1.1 Schematic representation of the MoFe nitrogenase and the structures of the MoFe cofactor and the P cluster.

references on page 18

In the newly described cofactor, imaginative ideas have been presented regarding the mode of dinitrogen binding. At the observed separation, the two iron atoms bound to "Y", may be privileged to accommodate a side-on bound dinitrogen molecule.[12] Theoretical studies done on the Mo-Fe cofactor also suggests that a dinitrogen ligand bound in a side-on fashion will be activated to a greater extent than the end-on case.[20] The most prevalently known end-on mode of binding is also possible at the same site, but accessed only by the expansion of the MoFe cage.

The role of molybdenum is still alive. The molybdenum centre which is at the +4 oxidation level during the resting state of the cofactor could possibly be reduced to the +2 oxidation level during its active state. This could lead to the dissociation of certain ligands attached to the molybdenum centre and thereby create a vacant site for the coordination of dinitrogen.[13]

1.3 Other Methods of Nitrogen Fixation

Lithium and some alkaline earth metals react with dinitrogen at ambient conditions to give metal nitrides, a process referred to as nitriding.[11] Vol'pin *et al.* showed that at elevated temperatures and pressures, nitriding of some main group metals could be catalyzed by transition metal salts in aprotic media. The nitrides thus formed are then hydrolyzed to form ammonia. A highly active system in this respect is formed by a mixture of $TiCl_4$, $AlCl_3$ and metallic aluminum, where greater than 200 moles of ammonia (after hydrolysis) per mole of titanium were produced. Circumstantial evidence suggests that reduced species of titanium formed during the reaction, form Lewis type adducts with $AlCl_3$. A species formulated as $C_6H_6 \cdot TiCl_2 \cdot 2AlCl_3$ has been isolated in benzene, which is a catalyst for nitriding of aluminum, and also reacts with dinitrogen in the absence of aluminum to give a nitride complex.[21,22]

The aprotic system described in Scheme **1.1** fixes dinitrogen at ambient conditions, where the operation is carried out in cycles. It is presumed that the low valent titanium species generated by the reaction of $Ti(OR)_4$ and sodium naphthalide reduces dinitrogen to some unknown nitride species. Operation of the cyclic process depends on the sequence involving

references on page 18

judicious addition of proton source (isopropyl alcohol); the addition of electron source (sodium metal) and removal of ammonia at the appropriate stages of the reaction sequence.[21,23] Systems similar to the ones described above also facilitate in the incorporation of nitrogen from dinitrogen into organic molecules as amine and nitrile functionalities.[21,24]

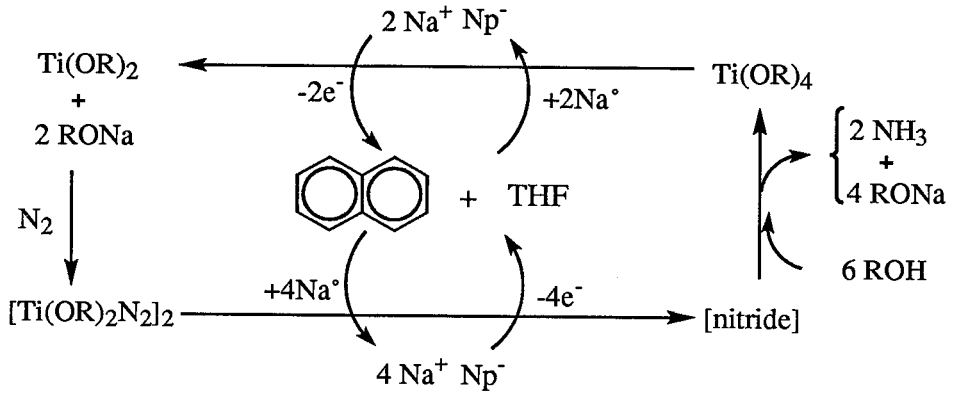

Scheme 1.1

Shilov *et al.* demonstrated that dinitrogen could be reduced in protic media. Two potent examples are the gels formed by the combination of salts, Mo^{5+} or $V^{4+}/Ti^{3+}/MgCl_2/KOH$ in an aqueous alcoholic medium.[25] These systems are catalytic with respect to molybdenum and vanadium ions and fix dinitrogen only in the presence of these ions. Mechanistic investigations suggest that the dinitrogen is probably activated within a preorganized bimetallic centre where the active metal centres are held by a complex arrangement of titanium and magnesium ions (Scheme **1.2**).[26]

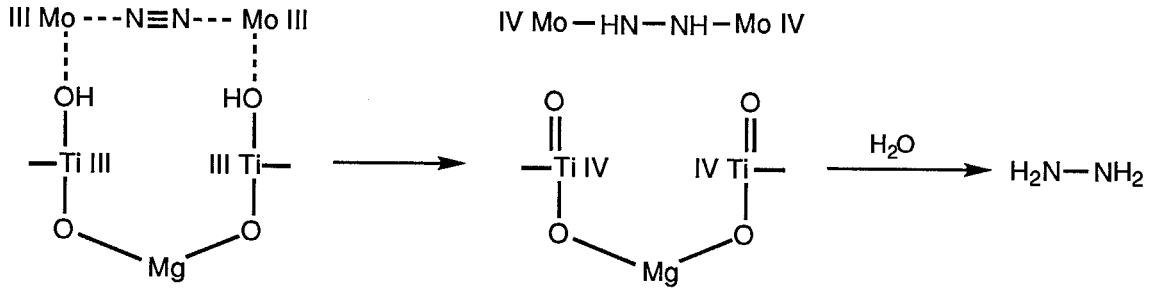

Scheme 1.2

Schrauzer *et al.* have suggested a different mechanism for the reduction of dinitrogen in aqueous gel matrices. The mechanism involve a side-on bound dinitrogen complex as the

references on page 18

intermediate, which is then reduced to give diazine*, HN=NH. The condition of the gel determines whether diazine undergoes disproportionation to give hydrazine $H_2N—NH_2$, and dinitrogen or will decompose to give dihydrogen and dinitrogen. (Scheme **1.3**).[27,28] Other than the methods described above, electrochemical[29, 73] and photochemical[30] studies have also been carried out. Recently, concerns have been raised regarding the reproducibility of the photochemical reduction of dinitrogen.[31]

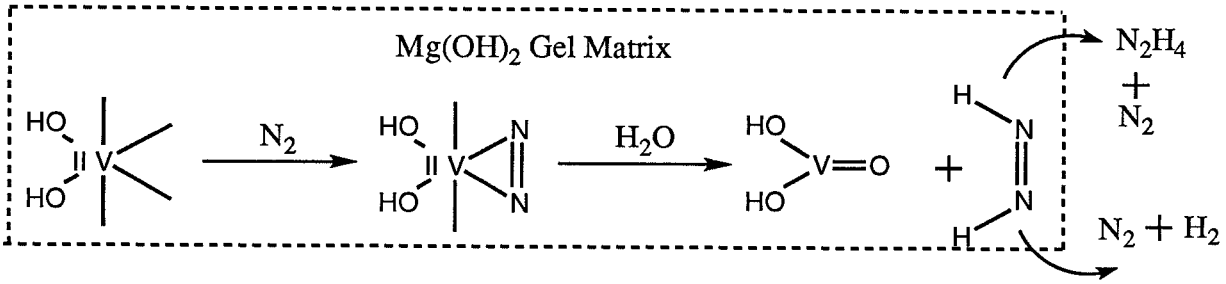

Scheme 1.3

1.4 Thermodynamic and Kinetic Factors

On the basis of the discussion presented above, one can gauge the difficulties in fixing** dinitrogen. The extraordinary stability of dinitrogen reflects the relatively high ionization potential (15.6 eV)*** making it difficult to oxidize.[32,33] A comparison of the dissociation energies of dinitrogen, 946 kJ mol^{-1}, diazine, 414 kJ mol^{-1}, and hydrazine, 159 kJ mol^{-1}, suggests that the cleavage of the first nitroge-nitrogen bond consumes most of the energy (≅ 532 kJ mol^{-1}).[34] Although the reduction of dinitrogen to ammonia is exothermic the calculated heat of formation of diazine is highly endothermic by 205 kJ mol^{-1}. Therefore a reaction path involving a diazine intermediate will require an activation energy not less than 205 kJ mol^{-1}. Such a high activation energy will correspond to a negligible

*Diazine is also refered to as diimide.

**The term fixation will refer to the partial or complete dissociation of the dinitrogen triple bond to give products such as hydrazine and ammonia. Activation will refer to the lengthening of the dinitrogen triple bond compared to its gaseous state. Degree of activation can be observed directly in structurally known complexes or indirectly by other spectroscopic methods, e.g., infrared spectroscopy.

***Comparable to the ionization energy of argon (15.75 eV)

references on page 18

rate of reaction between gaseous dinitrogen and dihydrogen.[26] Biological and industrial means of surmounting this kinetic barrier are by the use of metal catalysts.

$$N_2 + H^{\bullet} \longrightarrow {}^{\bullet}N_2H \qquad \Delta H^{\circ} = 88 \text{ kJ mol}^{-1} \qquad \textbf{1.2}$$

$$N_2 + 1\,H_2 \longrightarrow N_2H_2 \qquad \Delta H^{\circ} = 205 \text{ kJ mol}^{-1} \qquad \textbf{1.3}$$

$$N_2 + 2\,H_2 \longrightarrow N_2H_4 \qquad \Delta H^{\circ} = 92 \text{ kJ mol}^{-1} \qquad \textbf{1.4}$$

$$N_2 + 3\,H_2 \longrightarrow 2\,NH_3 \qquad \Delta H^{\circ} = -92 \text{ kJ mol}^{-1} \qquad \textbf{1.5}$$

Comparison of the heats of formation of diazine and hydrazine indicates that a simultaneous reduction of two of the three bonds of dinitrogen seems more favorable than a stepwise reduction (equations **1.3** and **1.4**). This analysis has been extended to rationalize the activation of dinitrogen coordinated between two metal centres, M←N≡N→M, where it is likely to undergo a four electron reduction to give a hydrazine type complex, M=N—N=M. Still, these metals would require such high reduction potentials that such reactions could not occur in protic media.[26]

Interestingly, in some diazine complexes the hydrogen atoms of the diazine ligand were found to be involved in hydrogen bonding with sulfur atoms of the ancillary ligand (Figure **1.2**).[35] In biological systems such multiple hydrogen bonds have been shown to exhibit bond energies up to 70 kJ mol^{-1}. Under such circumstances the formation of diazine intermediate would possibly become exothermic. Also for systems that operate in aqueous media, the heat of hydration* will aid in the stabilization of the intermediates.[26]

In the Haber process, the first step is the dissociative adsorption of dinitrogen and hydrogen to give surface bound nitrogen and hydrogen atoms. Under the conditions of Haber process the dissociative adsorption of dinitrogen is the rate-limiting step. The energy associated

---

*ΔH_{298K} in (H_2O) of N_2H_4 = 34 kJ mol^{-1}; ΔH_{298K} ($H_3O^{\oplus}$) of N_2H_4 = -7.5 kJ mol^{-1}; ΔH_{298K} in (H_2O) of (NH_3) = -161 kJ mol^{-1}; ΔH_{298K} ($H_3O^{\oplus}$) of (NH_3) = -168 kJ mol^{-1}.

references on page 18

with the formation of surface-atom bonds over the catalyst compensates for the relevant dissociation energy, making the overall adsorption reaction exothermic.** The adsorbed nitrogen atoms are then hydrogenated in a stepwise manner to give NH, NH_2 and NH_3 respectively. Although these steps are thermodynamically "uphill" they are easily overcome at the operating temperatures of the Haber process.[6]

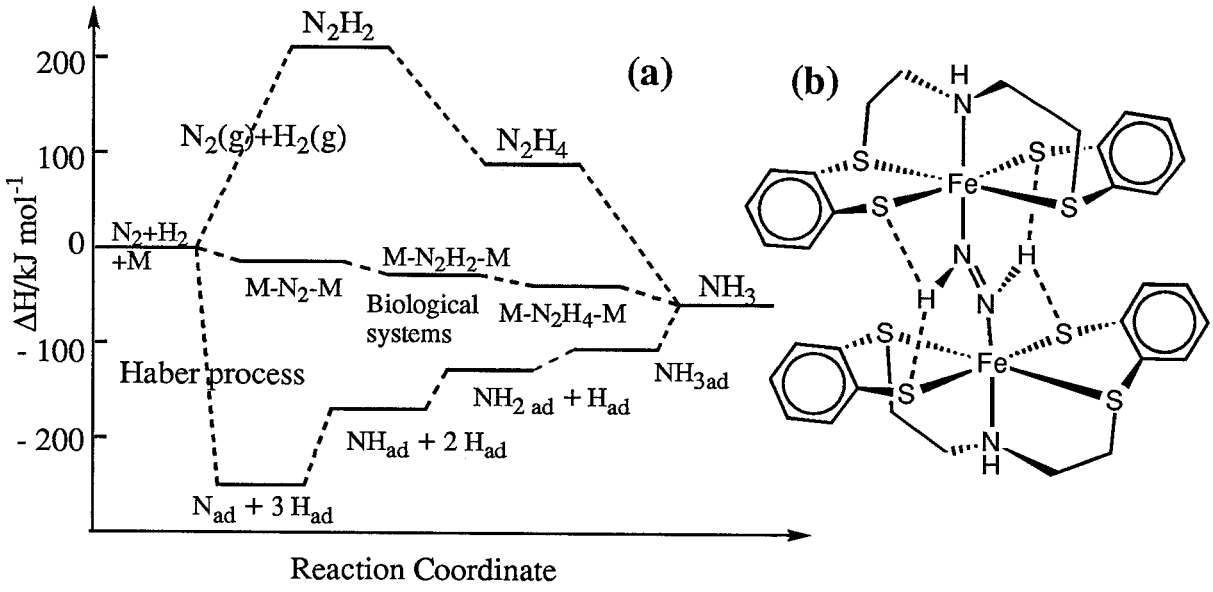

Figure 1.2 **(a)** A proposed energy diagram for the reaction of dinitrogen and dihydrogen; in gas phase (top), in biological systems (middle) and in the Haber process (bottom). N_{ad} and H_{ad} represent these atoms adsorbed on a catalytic surface. **(b)** An example of a diazine ligand involved in intramolecular hydrogen bonding.

1.5 Dinitrogen Complexes

In 1965 Allen and Senoff isolated the first dinitrogen complex, $[Ru(NH_3)_5N_2]^{2+}$.[36] Since then a wide variety of dinitrogen complexes have been prepared encompassing nearly all the transition metals. In most cases the coordinated dinitrogen ligand was derived from gaseous dinitrogen and in some cases was derived from hydrazine, azides, nitrous oxide etc.[37,38] A convenient way to present an overview of dinitrogen complexes is to group them on the basis of

---

**For the adsorption of one nitrogen and three hydrogen atoms the reaction is exothermic by 259 kJ mol^{-1}.

references on page 18

bonding of dinitrogen ligand as shown in Figure **1.3**. This figure will form the basis for discussion in the following section.

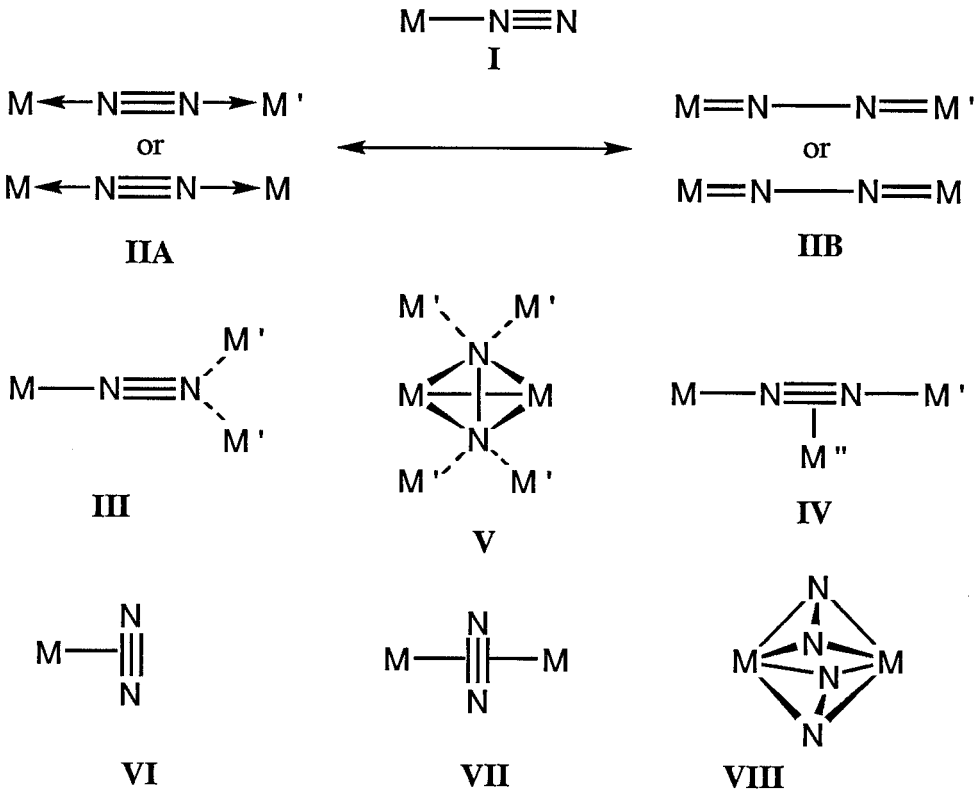

Figure 1.3 Dinitrogen bonding modes. M, M' and M" can be different metals or same metals with different ligand environments.

1.5.1 Mononuclear End-On Complexes

Mononuclear complexes with end-on bonded dinitrogen ligands, **I** (Figure **1.3**), are overwhelmingly represented. The bond distances of the nitrogen-nitrogen bond in these complexes range from 1.0 Å to 1.15 Å, and have a M—N≡N bond angle greater than 175°. This mode of coordination is scarcely known for Group 3, Group 4 and Group 5 metals. Recently an anionic vanadium complex with two terminally bound dinitrogen ligands has been structurally characterized, $[Na(THF)][V(N_2)_2(Ph_2PCH_2CH_2PPh_2)_2]$.[72] Monodentate and chelating phosphine ligands are the common ancillary ligands in mononuclear complexes.

Complexes with porphyrin ligands have also been reported.[39,40] Some dinitrogen complexes of iron, ruthenium and cobalt have been prepared by the addition of dinitrogen to

references on page 18

metal hydride complexes (equation **1.6**).[41] It has been proposed that in nitrogenase, hydrogen is evolved during the coordination of dinitrogen, which is comparable to the aforementioned reaction. Another pertinent reaction is the mutual exchange of hydride and dinitrogen ligands, where the metals involved are also present in nitrogenase (equation **1.7**).[42]

$$[RuH_4(PPh_3)_3] + N_2 \rightleftharpoons [RuH_2(N_2)(PPh_3)_3] + H_2 \qquad \textbf{1.6}$$

$$2\,[FeH(H_2)(dmpe)_2]^+ + [Mo(N_2)_2(dppe)_2] \longrightarrow 2\,[FeH(N_2)(dmpe)_2]^+ + [MoH_4(dppe)_2] \qquad \textbf{1.7}$$

1.5.2 Dinuclear End-On complexes

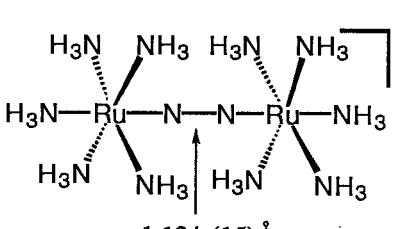

1.1

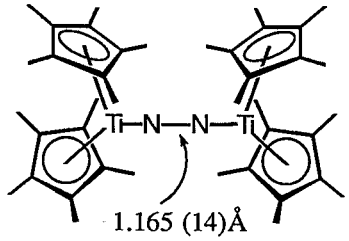

1.2

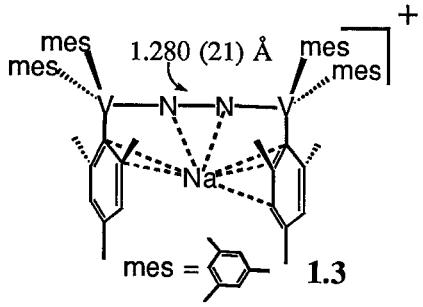

1.3

In the linearly bridged end-on binding mode, **II**, the dinitrogen ligand shows a wide range of activation. The observed nitrogen-nitrogen bond lengths range from 1.0 Å to 1.3 Å, and have a M—N≡N angle greater than 170°. Case **IIa** (examples **1.1** and **1.4**) [43,44] may be regarded as a Lewis acid-Lewis base type interactions where the nitrogen-nitrogen bond lengths are close to that of free dinitrogen (1.098 Å). In case **IIb** (examples **1.3** and **1.7**),[45,46] the bonded dinitrogen ligand is envisaged as a hydrazido type ligand, $(N_2)^{4-}$ where the nitrogen-nitrogen bond lengths are approximately 1.3Å. These two cases can be considered as the two limiting resonance forms for the bridging end-on case **II**. The intermediate cases (example **1.2** and **1.5**)[37,47] can be understood on the basis of different contributions from the two forms **IIa**

references on page 18

and **IIb**. Although the two limiting cases can be reasonably depicted, for the intermediate cases different authors seem to adopt different representations.

Interestingly, a close resemblance exists between complex **1.3** and the proposed intermediates in the systems which fix dinitrogen in protic media (Scheme **1.2**). In both cases the metal ions, sodium or magnesium, seem to aid in the stabilization of the bimetallic centre. A rare example of case **II** having porphyrin as the ancillary ligand (example **1.6**) is also known. These complexes are viewed as possible electrode catalysts for the reduction of dinitrogen.[48]

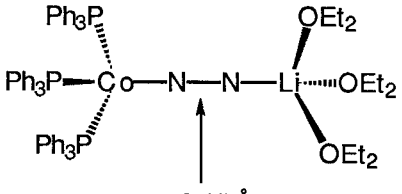

1.19 (4)Å

1.4

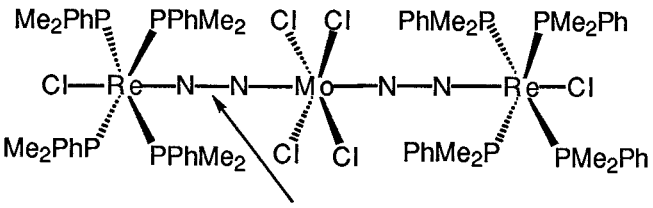

1.28 (5)Å

1.5

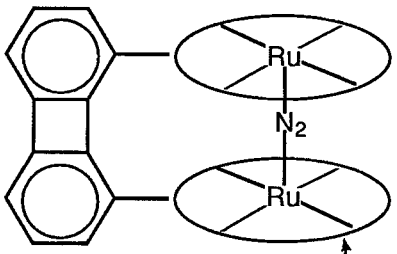

Porphyrin ligand

1.6

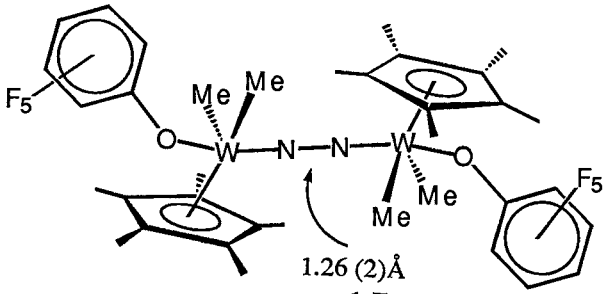

1.26 (2)Å

1.7

1.5.3 Protonation of Terminally Bonded Dinitrogen Complexes

1.8

Protonation reactions of ligated dinitrogen can be summarized as in equation **1.8**. Ratios of dinitrogen, ammonia and hydrazine produced vary widely, depending on the metal, proton source and solvent. The reaction of $[W(N_2)_2(PMe_2Ph)_4]$ with H_2SO_4 in methanol gave 1.86 moles of ammonia per mole of complex, which indicates almost a quantitative use of metal

references on page 18

electrons. The same complex reacted with HCl in dimethoxyethane gave 0.5 moles of ammonia and 0.3 moles of hydrazine per mole of complex.[49]

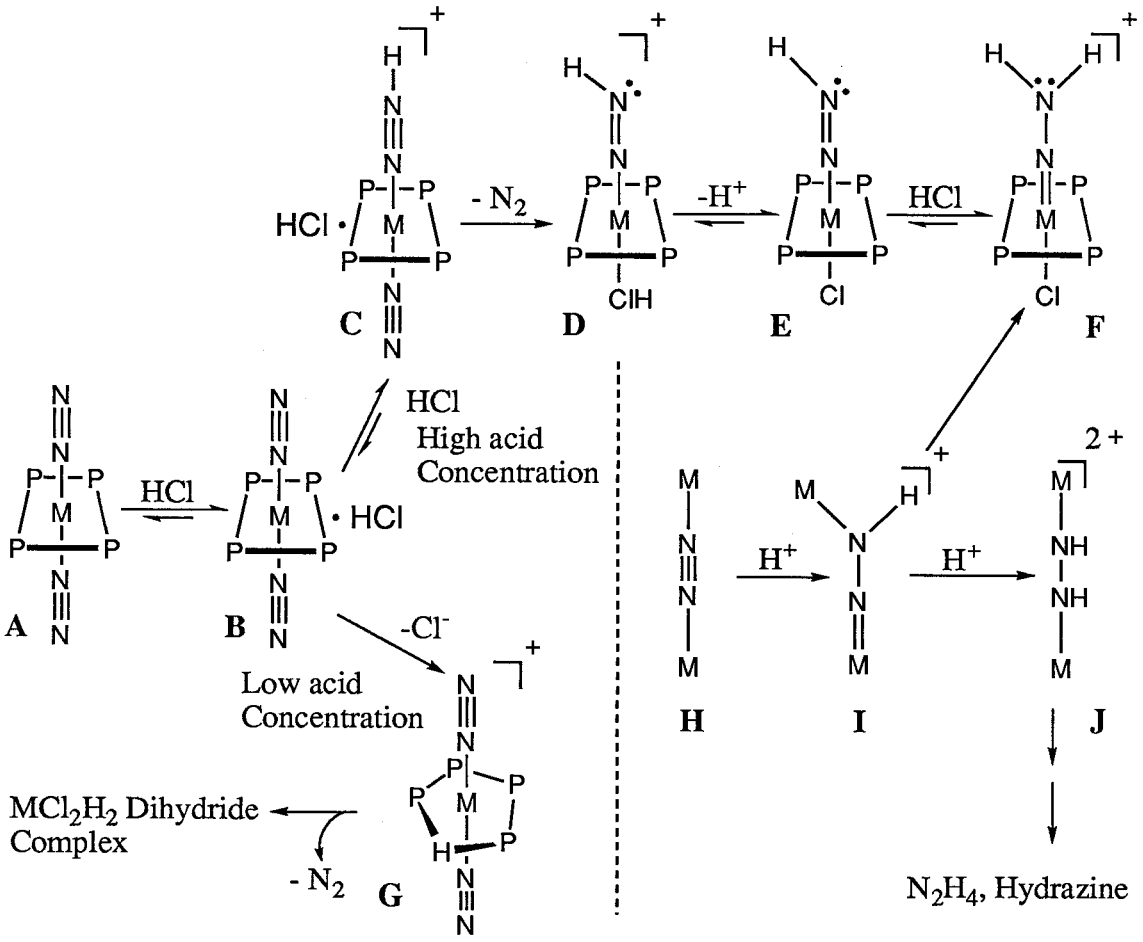

Figure 1.4 The proposed mechanism for the protonation of end-on bound dinitrogen in molybdenum(0) and tungsten(0) complexes by HCl in THF. The chelating phosphine ligand in this case is $Ph_2PCH_2CH_2PPh_2$. The intermediates **I** and **J** are proposed for the protonation of bridging complex **H**.

Some high oxidation state, dinuclear complexes of tantalum(V), niobium(V) and tungsten(VI), where the dinitrogen ligand is formulated as a hydrazido ligand $(N_2)^{4-}$, give quantitative yields of hydrazine upon protonation.[50,51] Conversely, complexes similar to **1.7** (example $[(\eta^5\text{-}C_5Me_5)MMe_3]_2(\mu\text{-}N_2)$, M = Mo or W) also formulated as tungsten(VI) and dinitrogen as hydrazido ligand $(N_2)^{4-}$, react with acid to give only 0.3 moles of ammonia per mole of complex. The yields of ammonia in these complexes were increased to 1.86 equivalents

references on page 18

when protonation was carried out under reducing conditions.[52] It is important to point out that a survey of numerous protonation reactions suggests no correlation between the degree of activation of the dinitrogen ligand and the observed fixation during protonation reactions.[53]

The protonation reactions of complexes $M(N_2)_2L_n$ where M = W or Mo and L_n = $(PPhMe_2)_4$ or L_n = $(Ph_2PCH_2CH_2PPh_2)_2$ have been extensively investigated.[37,38,54] Figure **1.4** depicts the intermediates involved during the first two proton transfers to the coordinated dinitrogen. Intermediates **B**, **C**, **D** and **E** are invoked on the basis of kinetic and spectroscopic studies. Diazenido $(NNH)^{-1}$ intermediates, similar to **D** or **E** are yet to be authenticated, but a Lewis acid adduct $(N—HN\rightarrow BPh_3)^{-1}$, has been structurally characterized.[49] The hydrazido $(NNH_2)^{2-}$ intermediate **F** has been substantiated by NMR spectroscopy and X-ray crystallographic analysis. An interesting feature in some structurally known examples of intermediate **F** (e.g., {[$W(NNH_2)Br(PMe_2Ph)_3(C_5H_4NMe\text{-}3)$](Br)}) is the presence of hydrogen bonding between the hydrogens of the hydrazido ligand and the halide ions.[37] Different mechanistic pathways have been proposed for the formation of ammonia and/or hydrazine from intermediate **F**.

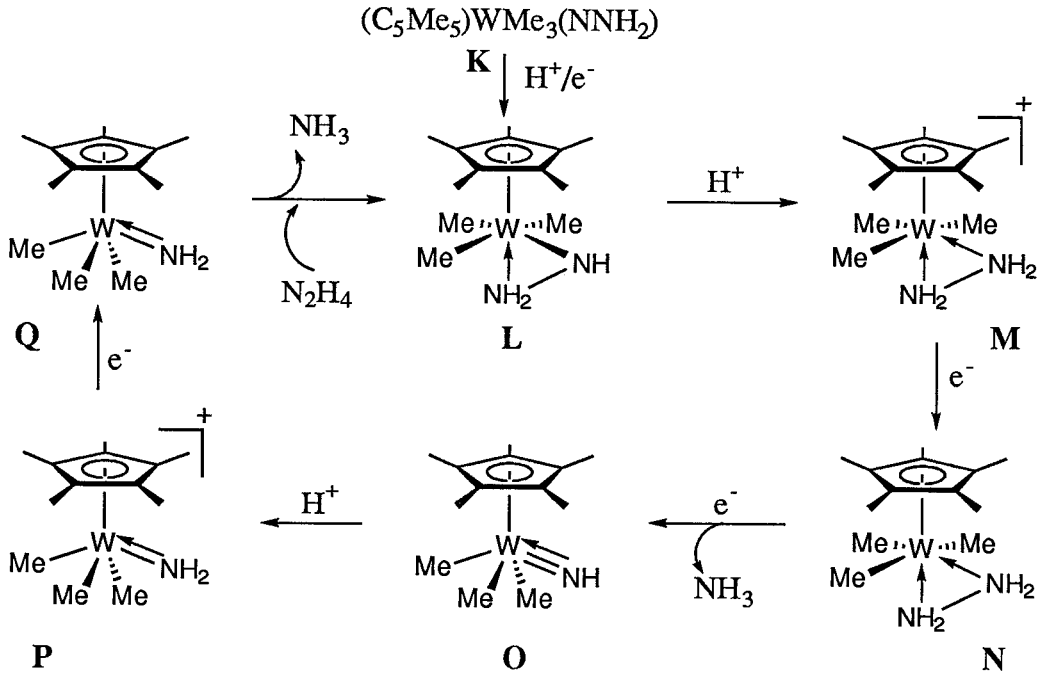

Figure **1.5** The proposed cycle for the catalytic reduction of hydrazine by complex $(\eta^5\text{-}C_5Me_5)WMe_3(NNH_2)$, **K**.

references on page 18

Schrock *et al.* have invoked similar hydrazido $(NNH_2)^{2-}$ intermediates during the protonation of dinuclear complexes, for example $(\eta^5\text{-}C_5Me_5)MMe_3]_2(\mu\text{-}N_2)$, M = Mo or W (Figure **1.5**). The hydrazido $(NNH_2)^{2-}$ intermediate formed in this case $((\eta^5\text{-}C_5Me_5)MMe_3(NNH_2)$ M = Mo or W) is formally in a higher oxidation state (+6) compared to the intermediates (e.g., **F**, Figure **1.4**) formed from mononuclear complexes. Therefore for the further reduction of the hydrazido ligand in **K** an external electron source is needed. The suggested mechanism for the protonation of $(\eta^5\text{-}C_5Me_5)WMe_3(NNH_2)$, under reducing conditions is shown in Figure **1.5**. In the absence of a suitable electron source some intermediates undergo disproportionation reactions to give ammonia and dinitrogen.[54,55] Also, intermediates **K** and **M** have been shown to catalytically reduce hydrazine (up to 10 equivalents of hydrazine). It is also noteworthy that some sulfur ligated molybdenum(IV) complexes (e.g. $[(Mo_2Cl_4(\mu\text{-}\eta^2\text{-}S_2)(\mu\text{-}2\text{-}SC_5H_3NH\text{-}3\text{-}SiMe_3)(2\text{-}SC_5H_3N\text{-}3\text{-}SiMe_3)_2]\bullet THF$) have shown to be effective in the catalytic disproportionation of hydrazine to ammonia and dinitrogen. However, in the presence of a reductant the conversion of hydrazine to ammonia occurs catalytically (up to 1200 cycles).[56]

1.5.4 Polynuclear Dinitrogen Complexes

In principle, the interaction of dinitrogen with three or more metal centres could generate numerous modes of bonding (eg. **III**, **IV** and **V** in Figure **1.3**). So far only a few different modes are known, each uniquely exemplified by **1.8**, **1.9**, **1.10** and **1.11**. In most of these cases the dinitrogen ligand is bound terminally as well as side-on.

These complexes usually show a higher degree of activation of dinitrogen, with nitrogen-nitrogen bond lengths greater than 1.3 Å. A few examples of case **III** (Figure **1.3**) are known, where M is tungsten or cobalt and M' is either lithium, aluminum or magnesium (e. g. **1.8**).[57,58] Complex **1.9** exemplifies case **IV**. Treatment of the complex **1.9** with acid gave four equivalents of dihydrogen and one equivalent of dinitrogen, whereas with water, a mixture of hydrazine and ammonia was obtained (greater than 90% fixation).[59] Until recently complex **1.10**, an example of case **V**, exhibited the longest nitrogen-nitrogen bond length of 1.36(2) Å.[60]

references on page 18

Although this complex showed a high degree of dinitrogen activation, reaction with ethylene smoothly displaced the dinitrogen ligand.[61]

The alkali-metal-cobalt complexes **1.4** and **1.11** are closely related, and in fact exhibit similar nitrogen-nitrogen bond lengths. However, the solid state structures of these two derivatives differ drastically. In **1.11** the dinitrogen interacts with the alkali metal both in an end-on and a side-on fashion.[62] Interestingly this type of coordination of dinitrogen closely resembles the environment of the isoelectronic carbide ion in the alkaline earth salts (C_2^{2-}; CaC_2, MgC_2, BaC_2, etc). Calcium carbide has a tetragonally distorted NaCl structure where each carbide ion is coordinated to six calcium ions. Four of these calcium ions interact side-on with the carbide ion and the other two end-on.[63]

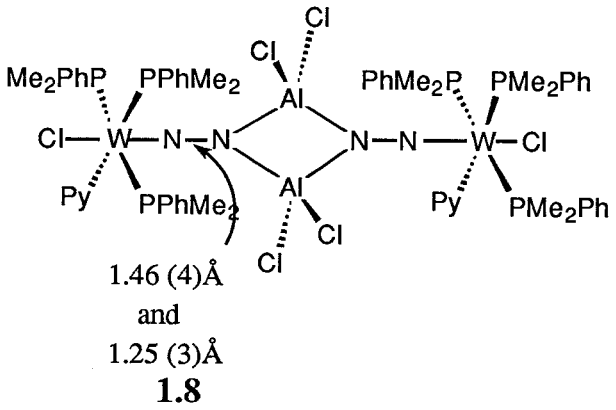

1.8

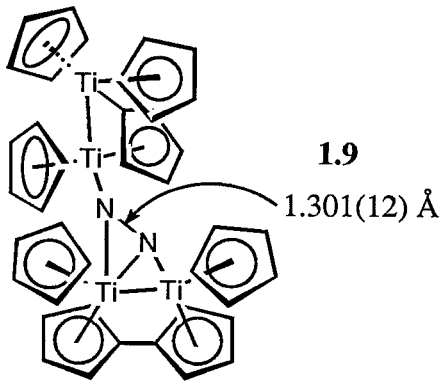

1.9

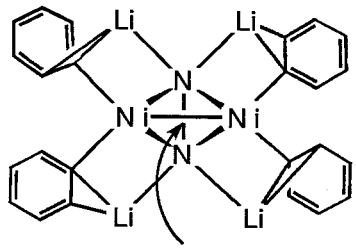

1.10

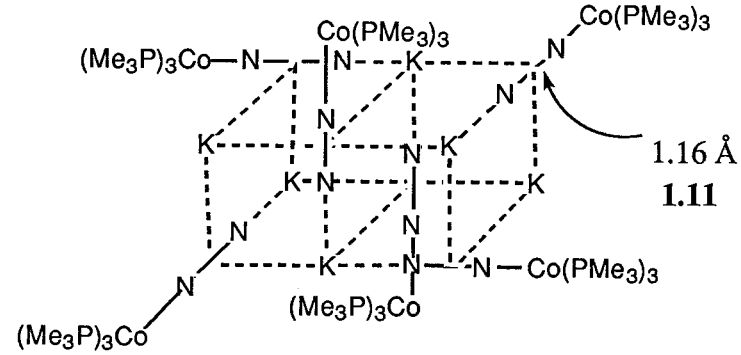

1.11

1.5.6 Mononuclear Side-On Complexes

On the basis of spectroscopic evidence only one example of a mononuclear side-on bound dinitrogen complex has been reported. The temperature invariant ESR spectrum of this zirconium(III) complex, $Cp_2Zr[CH(SiMe_3)_2](\eta^2\text{-}N_2)$, shows coupling due to two equivalent

references on page 18

nitrogen atoms. Upon protonation, this complex gave hydrazine and dinitrogen (25% fixation).[64,65]

In some cases side-on complexes have been implicated as intermediates. In the case of complex $(\eta^5\text{-}C_5Me_5)Re(CO)_2(\eta^{1\text{-}15}N\text{–}N^{14})$, the dinitrogen ligand was found to undergo end-to-end rotation in an intramolecular fashion. Inevitably the proposed mechanism involves a side-on bound intermediate (Scheme **1.4**).[66] Mononuclear dihapto dinitrogen complexes have been spectroscopically detected with many metals in low temperature matrices.[67]

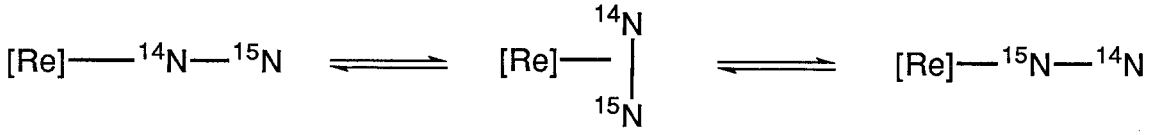

[Re] = $(\eta^5\text{-}C_5Me_5)Re(CO)_2(^{15}N\text{–}N^{14})$

Scheme 1.4

1.5.7 Dinuclear Side-On Complexes

In the past five years, two examples of case **VII** and one example of case **VIII** have been structurally characterized. Case **VII** examples are complexes of samarium (example **1.12**) and lithium (example **1.13**).

Although the complexes **1.12** and **1.13** are formed by different types of metals (lanthanide vs. alkali metal) the properties of the dinitrogen ligand are almost identical. The nitrogen-nitrogen bond lengths of these two complexes are identical to that of free dinitrogen and have a planar M—N_2—M core. Under vacuum the dinitrogen ligand can be stripped from the metals coordination sphere.[68,69] Reversible binding of dinitrogen in solid and in solution states have been demonstrated for complex **1.12**.[69] Stephan *et al.* have proposed that for complex **1.13**, the zirconium-phosphinidene dianion fortuitously favors the Li_2—N_2 dication rather than a fully solvated lithium counter ions.[68] Unfortunately, the mode of dinitrogen bonding in solution has not been verified for examples **1.12** and **1.13**.

The anionic complex **1.14** (example of case **VIII**), described by Gambarotta *et al.* has a pseudo octahedral $Ti(\mu\text{-}N_2)_2Ti$ core with the dinitrogen ligands defining the opposite edges of

references on page 18

an equatorial plane.[70] This anion is a mixed oxidation state complex where the titanium centres can be formulated as either titanium(I) and titanium(II) or as titanium(III) and titanium(IV) corresponding to neutral N_2 and $(N_2)^{2-}$ ligands respectively. Although the formalism predicts activation only to the extent of $(N_2)^{2-}$ the observed nitrogen-nitrogen bond length of (1.38(2) Å) in **1.14**, is much longer than a nitrogen-nitrogen double bound; by comparison PhN=NPh has a bond distance of 1.255 Å.[71] The nitrogen-nitrogen distance in **1.14** seems to correlate more closely to dinitrogen complexes where the dinitrogen is formulated as hydrazido ligand, $(N_2)^{4-}$.

The discussion presented so far on dinuclear side-on dinitrogen complexes seems to suggest that the degree of activation of dinitrogen as measured by bond lengths falls in two extreme ends. For the samarium and lithium cases dinitrogen is barely activated whereas in the titanium case the observed dinitrogen bond distances are much greater than what would be expected.

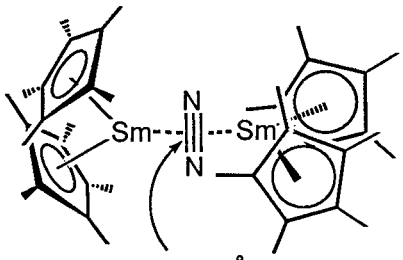

1.088 (12)Å

1.12

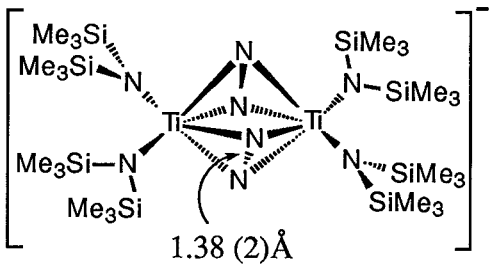

1.38 (2)Å

1.14

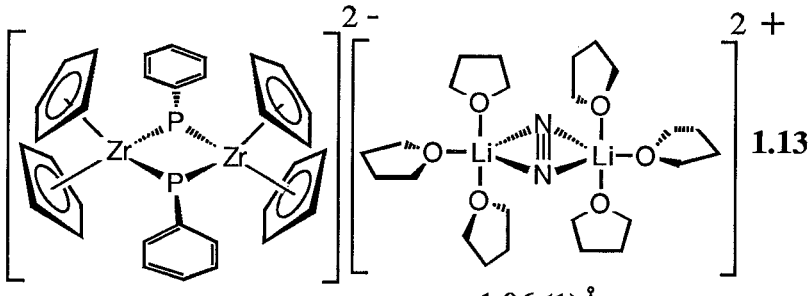

1.13

1.06 (1)Å

1.6 Summary

Terminally bound dinitrogen complexes have been synthesized with most transition metal complexes with varying degrees of activation. Although the motive for this type of research was eventually to develop complexes that could catalytically reduce dinitrogen, so far

references on page 18

mononuclear and dinuclear end-on complexes have been extensively investigated. Yet, compared to the mechanistic understanding of reactions involving other small molecules such as carbonmonoxide, dihydrogen etc., the protonation reactions of dinitrogen are limited. In the past five years, few side-on bound dinitrogen complexes have been structurally characterized. Another important milestone is the structural elucidation of the cofactor of the enzyme nitrogenase. Ironically, a few researchers have proposed that the dinitrogen might interact in a side-on fashion during its activation in the cofactor. Structural and theoretical studies seem to suggest that a side-on mode of bonding leads to a greater degree of activation of dinitrogen.

In the following chapter new side-on bound dinitrogen complexes of zirconium will be discussed. Aspects of the bonding both in solution and in the solid state, and some aspects of the reactivity of the coordinated dinitrogen will be considered.

1.7 References

(1) Miller, S. L. *J. Am. Chem. Soc.* **1955**, *77*, 2351.

(2) Lemmon, R. M. *Chem. Rev.* **1970**, *70*, 95.

(3) Ponnamperuma, C. *Quart. Rev. Biophys.* **1971**, *4*, 77.

(4) Price, C. C. *Synthesis of Life*; Dowden, Hutchingon & Ross, Inc.: Stroudsburg, Pennsylvania, 1974; Vol. 1.

(5) Crookes, W. In *The Report of the 68th meeting of the British Association for the Advancement of Science*; John Murray, London: Bristol, 1898; p 3.

(6) Jennings, J. R. *Catalytic Ammonia Synthesis: Fundamentals and Practice*; Plenum Press: New York and London, 1991; Vol. 1.

(7) Feldman, M. R.; Tarver, M. L. *J. Chem. Ed.* **1983**, *60*, 463.

(8) Haber, F.; vonOordt, G. *Z. Anorg. Chem.* **1905**, *44*, 341.

(9) Bortels, H. *Arch. Mikrobiol.* **1930**, *1*, 333.

(10) Dilworth, M. J.; Glenn, A. R. *Biology and Biochemistry of Nitrogen Fixation.*; Elsevier: New York, 1991, pp Chapter 4.

(11) Chatt, J.; Leigh, G. J. *Chem. Soc. Rev.* **1972**, *1*, 121.

(12) Orme-Johnson, W. H. *Science* **1992**, *257*, 1639.

(13) Sellmann, D. *Angew. Chem., Int. Ed. Engl.* **1993**, *32*, 64.

(14) Ciuril, S.; Holm, R. H. *Inorg. Chem.* **1989**, *28*, 1685.

(15) Coucouvanis, D. *Acc. Chem. Res.* **1991**, *24*, 1.

(16) Burgess, B. K. *Chem. Rev.* **1990**, *90*, 1377.

(17) Georgiadis, M. M.; Komiya, H.; Chakrabati, P.; Doo, D.; Komuc, J. J.; Rees, D. C. *Science* **1992**, *257*, 1653.

(18) Kim, J.; Rees, D. C. *Nature* **1992**, *360*, 553.

(19) Kim, J.; Rees, D. C. *Science* **1992**, *257*, 1677.

(20) Deng, H.; Hoffmann, R. *Angew. Chem., Int. Ed. Engl.* **1993**, *32*, 1062.

(21) vanTamelen, E. E. *Acc. Chem. Res.* **1970**, *3*, 361.

(22) Volpin, M. E.; Ilatovskaya, M. A.; Kosyakova, L. V.; Shur, V. B. *J. Chem. Soc., Chem. Commun.* **1968**, 1074.

(23) vanTamelen, E. E.; Fechter, R. B.; Schneller, S. W.; Boche, G.; Greeley, R. H.; Akermark, B. *J. Am. Chem. Soc.* **1969**, *91*, 1551.

(24) vanTamelen, E. E.; Rudler, H. *J. Am. Chem. Soc.* **1970**, *92*, 5253.

(25) Shilov, A.; Denisov, N.; Efimov, O.; Shuvalov, N.; Shuvalova, N.; Shilova, A. *Nature* **1971**, *231*, 460.

(26) Shilov, A. E. *Russ. Chem. Rev.* **1974**, *43*, 378.

(27) Zones, S. I.; Palmer, M. R.; Palmer, J. G.; Doemeny, J. M.; Schrauzer, G. N. *J. Am. Chem. Soc.* **1978**, *100*, 2113.

(28) Liu, N. H.; Strampach, N.; Plamer, J. G.; Schrauzer, G. N. *Inorg. Chem.* **1984**, *23*, 2772.

(29) Haight, G. P.; Scott, R. *J. Am. Chem. Soc.* **1964**, *86*, 744.

(30) Edwards, J. G.; Davies, J. A.; Boucher, D. L.; Mennad, A. *Angew. Chem., Int. Ed. Engl.* **1992**, *31*, 480.

(31) Edwards, J. G.; Davies, J. A.; Augugliaro, V.; Soria, J.; Palmisano, L.; Schiavello, M.; Sclafani, A. *Angew. Chem., Int. Ed. Engl.* **1993**, *32*, 550.

(32) Chatt, J. *Pure Appl. Chem.* **1970**, *24*, 425.

(33) Pelikan, P.; Boca, R. *Coord. Chem. Rev.* **1984**, *55*, 55.

(34) Jolly, W. L. *The Inorganic Chemistry of Nitrogen*; W. A. Benjamin, INC.: New York, 1964.

(35) Sellmann, D.; Soglowek, W.; Knoch, F.; Moll, M. *Angew. Chem., Int. Ed. Engl.* **1989**, *28*, 1271.

(36) Allen, A. D.; Senoff, C. V. *Chem. Commun.* **1965**, 621.

(37) Chatt, J.; Dilworth, J. R.; Richards, R. L. *Chem. Rev.* **1978**, *78*, 589.

(38) Henderson, R. A.; Leigh, G. J.; Pickett, C. J. *Adv. Inorg. Chem. Radiochem.* **1983**, *27*, 197.

(39) Buchler, J. W.; Smith, P. D. *Angew. Chem., Int. Ed. Engl.* **1974**, *13*, 745.

(40) Camenzind, M. J.; James, B. R.; Dolphin, D. *J. Chem. Soc., Chem. Commun.* **1986**, 1137.

(41) Knoth, W. H. *J. Am. Chem. Soc.* **1968**, *90*, 7172.

(42) Leigh, G. J.; Jimenez-Tenorio, M. *J. Am. Chem. Soc.* **1991**, *113*, 5862.

(43) Treitel, L. M.; Flood, M. T.; Marsh, R. E.; Gray, H. B. *J. Am. Chem. Soc.* **1969**, *91*, 6512.

(44) Yamamoto, A.; Miura, Y.; Ito, T.; Chen, H. L.; Iri, K.; Ozawa, F. *Organometallics* **1983**, *2*, 1429.

(45) O'Regan, M. B.; Liu, A. H.; Finch, W. C.; Schrock, R. R.; Davis, W. M. *J. Am. Chem. Soc.* **1990**, *112*, 4331.

(46) Ferguson, R.; Solari, E.; Floriani, C.; Chiesi-Villa, A.; Rizzoli, C. *Angew. Chem., Int. Ed. Engl.* **1993**, *32*, 396.

(47) Sanner, R. D.; Duggan, D. M.; McKenzie, T. C.; Marsh, R. E.; Bercaw, J. E. *J. Am. Chem. Soc.* **1976**, *98*, 8358.

(48) Collman, J. P.; Hutchison, J. E.; Lopez, M. A.; Guilard, R. *J. Am. Chem. Soc.* **1992**, *114*, 8066.

(49) Takahashi, T.; Mizobe, Y.; Sato, M.; Uchida, Y.; Hidai, M. *J. Am. Chem. Soc.* **1980**, *102*, 7461.

(50) Churchill, M. R.; Li, Y. J.; Theopold, K. H.; Schrock, R. R. *Inorg. Chem.* **1984**, *23*, 4472.

(51) Dilworth, J. R.; Henderson, R. A.; Hills, A.; Hughes, D. L.; Macdonald, C.; Stephens, N.; Watson, D. R. M. *J. Chem. Soc., Dalton Trans.* **1990**, 1077.

(52) Schrock, R. R.; Kolodziej, R. M.; Liu, A. H.; Davis, W. M.; Vale, M. G. *J. Am. Chem. Soc.* **1990**, *112*, 4338.

(53) Leigh, G. J. *Acc. Chem. Res.* **1992**, *25*, 177.

(54) Leigh, G. J. *J. Mol. Cat.* **1988**, *47*, 363.

(55) Schrock, R. R.; Glassman, T. E.; Vale, M. V.; Kol, M. *J. Am. Chem. Soc.* **1993**, *115*, 1760.

(56) Block, E.; Ofori-Okai, G.; Kang, H.; Zubieta, J. *J. Am. Chem. Soc.* **1992**, *114*, 758.

(57) Glassman, T. E.; Liu, A. H.; Schrock, R. R. *Inorg. Chem.* **1991**, *30*, 4723.

(58) Takahashi, T.; Kodama, T.; Watakabe, A.; Uchida, Y.; Hidai, M. *J. Am. Chem. Soc.* **1983**, *105*, 1680.

(59) Pez, G. P.; Apgar, P.; Crissey, R. K. *J. Am. Chem. Soc.* **1982**, *104*, 482.

(60) Jonas, K.; Brauer, D. J.; Kruger, C.; Roberts, P. J.; Tsay, Y. H. *J. Am. Chem. Soc.* **1976**, *98*, 74.

(61) Jonas, K. *Angew. Chem., Int. Ed. Engl.* **1973**, *12*, 997.

(62) Hammer, R.; Klein, H. F.; Friedrich, P.; Huttner, G. *Angew. Chem., Int. Ed. Engl.* **1977**, *16*, 485.

(63) Greenwood, N. N.; Earnshaw, A. *Chemistry of The Elements;* 1st edition ed.; Pergamon Press: Oxford, 1986, pp 318.

(64) Jerrery, J.; Lappert, M. F.; Riley, P. I. *J. Organomet. Chem.* **1979**, *181*, 25.

(65) Gyane, M. J. S.; Jeffery, J.; Lappert, M. F. *J. Chem. Soc., Chem. Commun.* **1978**, 34.

(66) Dengel, A. C.; Griffith, W. P.; O'Mahoney, C. A.; Williams, D. J. *J. Chem. Soc., Chem. Commun.* **1989**, 1720.

(67) Ozin, G. A.; Voet, A. V. *Can. J. Chem.* **1973**, *51*, 637.

(68) Ho, J.; Drake, R. J.; Stephan, D. W. *J. Am. Chem. Soc.* **1993**, *115*, 3792.

(69) Evans, W. J.; Ulibarri, T. A.; Ziller, J. W. *J. Am. Chem. Soc.* **1988**, *110*, 6877.

(70) Duchateau, R.; Gambarotta, S.; Bensimon, C. *J. Am. Chem. Soc.* **1991**, *113*, 8986.

(71) Allen, F. H.; Kennard, O.; Watson, D. G.; Brammer, L.; Orpen, A. G.; Taylor, R. *J. Chem. Soc., Perkin Trans.* **1987**, *II*, S1.

(72) Rehder, D.; Woitha, C; Priebsch, W; Gailus, H. *J. Chem. Soc., Chem. Commun.* **1992**, 365.

(73) Pickett, C. J; Ryder, K. S; Talarmin, J. *J. Chem. Soc., Dalton Trans.* **1986**, 1453.

Chapter 2

Dinitrogen Complexes of Zirconium

2.1 General

One of the on going research interests of our group involves the synthesis of transition metal complexes containing the tridentate ligand $[N(SiMe_2CH_2PR_2)_2]^{-1}$, abbreviated as PNP. This hybrid ligand was designed with a central amide unit flanked by two identical arms containing phosphine donors.[1-5] The incorporation of mismatched donor groups, i.e., the hard amide and the soft phosphine donors, has enabled the successful coordination of this ligand to hard, early and soft, late transition metals.[6,7] The formation of two fused five-membered chelate rings has also been shown to favour the complexation of this ligand.

As a formal six electron donor the PNP ligand is somewhat comparable to the isoelectronic Cp ligand. However, in certain instances, due to the availability of lone pair electrons on the nitrogen, PNP could donate a maximum of eight electrons, which would be manifested by shorter than usual metal-amide bond distances.[8] Also, in some late transition metal complexes the nitrogen lone pair has played an important role as an intramolecular Lewis base (e.g., Ir(2-propenyl)($AlMe_2$)-$[N(SiMe_2CH_2PPh_2)_2]$) and as a proton acceptor (e.g., $IrHMeBr[NH(SiMe_2CH_2PPh_2)_2]$).[9,10] The tridentate ligand usually exhibits meridional coordination, but occasionally facial coordination has been observed in the solid (e.g., $ZrCl_3[N(SiMe_2CH_2PMe_2)_2]$)[11] and in the solution (e.g., $IrH(\eta^3\text{-}C_3H_5)[N(SiMe_2CH_2PPh_2)_2]$)[12,13] states. Also, the ligand could influence the reactivity at the metal center by changing the coordination from tridentate to bidentate, or even monodentate, a process that could be compared to the ring slippage of the Cp ligand from η^5 to η^3 to η^1. The $^{31}P\{^1H\}$ NMR spectra of PNP derivatives are useful in assigning structures of these molecules and to monitor the reaction progress. The steric bulk of PNP can be readily altered by changing the size of the substituents on the phosphine donors, for example, the Me, Ph Pr^i and Bu^t derivatives are all available.

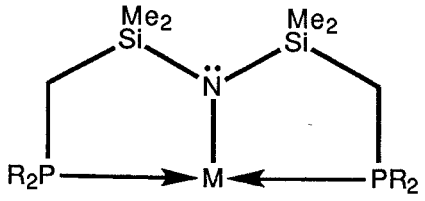

PNP

R = Me, Ph, Pr^i, Bu^t

M = metal ion

references on page 119

Investigations involving PNP as an ancillary ligand on zirconium led to the discovery of carbon-carbon bond formation between butadiene and allylic fragments.[14] Also some zirconium complexes have shown fluxional behavior (e.g., $Zr(\eta^4\text{-}C_4H_6)Cl[N(SiMe_2CH_2PPr^i_2)_2]$) and intriguing coordination geometries such as a bicapped tetrahedron (e.g., $ZrMe_3[N(SiMe_2CH_2\text{-}PMe_2)_2]$).[15,16]

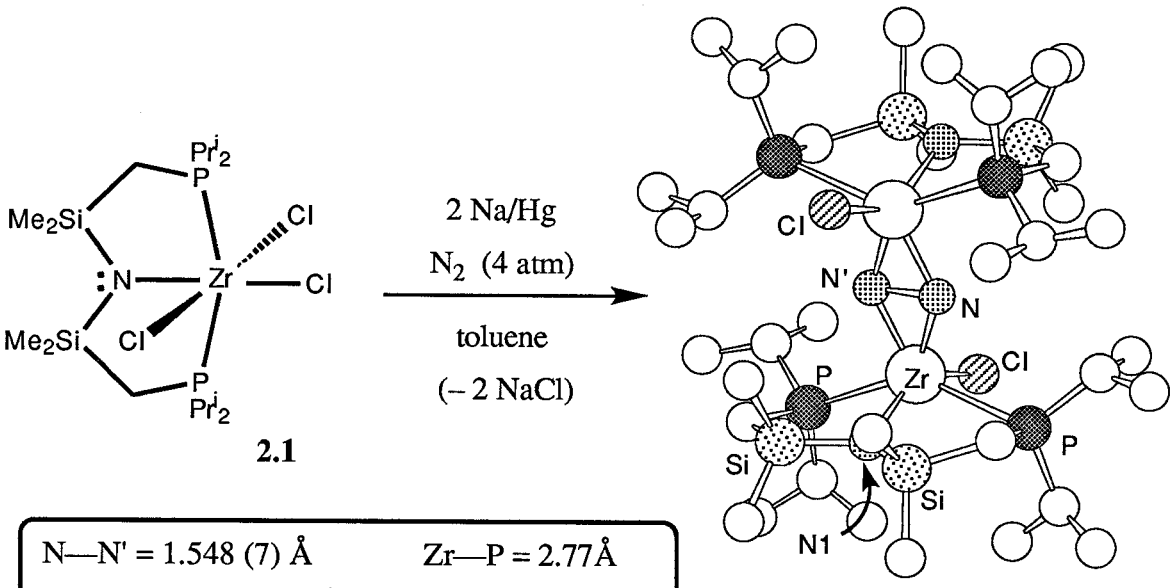

Scheme 2.1

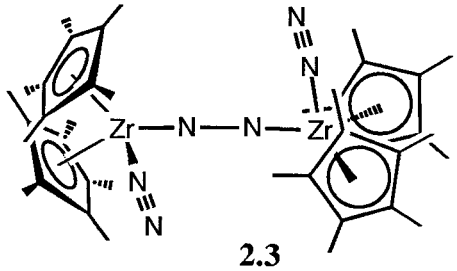

Bridging N_2 = 1.182Å
Terminal N_2 = 1.12Å

Investigations on the reduction of $ZrCl_3[N(SiMe_2CH_2PPr^i_2)_2]$ **2.1**, under a dinitrogen atmosphere gave rise to a deep blue complex. Structural analysis of the blue complex **2.2**, revealed it to be a dinuclear derivative containing a bridging side-on bound dinitrogen ligand (Scheme **2.1**).[8] The observed nitrogen-nitrogen bond distance of 1.548(7) Å in **2.2** was significantly longer than that observed for a nitrogen-nitrogen single bond; for example in hydrazine the nitrogen-nitrogen bond length is 1.46 Å.[17] Prior to this work there was only one other structurally characterized zirconium dinitrogen complex [(η^5-

references on page 119

$C_5Me_5)_2ZrN_2]_2$-(μ-η^1:η^1-N_2) **2.3**.[18-21] The dinuclear complex **2.3** has three dinitrogen ligands, two terminal and one bridging, and the bridging dinitrogen ligand has a nitrogen-nitrogen bond length of 1.182 Å, considerably shorter than that found in **2.2**.

To elaborate on the chemistry of side-on dinitrogen complexes similar to **2.2** we investigated the synthesis of other dinitrogen complexes of zirconium incorporating the PNP ligand. We were particularly interested in substituting the chloride ligand of **2.2** with other substituents such as Cp, alkoxide, etc. This chapter describes the synthesis of a series of dinitrogen complexes and aspects of their bonding. The mode of dinitrogen bonding in the solid versus the solution states was of interest along with some aspects of reactivity.

2.2 Synthesis of a Dinitrogen Complex Containing PNP and Cp Ligands

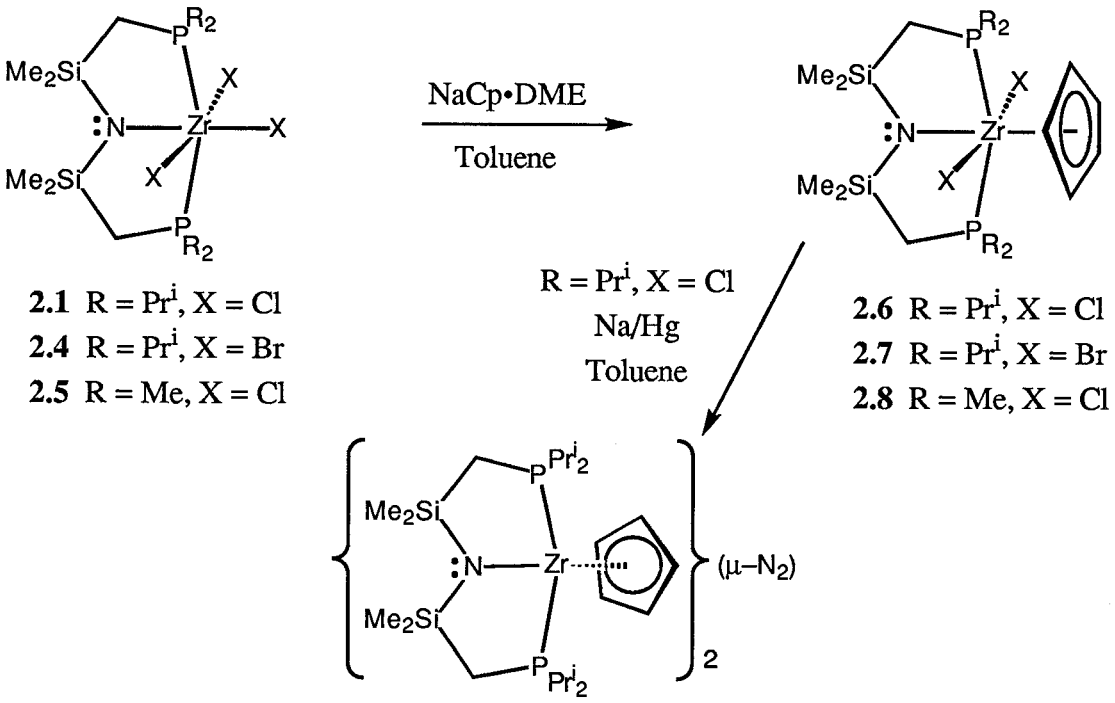

2.1 R = Pr^i, X = Cl
2.4 R = Pr^i, X = Br
2.5 R = Me, X = Cl

2.6 R = Pr^i, X = Cl
2.7 R = Pr^i, X = Br
2.8 R = Me, X = Cl

2.9

Scheme 2.2

Initial attempts to metathesize the zirconium-chloride bonds of the side-on dinitrogen complex **2.2** with alkyl lithium or sodium aryl oxides resulted in decomposition to unidentified products. Also the synthesis of **2.2** involves a tedious workup procedure, where optimum

references on page 119

conditions give only 40% yields. Therefore a two step reaction sequence starting with complex **2.1** was developed as shown in Scheme **2.2**. Selective metathesis of a single zirconium halide bond of the trihalo precursor and subsequent reduction did enable the synthesis of a new dinitrogen complex.

2.2.1 Synthesis of Precursors of the Type $ZrCpX_2[N(SiMe_2CH_2PR_2)_2]$

Synthesis of $ZrCpCl_2[N(SiMe_2CH_2PPr^i_2)_2]$ **2.6**, was readily achieved by reacting one equivalent of solid NaCp•DME with a toluene solution of $ZrCl_3[N(SiMe_2CH_2PPr^i_2)_2]$, **2.1**. After recrystallization, pure hexagonal shaped crystalline material was obtained in excellent yields (> 75%). The related complexes **2.7** and **2.8** were also synthesized via a similar reactions. A single resonance for the $SiMe_2$ moieties in the ^1H NMR spectrum and a single resonance in the $^{31}P\{^1H\}$ NMR spectrum suggest a symmetric structure for the complex **2.6** in solution.* The protons of the Cp ligand appear as a triplet, due to the coupling of two equivalent phosphines. These spectroscopic data are consistent with a C_{2v} structure for complex **2.6** in solution, i.e., assuming free rotation of the Cp ligand about the 119
axis defined by the zirconium and the centroid of the Cp (Scheme **2.2**). The principal C_2 axis coincides with the axis defined by the centroid of the Cp, the zirconium and the nitrogen, and the zirconium lies in a pseudo-octahedral environment. No evidence of fluxionality was observed in the ^1H NMR spectrum when a sample of **2.6** was cooled to -90 °C. This could imply that the Cp ligand is coordinated in an η^5 fashion in solution. The solution spectroscopic data obtained for the analogous complexes **2.7** and **2.8** also suggest geometries similar to complex **2.6**.

Figure **2.1** shows the X-ray structure of complex $ZrCpBr_2[N(SiMe_2CH_2PPr^i_2)_2]$, **2.7**. The Cp ligand is found to be trans to the amide linkage, and the nitrogen, zirconium and the centroid of the Cp are arranged almost linearly (Table **2.1**). The two phosphorus atoms and the two bromide atoms are slightly bent away from the Cp ligand. Assuming that in solution the Cp

* In the ^1H NMR spectrum of complexes containing PNP the resonances due to $Si(CH_3)_2$ group appear between 0.00 ppm and 0.75 ppm. The number of resonances observed for the $Si(CH_3)_2$ moieties, in conjunction with the $^{31}P\{^1H\}$ NMR spectrum enable us to predict the geometry of the molecule with reasonable accuracy.

references on page 119

ligand is undergoing rapid rotation about the zirconium centroid axis the overall geometry of the molecule in solid state agrees with the geometry inferred from solution spectroscopic data. The structure also shows the η^5 coordination of the Cp ligand.

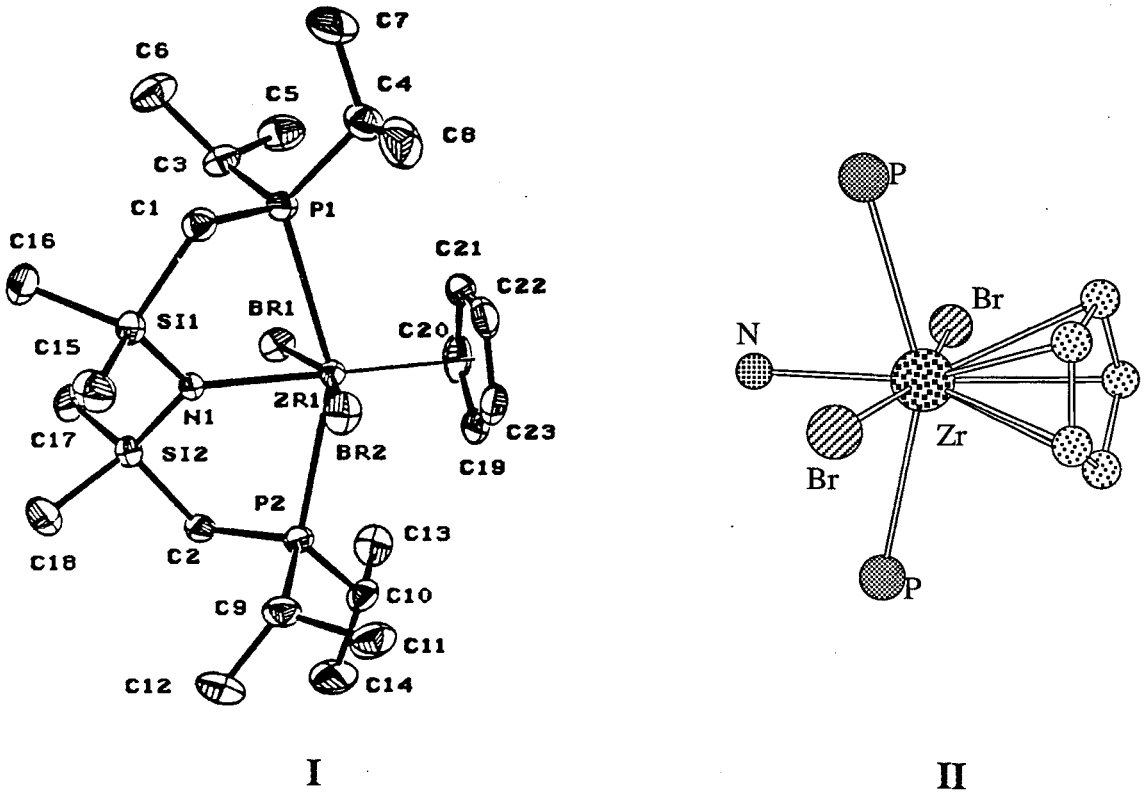

I **II**

Figure 2.1 **I** ORTEP view showing the complete atom labeling scheme of the complex $ZrCpBr_2[N(SiMe_2CH_2PPr^i_2)_2]$, **2.7**. **II** A Chem 3D® view showing the pseudo octahedral geometry at the zirconium.

The bond lengths (Table **2.1**) and bond angle (Table **2.2**) parameters associated with the "$Zr[N(SiMe_2CH_2PPr^i_2)_2]$" unit are similar to other structurally known complexes of zirconium(IV) with the PNP ligand.[11] The distance from zirconium to the centroid of the Cp, 2.286(2) Å is comparable to the distances observed for the bis(cyclopentadienyl) derivatives (e. g Cp_2ZrI_2, 2.20 Å)[22] and the monocyclopentadienyl derivatives (e.g. $[CpZrCl_3]_n$, 2.196 Å)[23].[24]

references on page 119

Table 2.1 Selected bond distances of complex **2.7** $ZrCpBr_2[N(SiMe_2CH_2PPr^i_2)_2]$.

atom	atom	distance (Å)	atom	atom	distance (Å)
Zr	Cp	2.286(2)	Zr	Br(1)	2.6871(7)
Zr	P(1)	2.817(1)	Zr	Br(2)	2.6842 (7)
Zr	P(2)	2.821(1)	Zr	C(average)	2.57
Zr	N	2.227(2)	N	Si(average)	1.736

Table 2.2 Selected bond angles of complex **2.7** $ZrCpBr_2[N(SiMe_2CH_2PPr^i_2)_2]$.

atom	atom	atom	angle (°)	atom	atom	atom	angle (°)
P(1)	Zr	P(2)	152.82(4)	P(1)	Zr	Cp	103.02(7)
Cp	Zr	N	179.2(1)	P(2)	Zr	Cp	104.16(7)
Br(1)	Zr	Br(2)	162.95(2)	P(1)	Zr	N	76.18(9)
P(1)	Zr	Br(1)	90.31(3)	P(2)	Zr	N	76.65(9)
P(1)	Zr	Br(2)	86.00(3)	Cp	Zr	Br(1)	99.02(7)
P(2)	Zr	Br(1)	85.08(3)	Cp	Zr	Br(2)	98.03(6)
P(2)	Zr	Br(2)	90.62(3)	N	Zr	Br(1)	81.50(8)

Much of what is known about the reactivity of organometallic complexes of zirconium arises from the work done on dihalo zirconocene derivatives, Cp'_2ZrX_2 (Cp' = any ligand containing a cyclopentadienyl unit, X = halide).[25-36] Because complexes **2.6**, **2.7** and **2.8** can be considered as isoelectronic to Cp'_2ZrX_2 useful comparisons are possible. An important difference in their physical properties is that the PNP derivatives are soluble in aliphatic

references on page 119

hydrocarbon solvents, whereas the zirconocene derivatives are usually soluble only in polar solvents.

Preliminary studies involving PNP derivatives and aluminoxanes have shown catalytic activity towards the polymerization of ethylene.[37] It is well established that zirconocene derivatives also function as excellent catalysts under similar conditions. Stereo-regular polymerization involving chiral zirconocene derivatives[38,39] could also be extended to the PNP systems by incorporating chiral cyclopentadienyl ligands or by using chiral phosphine donors.[40]

Reactions mediated by Cp'_2ZrX_2 complexes take place at adjacent sites, i.e., the sites occupied by the halide atoms. From a mechanistic viewpoint, the availability of adjacent reactive sites has been conducive to the successful utilization of these complexes (e.g., reductive elimination, α-H abstraction), particularly in their applications to organic synthesis.[25-36] In the case of PNP derivatives, the reactive sites, i.e., the sites occupied by the halides, are trans related. Therefore, for these sites to become involved in a mutual manner they have to be brought closer, either by the rearrangement of the PNP to a facial type coordination or by the dissociation of one of the phosphine donors.

2.2.2 Reduction of Complexes of the Type $ZrCpX_2[N(SiMe_2CH_2PR_2)_2]$

A toluene solution of complex $ZrCpCl_2[N(SiMe_2CH_2PPr^i_2)_2]$ **2.6**, was reduced with Na/Hg under 4 atmospheres of dinitrogen. The yellow color of the reaction mixture rapidly disappears to give a deep green solution which turns deep brown within a few days. The intermediate responsible for the green colour was also formed in the absence of dinitrogen (under an argon atmosphere) implying that it does not contain a dinitrogen ligand. A deep brown crystalline material was isolated from the brown solution which was formulated as a dinuclear dinitrogen complex (Scheme **2.2**) on the basis of spectroscopic and micro analytical data.

references on page 119

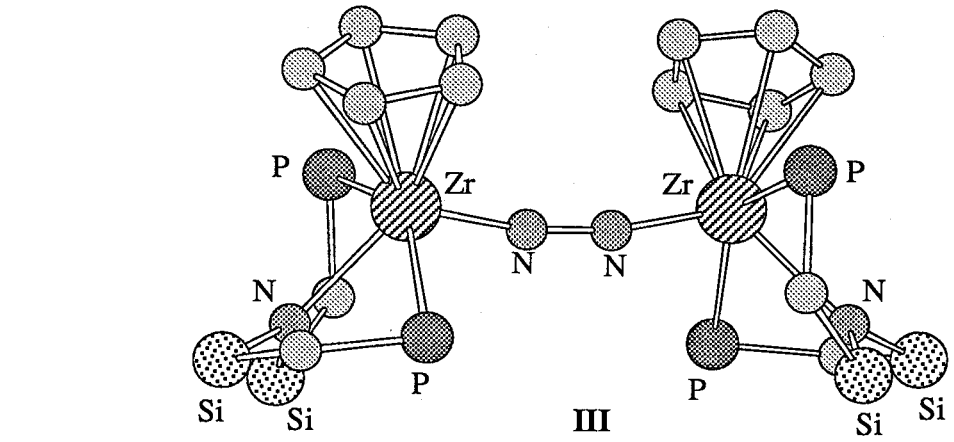

III

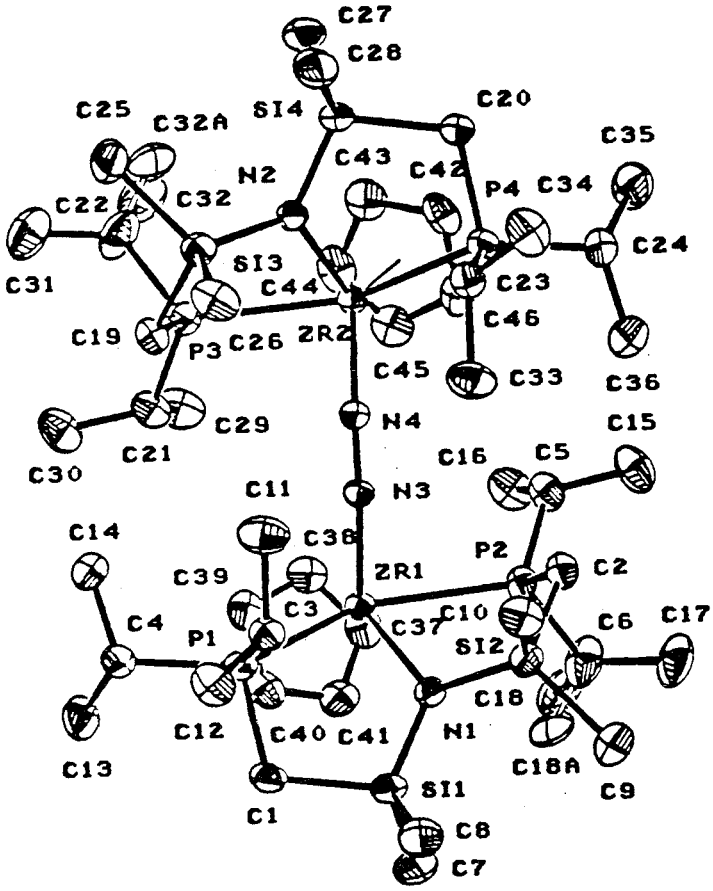

I

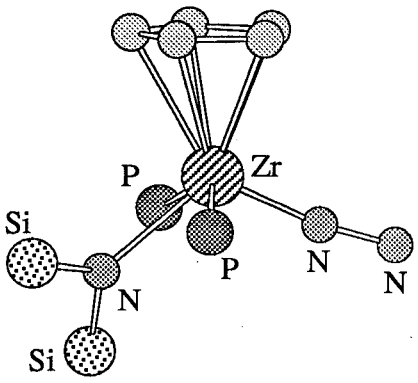

II

Figure 2.2 **I** ORTEP view showing the complete atom labeling scheme of complex $\{[(Pr^i_2PCH_2SiMe_2)_2N]Zr(\eta^5\text{-}C_5H_5)\}_2(\mu\text{-}\eta^1\text{:}\eta^1\text{-}N_2)$, **2.9**. **II** A Chem 3D® view of the arrangement of atoms around the zirconium centre. **II** A Chem 3D® view showing the arrangement of the PNP ligand and the Zr_2N_2 core.

references on page 119

The X-ray structure of the dinitrogen complex $\{[(Pr^i_2PCH_2SiMe_2)_2N]Zr(\eta^5\text{-}C_5H_5)\}_2\text{-}(\mu\text{-}\eta^1\text{:}\eta^1\text{-}N_2)$ **2.9**, is depicted in Figure **2.2**. The solid state structure unequivocally shows that the dinitrogen ligand is bound in an end-on fashion bridging two zirconium centres. The observed nitrogen-nitrogen bond distance of 1.301(3) Å (Table **2.3**) is significantly shorter in comparison to the similar distance of 1.548(7) Å in the side-on derivative **2.2**, but longer than (by 0.1 Å) the end-on derivative **2.3**, which is the only other zirconium complex with an end-on bound dinitrogen ligand that has been structurally characterized. When a comparison is made with end-on complexes in general where the nitrogen-nitrogen bond lengths range from 1.1 Å to 1.3 Å, the nitrogen-nitrogen distance in **2.9** falls in the upper limit (Chapter **1**, section **1.5.2**). Also, in complex **2.9** the zirconium-nitrogen distances associated with the dinitrogen ligand are approximately 0.1 Å shorter as compared to the side-on complex **2.2** or to the similar distance in complex **2.3***.[21] The dinitrogen ligand in **2.9** is slightly offset from the zirconium-zirconium axis, having a Zr–N–N angle of 170°.

Table 2.3 Selected bond distances of complex **2.9** $\{[(Pr^i_2PCH_2SiMe_2)_2N]Zr(\eta^5\text{-}C_5H_5)\}_2(\mu\text{-}\eta^1\text{:}\eta^1\text{-}N_2)$.

atom	atom	distance (Å)	atom	atom	distance (Å)
Zr(1)	Cp(1)	2.294 (2)	Zr(2)	Cp(2)	2.286 (2)
Zr(1)	P(1)	2.816 (1)	Zr(2)	P(3)	2.778 (1)
Zr(1)	P(2)	2.776 (1)	Zr(2)	P(4)	2.828 (1)
Zr(1)	N(1)	2.306 (3)	Zr(2)	N(2)	2.303 (3)
Zr(1)	N(3)	1.920 (3)	Zr(2)	N(4)	1.923 (3)
N(3)	N(4)	1.301 (3)	Zr	C(average)	2.58

* In complex **2.3** the zirconium-nitrogen bond distances for the bridging dinitrogen ligand are 2.087 (3) Å and 2.075 (3) Å, and for the terminal dinitrogen ligands is 2.188 (4) Å.

references on page 119

Table 2.4 Selected bond angles of the complex **2.9** $\{[(Pr^i_2PCH_2SiMe_2)_2N]Zr(\eta^5\text{-}C_5H_5)\}_2(\mu\text{-}\eta^1\text{:}\eta^1\text{-}N_2)$

atom	atom	atom	angle (°)	atom	atom	atom	angle (°)
P(1)	Zr(1)	P(2)	145.87 (4)	P(3)	Zr(2)	P(4)	145.65 (3)
N(1)	Zr(1)	N(3)	115.1 (1)	N(2)	Zr(2)	N(4)	115.3 (1)
N(1)	Zr(1)	Cp(1)	127.61 (9)	N(2)	Zr(2)	Cp(2)	127.49 (9)
N(3)	Zr(1)	Cp(1)	117.2 (1)	N(4)	Zr(2)	Cp(2)	117.1(1)
P(1)	Zr(1)	N(1)	71.74 (8)	P(3)	Zr(2)	N(2)	75.37 (7)
P(1)	Zr(1)	N(3)	98.92 (8)	P(3)	Zr(2)	N(4)	86.10 (8)
P(1)	Zr(1)	Cp(1)	102.89 (6)	P(3)	Zr(2)	Cp(2)	104.84 (6)
P(2)	Zr(1)	N(1)	75.66 (8)	P(4)	Zr(2)	N(2)	71.53 (8)
P(2)	Zr(1)	N(3)	85.76 (8)	P(4)	Zr(2)	N(4)	99.76 (8)
P(2)	Zr(1)	Cp(1)	104.84 (6)	P(4)	Zr(2)	Cp(2)	102.41 (6)
Zr(1)	N(3)	N(4)	170.6 (2)	Zr(2)	N(4)	N(3)	170.1 (2)

A comparison of the arrangement of the PNP ligand in complexes **2.2** and **2.9** shows that in the end-on case it is significantly twisted where as in the side-on case it is almost planar, reflecting the increased steric crowding around each metal centre in the end-on derivative. Also, the bond distances associated with the zirconium-amide bonds are approximately 0.1 Å longer than those observed in complex **2.2**. In fact, the zirconium-amide bond distances in **2.9** are the longest of any zirconium-nitrogen distances that have been measured for PNP coordinated to zirconium,[8,11] and are just slightly shorter than the distances of 2.443(1) Å and 2.412(2) Å found in neutral amine type adducts of zirconium(IV).[41,42] The zirconium-Cp bond distances of complexes **2.6** and **2.9** are identical. Analysis of the bond angles (Table **2.4**) around each

references on page 119

zirconium of **2.9** suggests an approximate trigonal bipyramidal geometry, with the phosphines occupying the apical positions, slightly bent away from the Cp ligand.

The ^1H NMR spectrum of **2.9** has only one resonance associated with the Cp ligand and two resonances associated with the $SiMe_2$ moieties; the $^{31}P\{^1H\}$ NMR spectrum consists of a single resonance at room temperature. These spectroscopic data suggest that complex **2.9** adopts a more symmetric structure (C_{2v}) in solution than that observed in the solid state (C_2). Variable temperature NMR spectroscopic studies with complex **2.9** show fluxionality. The variable temperature $^{31}P\{^1H\}$ NMR spectra show broadening and decoalescing of the singlet resonance which below -40 °C separates into an AB quartet ($^2J_{P\text{-}P}$ = 80 Hz). In the ^1H NMR spectra the two resonances associated with the $SiMe_2$ groups give rise to four peaks at low temperature. These low temperature spectroscopic data are consistent with the structure observed in the solid state. The ^1H and $^{31}P\{^1H\}$ NMR spectra were virtually unchanged through the temperature range from -40 °C to -90 °C, suggesting that phosphine dissociation is not involved in this particular fluctional process. Imagining a fluctional process involving synchronized pivoting of the zirconium-amide bonds with respect to the Zr_2N_2 core would render the two phosphines equivalent (Scheme **2.3**).

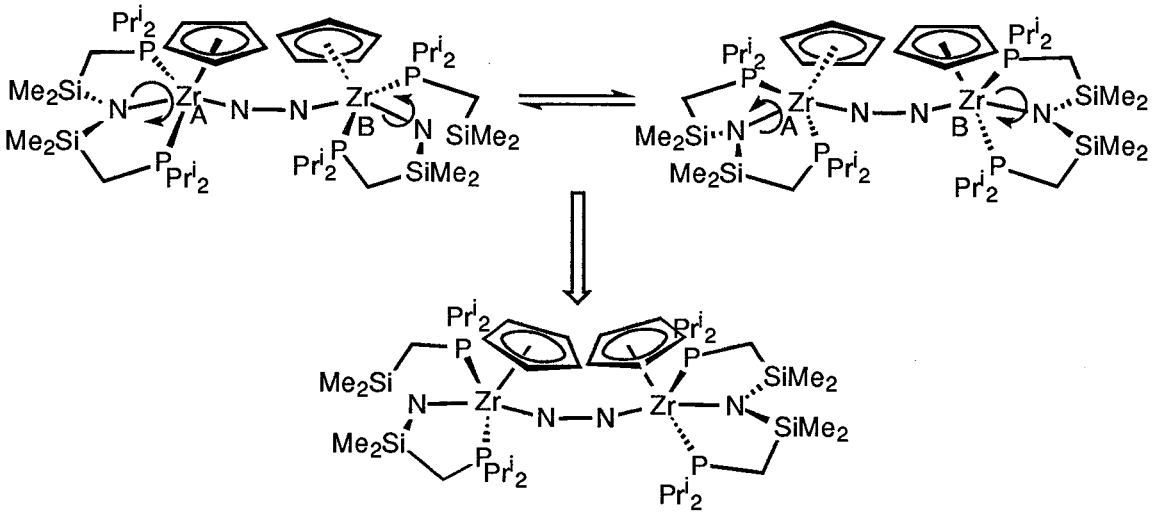

Scheme 2.3

references on page 119

The replacement of a chloride ligand of the side-on dinitrogen complex **2.2** by a Cp would dramatically increase the steric interactions between the two zirconium centres. By this rationale, substituting the chloride ligands of **2.2** with Cp ligands would favor the formation of the end-on complex over the side-on complex. In the side-on complex **2.2** the two metal atoms are separated by 3.7 Å which is significantly closer than the comparable distance of 5.1 Å in the end-on complex **2.9**. The important difference in the electronic properties of the two complexes is that the Cp ligand in **2.9** is bonded to the metal by a σ and two π-bonds whereas in **2.2** the Cl ligand is mainly bonded via a σ-bond. These interactions will significantly alter the type of orbitals available for dinitrogen bonding. Considering electron donor properties, the Cp ligand is likely to make the metal more electron rich. Although this would increase metal to dinitrogen backbonding interactions it is difficult to predict how this would influence the mode of dinitrogen bonding.

2.3 Attempted Synthesis of a Dinitrogen Complex Containing PNP and Allyl ligands

Considering the discussion presented in Section **2.2**, replacing the chloride ligand of the dinitrogen complex **2.2** with an allyl ligand would be a suitable extension of our investigation. Sterically, an allyl ligand is less bulky than a Cp ligand. Electronically, it donates less electrons to the metal than a Cp ligand and is bonded to the metal via one σ and one π-bond. Synthesis of the monoallyl derivative was achieved by a metathesis reaction involving 1 equivalent of C_3H_5MgCl and **2.1** (Scheme **2.4**). However, initial attempts to synthesize the allyl derivative using C_3H_5MgBr and **2.1**, gave a mixture of products. Spectroscopic and elemental analysis suggests that the mixture consists of two products, the desired complex $Zr(\eta^3\text{-}C_3H_5)Cl_2\text{-}[N(SiMe_2CH_2PPr^i_2)_2]\}$ **2.10**, and $Zr(\eta^3\text{-}C_3H_5)ClBr[N(SiMe_2CH_2PPr^i_2)_2]$, **2.10a**.

In the ^1H NMR spectrum of **2.10** the $SiMe_2$ moieties gives rise to two resonances and the $^{31}P\{^1H\}$ NMR spectrum consists of a single peak. The syn, anti and central protons of the allylic group appear as three separate resonances in the ^1H NMR spectrum suggesting that the allyl group is rigid within the observed time scale. The $^{31}P\{^1H\}$ NMR spectrum of a

references on page 119

recrystallized sample from the reaction of C_3H_5MgBr and **2.1** consists of a singlet and a set of AB quartets ($^2J_{P-P}$ = 7.9 Hz) corresponding to **2.10** and **2.10a**, respectively. Assuming that **2.10** and **2.10a** are isostructural in solution the $^{31}P\{^1H\}$ NMR data can be explained only if the PNP ligand adopts a facial geometry. The suggested geometry for **2.10**, shown in Scheme **2.4** has C_s symmetry, which intuitively suggests that **2.10a** will be asymmetric. The ^1H NMR data suggests that in **2.10** the symmetry plane containing the central proton of the allylic ligand and bisects the molecule into two chemically equivalent halves.

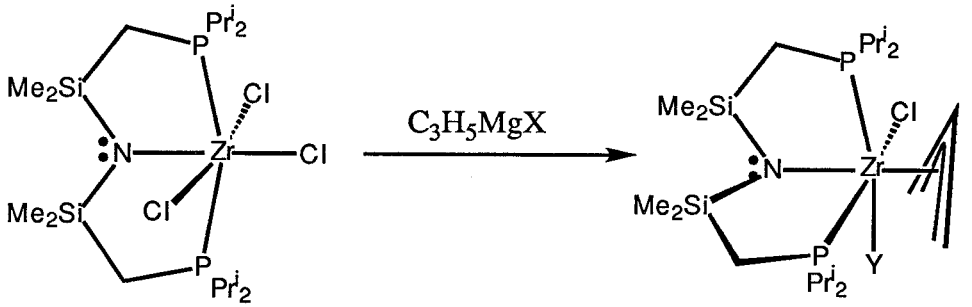

2.1

X = Cl, Y = Cl, **2.10**
X = Br, Y = Br, **2.10a** and Cl, **2.10**

Scheme 2.4

NOEDIFF experiments involving the irradiation of the syn or the anti protons of the allylic ligand resulted in the spin saturation of both the syn and the anti protons and showed enhancement of the resonance due to central proton. Irradiating the central proton resulted in the enhancement of the resonances due to syn and anti protons. This seems to suggest that the allyl ligand undergoes syn anti exchange with a time scale comparable to the duration of radiation during the NOEDIFF experiment.

When a toluene solution of complex **2.10** was reduced with Na/Hg or with Mg under 4 atmospheres of dinitrogen the yellow colour of the reactant rapidly changed to give a green solution. Upon further reaction the green colour slowly changed to give a deep brown solution. Attempts to isolate solid materials from these solutions only resulted in impure oils.

references on page 119

2.4 Synthesis of a Dinitrogen Complex Containing PNP and Aryl Oxide Ligands

After exploring the effects of substituting the Cl ligand of **2.2** with π-type ligands such as Cp and allyl, attention was focused on investigating the preparation of the following monodentate ligands: amide (NPh_2), alkyl (CH_2SiMe_3), alkoxides ($OCHPh_2$ and OBu^t) and aryl oxides (OPh and OAr^* where Ar^* = ($C_6H_3Me_2$-2,6). Of these, OAr^* was the most successful in leading to the synthesis of a dinitrogen complex, hence the chemistry associated with OAr^* ligand will be discussed in detail.

2.4.1 Synthesis of $Zr(OAr^*)Cl_2[N(SiMe_2CH_2PPr^i_2)_2]$

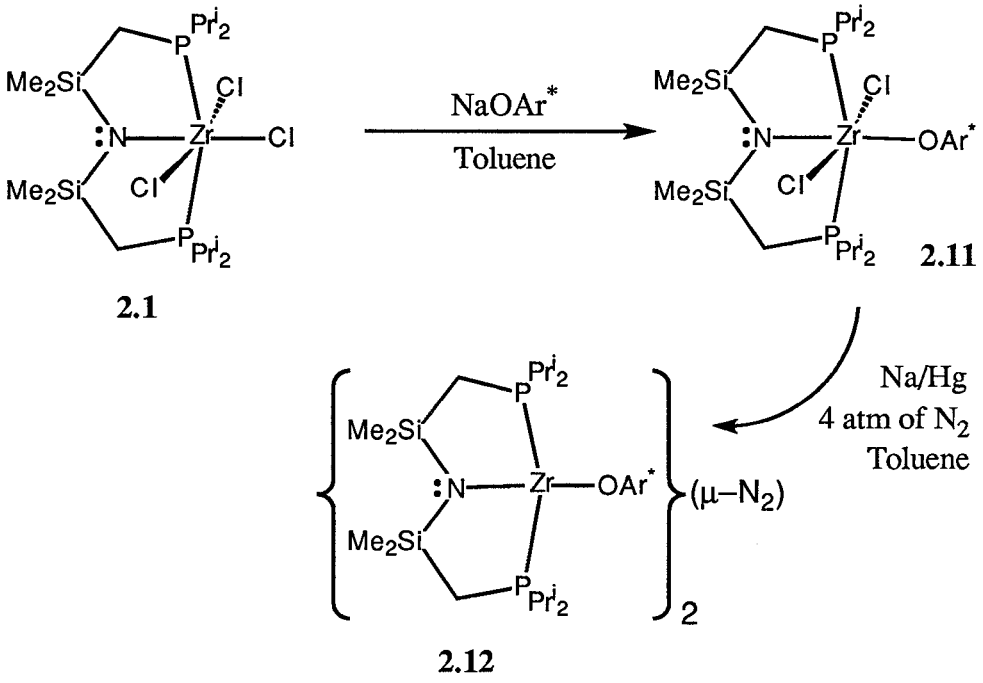

2.1 **2.11** **2.12**

Scheme 2.5

Addition of solid $NaOAr^*$ to a toluene solution of the trichloro starting material **2.1** led to the synthesis of $Zr(OAr^*)Cl_2[N(SiMe_2CH_2PPr^i_2)_2]$, **2.11** in good yields (Scheme **2.5**). It is important that toluene be used as the solvent to obtain high yields of the monoaryloxide complex. During test runs in THF it was found that the reaction yielded a mixture of mono and

references on page 119

bis OAr* substituted products in approximately a 3:1 ratio, respectively. When the reaction was carried out in an NMR tube containing a solvent mixture of THF/C_6D_6 (THF:C_6D_6 = 4:1), the $^{31}P\{^1H\}$ NMR spectrum showed two resonances: one corresponds to unreacted **2.1** and the other to the uncoordinated phosphine of PNP. A sample prepared in C_6D_6 after stripping the THF solvent did not show any resonances due to uncoordinated phosphines. This spectroscopic evidence seems to suggest that soon after the formation of mono OAr* the phosphines become labile in THF solution (Scheme **2.6**). The substitution of bulky phosphine donors by THF ligands is likely to decrease the steric crowding around the metal center, allowing further metathesis reactions. When the reaction was carried out in toluene, after the formation of the mono OAr* derivative the phosphine donors remained coordinated. This makes the metal centre sterically more crowded and therefore the metathesis of the second zirconium-chloride bond is significantly slower.

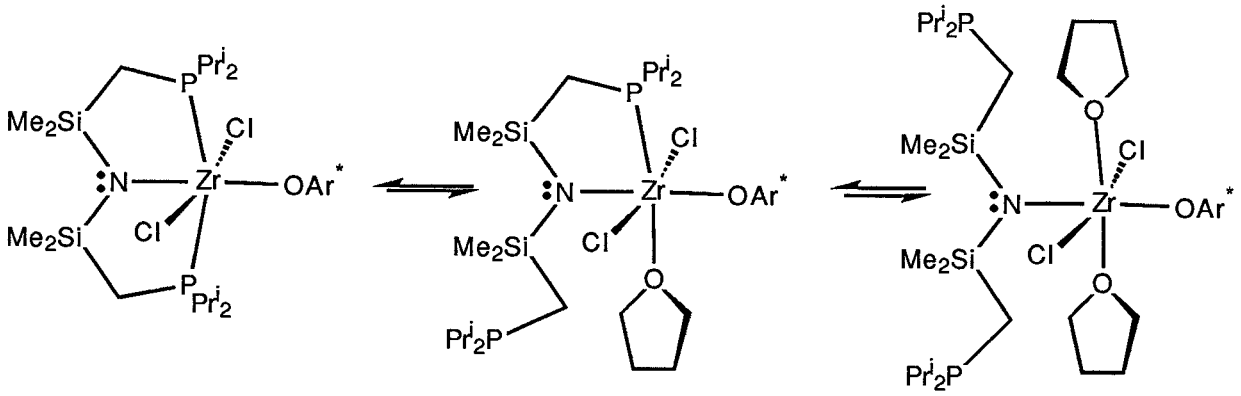

Scheme 2.6

The ^1H and $^{31}P\{^1H\}$ NMR spectra of the monoaryloxide **2.11** show that the complex essentially has the same symmetry (C_{2v}) as complexes **2.1** or **2.6**. As depicted in Scheme **2.5** the molecule adopts an approximately octahedral geometry having trans geometry.

2.4.2 Reduction of $Zr(OAr^*)Cl_2[N(SiMe_2CH_2PPr^i_2)_2]$

During the reduction of **2.11** with Na/Hg under a dinitrogen atmosphere, depending on the purity of the dinitrogen gas, two types of materials were isolated. When the reaction was

references on page 119

carried out under normal dinitrogen (refer to experimental for the purification of dinitrogen) the crude material contained many impurities. The crude material was washed with hexanes and then recrystallized from a toluene solution to give pure material directly. When the reduction was carried out under $^{15}N_2$ gas the crude product had fewer impurities, and washing with hexanes afforded pure material. The spectroscopic analysis ($^{31}P\{^1H\}$ NMR spectroscopy) of the pure material obtained with normal dinitrogen showed the presence of one compound, whereas the product obtained from the $^{15}N_2$ reduction showed the presence of two compounds in approximately 2:1 ratio. In the latter case the chemical shift of the major peak was identical to that obtained under normal dinitrogen. The elemental analysis of both materials gave identical results, and was consistent with the formula $\{[(Pr^i_2PCH_2SiMe_2)_2N]Zr(OAr^*)\}_2(N_2)$, **2.12.**

The above experimental details show that the reduction of **2.11** under dinitrogen gives rise to two isomers of complex **2.12**. The major isomer, **2.12a** has slightly better solubility properties than complex **2.2** whereas the minor isomer **2.12b** dissolves readily in hexanes and toluene. Therefore when reductions were carried out under normal dinitrogen, during workup most of the minor isomer was removed along with the hexane washings.

Single crystals suitable for X-ray analysis were obtained for the major isomer **2.12a**. The solid state structure unequivocally shows that the dinitrogen is bound in a side-on fashion bridging the two zirconium centers (Figure **2.3**). The observed nitrogen-nitrogen bond length of 1.528(7) Å (Table **2.5**) is identical to the other side-on derivative **2.2**, and is significantly longer than the bridging end-on complexes where, as already mentioned, the nitrogen-nitrogen bond lengths range from 1.12 Å to 1.3 Å. A compilation of nitrogen-nitrogen bond lengths, presented in Table **2.6**, provides a comparison with other dinitrogen complexes and also to selected other molecules of interest. The dinitrogen bond lengths in complexes **2.2** and **2.12a** are not only longer than that of free hydrazine but also longer than that found for coordinated hydrazine ligand (N_2H_4), or hydrazido ligand $(NHNH)^{2-}$ (Table **2.6**).

references on page 119

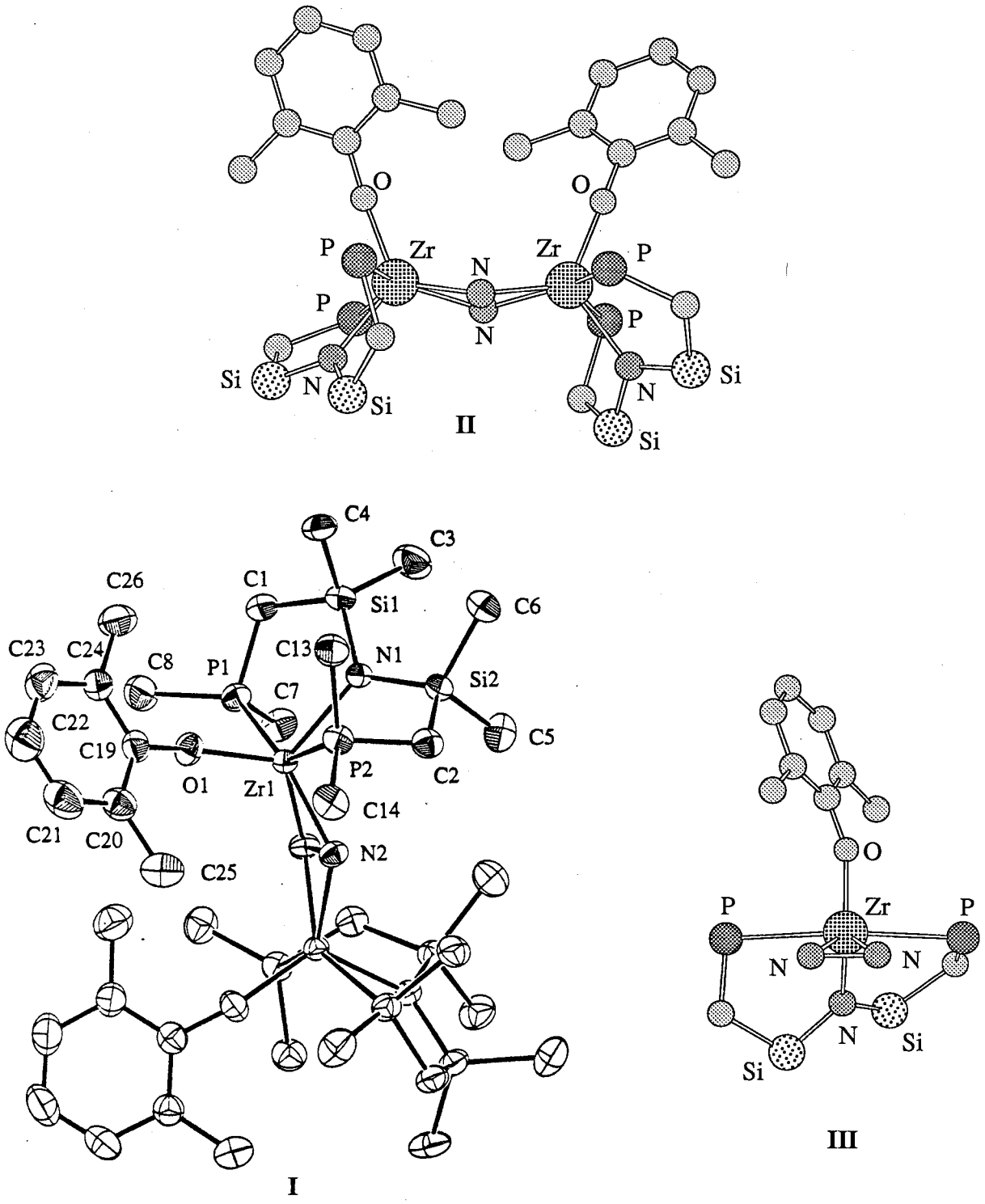

Figure 2.3 **I** ORTEP view showing the complete atom labeling scheme of complex $\{[(Pr^i_2PCH_2SiMe_2)_2N]Zr(OAr^*)\}_2(\mu\text{-}\eta^2\text{:}\eta^2\text{-}N_2)$, **2.12a**. **II** A Chem 3D® view showing the arrangement of the PNP ligand and the Zr_2N_2 core. **III** A Chem 3D® view of the arrangement of atoms around the zirconium centre.

references on page 119

Table 2.5 Selected bond distances of complex **2.12a**, $\{[(Pr^i_2PCH_2SiMe_2)_2N]Zr(OAr^*)\}_2(\mu\text{-}\eta^2\text{:}\eta^2\text{-}N_2)$.

atom	atom	distance (Å)	atom	atom	distance (Å)
Zr(1)	O(1)	2.020 (3)	Zr(1)	N(1)	2.211 (3)
Zr(1)	P(1)	2.818 (1)	Zr(1)	N(2)	2.034 (4)
Zr(1)	P(2)	2.846 (1)	Zr(1)	N(2)'	2.082 (4)
N(2)	N(2)'	1.528 (7)	N(1)	Si(1)	1.718 (4)

Table 2.6 Compilation of nitrogen-nitrogen bond lengths for some selected compounds.

Compound	Bond Length (Å)	ref.
N_2	1.0975 (2)	43
Ph–N=N–Ph	1.255	44
$ON–NO_2$	2.08	69
$O_2N–NO_2$	1.75	69
$H_2N–NH_2$	1.46	17
$\{[(Pr^i_2PCH_2SiMe_2)_2N]Zr(OAr^*)\}_2(\mu\text{-}\eta^2\text{:}\eta^2\text{-}N_2)$ **2.12a**	1.528 (7)	this work
$\{[(Pr^i_2PCH_2SiMe_2)_2N]ZrCl\}_2(\mu\text{-}\eta^2\text{:}\eta^2\text{-}N_2)$ **2.2**	1.548 (7)	8,45
$[Cp^*_2Sm]_2(\mu\text{-}\eta^2\text{:}\eta^2\text{-}N_2)$ **1.12**	1.088 (12)	46
$W(NPh)Me_3]_2(\mu\text{-}\eta^1\text{:}\eta^1NH_2NH_2)(\mu\text{-}\eta^2\text{:}\eta^2NHNH)$		47
$\mu\text{-}\eta^1\text{:}\eta^1NH_2NH_2$	1.434 (14)	
$\mu\text{-}\eta^2\text{:}\eta^2NHNH$	1.391 (15)	
$\{[(Pr^i_2PCH_2SiMe_2)_2N]Zr(\eta^5\text{-}C_5H_5)\}_2(\mu\text{-}N_2)$ **2.9**	1.301 (3)	this work
$\{[(Pr^i_2PCH_2SiMe_2)_2N]TiCl\}_2(\mu\text{-}N_2)$	1.275 (7)	48
$\{[(Pr^i_2PCH_2SiMe_2)_2N]VCl\}_2(\mu\text{-}N_2)$	1.257 (8)	48
$\{(Me_3P)_2(Me_3CCH_2)Ta=CHCMe_3\}_2(\mu\text{-}N_2)$	1.298 (12)	49

references on page 119

The very long nitrogen-nitrogen bond distances of complexes **2.2** and **2.12a** vindicates the discussion presented for the titanium complex with a "$Ti_2(\mu\text{-}\eta^2\text{:}\eta^2\text{-}N_2)_2$" core, **1.14** (Chapter **1**, Section **1.5.7**). In complexes **2.2** and **2.12a** the dinitrogen ligand can have a maximum formal charge of 4-, $(N_2)^{4-}$. However, comparison with end-on complexes where the dinitrogen ligand can be formulated as a $(N_2)^{4-}$ ligand, for example, as found in complexes with nitrogen-nitrogen bond distances closer to 1.3 Å, the side-on complexes of zirconium exhibit extravagant nitrogen-nitrogen bond lengths, in fact they are longer than that found in hydrazine.

A conspicuous difference between the side-on complexes **2.2** and **2.12a** is that the Zr_2N_2 core in **2.12a** is hinged along the nitrogen-nitrogen axis, whereas in the chloro derivative **2.2** it is planar. In complex **2.12a** the triangular planes defined by each zirconium and the nitrogens of the Zr_2N_2 core form an angle of 156.2°, and the orientation of the PNP ligands with respect to the Zr_2N_2 core can be described as syn. Considering the structure of **2.12a** as a whole, the bending of the core perhaps eases any steric interactions that might arise if the core was planar, since with a bent core, PNP ligands are moved away from each other. The calculated zirconium-zirconium separation of 3.7 Å in **2.12a** is identical to that of **2.2**.

The bond distances associated with the phosphine donors and zirconium are comparable to other PNP complexes of zirconium.[8,11,50] The bond lengths from the zirconium to each of the bridging nitrogens Zr-N(2), are 2.034(4) and 2.082(4) Å, and this is shorter than the zirconium-amide bond length, Zr-N(1), 2.211(3) Å of the ancillary ligand, PNP; and are comparable to the same bond parameters of **2.2**. Also the zirconium-amide bond, Zr-N(1), 2.211(3) Å, is significantly shorter than the comparable bond length of the cyclopentadienyl dinitrogen complex **2.9**, which is 2.306 (3)Å. Other zirconium-nitrogen bond distances in the literature range from 1.826(4) Å for a zirconium-nitrogen double bond in $Cp_2Zr{=}NBu^t(THF)$[51] to 2.443(1) Å in Schiff base chelate derivatives.[52]

The zirconium-oxygen bond separation, Zr-O(1) is 2.020(3) Å and the bond angle defined by the atoms Zr, O(1) and C(19) is 161.5(4)° (Table **2.7**). These two interrelated structural features are indicators of metal-oxygen d_π-p_π interactions where larger bond angles and shorter bond lengths are correlated with π-electron donation from the oxygen.[53] By

references on page 119

comparison, parameters associated with the zirconium-oxygen bond for $\{[(Bu^t)_3CO]_2ZrCl_3 \bullet Li(OEt_2)_2\}$[53] are 1.859 Å and 169°; for $[Cp_2Zr(NMe_2)(OC_6H_3Bu^t_2\text{-}2,6)]$[24] they are 2.056(1) Å and 142.7(7)° and for $[(Cp_2ZrMe)_2O]$[54], 1.945 Å and 174.1° are found. In the solid state structure of **2.12a** the OAr* ligand is oriented such that the methyl substituents are directed away from the isopropyl substituents of the phosphine donors.

Table 2.7 Selected bond angles of complex **2.12a**, $\{[(PPr^i_2CH_2SiMe_2)_2N]Zr(OAr^*)\}_2(\mu\text{-}\eta^2\text{:}\eta^2\text{-}N_2)$.

atom	atom	atom	angle	atom	atom	atom	angle
P(1)	Zr(1)	P(2)	145.54 (4)	P(1)	Zr(1)	N(2)	128.10 (10)
N(1)	Zr(1)	N_2	114.9*	P(2)	Zr(1)	N(2)	82.89 (10)
N(1)	Zr(1)	O(1)	123.0 (1)	P(1)	Zr(1)	N(2)'	85.10 (10)
O(1)	Zr(1)	N_2	122.3*	P(2)	Zr(1)	N(2)'	126.19 (10)
O(1)	Zr(1)	N(2)	119.8 (1)	P(1)	Zr(1)	O(1)	87.6 (1)
O(1)	Zr(1)	N(2)'	119.1 (1)	P(2)	Zr(1)	O(1)	88.1 (1)
N(1)	Zr(1)	N(2)	111.4 (1)	P(1)	Zr(1)	N(1)	79.4 (1)
N(1)	Zr(1)	N(2)'	114.7 (1)	P(2)	Zr(1)	N(1)	74.5 (1)
N(2)	Zr(1)	N(2)'	43.6 (2)	Zr(1)	N_2	Zr(1)'	156.2*
P	Zr(1)	N_2	106.4*	Zr(1)	N(2)	N(2)'	69.9 (2)
P	Zr(1)	N_2	104.8*	Zr(1)	N(2)	Zr(1)'	130.7 (2)
Zr(1)	O(1)	C(19)	161.5 (4)				

* These data were measured from a molecule constructed by using the structural data of **2.12a** in a CAChe work station.

The room temperature ^1H NMR spectrum of the major isomer shows two resonances for the $SiMe_2$ moieties and a singlet for the protons of the two ortho methyl groups of OAr*; the $^{31}P\{^1H\}$ NMR spectrum consists of a singlet. An averaged solution structure depicted in **2.12a**

references on page 119

having C_{2v} symmetry accounts for both ^1H and $^{31}P\{^1H\}$ NMR spectral features. The spectroscopic analysis of the sample containing a mixture of both isomers suggests that the minor isomer adopts a less symmetric structure, where the $SiMe_2$ protons give rise to four overlapping signals and the phosphines give rise to two singlet resonances in the ^1H and $^{31}P\{^1H\}$ NMR spectra, respectively. On the basis of the assumption that the minor isomer has the same type of $Zr_2(\mu\text{-}\eta^2\text{:}\eta^2\text{-}N_2)$ core as the major isomer the structure depicted as **2.12b** is proposed, having C_s symmetry. By having the bent Zr_2N_2 core, the ends of the molecule are now different, consistent with the solution spectral data. Considering the arrangement of the ligands with respect to the Zr_2N_2 core, the two isomers can be envisaged as the syn **2.12a** and the anti **2.12b** isomers.

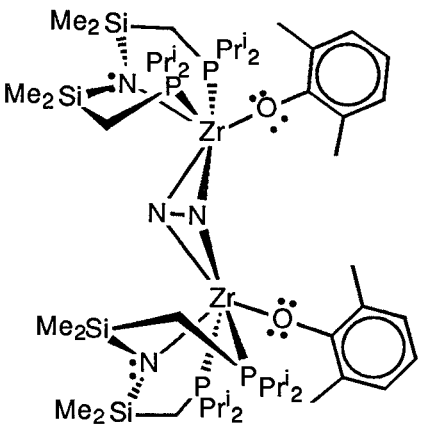

2.12a

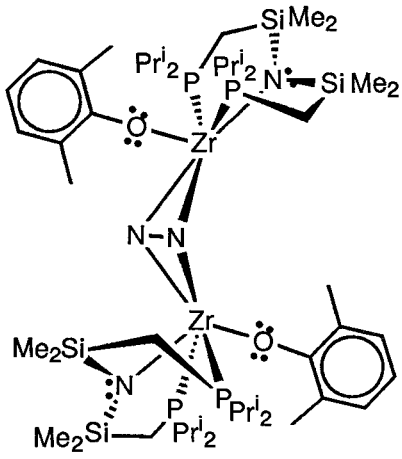

2.12b

A variable temperature $^{31}P\{^1H\}$ NMR analysis of **2.12a** showed an unsymmetrical broadening of the singlet resonance at 8.69 ppm. At temperatures below -70 °C a new resonance began to appear around 4.0 ppm which increased in intensity as the temperature was lowered to -90 °C. Upon cooling, it was expected that the singlet resonance would decoalesce in a symmetric manner to give an AB quartet or two singlets which could be related to the solid state structure of **2.12a**. However, none of the low temperature $^{31}P\{^1H\}$ NMR features correspond to the solid state structure of **2.12a** (Figure **2.4**). Considering the room temperature ^1H NMR spectrum of **2.12a**, the appearance of a singlet due to the methyl protons of OAr^*

references on page 119

group can result from rotation about the oxygen-carbon bond; but the appearance of only two peaks for the $SiMe_2$ units, instead of four as predicted by the solid state structure, would require the rotation of the OAr^* group about the zirconium-oxygen bond, averaging the inequivalent phosphine environments.

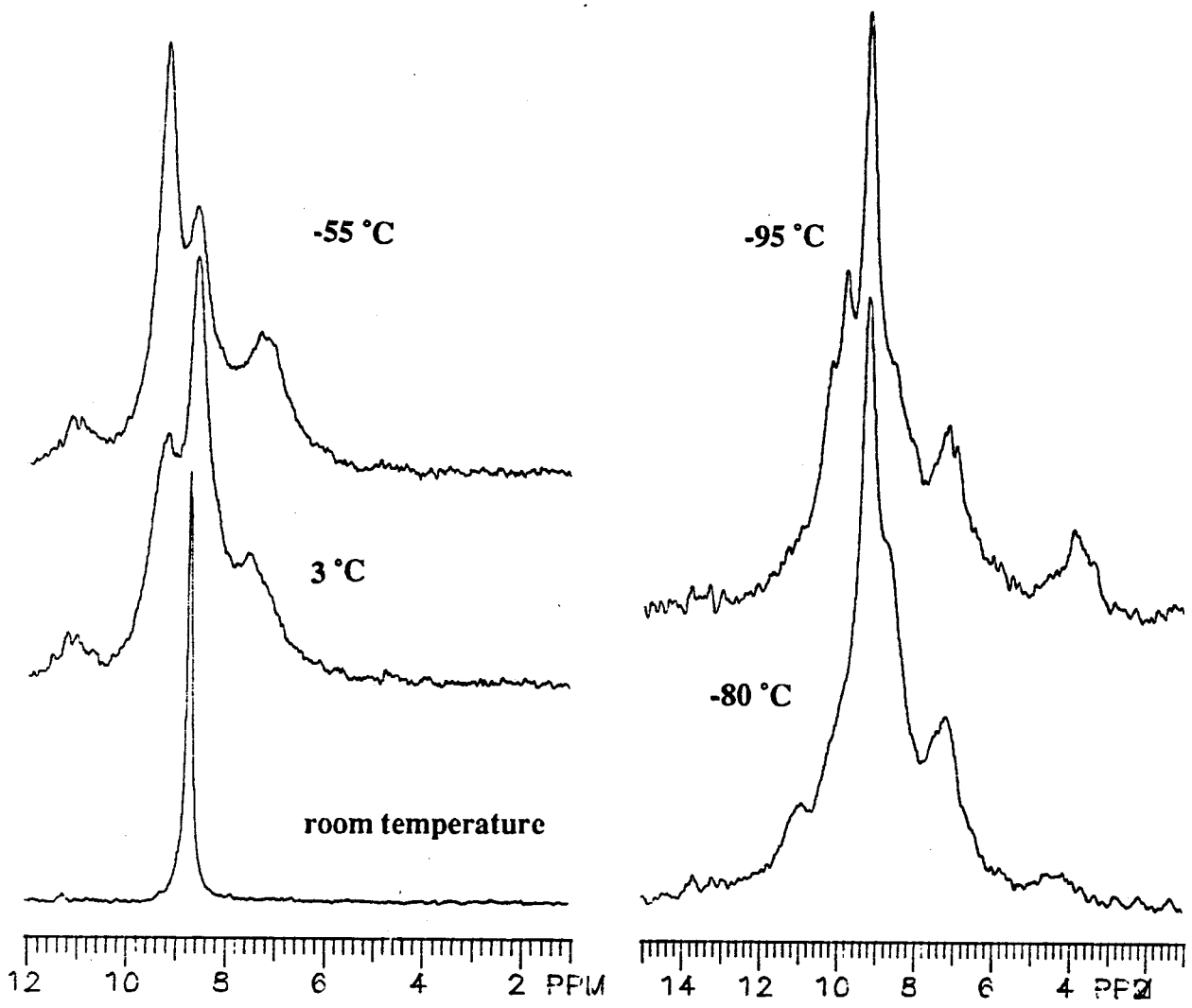

Figure 2.4 Variable temperature 121 MHz $^{31}P\{^1H\}$ NMR spectra of **2.12a** recorded in C_7D_8.

Studies associated with zirconium aryloxide complexes (e.g., $[Cp_2Zr(NMe_2)(OC_6H_3\text{-}2,6\text{-}Bu^t_2)]$) suggest restricted rotation about the zirconium-oxygen bond, where the calculated $\Delta G^{\ddagger}$ values were around 73 kJ mol^{-1}. It is possible that in complex **2.12a** rotation about the zirconium-oxygen bond could be sterically hindered. The complex probably undergoes

references on page 119

reversible dissociation of one of the phosphine arms of PNP during which the OAr* group swings from one end of PNP to the other end. The intermediate observed in the variable temperature $^{31}P\{^{1}H\}$ NMR spectrum may be due to the rapid equilibrium between the two intermediates which have one phosphine arm dissociated (Scheme **2.7**).

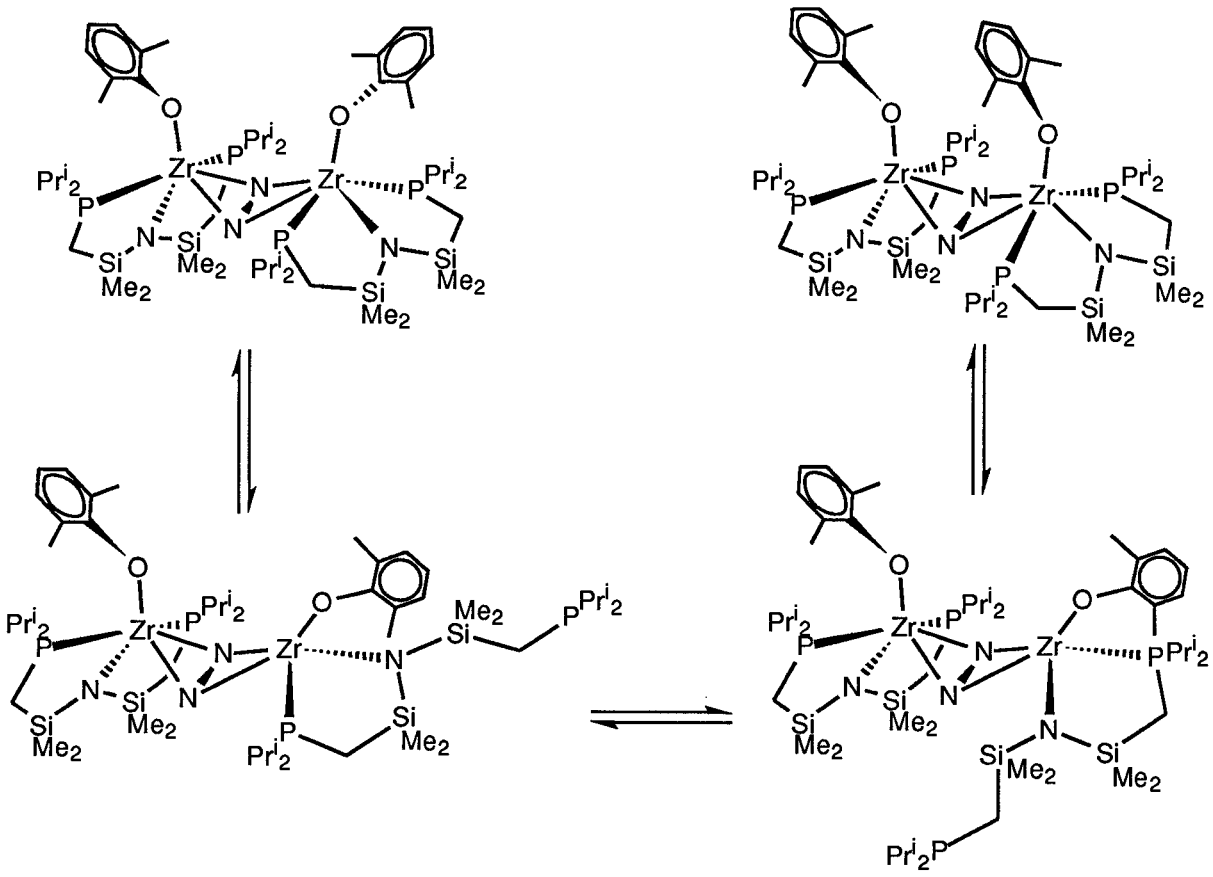

Scheme 2.7

Replacing the chloride of **2.1** with OAr* ligand has not altered the mode of dinitrogen bonding nor the degree of activation. The structural parameters associated with the zirconium-oxygen bond indicate that there is π-bonding between the two atoms, which would make the metal centers of **2.12** more electron rich than the metal centers in the side-on derivative with the chloride ligand **2.2**. The increased steric crowding caused by the replacement of the chloride ligand of **2.2** with OAr* is overcome by the bending of the Zr_2N_2 core. A favorable physical

references on page 119

property attained by the substitution of the chloride ligand with OAr^* is the increased solubility of the minor isomer **2.12b** in hydrocarbon solvents.

2.5 Synthesis of $\{[(Pr^i_2PCH_2SiMe_2)_2N]Zr(OBu^t)\}_2(\mu\text{-}\eta^2\text{:}\eta^2\text{-}N_2)$

Selective metathesis of only one chloride of **2.1** with one tert-butoxide (OBu^t) group to yield the precursor $Zr(OBu^t)Cl_2[N(SiMe_2CH_2PPr^i_2)_2]$ **2.13**, was partially successful. Reactions carried out under different conditions gave oily mixtures of mono and bis substituted complexes which were difficult to separate. The reduction of the crude precursor (containing approx. 80% of the monosubstituted derivative **2.13**) with Na/Hg gave a deep purple solution. The $^{31}P\{^1H\}$ NMR spectrum of the reduced material has a broad peak at 8.16 ppm, which is comparable to other side-on bound dinitrogen complexes **2.2** and **2.12**. Unfortunately the complex **2.14** was extremely soluble in hydrocarbon solvents (pentane) and remains as an impure oil even at -78 °C. This could be partly attributed to the build up of impurities, since the precursor also could not be purified. The ^1H NMR features were similar to the side-on dinitrogen complexes **2.12** having two resonances for the $SiMe_2$ group and a singlet for the OBu^t group.

A compilation of $^{31}P\{^1H\}$ NMR chemical shifts for some zirconium precursors and the dinitrogen complexes derived from them is given in Table **2.8**. The data suggest that the phosphorus-31 chemical shifts for a given precursor will shift to high-field upon formation of a side-on dinitrogen complex and shift to low-field upon the formation of an end-on dinitrogen complex. The zirconium tert-butoxy precursor, having a ^{31}P chemical shift of 11.6 ppm, shifts to a lower field upon its reduction under dinitrogen atmosphere. Therefore, it is presumed that the product is a side-on dinitrogen complex and is formulated as $\{[(Pr^i_2PCH_2SiMe_2)_2N](OBu^t)\text{-}Zr\}_2(\mu\text{-}\eta^2\text{:}\eta^2\text{-}N_2)$, **2.14**. In the absence of other corroborating evidence, however, this proposal is speculative.

The methyl-PNP derivative $Zr(OBu^t)Cl_2[N(SiMe_2CH_2PMe_2)_2]$ **2.15**, can be synthesized and isolated as a pure material. The reduction of this complex under dinitrogen atmosphere was slow and prolonged reaction times afforded many products as detected by $^{31}P\{^1H\}$ NMR spectroscopy. Also, the final reaction mixture was only faintly colored, whereas the reduction

references on page 119

of other precursors that yielded dinitrogen complexes always gave deeply colored solutions. A different alkoxide precursor $Zr(OCHPh_2)Cl_2[N(SiMe_2CH_2PPr^i_2)_2]$ **2.16**, upon reduction (Na/Hg or Mg) gave uncoordinated PNP ligand. The mono amide precursor $Zr(NPh_2)Cl_2[N(SiMe_2CH_2PPr^i_2)_2]$ **2.17**, and the mono alkyl precursor $Zr(CH_2SiMe_3)Cl_2[N(SiMe_2CH_2PPr^i_2)_2]$ **2.18**, gave intractable materials upon reduction.

Table 2.8 Compilation of $^{31}P\{^1H\}$ NMR chemical shifts for some zirconium precursors and the dinitrogen complexes derived from them. In all these complexes PNP corresponds to $[N(SiMe_2CH_2PPr^i_2)_2]$.

Precursors	Chemical Shift (ppm)	Dinitrogen Complexes	Chemical Shift (ppm)
$(PNP)ZrCl_3$	15.4	$[(PNP)ZrCl]_2(\mu\text{-}\eta^2\text{:}\eta^2\text{-}N_2)$	10.0
$(PNP)ZrBr_3$	16.5	$[(PNP)ZrBr]_2(\mu\text{-}\eta^2\text{:}\eta^2\text{-}N_2)$	10.0
$(PNP)Zr(OAr^*)Cl_2$	15.0	$[(PNP)Zr(OAr^*)]_2(\mu\text{-}\eta^2\text{:}\eta^2\text{-}N_2)$	8.7, 8.9 &11.3
$(PNP)Zr(OBu^t)Cl_2$	11.6	$[(PNP)Zr(OBu^t)]_2(\mu\text{-}\eta^2\text{:}\eta^2\text{-}N_2)$	8.2
$(PNP)ZrCpCl_2$	16.1	$[(PNP)ZrCp]_2(\mu\text{-}\eta^1\text{:}\eta^1\text{-}N_2)$	20.3
$(PNP)TiCl_3$	-1.9	$[(PNP)TiCl]_2(\mu\text{-}\eta^1\text{:}\eta^1\text{-}N_2)$	21.2
$(PNP)Ta(=CHBu^t)Cl_2$	37.5	$[(PNP)Ta(=CHBu^t)]_2(\mu\text{-}\eta^1\text{:}\eta^1\text{-}N_2)$	48.8
$(PNP)Ta(=CHPh)Cl_2$	40.1	$[(PNP)Ta(=CHPh)]_2(\mu\text{-}\eta^1\text{:}\eta^1\text{-}N_2)$	51.1

2.6 Spectroscopy as a Diagnostic Tool for End-On and Side-On Dinitrogen Complexes

Although X-ray structure determination of dinitrogen complexes will unequivocally show the mode of dinitrogen binding in the solid state, it does not necessarily relate to the mode of dinitrogen binding in the solution state. Also, X-ray analysis inevitably requires the isolation of single crystals which ultimately relies on serendipity. Therefore, any spectroscopic technique that could differentiate between these two modes of bonding would not only help in the assignment of dinitrogen bonding in complexes that are difficult to crystallize but would also

references on page 119

enable one to ascertain the mode of dinitrogen bonding both in the solid and the solution states. We were particularly interested in discerning the mode of dinitrogen bonding in the side-on complex **2.2** in the solution state.

2.6.1 ^{15}N NMR Spectroscopy

The nitrogen-15 analogues of complexes **2.2**, **2.9** and **2.12** were prepared by introducing $^{15}N_2$ gas during the reductions of the corresponding precursors. Originally, we had hoped that the measurement of the nitrogen-15 chemical shifts[55] would provide a diagnostic handle on the mode of binding in these derivatives, that is, side-on bridging versus end-on bridging. However, as is evident from the chemical shifts compiled in Table **2.9**, there is no obvious correlation between the two modes of coordination. For example, the chemical shift of the side-on complex **2.2**, whether in the solid or in the solution state, is in the range of 345 to 351 ppm while the end-on derivative **2.9** is at 354 ppm. In fact, the only correlation seems to be related to which metal the dinitrogen ligand is attached, since the zirconium complexes resonate around 350 ppm, with the exception of the bridging dinitrogen ligand of $[Cp^*_2Zr(N_2)]_2(\mu\text{-}N_2)$. The dinuclear tantalum complexes also seems to display very similar chemical shifts irrespective of the ancillary ligands. But, also notable is that the formally tungsten(VI) derivative, $[Cp^*WMe_3]_2\text{-}(\mu\text{-}N_2)$, and the mononuclear molybdenum(0) complex, *trans*-$Mo(N_2)_2(PMePh_2)_4$, show similar chemical shifts to the tantalum dinitrogen complexes. The chemical shift of the bridging dinitrogen ligand in the diamagnetic titanium dinitrogen complex having PNP as the ancillary ligand appears around 375 ppm. Dinuclear titanium dinitrogen complexes reported in the literature are paramagnetic complexes.[56-58] None of the dinitrogen complexes containing PNP as the ancillary ligand showed any observable coupling to the phosphine donors in their ^{15}N NMR spectra.[59,60]

references on page 119

Table 2.9 Compilation of some ^{15}N chemical shifts[a] for some selected compounds.

Compound	Chemical Shift (ppm)	Reference
$\{[(Pr^i_2PCH_2SiMe_2)_2N]ZrCl\}_2(\mu\text{-}\eta^2\text{:}\eta^2\text{-}N_2)$	350.9 (solution)	this work
	345.0 (solid)	
$\{[(Pr^i_2PCH_2SiMe_2)_2N]ZrBr\}_2(\mu\text{-}\eta^2\text{:}\eta^2\text{-}N_2)$	345.8	this work
$\{[(Pr^i_2PCH_2SiMe_2)_2N]Zr(OAr^*)\}_2(\mu\text{-}\eta^2\text{:}\eta^2\text{-}N_2)$	342.9 and 339.1	this work
$\{[(Pr^i_2PCH_2SiMe_2)_2N]Zr(\eta^5\text{-}C_5H_5)\}_2(\mu\text{-}\eta^1\text{:}\eta^1\text{-}N_2)$	354.0	this work
$\{[(Pr^i_2PCH_2SiMe_2)_2N]TiCl\}_2(\mu\text{-}\eta^1\text{:}\eta^1\text{-}N_2)$	375.5	48
$[Cp^*_2Zr(\eta^1\text{-}N_2)]_2(\mu\text{-}\eta^1\text{:}\eta^1\text{-}N_2)$	452.0[b] (bridging)	61
	354.0[b] (terminal)	
$\{[(Pr^i_2PCH_2SiMe_2)_2N]Ta{=}CHBu^t\}_2(\mu\text{-}\eta^1\text{:}\eta^1\text{-}N_2)$	301.2	62
$\{(Me_3P)_2ClTa{=}CHCMe_3\}_2(\mu\text{-}\eta^1\text{:}\eta^1\text{-}N_2)$	296.2[c]	63
$[Cp^*WMe_3]_2(\mu\text{-}\eta^1\text{:}\eta^1\text{-}N_2)$	310.9[c]	64
trans-$Mo(\eta^1\text{-}N_2)_2(PMePh_2)_4$	298.3 & 305.4[d]	60

[a]All chemical shifts are referenced to external neat formamide set at 0.0 ppm. [b]Originally referenced to nitric acid. [c]Originally referenced to liquid ammonia. [d]Originally referenced to nitromethane.

A different approach to probe the binding of the dinitrogen ligand in the binuclear side-on zirconium complexes is to synthesize closely related complexes where the two zirconium centers are chemically different. For example, substituting one of the chloride ligands of complex **2.2** with a different ligand (e.g., Br or OAr^*) will render the two zirconium centers chemically different, and also change the symmetry of **2.2** from C_{2h} to C_s. Assuming that the ancillary ligand arrangements are similar in the solid and in the solution states, the solution ^{15}N NMR spectrum of the complex corresponding to C_s symmetry should give a singlet resonance, if the dinitrogen ligand is bound in a side-on manner in solution. Conversely, if the

references on page 119

dinitrogen is bound in an end-on fashion the ^{15}N NMR spectrum may consist of two singlets or a doublet-of-doublets corresponding to an AB type spin system.

Since attempts to selectively metathesize the zirconium-chloride bonds of **2.2** were futile,[65,66] mixtures containing a 1:1 ratio of two different precursors were reduced under $^{15}N_2$ atmosphere. When an equimolar mixture of **2.1** and **2.11** was reduced under dinitrogen it gave mainly complex **2.2** and none of the desired dinitrogen complex containing one chloride and one OAr^* ligand. Conversely, when a similar reduction was carried out with complex **2.1** and the bromide analogue $ZrBr_3[N(SiMe_2CH_2PPr^i_2)_2]$ **2.4**, it gave a mixture of three dinitrogen complexes. The $^{31}P\{^1H\}$ NMR spectrum of the mixture had four singlet resonances, which were very close in their chemical shifts. Two of these resonances were assigned to complex **2.2** and to the dibromo analogue **2.19**, and the other two resonances were assigned to the mixed halogen derivative, **2.20** where each signal is associated with one type of zirconium centre (Figure **2.5**). The ^1H NMR spectrum of the mixture shows the presence of eight equal intensity resonances (some overlapping) in the $SiMe_2$ region. This spectroscopic analyses shows that the above reaction produces a mixture of three complexes, **2.2**, **2.20** and **2.19** in approximately a 1:2:1 ratio (Scheme **2.8**).

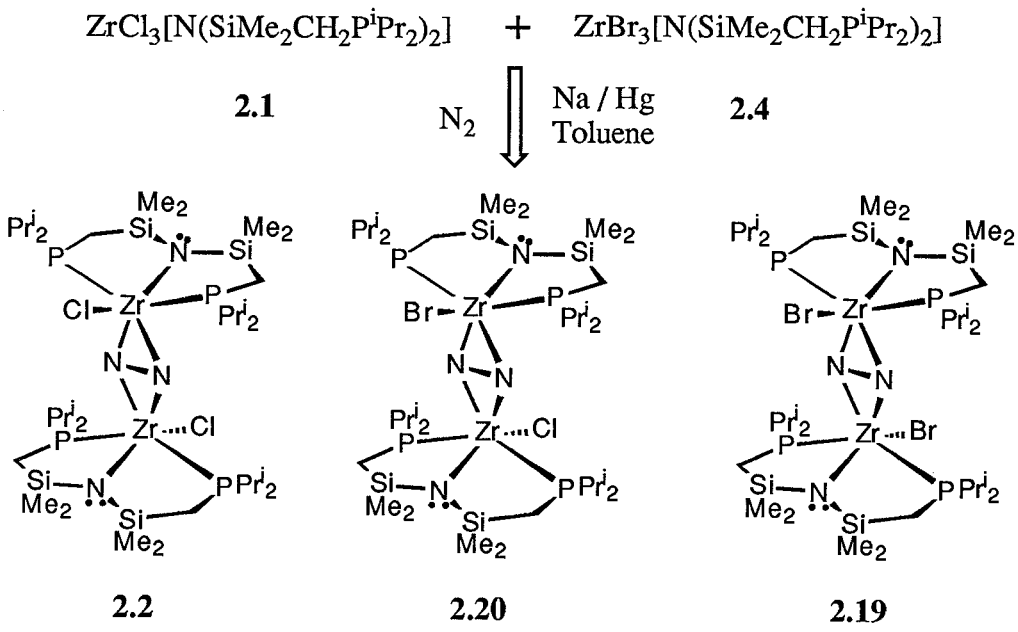

Scheme 2.8

references on page 119

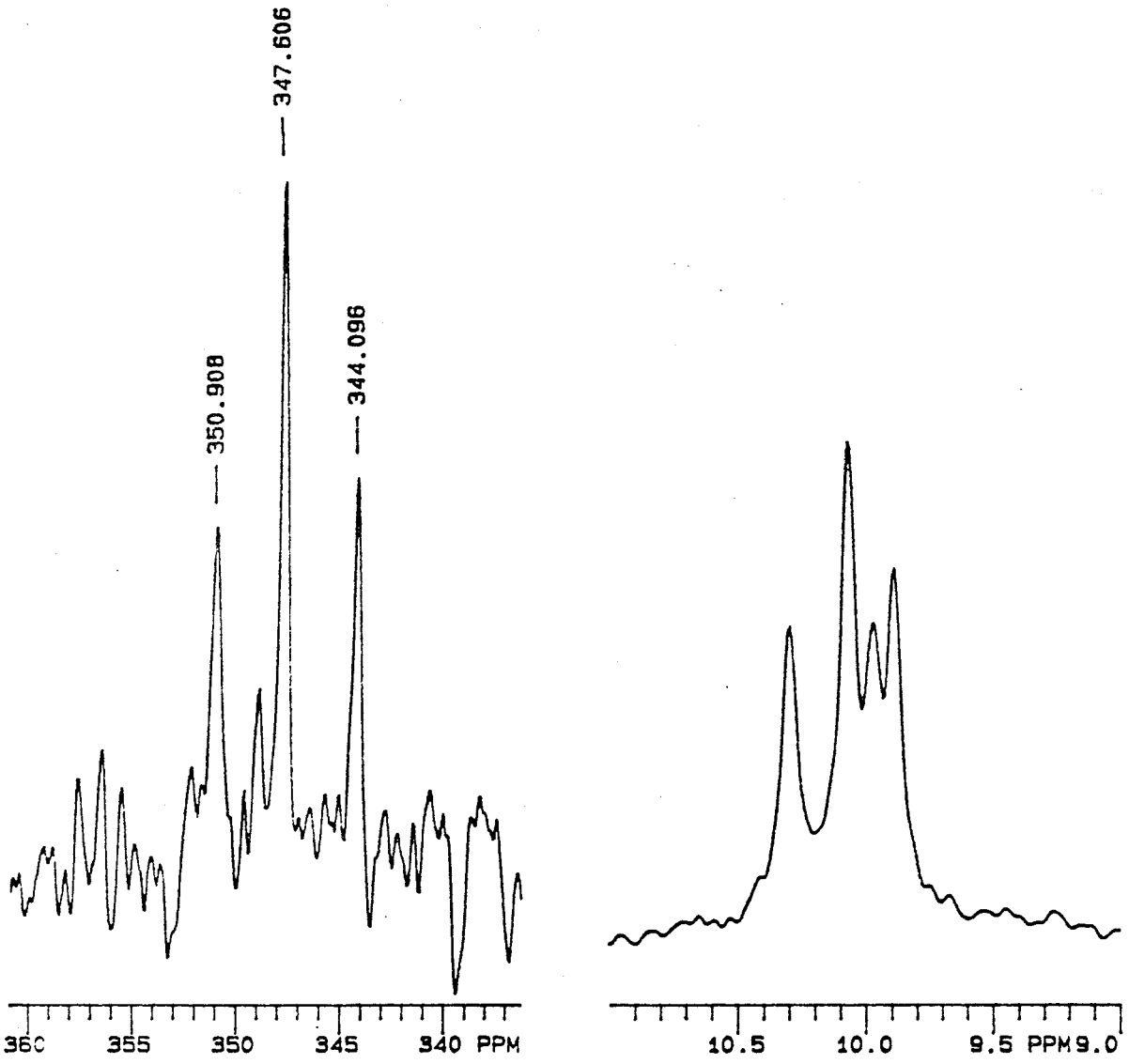

Figure 2.5 (right) $^{31}P\{^{1}H\}$ NMR spectrum of the sample obtained from the reaction described in Scheme **2.8**. (left) ^{15}N NMR spectrum of the same sample

The solution ^{15}N NMR spectrum of the sample containing the three dinitrogen complexes has three singlet resonances in approximately 1:2:1 ratio, of which the two low intensity peaks were assigned to complexes **2.2** and **2.19** (Figure **2.5**). The high intensity peak was assigned to the mixed halogen derivative, **2.20** which, being a singlet resonance suggests that the dinitrogen ligand is bound in a side-on fashion in solution. It is theoretically possible that the observed singlet resonance of **2.20** is a time averaged signal resulting from a rapid

references on page 119

fluxional process that involves intermediates containing end-on and side-on bound dinitrogen ligand. However, the dinitrogen ligand is highly activated in these complexes, and therefore the metal-nitrogen interactions are likely to be strong, which in turn would imply that the rotation of the dinitrogen ligand may have a high activation barrier.

To confirm that the bromide ligand also favors the formation of a side-on dinitrogen complex the pure dibromo derivative **2.20** was synthesized from **2.19**. A preliminary X-ray analysis of this complex showed that in the solid state the Zr_2N_2 core is identical to that of complex **2.2**.

2.6.2 Resonance Raman Spectroscopy

Further evidence for the mode of dinitrogen coordination in the zirconium complexes has been obtained from resonance Raman spectroscopic analysis.[67] Resonance Raman spectra of both isotopomers, nitrogen-15 and nitrogen-14, were obtained for solid samples and for solution samples made up in THF. The most prominent feature in the solid state resonance Raman spectrum of the end-on complex **2.9** is the peak at 1211 cm^{-1}, which shifts to 1172 cm^{-1} upon substitution of the $^{14}N_2$ ligand with $^{15}N_2$ (Figure **2.6**, page 52). The magnitude of this isotope shift, 39 cm^{-1}, is essentially equal to the calculated value of 41 cm^{-1}. The solution spectra of the two isotopomers are very similar to the solid state spectra, except for the presence of some solvent peaks. These spectral data imply that the dinitrogen ligand in **2.9** is bound in an end-on manner both in the solid and in the solution states.

The solid state resonance Raman spectrum of the side-on derivative **2.2** has two intense peaks at 317 cm^{-1} and 731 cm^{-1} and a few low intensity peaks. Substituting the dinitrogen ligand with nitrogen-15 isotopomer the peaks at 731 cm^{-1}, 991 cm^{-1} and 1046 cm^{-1} shift to 709 cm^{-1}, 968 $^{-1}$ and 1024 cm^{-1} respectively (Figure **2.7**, page 53). The isotopic shift of 22 cm^{-1} observed for the peak at 731 cm^{-1} is within 2 cm^{-1} of the calculated value, suggesting almost pure nitrogen-nitrogen bond stretching character.

references on page 119

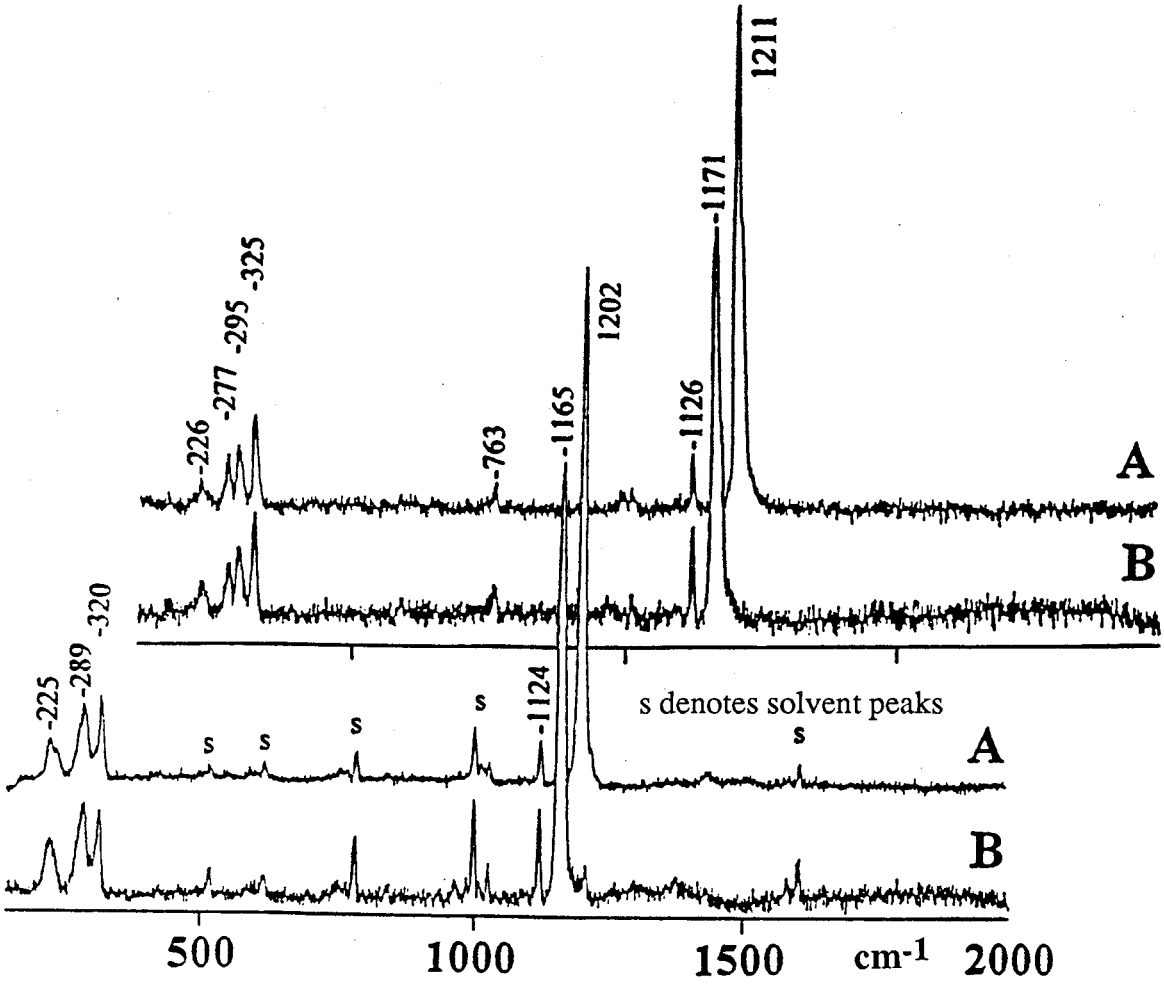

Figure **2.6** The resonance Raman spectra of complex **2.9** recorded at approximately 90 K. **A** and **B** correspond to the (μ-$^{14}N_2$) and (μ-$^{15}N_2$) complexes respectively. The top two traces were recorded in the solid state and the bottom two were recorded in the solution (THF) state. Each trace is a sum of 5 scans, each recorded at 2 cm^{-1}/s using 40 mW of 514. 5 nm laser excitation (Appendix **A.1**).

The resonance Raman studies done on the oxyhemocyanin model complex {Cu[HB(3,5-$Ph_2pz)_3$]}(μ-η^2:η^2-O_2) were used as the basis for the interpretation of the resonance Raman features of complex **2.2**.[68] It is important to note that both complexes have planar M_2X_2 (where M = Zr and X = N or M = Cu and X = O) type cores with the X_2 moiety bound in an identical side-on fashion.

references on page 119

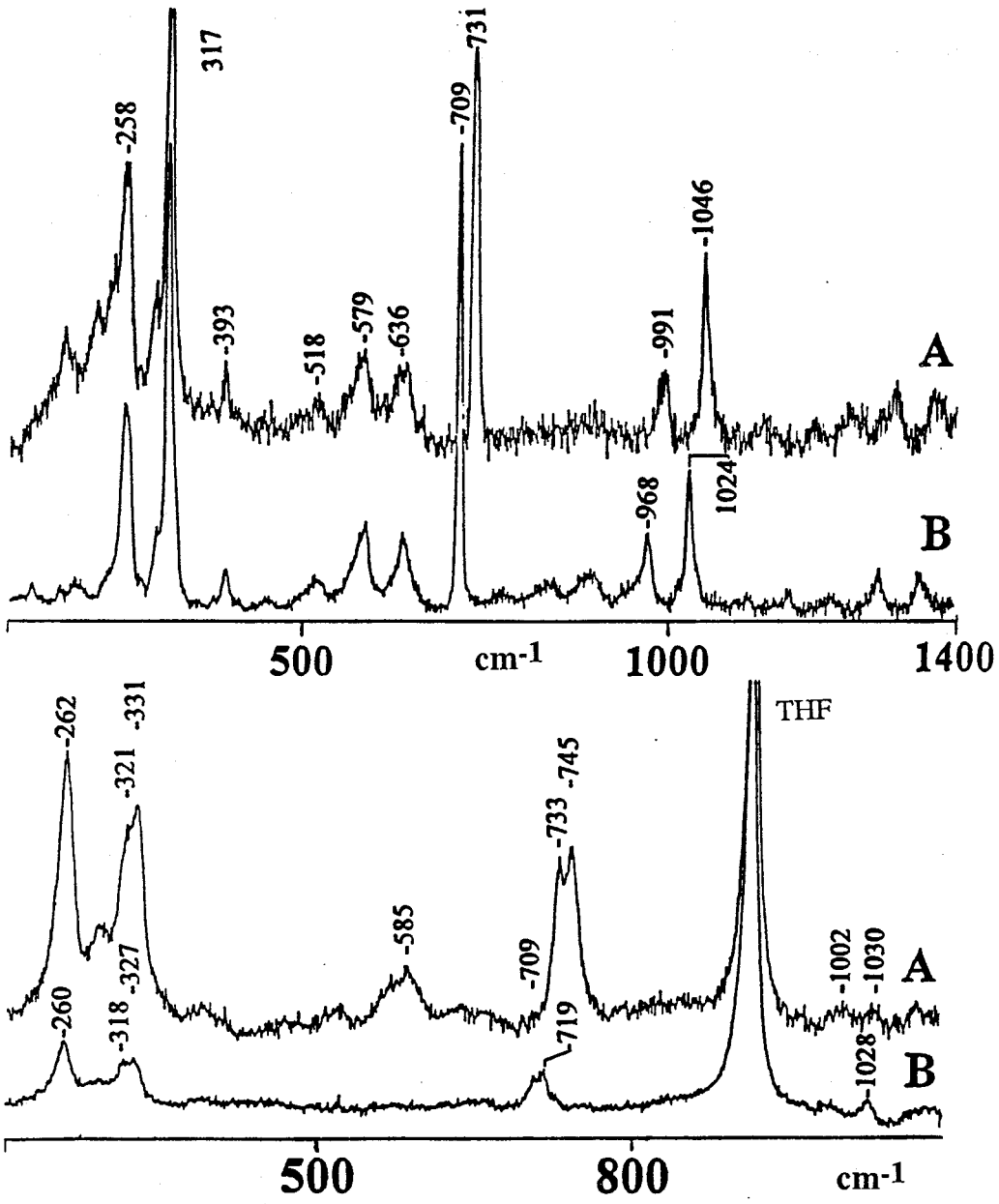

Figure **2.7** The resonance Raman spectra of complex **2.2** recorded at approximately 90 K. **A** and **B** correspond to the (μ-$^{14}N_2$) and (μ-$^{15}N_2$) complexes respectively. The top two traces were recorded in the solid state (sum of 9 scans) and the bottom two were recorded in the solution (THF) state (sum of 5 scans). Each scan was recorded at 1 cm^{-1}/s using 20 mW of 647.1 nm laser excitation (Appendix **A.1**).

The vibrational modes derived from normal coordinate analysis of the Cu_2O_2 core are depicted in Figure **2.8**. The peak observed at 731 cm^{-1} for the complex **2.2** has been assigned to the symmetric mode A_g where the dominant stretch involves the nitrogen-nitrogen bond

references on page 119

(Figure-**2.8**). By comparison, the similar stretching mode in the copper peroxide complex gives a value of 763 cm^{-1} for the $^{16}O_2$ complex which shifts to 723 cm^{-1} upon $^{18}O_2$ substitution.

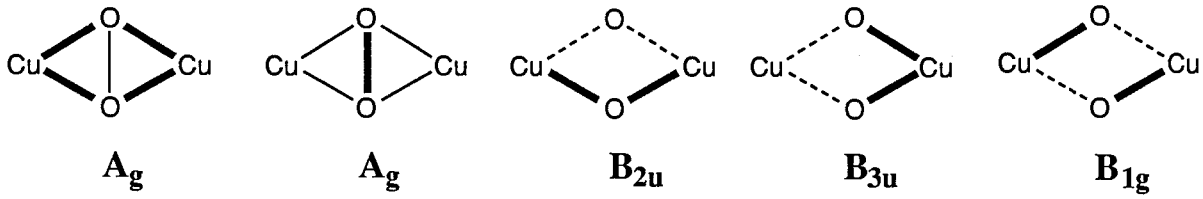

Figure 2.8 Depiction of the in-plane normal vibrational modes of the side-on peroxide bridged copper dimer.[68] Broken lines increase in length as solid lines decrease in length. Bonds which do not change in length during a given vibration are not shown. Thicker lines indicate the dominant motion in the two A_g modes.[68] The B_{1u} deformation mode is not shown.[114]

The other two isotope sensitive peaks of the side-on derivative **2.2**, 991 cm^{-1} and 1046 cm^{-1} shift by 23 cm^{-1} and 22 cm^{-1} respectively, upon substitution with the ^{15}N isotope. These two peaks are assigned as combination bands where the former is due to the peaks at 258 cm^{-1} and 731 cm^{-1} and the latter is due to the peaks at 317 cm^{-1} and 731 cm^{-1}. Since the peaks at 258 cm^{-1} and 317 cm^{-1} are not isotope sensitive, the shifts in the combination bands can be attributed to the isotope sensitive band at 731 cm^{-1}. Overall the spectrum consists of a few fundamental bands and the rest of the peaks are a result of overtones or combination bands.

The solution resonance Raman spectrum of **2.2** was different in some aspects. The peak due to the nitrogen-nitrogen stretching at 731 cm^{-1} in the solid state was split into two resonances at 745 cm^{-1} and 733 cm^{-1}. These two peaks shift to 719 cm^{-1} and 709 cm^{-1} respectively, upon substitution with nitrogen-15 dinitrogen ligand. The magnitude of the shifts (26 cm^{-1} and 24 cm^{-1}) are similar to the shifts observed in the solid state spectra. Also the feature at 317 cm^{-1} of the solid state spectrum was split into two resonances at 331 cm^{-1} and 321 cm^{-1}. The fact that the peaks corresponding to the nitrogen-nitrogen stretching are very close in the solid and in the solution state spectra strongly suggests that the mode of dinitrogen binding is very similar in the solid and in the solution states.

references on page 119

It is possible that the appearance of two peaks associated with the nitrogen-nitrogen stretching of the side-on complex **2.2** in the solution (THF) state is due to some solvent effects. However, recording the spectra in a relatively non-coordinating solvent like pentane also showed two peaks. Therefore it is believed that the molecule is undergoing some fluxional process, for example, a process that involves the bending of the planar Zr_2N_2 core along the nitrogen-nitrogen axis (Equation **2.1**). An isomer with a bent core is comparable to the OAr^* derivative, **2.12**.

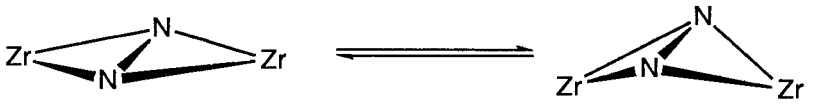

Planar Core Bent Core **2.1**

Curiously, the solution spectrum of the ^{15}N isotopomer of the side-on complex **2.2** had a peak at 1028 cm^{-1} which was comparable to the dinitrogen stretching of the end-on complex **2.9**. To ascertain the origin of this peak, polarization studies were carried out on the nitrogen-15 isotopomer in solution. It was found that the peaks at 719 cm^{-1} (ρ, 0.32), 709 cm^{-1} (ρ, 0.32), 327^{-1} (ρ, 0.40), 318 cm^{-1} (ρ, 0.40) and 260 cm^{-1} (ρ, 0.35) were polarized and the peak at 1028 cm^{-1} (ρ, 0.76) was depolarized. The lower polarization associated with the peaks at 700 cm^{-1} and the peak at 260 cm^{-1} suggest that they are due to the A_g modes, where the former peak corresponds to the nitrogen nitrogen stretching mode and the latter to the breathing mode of the Zr_2N_2 core (Figure **2.8**). The peaks around 300 cm^{-1} also share some A_g character. Also the depolarized peak at 1028 cm^{-1} is not associated with any totally symmetric mode and is probably due to solvent (THF).

The resonance Raman spectra of the sample containing a mixture of three complexes **2.2**, **2.21** and **2.20** gives only a single peak at 709 cm^{-1} (Figure **2.9**). The absence of a center of symmetry in the mixed halogen complex **2.18** does not seem to affect the A_g stretching mode associated with the dinitrogen ligand. This is in agreement with our previous suggestion that the peaks around 700 wave numbers are almost purely of dinitrogen stretch in character. The

references on page 119

resonance Raman spectra of the aryloxy derivative **2.12** also gives a strong Raman feature at 730 cm^{-1}.

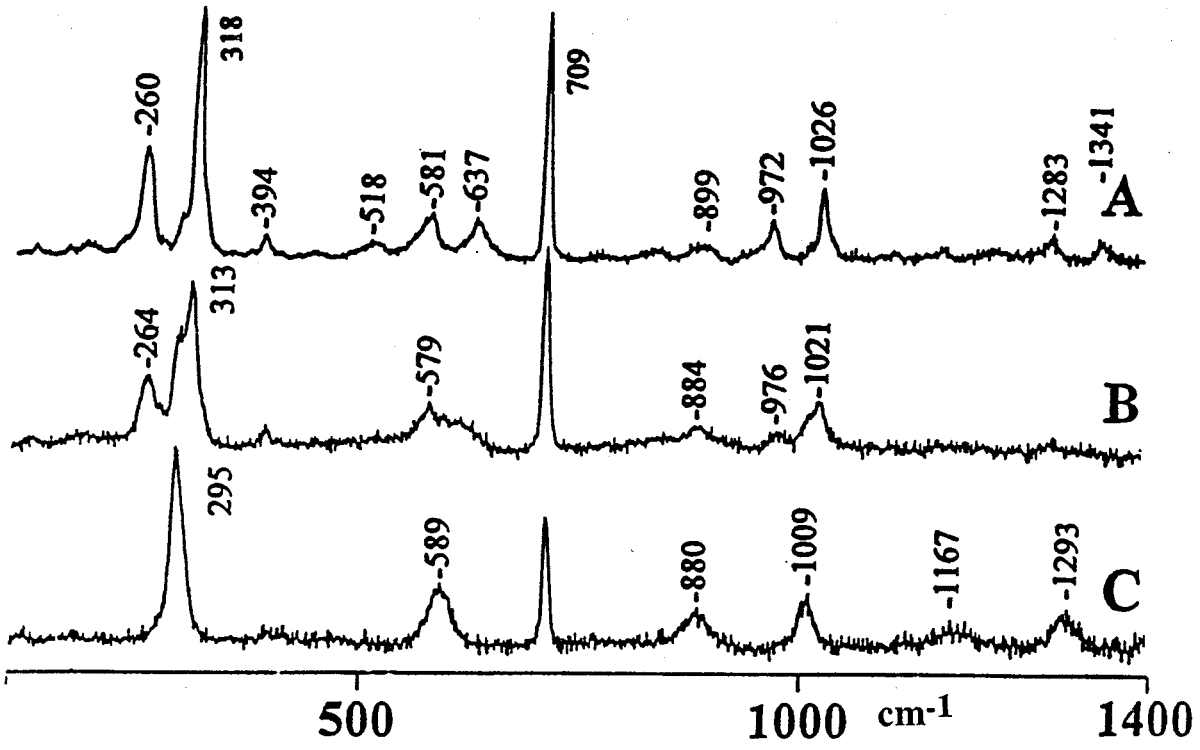

Figure **2.9** The solid state resonance Raman spectra of **2.2**, (**A**) and **2.19**, (**C**) and of the sample (**B**) obtained from the reaction shown in Scheme **2.6**. All of the samples contain a (μ-η^2:η^2-$^{15}N_2$) ligand. Spectral conditions are similar to Figure **2.8**.

A compilation of various bond lengths and stretching frequencies associated with a nitrogen-nitrogen bond are shown in Table **2.10**. The stretching frequencies associated with the dinitrogen ligand in the side-on complexes are significantly lower than what has been observed for hydrazine, whereas the comparable feature of the end-on derivative, **2.9** is higher; i.e., in these zirconium complexes the stretching frequencies seems to corroborate well with the observed nitrogen-nitrogen bond distances. Also these data suggest that the end-on zirconium derivative has a bond order higher than that of hydrazine whereas the side-on derivatives have a bond order of less than one.

references on page 119

Table 2.10 Compilation of some nitrogen-nitrogen bond lengths and stretching frequencies associated with them.

Compound	Bond length Å	ν cm^{-1}	references
N≡N	1.0975(2)	2331	115
Me—N=N—Me	1.247[70]	1576	71
Ph—N=N—Ph	1.255	1442	71
H_2N—NH_2	1.46	1111	71
F_2N—NF_2		600, 588	71
$[Ru_2(NH_3)_{10}(\mu\text{-}\eta^1\text{:}\eta^1\text{-}N_2)]^{4+}$	1.124(15)	2050-2100	72
$\{[(Pr^i_2PCH_2SiMe_2)_2N]Zr(\eta^5\text{-}C_5H_5)\}_2(\mu\text{-}\eta^1\text{:}\eta^1\text{-}N_2)$	1.301(3)	1211	this work
$\{[(Pr^i_2PCH_2SiMe_2)_2N]Zr(X)\}_2(\mu\text{-}\eta^2\text{:}\eta^2\text{-}N_2)$			
X = Cl	1.548(7)	731	this work
X = OAr*	1.51(1)	732	

2.7 Bonding Considerations

2.7.1 General

The Dewar-Chatt-Duncanson bonding model developed for the qualitative understanding of metal-olefin interactions has been extended to explain the bonding of transition metal dinitrogen complexes.[73,74] This synergic bonding formalism involves electron donation from a filled ligand orbital into a vacant metal orbital, and concomitant back donation of electrons from a filled metal orbital into a vacant ligand orbital. In mononuclear end-on complexes, the lone-pair orbitals of the end-on bound dinitrogen ligand act as the donor orbitals and the vacant π^*-orbitals act as the acceptor orbitals.[75] The bonding in mononuclear side-on dinitrogen complexes can be rationalized by invoking the filled π-orbitals as the donor orbitals and the vacant π^*-orbitals as the acceptor orbitals.[76]

To explain the bonding in dinuclear metal complexes having an end-on bridging dinitrogen unit, M—N≡N—M, Chatt *et al.* proposed the qualitative molecular orbital (MO) analysis depicted in Figure **2.10**.[77,78] For this four-center M–N–N–M interaction, the atomic

references on page 119

orbitals (AO) of each center (i.e., of both the metals and the two nitrogens) contribute equally towards each MO.

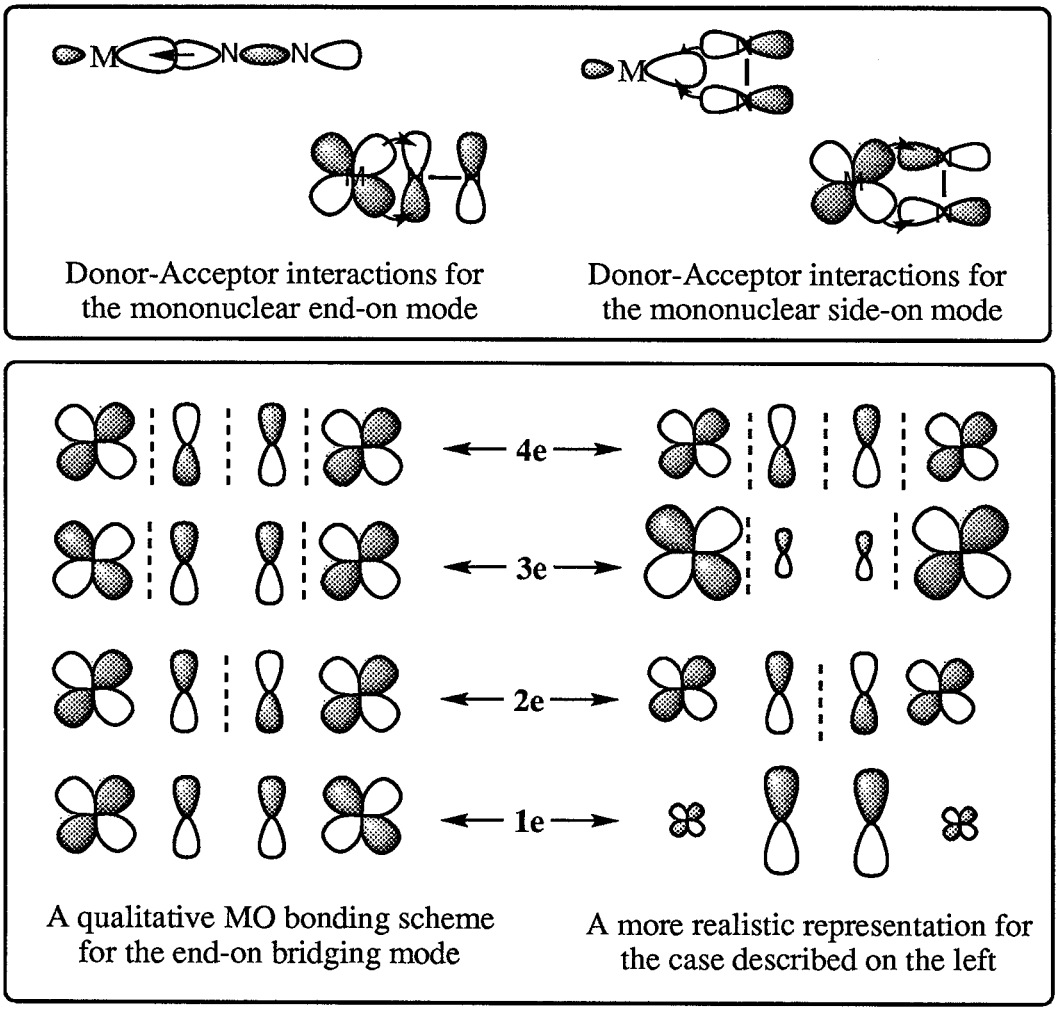

Figure 2.10 Qualitative bonding description for mononuclear complexes (top) and end-on bridging dinuclear complexes (bottom).

Molecular orbital calculations performed on structurally known complexes give a slightly different picture.[79] Fenske-Hall type calculations performed on the end-on dinuclear complexes, $\{[Ru(NH_3)_5]_2(\mu\text{-}N_2)\}^{4+}$, $\{[Nb(CH_2)(CH_3)(PH_3)_2]_2(\mu\text{-}N_2)\}$ and $(Cp^*_2ZrN_2)_2(\mu\text{-}N_2)$, **2.3**, suggest that the MOs labelled **3e** for all of the $\mu\text{-}\eta^1\text{:}\eta^1\text{-}N_2$ complexes are either non-bonding or weakly bonding in character so that their occupation cannot affect the nitrogen-nitrogen bond length.[79] Thus, the character of the **2e** MOs must control the strength of the

references on page 119

metal-nitrogen and nitrogen-nitrogen bonds. The AO composition of the **2e** MOs vary considerably for different complexes. It was found that the participation of the dinitrogen π^*-orbitals in the **2e** MOs was greater for the zirconium and niobium cases and was less for the ruthenium case, which also corroborates with the longer nitrogen-nitrogen bond distances observed in the zirconium and niobium complexes. For the niobium and zirconium complexes, $\{[Nb(CH_2)(CH_3)(PH_3)_2]_2(\mu\text{-}N_2)\}$ and $(Cp^*_2ZrN_2)_2(\mu\text{-}N_2)$, a push-pull type of bonding mechanism has been postulated that parallels the synergic bonding in mononuclear complexes.[21,79] In these examples, of the two d-orbitals (one from each metal) that contribute towards the **2e** MOs, only one is filled and the other is vacant. As a result, metal to dinitrogen $M \rightarrow N_2$, and dinitrogen to metal $N_2 \rightarrow M$, electron flow can occur without significant charge build up on the dinitrogen ligand.[21,79]

2.7.2 Bonding in $\{[(Pr^i_2PCH_2SiMe_2)_2N]Zr(\eta^5\text{-}C_5H_5)\}_2(\mu\text{-}N_2)$

INDO/1-MO calculations were performed on the idealized metal complex $[(H_3P)_2(H_2N)Zr(\eta^5\text{-}C_5H_5)]_2(\mu\text{-}\eta^1\text{:}\eta^1\text{-}N_2)$ **A**, which was restricted to C_{2v} symmetry.[45] The fragment MO analysis was carried out on the idealized fragment $[(H_3P)_2(H_2N)Zr(\eta^5\text{-}C_5H_5)]$ **B** with an imposed C_s symmetry. In these models, the relative spatial arrangement of the atoms directly bonded to zirconium was kept very close to that of the X-ray structure.[45] In order to minimize the total number of AOs associated with the model the isopropyl groups on the phosphine donors were replaced with hydrogen atoms. The isopropyl substituents are important in view of their steric contribution but in a semi-empirical level of calculations they are unlikely to have a significant influence in the electronic properties associated with the metal.

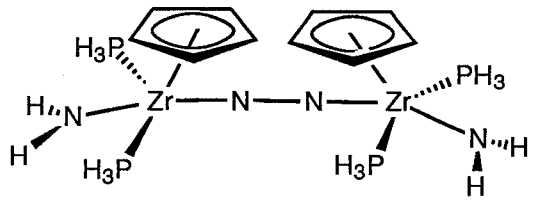

A

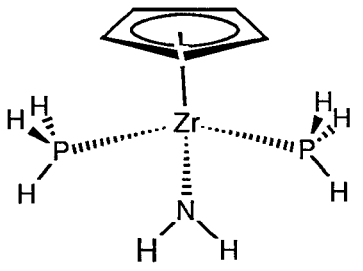

B

references on page 119

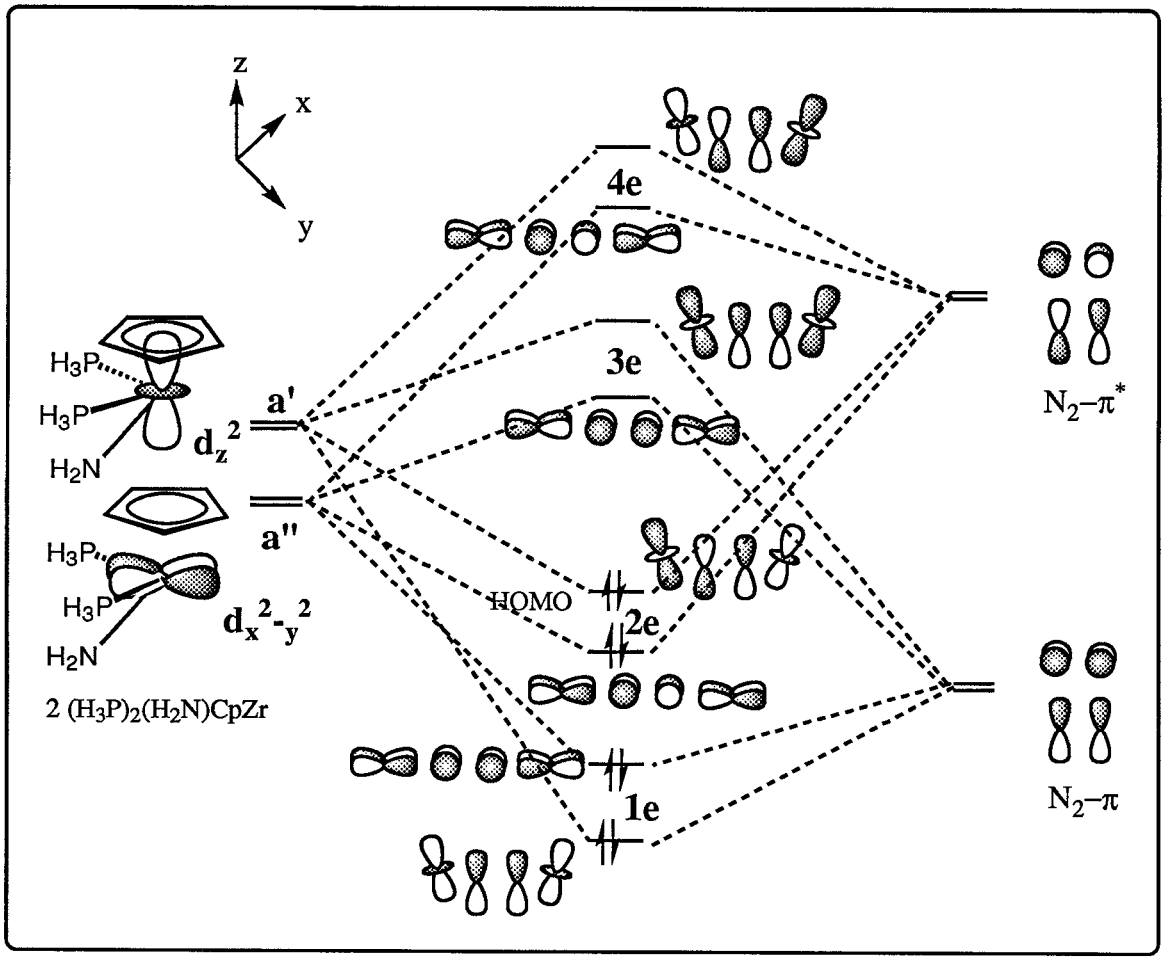

Figure 2.11 Bonding scheme for the model **A**.

From the dinitrogen ligand the lone-pair orbital $3\sigma_g$, the bonding π_u-orbitals and the antibonding π^*-orbitals are available for bonding. MO analysis of the fragment **B** indicated that there are two metal-based orbitals **a'** and **a"** which are available for bonding with dinitrogen. These frontier orbitals **a'** and **a"** mainly consist of d_z^2 (52%) and d_x^2-$_y^2$ (68%) respectively (Table **2.11**).* The d_z^2 lies along the axis containing the metal and the centroid of the Cp ligand, and is therefore higher in energy than the d_x^2-$_y^2$, which lies between the phosphine and the amide ligands.** The d_{xz} and d_{yz} orbitals are involved in bonding with the Cp ligand and the d_{xy}-orbital is directed towards the ancillary ligand atoms. This formalism is consistent with the

* The total d-orbital contribution towards the frontier orbital **a'** (-0.674 eV) is 63% and **a"** (1.556 eV) is 85%. Orbital **a'** has a significant zirconium p-orbital (p_z-17%) contribution as well.

** If the symmetry of the major d-orbital contributing towards a frontier orbital agrees with the adopted coordinate system then that frontier orbital will be referred to by the symmetry symbol of the d-orbital.

references on page 119

isoelectronic and qualitatively isolobal fragment $[(C_5Me_5)WMe_3]$*[80] where the two isolobal **a'** and **a"** orbitals mainly consist of d_z^2 and d_{xy} orbitals.[64,81]

Table 2.11 Some orbital parameters of **1e** and **2e** MOs of model complex **A**.

Molecular orbital	Energy (eV)	Zr d-orbital contribution per metal	N_2 p-orbital contribution per nitrogen
HOMO (**2e**)	-5.824	10%	23% (p_y = 18%)
HOMO-1 (**2e**)	-6.594	24%	21% (P_z = 14%)
HOMO-9 (**1e**)	-11.065	8%	26% (p_z = 17%)
HOMO-11 (**1e**)	-12.363	9%	24% (p_y = 19%)

The bonding scheme for model **A** is shown in Figure **2.11**. The symmetric combination of the $d_{x^2-y^2}$-orbital with one of the π-orbitals of dinitrogen gives rise to HOMO-9 and the symmetric combination of the d_z^2-orbitals with the second π-orbital of dinitrogen gives rise to HOMO-11. These two MOs correspond to the **1e** MOs depicted in Figure **2.11** and consist mainly of π-N_2 in character.* In a similar fashion the anti-symmetric combinations of the d_z^2 and $d_{x^2-y^2}$ orbitals can interact with the π*-orbitals of dinitrogen to give the **2e** MOs, which correspond to HOMO and HOMO-1 respectively. The relative energies and orbital contributions (for one Zr and one nitrogen atom of the dinitrogen ligand) of **1e** and **2e** MOs are given in Table **2.11**. With regard to the AO contributions towards the **2e** MOs, the HOMO has a significantly greater dinitrogen p-orbital character than the d-orbital character of zirconium, which in turn suggests that the occupation of the HOMO would lead to a charge build up on the dinitrogen ligand. The **1e** and **2e** MOs are occupied by eight electrons, four of which are from the dinitrogen and the remainder from the metal orbitals where each metal formally contributes

* The $CpZr(PH_3)_2(NH_2)$ fragment deviates from being ideally isolobal to the $(C_5Me_5)_2WMe_3$ fragment due to the π interactions of the amide lone pair with the metal d-orbital. Both fragments belong to C_s point group.

* Since these two MOs have different energy they are not strictly **1e** MOs. They are comparable to **1e** MOs only on the basis of the number of nodes and the type of interactions between the metal and N_2. Similar reasoning is adopted for the **2e**, **3e** and **4e** MOs.

references on page 119

two electrons. The unoccupied **3e** MOs (LUMO+2, 0.602 eV and LUMO+4, 1.392 eV) are mainly metal d-orbital in character, i.e., these MOs can be considered as virtual non-bonding orbitals. In principle therefore, addition of electrons into the **3e** MOs (i.e., further reduction of **2.9**, e.g., electrochemical reduction) is unlikely to lead to any significant activation of dinitrogen.

The values for the Wiberg indices[82-84] (Table **2.12**) clearly show a weak nitrogen-nitrogen bond in **A**; by comparison, the calculated bond indices of diazenido $(N_2)^{2-}$ and hydrazido $(N_2)^{4-}$ ligands give rise to bond orders of 2 and 1, respectively.[85,86] Therefore the calculated bond order of 1.15 for the nitrogen-nitrogen bond in **A**, agrees well with the formalism of the dinitrogen ligand as a hydrazido $(N_2)^{4-}$ ligand and is also in line with the resonance Raman data where the observed nitrogen-nitrogen stretch for the end-on derivative **2.9** was approximately 100 cm^{-1} higher than that of hydrazine. Also the calculated bond order of 2.18 for the zirconium-nitrogen bond of the Zr_2N_2 core supports the formulation of the Zr_2N_2 core as a Zr=N—N=Zr unit. The population analysis shows a net donation of 0.22 electrons from the dinitrogen lone pairs (on the basis of a decrease of electron density of the nitrogen s and p_x orbitals). It also shows a net gain of 0.61 electrons into the π^*-orbitals. The calculated total charge on the dinitrogen ligand is -0.76 (-0.38×2).

Table 2.12 Bond indices and population analysis of model complex **A**.

Wiberg Bond Index		Mulliken Orbital Populations of N_2 per nitrogen		
Bond	Index	Orbital	N_2 complex	free N_2 (N—N = 1.096Å)
Zr—N (N_2)	2.18	s	1.684	1.906
Zr—N (amide)	1.00	p_x	1.086	1.096
N—N	1.15	P_y	1.276	1.000
Zr—P	0.63	P_z	1.333	1.000

references on page 119

2.7.3 Bonding in Side-On Complexes

Due to the lack of experimental evidence for side-on bound dinitrogen complexes, only a few publications have addressed the issue of bonding in these complexes. Theoretical studies on some mononuclear dinitrogen complexes have shown that the nitrogen-nitrogen bond is weakened (i.e., on the basis of longer nitrogen-nitrogen distances) to a greater extent in the side-on mode of coordination as compared to the end-on mode.[76,87] For example, the simple interaction of a CH_2 fragment with dinitrogen in an end-on (diazomethane) fashion versus the corresponding side-on form (diazirine) showed a greater weakening of the dinitrogen bond in the latter case.[87] Also, calculations done on model complexes $[Ru(NH_3)_5(N_2)]^{2+}$ and $[CoH(PH_3)_3(N_2)]$ indicate that the metal nitrogen bond strengths are stronger for side-on cases, whereas the nitrogen-nitrogen bond strengths (i.e., calculated bond energies) were greater for the end-on cases.

It has been suggested[87] that the paucity of side-on complexes may be attributed to the overwhelming destabilization of the nitrogen-nitrogen bond upon complexation which in turn is not stabilized adequately by the formation of the metal-nitrogen bond. In the case of the model complex $[Ni(PH_3)_2(N_2)]$ the SCF binding energies are calculated to be -15.1 kcal mol^{-1} and -12.6 kcal mol^{-1} for side-on and end-on cases respectively, favoring the side-on mode. It was also shown that the nitrogen-nitrogen bond was more elongated in the side-on case and also the negative charge on the nitrogens of the dinitrogen ligand was greater (0.30 electrons for side-on versus 0.02 electrons for end-on), implying increased π-backdonation for the former.[76] Conversely, calculations done on a different nickel complex, $[Ni(O_2)(N_2)]$ showed that the end-on mode of coordination is favored.[88]

Hoffmann *et al.* have performed MO calculations on dinuclear complexes containing side-on bound dinitrogen unit where the $M–N_2–M$ core adopts a bent geometry (Figure **2.12**). They considered the cobalt complex **C** as a possibility and the nickel complex **D** as a model for example **1.10** (Chapter **1**).[89] The two important π-acceptor interactions of the bridging dinitrogen are shown in Figure **2.12**. The in-phase and out-of-phase combinations of the fragment orbitals overlap with the two π^*-orbitals to give two π MOs, $\mathbf{b_1}$ and $\mathbf{a_2}$. Also, the

references on page 119

EH-MO calculations on **C** and **D** gave a substantial energy separation (3 eV) between the HOMO and LUMO for the side-on mode, whereas similar energy separation for the parallel end-on case **E** was only 0.02 eV. These energy values clearly indicate higher thermodynamic and kinetic stability for the side-on modes.[89]

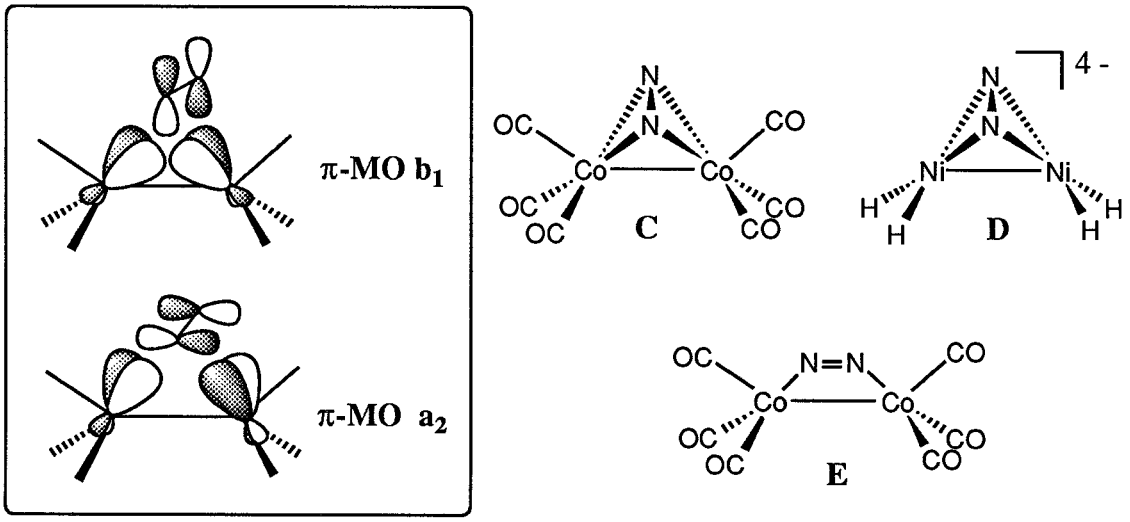

Figure 2.12 Bonding scheme (in the box) describes the edge-on bridging dinitrogen complexes of Co and Ni.

2.7.4 Bonding in $\{[(Pr^i_2PCH_2SiMe_2)_2N]ZrCl\}_2(\mu\text{-}N_2)$

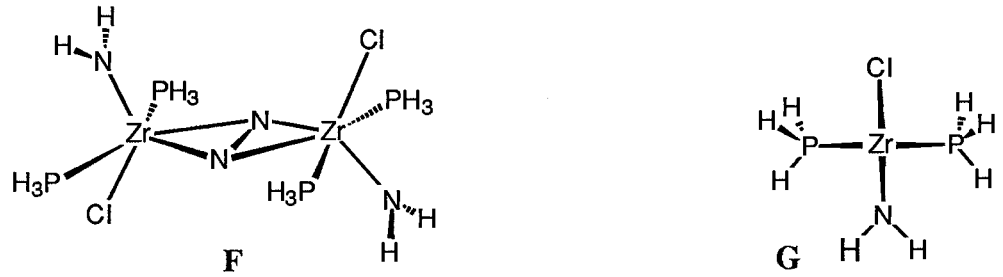

Using the INDO1/MO level, semi-empirical calculations were performed on this side-on complex using the idealized form $\{(H_3P)_2(H_2N)ZrCl\}_2(\mu\text{-}N_2)$, **F**, with an imposed C_{2h} symmetry.[45,62] The fragment MO analysis was carried out on the species $[(H_3P)_2(H_2N)ZrCl]$, **G**, with an imposed C_s symmetry.[45,62] In these models, the relative spatial arrangement of the atoms directly bonded to zirconium was kept very close to what was observed in the X-ray

references on page 119

structure.[8] The isopropyl substituents are important in view of their steric contribution but in a semi-empirical level of calculations they are unlikely to have a significant influence in the electronic properties associated with the metal. The $SiMe_2$ groups associated with the amide were also replaced with hydrogens, and a comparison of the theoretical electronic data for **F** and the silyl substituted analogue, $\{(H_3P)_2[(H_3Si)_2N)]ZrCl\}_2(\mu\text{-}N_2)$ gave identical results.

The fragment orbitals **1a"** and **2a"** of **G** have the appropriate symmetry to form a π-MO and a δ-MO, respectively. The frontier orbital **1a"** has 84% d-character (55%, d_z^2; 23%, $d_{x^2-y^2}$ and 6%, d_{xz}) and **2a"** has 80% d-character (38%, d_{xy}; 25%, d_{xz} and 16%, d_{yz}). In the case of **G**, due to the extensive mixing of the d-orbitals the frontier orbitals **1a"** and **2a"** will be referred to as virtual-d_{xz} and virtual-d_{xy} orbitals* respectively (Table **2.13**).

Table 2.13 Some orbital parameters of π and δ MOs of complex **F**.

Molecular orbital	Energy (eV)	Zr d-orbital contribution per metal	p-orbital contribution N_2 per nitrogen
HOMO (δ)	-6.937	12%	34% (p_x = 12.4%; p_z = 15%)
HOMO-9 (π)	-10.329	20%	27% (p_z = 5.7%; p_y = 21%)

From a symmetry point of view the acceptor interactions of the dinitrogen π*-orbitals with the metal in the side-on case **F** differ considerably from that of the end-on model **A**. In **F** the π*-orbitals in the plane of Zr_2N_2 core overlap with a virtual d_{xz}-orbital, which is also contained in the same plane to give a π-MO (Figure **2.13**). This MO has 27% zirconium-d and 20% dinitrogen-p character, which is similar to the orbital contributions calculated for the HOMO-1 of the model complex **A** (Table **2.13**). But, an important difference is that the π-MO of **F** is much lower in energy than the π-MOs of **A**. This is probably due to the fact that the dinitrogen π*-orbitals overlap better with the metal d-orbitals in the side-on mode than in the

* These frontier orbitals are referred to as virtual orbitals because they are assigned according to the adopted coordinate system and not on the basis of which atomic orbital contributes the most.

references on page 119

end-on mode. By comparison, the overlap values calculated for the π-type interaction between the π*-orbital of dinitrogen and titanium d-orbitals give a value of 0.227 for the side-on bonding and 0.155 for the end-on bonding.[90]

The out of plane π*-orbitals of the dinitrogen in **F** overlap with a virtual d_{xy}-orbital, which is contained in a parallel plane to form a δ-MO (Figure **2.13**). This MO has 12% zirconium-d and 34% nitrogen-p character and suggests that there is considerable ionic character with electron density mainly located on the nitrogens of the dinitrogen ligand. A survey of the low lying LUMOs of **F** (up to LUMO+5) showed that they are mainly non-bonding metal-based orbitals.

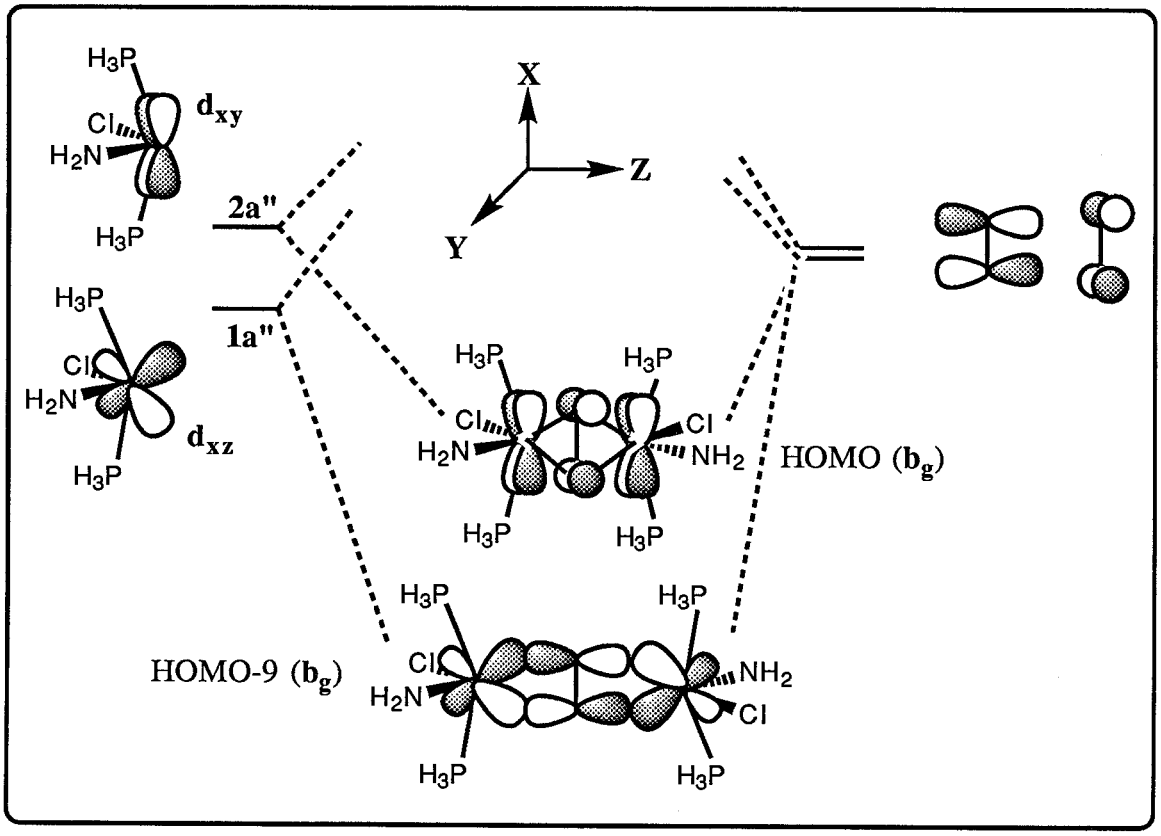

Figure 2.13 Bonding scheme illustrating the types of overlap leading to the formation of the π-MO and the δ-MO.

references on page 119

The large energy gap (6.4 eV) between the HOMO and LUMO is consistent with the observed stability of this complex. When the hypothetical end-on complex* having identical ligand arrangements around the zirconium core, as that of **F**, was subjected to INDO/1-MO analysis the HOMO-LUMO gap (6.3 eV) was found to be very close to the gap for **F**. Therefore, an analysis on the basis of HOMO-LUMO gap does not favor the side-on mode over the end-on.[89] However, the SCF energy value does favor the side-on case **F**, by greater than 1 eV.

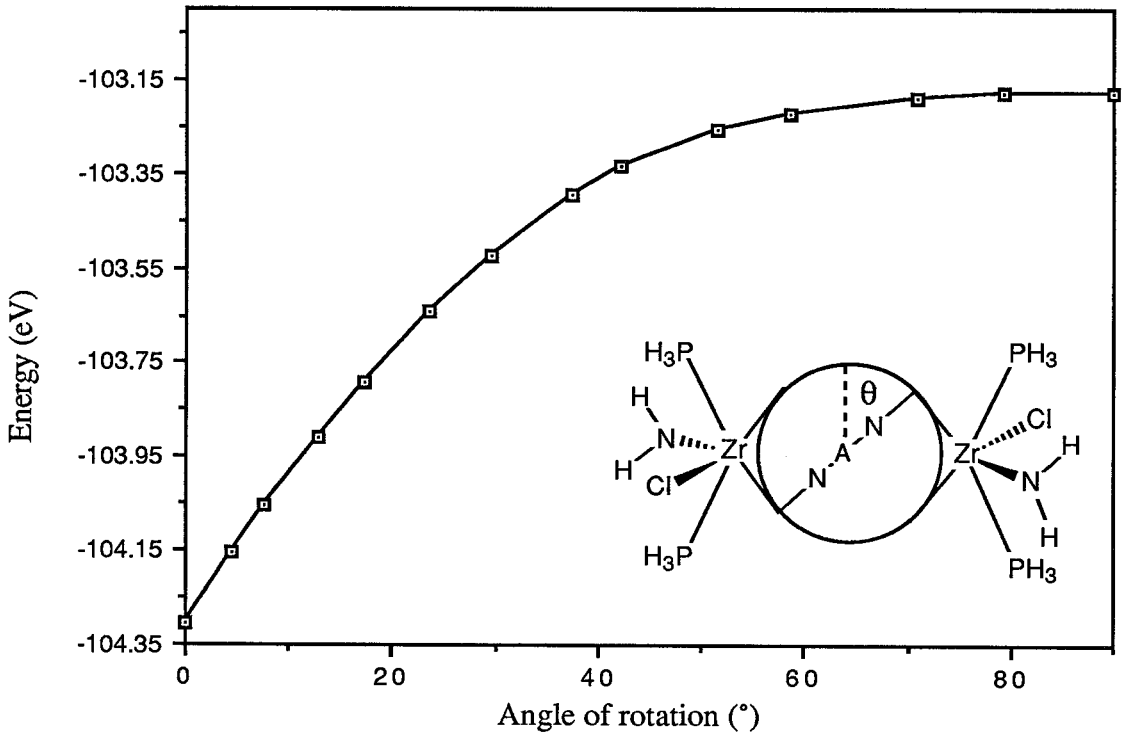

Figure 2.14 Plot showing the change of energy in the model complex **F** with the rotation of the dinitrogen ligand.

To evaluate the barrier for the conversion of the side-on complex to the end-on complex, the dinitrogen ligand was rotated in a stepwise manner on the plane of the Zr_2N_2 core until the dinitrogen ligand became coordinated end-on. The angle of rotation θ is depicted in

* The Zr_2N_2 core of **F** was changed to a linear end-on mode, Zr–N–N–Zr; Zr–N = 1.92 Å, N–N = 1.30Å. Bond length parameters of the ligands were kept identical to **F**.

references on page 119

Figure **2.14** where it was increased from 0° to 90°. During rotation the closest distances between a zirconium center and a nitrogen of the dinitrogen ligand were kept constant. The curve obtained from the plot of θ vs. energy (at the SCF level) suggests that the barrier for the rotation from an end-on to side-on coordination is greater than 1 eV. More importantly, from a thermodynamic viewpoint the shape of the curve suggests that this particular end-on complex should spontaneously convert to the side-on complex. It is of interest to point out that *ab initio* calculations done on naked dinuclear side-on dinitrogen complexes of the type $M_2(\mu\text{-}\eta^2\text{:}\eta^2\text{-}N_2)$, where M = Ti, Zr and Y, suggested that zirconium and yttrium favor a side-on bound dinitrogen ligand. The calculated nitrogen-nitrogen bond distances for the ligand-free zirconium case (Zr_2N_2) was 1.48 Å, which was only 0.07 Å shorter than the experimental value 1.55 Å found for complex **2.2**.[91]

In the model **F**, the calculated value of 0.85 (Table **2.14**) for the nitrogen-nitrogen bond order, is less than the value of 1.15 found for the end-on case **A**, and this corroborates well with the resonance Raman data of complex **2.2**, where the observed nitrogen-nitrogen stretching frequency was approximately 300 cm^{-1} lower than that of hydrazine. But, comparison with the observed differences in the nitrogen-nitrogen bond lengths of end-on and side-on complexes (e.g., **2.2** versus **2.9**) the differences in bond indices are not significant. By the definition of bond order, i.e., the net bonding electrons are equal to twice the value of bond order, in going from models **A** to **F** the number of bonding electrons associated with the dinitrogen ligand have decreased by 0.6. This would imply greater backbonding in the side-on complexes and is consistent with other theoretical studies done on side-on complexes. The overall bond order between the dinitrogen and zirconium in the side-on case was found to be 2.38 (2×1.19), and suggests stronger metal dinitrogen interactions than in the end-on case. The calculated bond order between the amide nitrogen and zirconium was found to be greater than 1, implying significant π interactions. The significance of this interaction will be discussed later.

references on page 119

Table 2.14 Bond indices and population analysis of model complex **F**.

Wiberg Bond Index		Mulliken Orbital Populations of N_2 per nitrogen		
Bond	Index	Orbital	N_2 complex	free N_2 (N-N = 1.548 Å)
Zr—N (N_2)	1.19	s	1.845	1.937
Zr—N (amide)	1.13	p_x	1.152	1.063
N—N	0.85	P_y	1.284	1.000
Zr—P	0.61	P_z	1.260	1.000

Population analysis of **F** shows only a small decrease in the s-orbital population of dinitrogen, but the populations of all the p-orbitals have been increased. The calculated formal charge of -1.08 on the dinitrogen ligand is significantly higher than what was found for the end-on species **A** (-0.76). It is possible that the increased coulombic repulsion (due to the higher charge) between the two nitrogens of the dinitrogen ligand and weak bonding interactions (on the basis of Wiberg indices) are important factors contributing to the long nitrogen-nitrogen distances observed in the side-on complex **2.2**. With regard to this coulombic repulsion, the changes in nitrogen-nitrogen bond lengths in neutral hydrazine and its protonated derivatives are important. The observed nitrogen-nitrogen bond length decreases consistently upon successive protonation of hydrazine, i.e., the nitrogen-nitrogen bond lengths for H_4N_2, $(H_5N_2)Br$, and $(H_6N_2)SO_4$ are 1.47 Å, 1.45 Å and 1.40 Å respectively. This decrease in bond length has been attributed to the removal of the highly repulsive lone-pair interactions by protonation.[69]

2.7.5 Bonding in $\{[(Pr^i_2PCH_2SiMe_2)_2N]Zr(OAr^*)\}_2(\mu\text{-}N_2)$

Using the INDO1/MO level, semi-empirical calculations were performed on this side-on complex using the idealized form $\{(H_3P)_2(H_2N)Zr(OH)\}_2(\mu\text{-}N_2)$, **H**, with an imposed C_2 symmetry. The relative positions of the ligands around each zirconium are within 1° of the actual parameters found in the solid state structure. When model **H** was subjected to INDO/1-MO analysis, the MOs changed considerably from those found for **F**. Most

references on page 119

importantly, the π-MO associated with the dinitrogen ligand was split into two separate MOs, which also showed some d_{π}-p_{π} type interactions with the lone-pairs of the oxygen. To evaluate the cause of this change the model **J** was constructed as follows: the bent core of model **H** was made planar and one zirconium was rotated by 180° with respect to the other and then the OH groups were replaced by chloride (Zr–Cl = 2.5Å). Model **J** now mimics model **F** and they differ only in their angle parameters associated with the zirconium and the ancillary ligands.

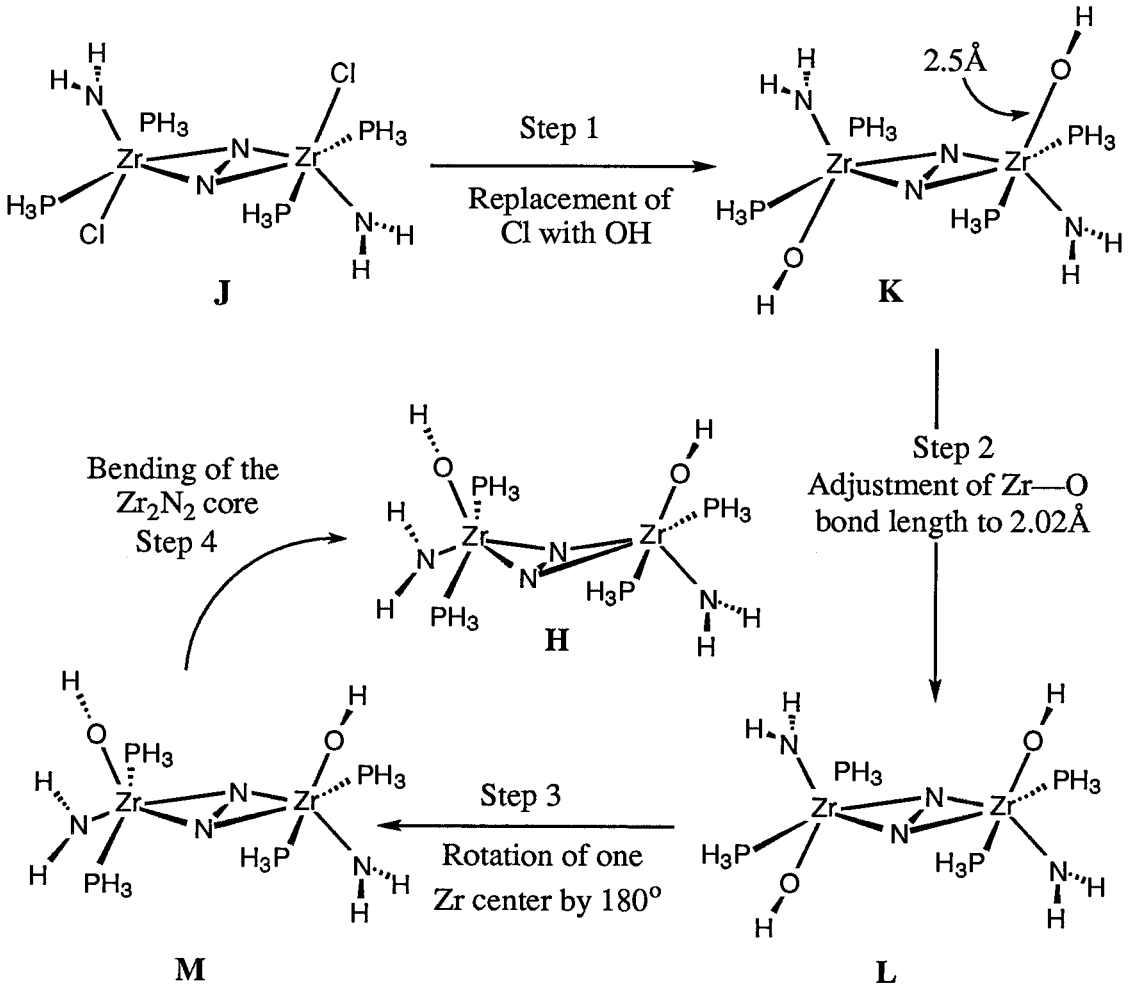

Scheme 2.9

Then model **J** was changed to model **H** in a stepwise manner, as described in Scheme **2.9**; in each case the MOs were compared to the previous case. The results of this step-wise analysis are shown in Table **2.15**. The SCF-energy values of the models **J** and **K** were within

references on page 119

0.02 eV, and the bonding interactions associated with the dinitrogen ligand, i.e., the π and the δ MOs were similar to **F**.

Table 2.15 SCF energy values and the energies of some MOs of models **H**, **J**, **K**, **L**, **M** and **F**.

Model	Energy (SCF)	δ-MO	π-MO
J	-104.070 eV	-6.830 eV (HOMO)	-10.229 eV (HOMO-9)
K	-104.046 eV	-6.640 eV (HOMO)	-10.049 eV (HOMO-7)
L	-104.597 eV	-5.924 eV (HOMO)	-9.213 eV (HOMO-3)
			-11.070 eV (HOMO-8)
M	-104.597 eV	-5.930 eV (HOMO)	-9.190 eV (HOMO-3)
			-11.001 eV (HOMO-9)
H	-104.616 eV	-6.093 eV (HOMO)	-9.019 eV (HOMO-3)
			-11.041 eV (HOMO-9)
F	-104.306 eV	-6.937 eV (HOMO)	-10.329 eV (HOMO-9)

The shortening of the zirconium-oxygen bond of **K** gave model **L**, which was stabilized by 0.6 eV than models **J** and **K**. Analyzing the contours of the MOs corresponding to **L** shows that the zirconium-dinitrogen bonding had significantly changed. The π-MO has been split into two separate MOs and their contours suggest a d_{π}-p_{π} type interaction between the zirconium orbitals and the oxygen lone-pair orbitals. These interactions are depicted in Figure **2.15**, which also qualitatively explain the relative contributions of different AOs to each MOs (also see Table **2.16**). The lower energy π-MO was largely oxygen p-orbital in character with a bonding interaction with the metal orbital. The higher energy π-MO was mainly a metal dinitrogen bonding interaction with antibonding character between the metal and oxygen orbitals. Further modifications from **L** to **H** do not seem to cause any major changes in the type of overlaps or in the total energies of the models.

references on page 119

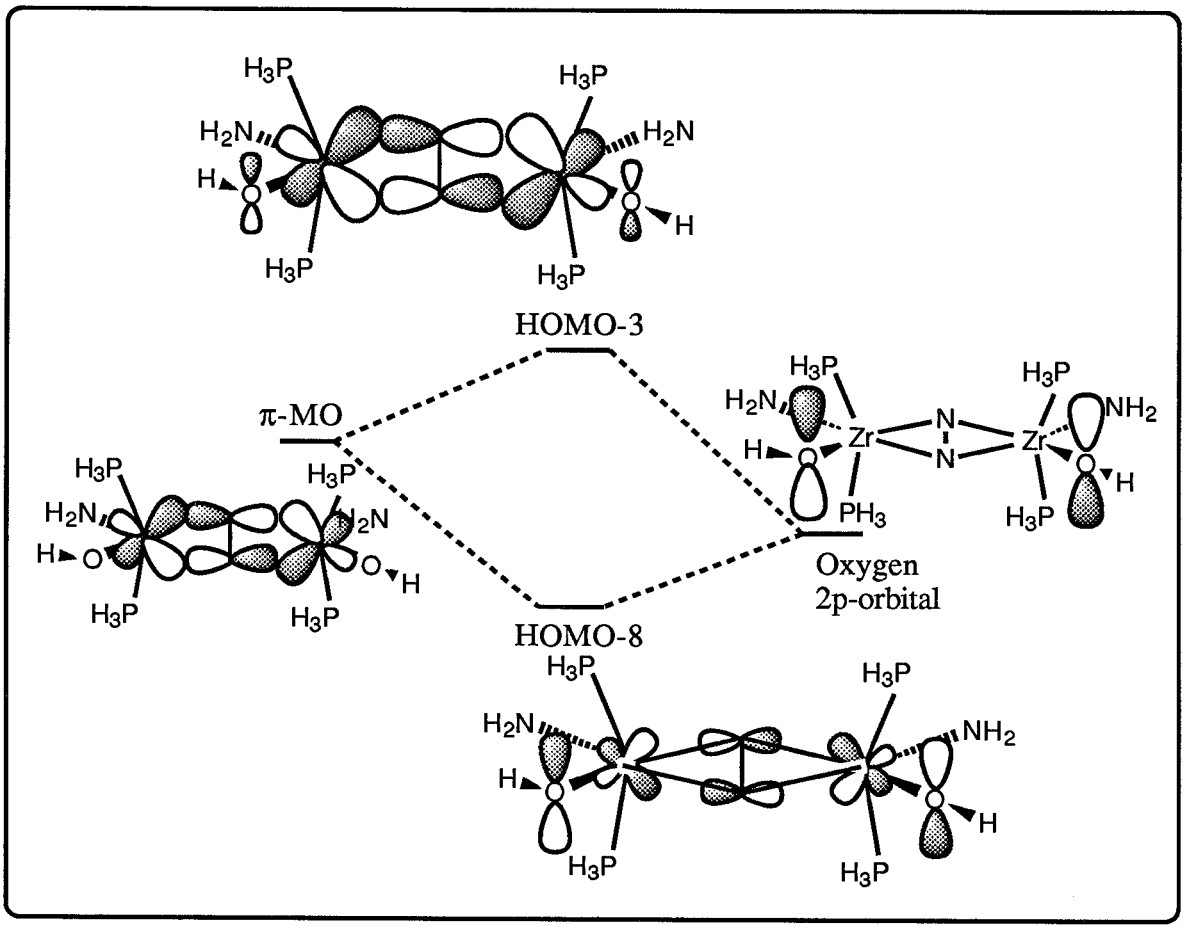

Figure 2.15 Splitting of the π-MO in complex **H**.

Table 2.16 Some orbital parameters of model **H**.

Molecular orbital	Energy (eV)	Zr d-orbital contribution per metal	N_2 p-orbital contribution per nitrogen	O p-orbital contribution per oxygen
HOMO (δ)	-6.098	9%	36% (p_x = 21%; p_y = 14%)	< 1%
HOMO-3 (π)	-9.018	17%	22% (p_y = 18%)	4%
HOMO-9 (π)	-11.041	5%	3%	31% (p_z = 23%; p_x = 8%)

references on page 119

The metal and dinitrogen orbital contributions of HOMO and HOMO-3 are similar to that in model **F** (Table **2.17**). Comparison of bond orders associated with similar bonds of models **F** and **H** show that the zirconium-amide bond and the zirconium-phosphine bonds are slightly weaker in **H** than in **F**.* A bond order of 1.16 between the zirconium-oxygen bond, comparable to the bond orders between the zirconium and nitrogens of the dinitrogen ligand, confirms the presence of p_π-d_π bonding, which was previously suggested on the basis of structural features. The bond indices associated with the Zr_2N_2 core are also comparable to model **F**. For **H**, the indices indicate a weakening of the zirconium-amide bond compared to the same indices of model **F**. This could probably be due to the increased π interactions of the oxygen lone pairs since the bond order between the zirconium and oxygen was greater than one.

Table 2.17 Wiberg bond indices and Mulliken orbital populations of model **H**.

Wiberg Bond Index		Mulliken Orbital Populations of N_2 per nitrogen		
Bond	Index	Orbital	N_2 Complex	free N_2 (N-N = 1.548 Å)
Zr—N (N_2)	1.17	s	1.85	1.937
Zr—N (NH_2)	1.07	p_x	1.25	1.063
N—N	0.87	p_y	1.22	1.000
Zr—P	0.55	p_z	1.23	1.000
Zr—O	1.16			

Alkaline salts of chloride and hydroxide ions were analyzed to estimate the relative energies of the lone-pair electrons of the anions. It was assumed that in these alkaline salts there would be no π-type interactions, and therefore this enables the estimation of the energies of the lone-pairs. Calculations suggest that the oxygen lone-pairs are relatively lower in energy than those on the chloride. Comparison of these energies with the π-MO of **F** shows that the oxygen

* The ZINDO output files gives the values of Mulliken populations and Wiberg bond indices to six significant figures.

references on page 119

lone pairs are the closest in energy (Table **18**). The calculated π overlap values for **F** were also greater for oxygen p-orbitals than those of the chloride p-orbitals* . These factors are likely to contribute towards the mixing of the π-MO with the oxygen lone pair resulting in the formation of two π-MOs. When the hydroxyl ligand of model **L** was replaced with a chloride ligand without altering the zirconium-chloride distance (2.02 Å), analysis gave almost identical results to those obtained for **L**. This could be explained on the basis of the lowering of the energy of the chloride lone pair (with the shortening of distances) and also increasing the overlap with the d-orbitals.

Table 2.18 A comparison of the energies of the lone pair electrons of Cl, NH_2 and OH ions.

Salt	Distance	Lone pair Energy (eV)	Salt	Distance	Lone pair Energy (eV)
$LiNH_2$	2.20 Å	-7.789	LiCl	2.50 Å	-8.548
LiOH	2.02 Å	-9.344	NaCl	2.50 Å	-8.793
LiCl	2.02 Å	-9.002	NaOH	2.02 Å	-9.391

The angular overlap model[92] suggests that the frontier orbital requirements for a side-on bound dinitrogen ligand with a bent core can be different from those of a planar core. With reference to the planar case depicted in Figure **2.16**, the frontier orbitals shown can only overlap with one π^*-orbital of the dinitrogen, which is also contained on the same plane, whereas the other π^*-orbital of dinitrogen is perpendicular to the plane and will require a different metal based orbital for bonding, for example see the bonding scheme for the planar side-on model **F** depicted in Figure **2.13**. It is also important to note in Figure **2.13**, that each set of frontier orbitals (i.e., the set corresponding to the π-MO and the set corresponding to the δ-MO), can have a symmetric and an anti-symmetric combination, of which only the anti-symmetric combination is involved in bonding. In the absence of bonding, i.e., in the absence of a

* Calculated overlap integerals for Zr–Cl, 2.50 Å; Zr–Cl, 2.02 Å and Zr–OH, 2.02 Å are 0.087, 0.192 and 0.110 respectivly.

references on page 119

dinitrogen ligand in between the two metal centers, these two combinations corresponding to each set will be degenerate (i.e., in Figure **2.13**). In fact, during the MO analysis of models **F** and **M** the symmetric combinations were found to be non-bonding, because they do not have a suitable dinitrogen based orbital for bonding.

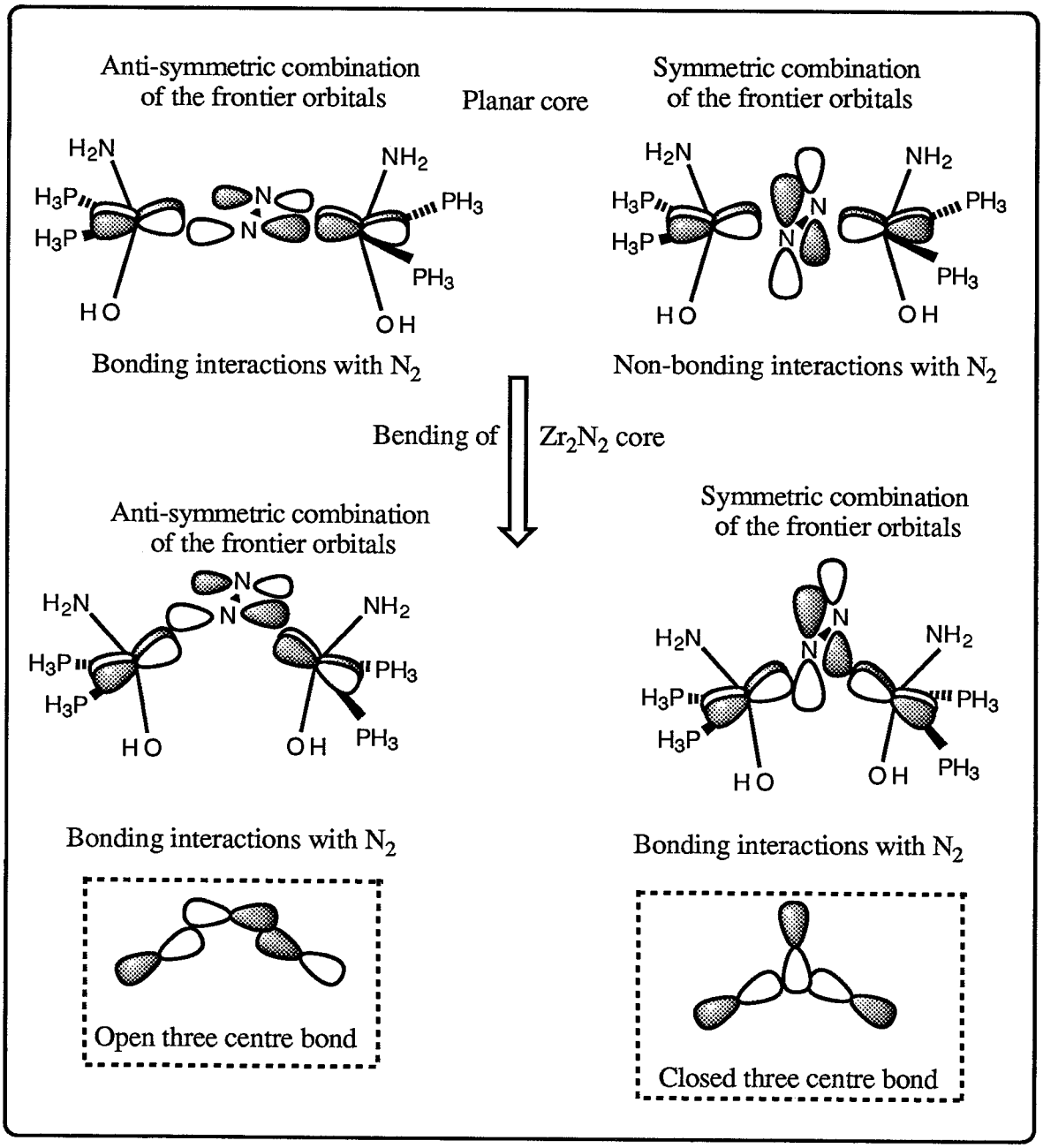

Figure 2.16 The angular overlap for the side-on bonded dinitrogen with a bent Zr_2N_2 core.

references on page 119

Figure **2.16** illustrates the bonding of a side-on bound dinitrogen ligand where the Zr_2N_2 core is bent. It can be seen that the bonding in this case can be rationalized by using only one set of frontier orbitals, where both, the symmetric and anti symmetric combinations are used in bonding with the dinitrogen ligand.[89] The interaction of the anti-symmetric combination (i.e., in the bent mode shown on the right) with the dinitrogen π^*-orbital is comparable to an open three-center bond whereas the interaction of the symmetric combination is comparable to a closed three-center bond.

To evaluate this hypothesis the model **M** was bent in a step-wise manner using the nitrogen-nitrogen bond as a hinge. To perform this calculation, a phantom atom X was placed in the middle of nitrogen-nitrogen bond and the bend angle was measured by taking the Zr–X–Zr angle, θ. Calculations were done for different models which were constructed by decreasing the Zr–X–Zr angles by approximately 5° from that of the planar case **M** (i.e., decreased from 180°), and for each case the SCF energy and the contours of 13 HOMOs (from HOMO to HOMO-12) were analyzed. The contours of the models with values of θ greater than 150° show the involvement of two different frontier orbitals (i.e., similar to the bonding described for model **H**) with the π^*-orbitals of dinitrogen. These interactions are shown in Figure **2.17**. It is important to note that the δ-interaction is weakened above the Zr_2N_2 core and is strengthen below the core. For smaller values θ, i.e., less than 120°, the contours seem to suggest the involvement of only one frontier orbital (i.e., from each metal) as described in Figure **2.16**. Because of extensive mixing of atomic orbitals during the ZINDO/1-MO analysis a more definite evaluation was not possible.

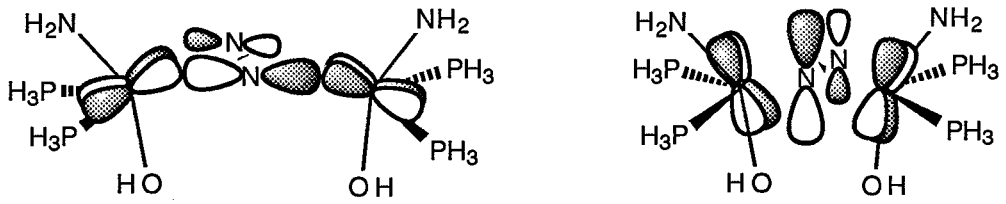

Figure 2.17 The orbital interactions for a bent Zr_2N_2 core of complex **2.12** where the bend angles are greater than 150°.

references on page 119

The change in the SCF energy values of the models with different values of θ is shown in Figure **2.18**. The curve suggests that the bending of the planar Zr_2N_2 core, even by a small angle (5°) increases the energy of the model by approximately 0.1 eV, but upon further bending the energies of the model decreases. The energies become comparable to the planar model **H** when the core is bent by about 135°. In fact, the shape of the curve suggests that continued bending produces even more stable geometries, although presumably steric factors will become dominant as the angle decreases.

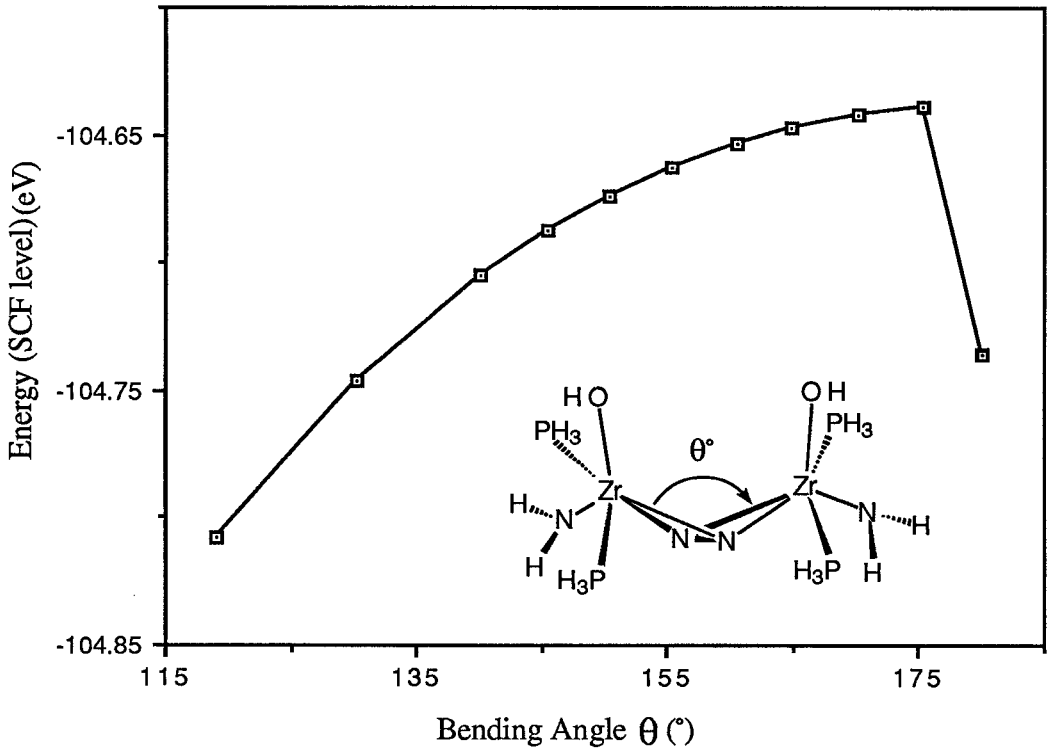

Figure 2.18 The change in SCF energy with respect to the bending of the Zr_2N_2 core of model **M**. The core was bent along the nitrogen-nitrogen axis.

2.7.6 Factors Influencing the Side-On Mode of Coordination

On the basis of the discussion presented on dinuclear dinitrogen complexes in Chapter **1** it is clear that the precedence for the formation of end-on bonded complexes is overwhelming.

references on page 119

The bonding description that has been presented so far has been mainly concerned with the analysis of the MOs of complexes **2.2**, **2.9** and **2.12** and how they relate to their structural features. So far no attempts have been made to address the question that why complexes **2.2** and **2.12** did not form the end-on complexes, despite the overwhelming experimental evidence for their formation.

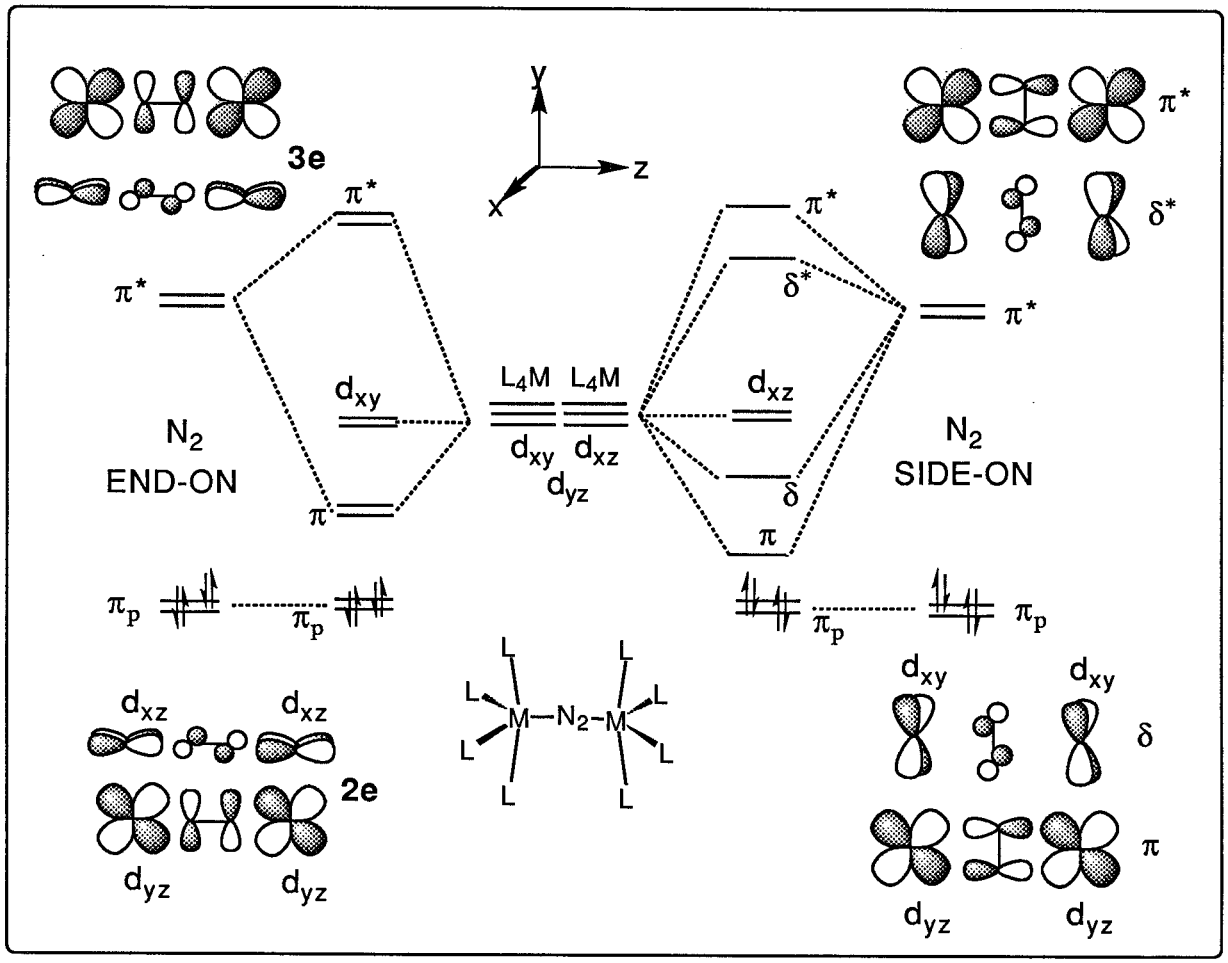

Figure 2.19 Bonding scheme illustrating the symmetry based orbital requirements for the dinitrogen binding in bridging side-on and end-on modes involving ML_4 fragments.

In an attempt to evaluate the electronic factors which favored the formation of side-on complex **2.2** a simple, back of the envelope type MO analysis was considered (Figure **2.19**). During analysis two ML_4 fragments having C_{4v} symmetry, were arranged to satisfy an overall

references on page 119

D_{4h} symmetry, with ligands pointing away from the center of metal-metal axis (Figure **2.19**). The metal-centers were separated by sufficient distance, such that a dinitrogen ligand could be inserted in an end-on or side-on manner.

The $d_{x^2-y^2}$ and d_{z^2} orbitals which point toward the ligands are used for σ-bonding with ligands L of ML_4 and also with the dinitrogen. The remaining three d-orbitals, the d_{xy}, d_{xz} and d_{yz}, pointing in between the ligands, are available for bonding.[80] Since it is already established that the π acceptor interactions of dinitrogen are the most crucial, only the bonding of π^*-orbitals of dinitrogen with the metal d-orbitals are considered.[79,90] Simple analysis shows that the end-on mode results in the formation of two degenerate π-MOs which correspond to the **2e** MOs described previously (Figure **2.10**). In the side-on mode the dinitrogen π^*-orbital in the plane of M–N_2–M will form a π-MO; however, the π^*-orbital perpendicular to the plane will form the δ-MO, with the π-MO is placed lower in energy.[90] Although this relative positioning of the MOs agree with the conventional wisdom that π-orbitals are more stable than δ-orbitals, a comparison of the π-MOs of the end-on case, **A** and the side-on case, **F** show that the π-MO of side-on is much lower in energy. A rationale for the formation of lower energy π-MOs in the side-on case is that the respective overlaps of the AOs leading to the formation of the π-MO is greater for the side-on mode than that of the end-on mode. By comparison, the overlap values calculated for the interaction of naked titanium metal with dinitrogen ligand are 0.227 and 0.155 for side-on and end-on cases respectively.[90]

In the two analyses described in Figure **2.19** only two of the three available d-orbitals are used in bonding. In the end-on case the two d_{xy}-orbitals and in the side-on case the two d_{xz}-orbitals are non-bonding. Therefore, any π-type interactions with one of these three metal d-orbitals with an appropriate ligand orbital (excluding the dinitrogen ligand) will leave only two d-orbitals available for bonding with the π^*-orbital of dinitrogen. In the case where the d_{xy} orbital is not available then only the end-on complex can be formed. If the d_{xz} or d_{yz} orbital is not available then the result would be the formation of a side-on complex.

When the HOMOs of **F** were carefully analyzed at the INDO1/MO level, the orbital HOMO-8 (Figure **2.20**) was intriguing in that one of the d-orbitals on the metal was involved in

references on page 119

π-bonding with the amide lone pair and σ-bonding with the chloride ligand. Principally, this is one of the non-bonding d-orbitals described in Figure **2.19**, which according to the symmetry based analysis can only form a π-MO. Therefore, due to the formation of HOMO-8 the remaining d-orbitals can only form one π-MO and one δ-MO resulting in the formation of the side-on complex. In the model complex **H** the d-orbital that is required for the second π-MO was π-bonded to oxygen and σ-bonded to the amide.

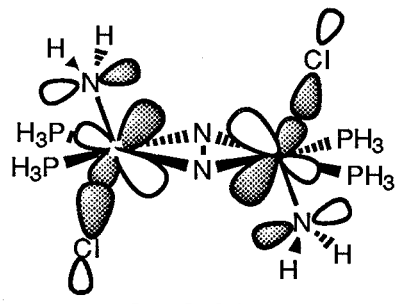

HOMO-8 in **F**

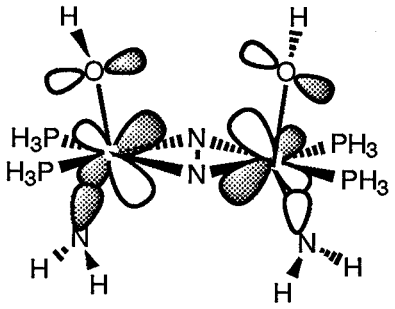

HOMO-12 in **H**

Figure 2.20 Important π-type interactions that determine the type of dinitrogen bonding in model complexes **F** and **H**.

To vindicate this claim the MOs of the fragment **G** and those of the fragment **N**, obtained by rotating the plane of the amide by 90°, were analyzed. In Figure **2.21** the fragment MOs corresponding to **G** (on the left) and those of **N** (on the right) are arranged such that their energies decrease in going from top to bottom. For both cases the set of orbitals **1a"** and **2a"** will favor the side-on mode and the set **1a"** and **1a'** will favor the end-on mode of bonding. The calculated energy for the **1a'** orbital of **G** was found to be much higher (37 kJ mol^{-1}) than the nearest orbital **2a"**. The **1a'** orbital of **G** is raised in energy partly due to the amide d_{π}-p_{π} interactions and also due to the σ interactions with the chloride ligand. Therefore, on the basis of symmetry the available orbitals that will lead to the side-on complex are **1a"** and **2a"**.

When the plane of the amide in model **G** was rotated by 90°, the model **N** was obtained. Calculations on model **N** show that, due to the removal of the d_{π}-p_{π} interactions, the orbital **1a'** was lowered in energy. Also, due to the newly imposed d_{π}-p_{π} interactions, the frontier orbital **2a"** is raised in energy. It was found that orbitals **1a'** and **2a"** were only separated by 0.5 kJ

references on page 119

mol^{-1}. Therefore **1a'** can form two sets of orbitals (i.e., **1a'** and **1a"** or **1a'** and **2a"**) which are energetically similar, where each set will lead to different mode of bonding. The case leading to the end-on mode will generate two π-MOs, while the other will generate a π-MO and a δ-MO, where the formation of two π-MOs will be energetically more favorable. Therefore in theory the fragment **N** should lead to an end-on complex.

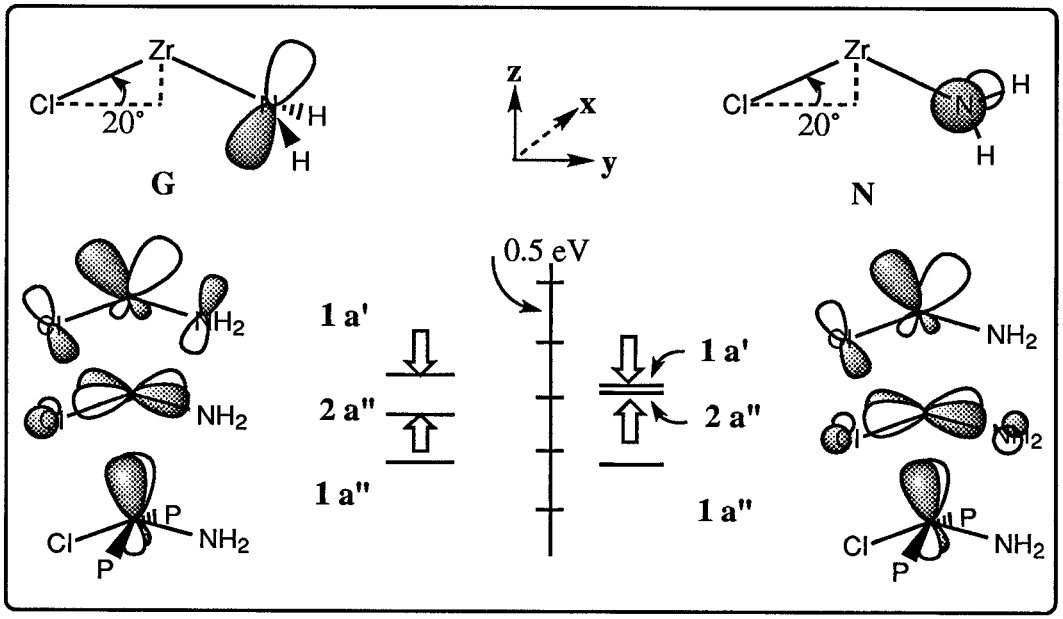

Figure 2.21 The frontier orbitals of the fragments **G** and **N** arranged in increasing order of their energy

Support for this analysis can be found in two recent X-ray structures of related isoelectronic dinuclear titanium dinitrogen complexes, shown in **2.27** and **2.28**, both of which display the bridging end-on mode.[57,58] In **2.27**, having cis disposed neutral amine donors rather than trans disposed phosphine ligands, the major difference is that the bis(trimethylsilyl)amide ancillary ligand is arranged perpendicular to the plane defined by the donor atoms; this is also found in **2.28** but now the neutral pyridine donors are trans disposed. Both of these complexes are similar to that proposed in model conformer **N** and their structures are a reasonable consequence of the fact that both **2.27** and **2.28** have no conformational restrictions to force the

references on page 119

amide ligand to bond in a manner as is found in the chelating amido-diphosphine ligand of the side-on derivative **2.2**.

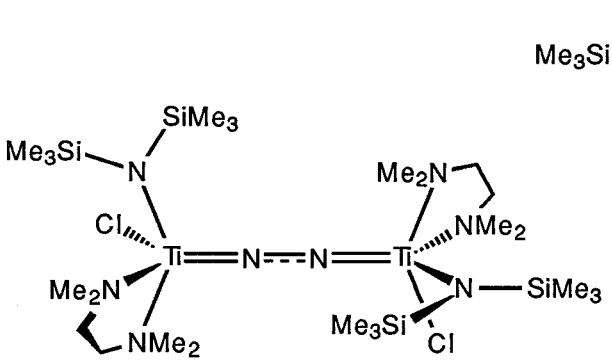

2.27

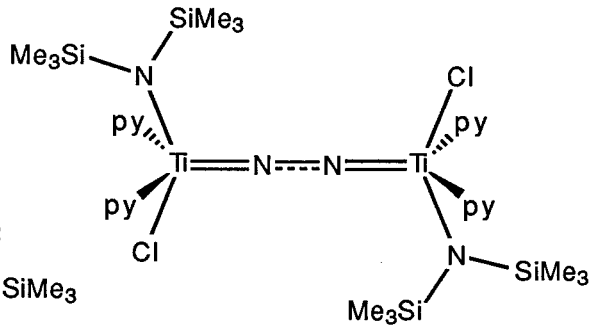

2.28

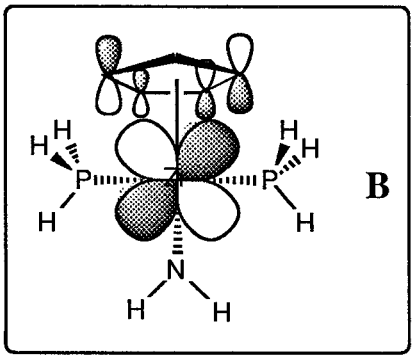

B

This rationale could be also extended to explain the formation of the end-on complex **2.9**. The replacement of the chloride ligand of **2.2** by a cyclopentadienyl group has altered the available d-orbitals for dinitrogen bonding. Analysis of the molecular orbitals of the fragment **B** shows that the d-orbital that would be used to generate the δ-molecular orbital for a side-on dinitrogen fragment overlaps with the π-orbitals of the cyclopentadienyl ligand. Also an important structural feature that correlates well with the electronic description is the zirconium amide bond distances. Since the fragment orbital that has the correct symmetry to overlap with the amide p-orbital is involved in π-bonding with the dinitrogen ligand, one would expect a long zirconium amide bond length (see section **2.2.2**). It is noteworthy that in the solid-state structure, the NSi_2 plane in the tridentate ligand is twisted with respect to the plane of the three donors (NP_2) and this would be expected to further minimize overlap between the lone pair on the amide and the d orbital.

references on page 119

2.7.7 Bonding in the Samarium and Lithium Dinitrogen Complexes

The dinuclear samarium and lithium dinitrogen complexes discussed in Chapter **1** have a very weak, side-on bound dinitrogen ligand.[93,94] This is in stark contrast to the side-on dinitrogen complexes of zirconium where the dinitrogen ligand is highly activated and is strongly bound to the metal. For comparative reasons some suggestions can be made with regard to the weak bonding interactions of the samarium complex, **1.12**, and the lithium derivative, **1.13**.

To understand the origin of molecular interactions in electron donor-acceptor complexes (e.g., $H_3N{\rightarrow}BH_3$), the total interaction energy of these complexes can be decomposed into five components; electrostatic (ES), polarization (PL), exchange repulsion (EX), charge transfer (CT) and coupling (MIX).[95] This *ab initio* SCF method has been extended to the donor-acceptor interactions of a dinitrogen ligand with a transition metal, for example, in the complex $[Ru(NH_3)_5(N_2)]^{2+}$ having the dinitrogen end-on, the calculated energy for the metal dinitrogen interaction was -15.52 eV of which -0.68 eV has been attributed to the ES interaction, whereas for the side-on mode of bonding, the calculated energy for the metal dinitrogen bond was -18.64 eV of which -1.15 eV has been attributed to the ES interaction.[87,88]

It is therefore possible that in the samarium and lithium complexes **1.12** and **1.13** the primary interaction between the dinitrogen and the metals is weakly electrostatic in nature. On the basis of this assumption, the bonding in these complexes can be compared to the bonding in dilithioacetylide, Li_2C_2 where the interactions between the lithium and the acetylide are ionic in nature. X-ray structure analysis and theoretical studies done on dilithioacetylide have shown that the favored mode of coordination is side-on: $Li_2(\mu\text{-}\eta^2\text{:}\eta^2\text{-}C_2)$.[29,30] Therefore, in complexes **1.12** and **1.13** if the metal dinitrogen interactions are mainly ionic in nature the favored mode of dinitrogen coordination could be side-on. However, it is important to note that the mode of dinitrogen coordination in the solution state has not been determined for these complexes. Also, in the case of the lithium complex it has been suggested that the solid state structure could be attributed to solid state effects.[94]

references on page 119

2.8 Reactions

2.8.1 Conversion of the Side-On Complex to the End-On Complex

When the side-on complex **2.2** was reacted with NaCp•DME in THF the deep blue colour of the solution changed to give a deep brown solution over a period of 1 week. The ^{1}H and $^{31}P\{^{1}H\}$ NMR spectra of the final product showed only the presence of the end-on derivative **2.9** (Equation **2.2**). Monitoring the reaction shown in Equation **2.2** by NMR spectroscopy showed only the depletion of the side-on complex **2.2**, and concomitant formation of the end-on derivative, **2.9**. This seems to suggest that the mono cyclopentadienyl intermediate formed by the metathesis of only one zirconium-chloride bond of **2.2** is rapidly converted to the bis cyclopentadienyl derivative **2.9**.

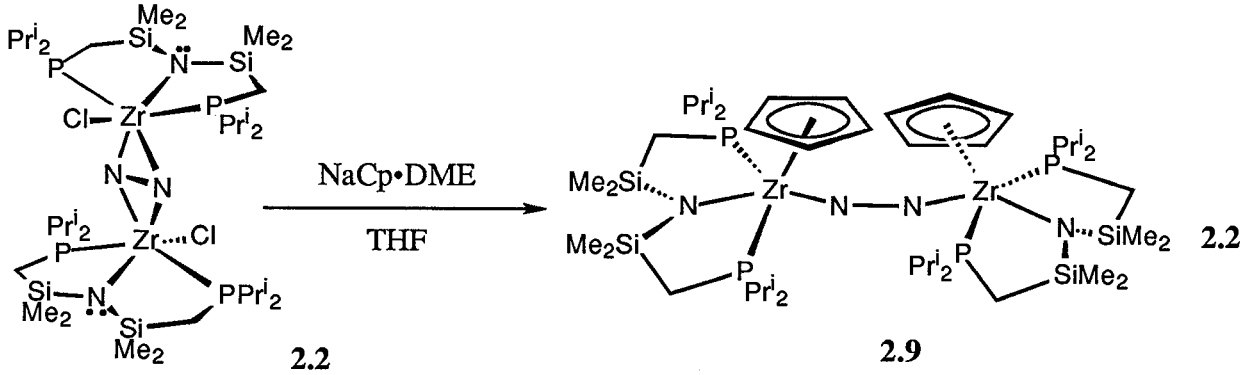

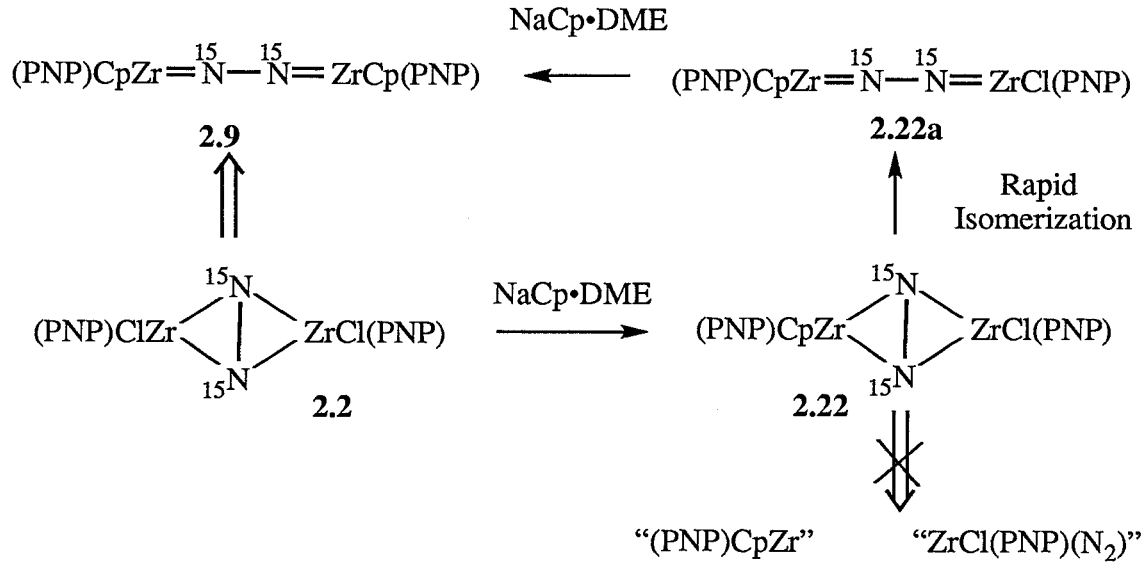

Scheme 2.10

references on page 119

One possible mechanistic proposal for the reaction shown in Equation **2.2** is given in Scheme **2.10**. The elusive mono cyclopentadienyl intermediate, $\{[(Pr^i_2PCH_2SiMe_2)_2N]Zr\}_2$-ClCp($\mu$-$N_2$) **2.22**, could dissociate into mononuclear zirconium species and then recombine to form complexes **2.2** and **2.9**. In accordance with this postulate, before or during the recombination of the monomers the coordinated dinitrogen may be exchanged with free dinitrogen from the surroundings.

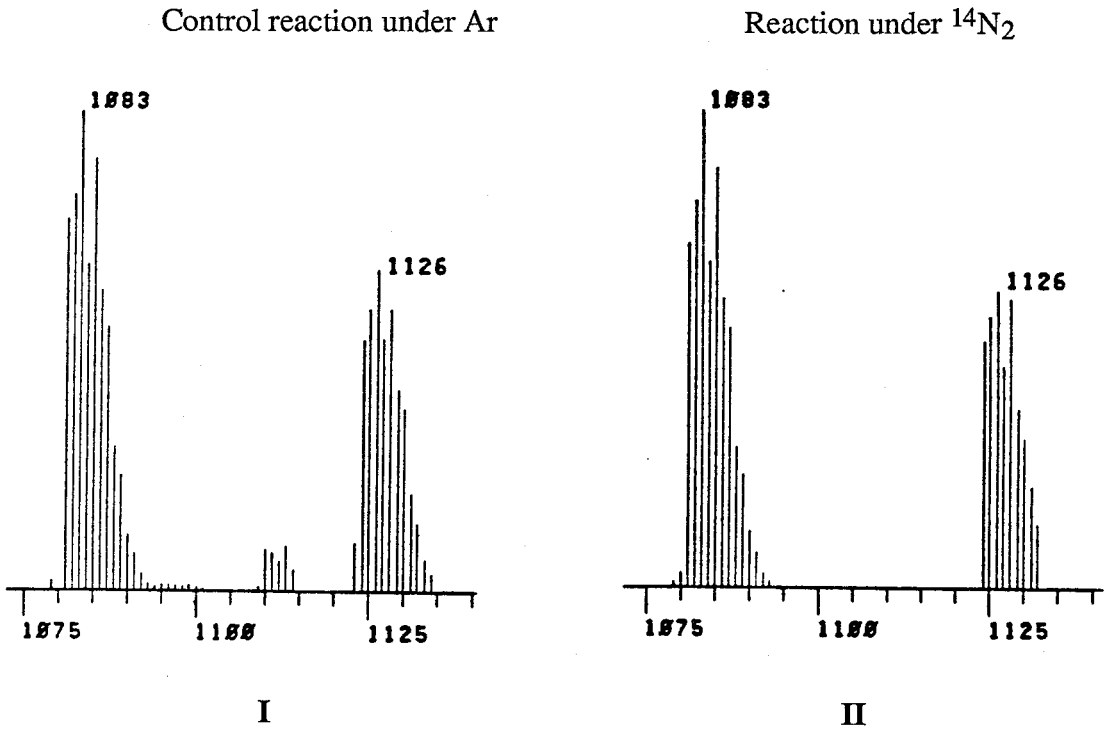

Figure 2.22 **I** The parent ion peaks of the $^{15}N_2$ analogue of **2.9**. **II** Parent ion peaks of **2.9** formed from the reaction of $^{15}N_2$ analogue of **2.2** with NaCp•DME under an atmosphere of $^{14}N_2$.

Aforementioned hypothesis was tested by performing the reaction with the nitrogen-15 labelled material of **2.2**, under an atmosphere of normal dinitrogen ($^{14}N_2$). When the product of this reaction was analyzed by mass spectroscopy, the relative intensities of the peaks associated with the parent ions were virtually identical to the parent ion peaks found for an authentic sample of the $^{15}N_2$ analogue of complex **2.9** (Figure **2.22**). This experiment suggests that there

references on page 119

is no exchange between the coordinated dinitrogen and the dinitrogen from the surroundings. Therefore, it is possible that the side-on bound dinitrogen ligand in the intermediate **2.22** rotates in an intramolecular fashion to give an end-on intermediate **2.22a** (Scheme **2.10**). Also, the end-on isomer **2.22a** is sterically less hindered than the side-on isomer, **2.22**, and therefore kinetically more favored to react with the second equivalent of NaCp•DME to give complex **2.9**.

2.8.2 Reaction of Side-On Complexes With $LiBEt_4$

Earlier work in our laboratory has shown that in the case of the dinuclear palladium complex **2.23** the $Pd_2(\mu\text{-}H)_2$ core interacts with a $LiBEt_4$ unit, where the lithium ion is found sandwiched between the borate moiety and the $Pd_2(\mu\text{-}H)_2$ core.[96] It is postulated that the interaction between the $Pd_2(\mu\text{-}H)_2$ core and the lithium cation is a Lewis acid, Lewis base type. By comparison, complex **2.2** has a planar Zr_2N_2 core, with considerable negative charge on the nitrogen atoms. Therefore reacting complex **2.2** and $LiBEt_4$ may lead to the synthesis of a complex that would resemble **2.23**, for example a complex having a core similar to **T**. Furthermore, an X-ray structure elucidation of such an adduct of $LiBEt_4$ could provide some experimental evidence for the suggestion that the very long nitrogen-nitrogen bond length of **2.2** is partly attributed to the higher charge densities on the nitrogens of the dinitrogen ligand.

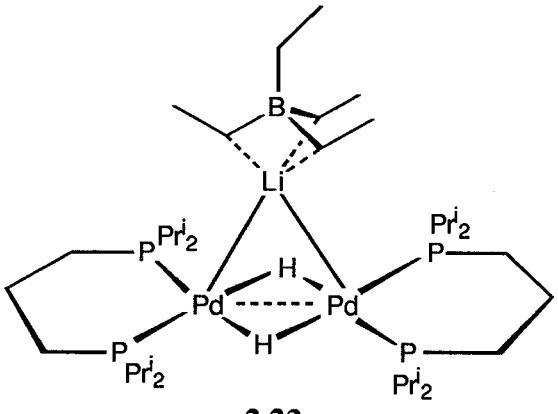

2.23

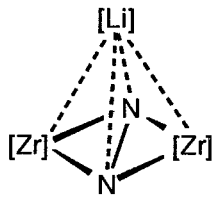

T

[Li] = $LiEt_4B$

[Zr] = "$ZrX[N(SiMe_2CH_2PPr^i_2)_2]$ where X = Cl or OAr^*

Reacting the side-on derivative, **2.2** with $LiBEt_4$ in toluene over a period of 7 days gave a yellow solution. The $^{31}P\{^1H\}$ NMR spectrum of the yellow material had a spectral pattern

references on page 119

which is consistent with an ABMX spin system (Figure **2.23**). The $^{1}H\{^{31}P\}$ NMR spectrum consists of 8* resonances in the $SiMe_2$ region, which implies that the complex is an unsymmetrical dimeric species. The resonance at 4.81 ppm is attributed to a hydride ligand. The multiplet at 0.03 ppm is probably an overlapping doublet of quartets with small coupling to phosphorus nuclei. This suggest that the peak at 0.03 ppm probably corresponds to one of the methylene protons of an ethyl ligand, and the other methylene proton is probably beneath the $SiMe_2$ resonances. The ^{15}N NMR spectrum has two doublets centered at 250.5 ppm and 185.9 ppm, with $^{2}J_{N\text{-}N}$ = 12 Hz. The $^{11}B\{^{1}H\}$ NMR spectrum has a broad resonance** centered around -41.6 ppm. On the basis of the aforementioned spectroscopic evidence the complex can be formulated as $\{\{[(Pr^{i}_2PCH_2SiMe_2)_2N]ZrH\}\{[(Pr^{i}_2PCH_2SiMe_2)_2N]ZrEt\}\}(\mu\text{-}N_2{\bullet}BEt_3)$, **2.24.**

The reaction of $LiBEt_4$ with other side-on derivatives, **2.12**, **2.20** and **2.21** also gave a yellow material which had identical spectral features to that of **2.24**. This seems to suggest that during the reaction the zirconium-X bond, where X = Cl, Br or OAr*, undergoes a metathesis reaction to give a diethyl intermediate, "$\{[(Pr^{i}_2PCH_2SiMe_2)_2N]ZrEt\}_2(\mu\text{-}N_2)$" where one of the ethyl group undergoes a β-hydride elimination reaction. Monitoring the reaction (inside a sealed NMR tube) by ^{1}H and $^{31}P\{^{1}H\}$ NMR spectroscopy failed to provide any useful information; however, the ^{1}H NMR spectrum showed the formation of ethylene. Also, the presence of free Et_3B in the $^{11}B\{^{1}H\}$ NMR suggests that only one of the BEt_3 is associated with the complex **2.24**.

---

* One of the methyl group of a $SiMe_2$ seems to have shifted into the region where the isopropyl methyl resonances appear. By comparison with the ^{1}H and $^{1}H\{^{31}P\}$ NMR spectra the resonance at 0.95 ppm was assigned to one methyl group of a $SiMe_2$ moiety.

** The broad resonances due to the glass of the NMR tube also appears from -20 to -140 ppm. The peak at -41.6 was found by subtracting the spectra due to the glass.

references on page 119

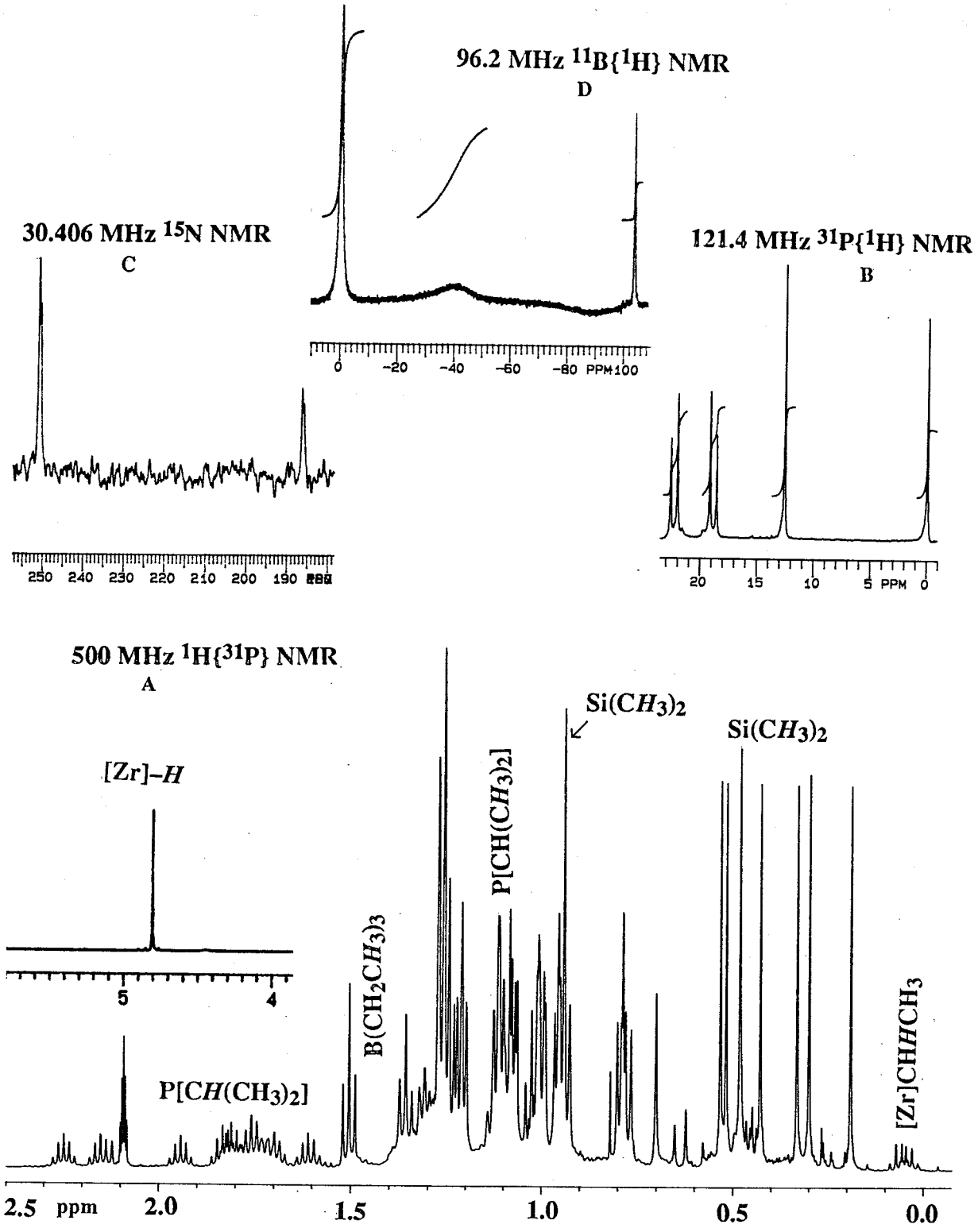

Figure 2.23 **A** The 500 MHz $^1H\{^{31}P\}$ NMR; **B** 121.4 MHz $^{31}P\{^1H\}$ NMR; **C** 30.406 MHz ^{15}N NMR and **D** 96.2 MHz $^{11}B\{^1H\}$ NMR spectra of the crude reaction mixture obtained from the reaction of **2.2** and $LiBEt_4$ in C_7D_8.

references on page 119

The ^{15}N NMR chemical shifts of the nitrogens of the dinitrogen ligand are centered around 250.5 and 185.9 ppm, which by comparison with the side-on complexes are shifted by more than a 100 ppm. Also, comparison of the chemical shifts of the two nitrogens, which are separated by 65 ppm, suggests that the BEt_3 is probably interacting with one of the nitrogens of the dinitrogen ligand. In the $^{31}P\{^1H\}$ NMR spectrum the two high field singlet resonances are probably due to a PNP ligand that is facially coordinated*, whereas the two low field doublets are due to a meridionally coordinated PNP ligand where the observed coupling constant $^2J_{A\text{-}B}$ = 72 Hz is comparable to other zirconium complexes containing a meridional PNP ligand.[15] The structure depicted as **2.24** seems to fit most of the NMR spectroscopic data.

A structure involving an η^2-dinitrogen ligand, **2.24a** with one of the nitrogens interacting with BEt_3 is also possible. The coordination around the dinitrogen ligand in **2.24a** is comparable to the tetranuclear titanium dinitrogen complex **1.9**. Although the complex **2.24** gave good crystals at -40 °C, upon warming to room temperature they melted, which hampered attempts to obtain an X-ray structure.

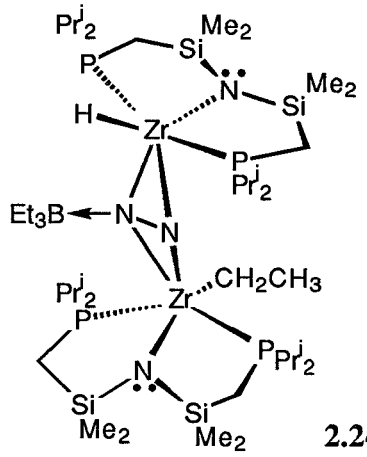

2.24

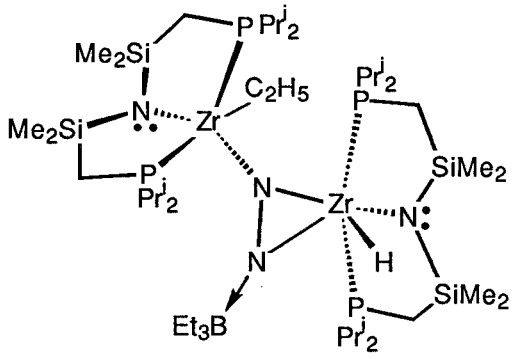

2.24a

* The chemical shift for uncoordinated phosphine is usually between -4.5 and -4.8 ppm. It is believed that facial coordination of the PNP ligand with isopropyl substituents is not sterically favored. However, it could approach facial coordination by lengthening the zirconium-phosphorus bond which would enable the bulky isopropyl substituents to be further away. Therefore, the $^{31}P\{^1H\}$ NMR chemical shifts of such phosphines are also likely to shift towards that of the uncoordinated phosphines.

references on page 119

2.8.3 Protonation Reactions

When a toluene solution of **2.9** was reacted with anhydrous HCl gas 1 equivalent of hydrazine was produced. By comparison, the side-on derivative **2.2** also gave 1 equivalent of hydrazine under similar conditions. However, when the end-on derivative **2.9** was reacted with 1M $HCl_{(aq)}$ or with water, approximately 0.8 equivalents of gas was produced, and a qualitative test of the aqueous solutions after the reaction showed the presence of hydrazine. Also, when **2.9** was decomposed with D_2O inside a NMR tube, the ^1H NMR spectrum showed the formation of only a small amount of cyclopentadine (< 2%), suggesting that the hydrolysis of the zirconium-Cp bonds is minimal during protonation in aqueous media.* The gaseous mixture probably consists mainly of dinitrogen and dihydrogen in approximately a 1:1 ratio. When complex **2.9** is decomposed to give dinitrogen it would also generate a zirconium(II) species which, under aqueous conditions, is likely to reduce hydrogen ions to dihydrogen (Scheme **2.11**). Therefore depending on the strength of the acid, complex **2.9** could either give only hydrazine, or a mixture of hydrazine, dinitrogen and dihydrogen.

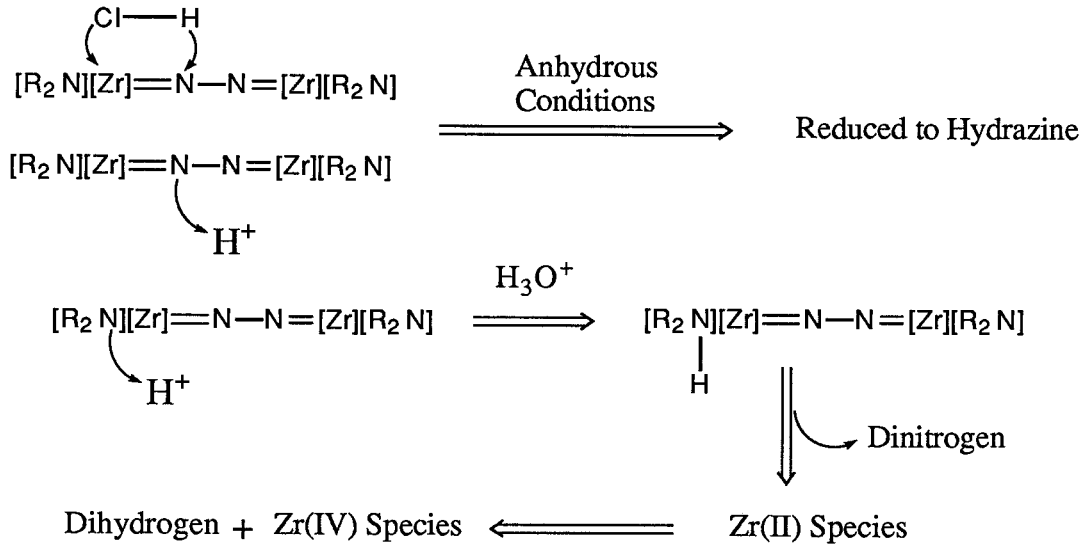

Scheme 2.11

* This reaction was done to show that the amount of gas measured did not contain any volatile cyclopentadiene.

references on page 119

Under anhydrous conditions and in a non-polar solvents like toluene, HCl acts as a weak acid,*[97] and therefore is likely to react at the most basic site of the molecule which is probably the reduced dinitrogen ligand, $(N_2)^{4-}$. The reaction in toluene can also be envisaged as an addition of HCl across the zirconium-dinitrogen bonds (Scheme **2.11**). Under aqueous conditions the strength of HCl is many orders of magnitude greater than its strength in toluene and therefore protonation at different sites of the complex becomes possible. When a C_7D_8 solution of **2.9** was reacted with pyridinium hydrochloride inside a sealed NMR tube, the $^{31}P\{^1H\}$ NMR spectrum showed a clean conversion of **2.9** to the uncoordinated amine of PNP, and no signals were found around 4 ppm that would correspond to hydrazine. This observation suggests that the protonation probably takes place at the nitrogen of the amide ligand which in turn could result in the decomposition of the complex.

Table 2.19 A compilation of chemical shifts of NH protons associated with hydrazido ligands.

Compound	δ (NH) ppm	references
$Cp^*Me_3W{=}NNH_2$	4.48	98
$Cp^*Me_3W{=}NNH(SiMe_3)$	5.12	98
$[Cp^*Me_3W{=}NNHLi]_x$	6.10	98
$[Cp^*Me_3W{=}NNH]_2ZrCp_2$	7.81	98
$Cp^*Me_3W{=}NNH(ZrCp_2Me)$	8.03	98
$[W(C_5Me_4Bu^t)(CCMe_3)Cl]_2(\mu\text{-}\eta^1{:}\eta^1NHNH)$	10.7	99,100
$W(NPh)Me_3]_2(\mu\text{-}\eta^1{:}\eta^1NH_2NH_2)(\mu\text{-}\eta^2{:}\eta^2NHNH)$		47
$\mu\text{-}\eta^1{:}\eta^1NH_2NH_2$	4.26	
$\mu\text{-}\eta^2{:}\eta^2NHNH$	5.70	

When the side-on complex **2.2** was reacted with pyridinium hydrochloride in C_7D_8 the $^{31}P\{^1H\}$ NMR spectrum showed the presence of one intermediate, **2.25** (amounts to approx.

* The K_a for the dissociation of HBr in CH_3CN solvent was found to be 3.16×10^{-6}.
$HBr + CH_3CN = CH_3CNH^+ + Br^-$.

references on page 119

30%) along with the trichloro complex **2.1** (20%) and the uncoordinated amine of the ligand PNP, [($Pr^i_2PCH_2SiMe_2)_2NH$] (40%). Repeating the reaction with the $^{15}N_2$ analogue of **2.2** the ^1H NMR spectra showed that the resonance at 4.99 ppm was split into a doublet ($^2J_{N-H}$ = 59.7 Hz), suggesting that the intermediate has a hydrazido type ligand, $(N_2H_x)^{n-}$. Comparison of the chemical shifts (Table **2.19**) of different types of hydrazido ligands suggest that the peak at 4.99 ppm probably corresponds to a hydrazido ligand of the type, $(NNH_2)^{2-}$.

The mononuclear structures, for example **2.25a** are excluded on the basis of the integration of $(NNH_2)^{2-}$ protons with respect to the $SiMe_2$ resonances. The structure depicted in **2.25** (Scheme **2.12**) is proposed for the intermediate which has a bridging hydrazido $(N_2H_2)^{2-}$ ligand. Although the structure is drawn with an overall C_2 symmetry, a fluxional process that would enable the chloro ligands trans to the amide nitrogen to exchange positions would give a time averaged C_{2v} symmetry to the molecule. This would be consistent with a broad $^{31}P\{^1H\}$ NMR signal and two singlets for the $SiMe_2$ groups in the ^1H NMR spectra.

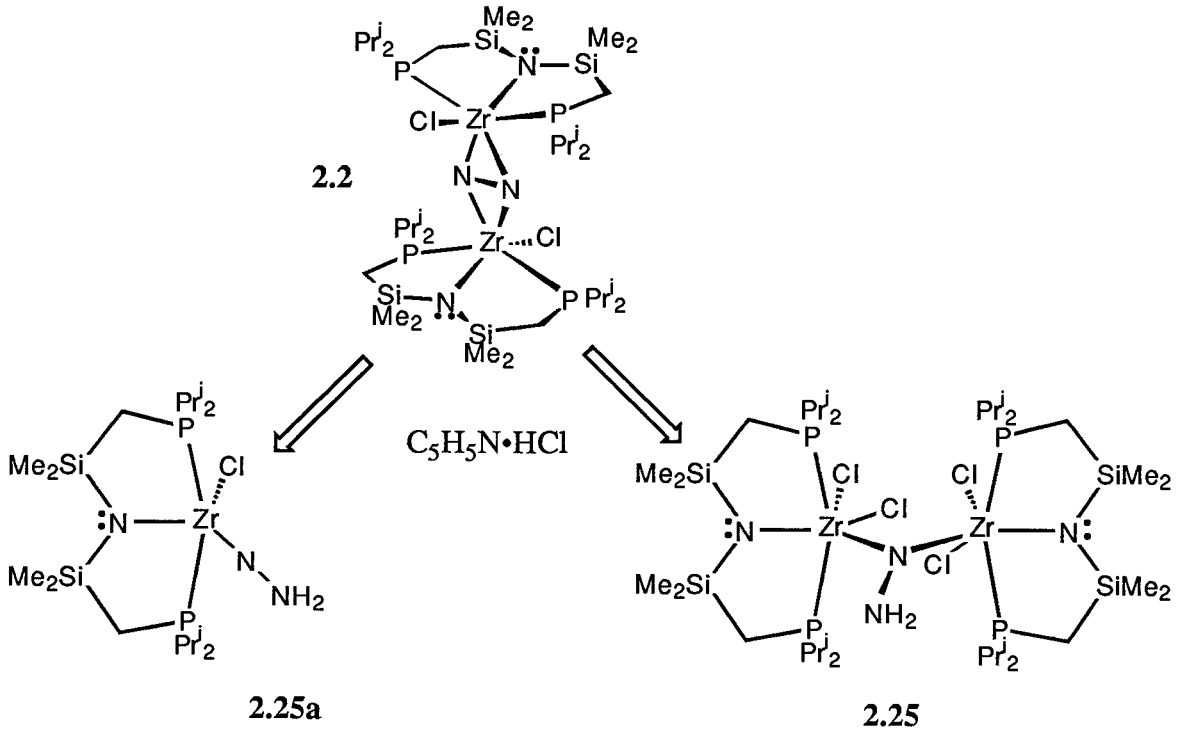

Scheme 2.12

references on page 119

2.8.4 Reactions With Halo Alkanes

Although the chemistry associated with dinitrogen is mainly directed towards the protonation of the coordinated dinitrogen ligand, occasionally attention has been focused towards incorporating nitrogen from dinitrogen into organic molecules. Reactions involving N_2 complexes and alkyl or aryl halides have led to the synthesis of alkyl or aryl amines.[101,102] Recently, molecular nitrogen has been incorporated into N-heterocycles by using titanium and palladium as catalysts.[103]

In some instances, the reactivity of the coordinated dinitrogen has been helpful in understanding the nature of metal-dinitrogen interactions, e.g., some tantalum dinitrogen complexes react with ketones to form hydrazones, where the (formulated) Ta=N—N=Ta unit has been transformed into R_2C=N—N=CR_2.[49]

2.8.4a Reactions of the End-On Complex With BzBr and CH_3I

When the reactivity of **2.9** was investigated with CH_3I or $C_6H_5CH_2Br$ (BzBr), even under carefully controlled conditions, a complex mixture of products was obtained. On the basis of $^{31}P\{^1H\}$ NMR spectral analysis the only identifiable product was the dihalide derivative of $ZrCpX_2[N(SiMe_2CH_2PPr^i_2)_2]$ (X = Br or I), which corresponds to a resonance around 15 ppm. Fortunately, when the reaction of **2.9** with approximately 1 equivalent of BzBr was monitored by variable temperature $^{31}P\{^1H\}$ NMR spectroscopy from -78 °C to room temperature, the formation of two products was observed. The crude material from the reaction of **2.9** with BzBr consisted of three compounds: $ZrCpBr_2[N(SiMe_2CH_2PPr^i_2)_2]$ **2.7**, the intermediate **2.26**, along with some unreacted **2.9** (Figure **2.24**). Persistent attempts, by repeated fractional crystallization, eventually led to the isolation of the intermediate **2.26** as pale yellow crystals. Elemental analysis of this intermediate was consistent with a product formed by the addition of one equivalent of BzBr to the dimer **2.9**. It was found that in solution the intermediate **2.26** slowly reacts to give the end-on complex **2.9** and other unidentified products.

references on page 119

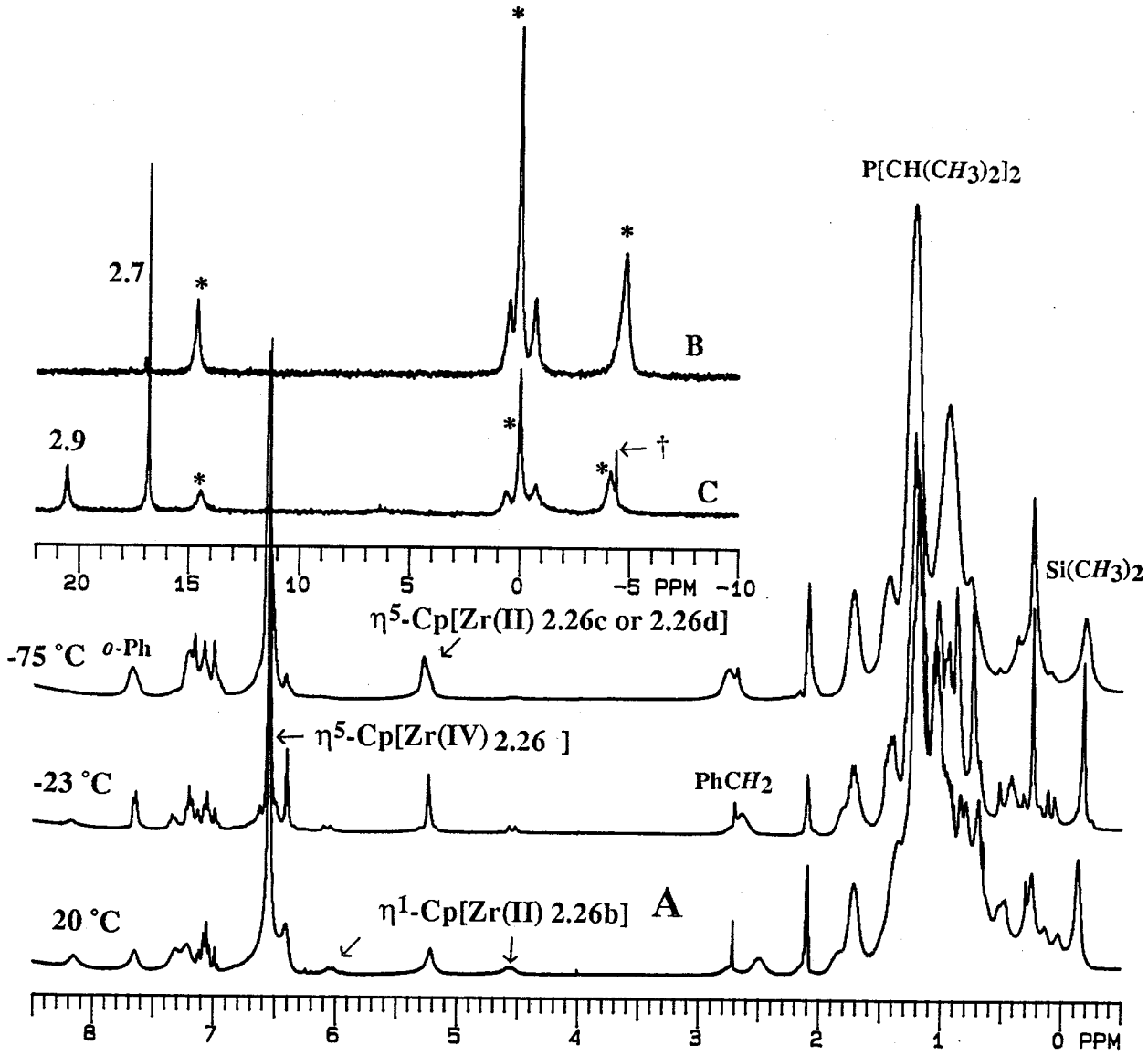

2.7 $ZrCpBr_2[N(SiMe_2CH_2PPr^i_2)_2]$

2.9 $\{[(Pr^i_2PCH_2Me_2Si)_2N]ZrCp\}_2(\mu\text{-}N_2)$

* 2.26

† (PNP)H

Figure 2.24 **A** Variable temperature ^1H NMR spectra (300 MHz) of complex **2.26** recorded in C_7D_8. **B** and **C** are $^{31}P\{^1H\}$ NMR (121 MHz) spectra of **2.26** and of the crude reaction mixture obtained from the reaction of **2.9** and $PhCH_2Br$.

references on page 119

The complexity of the variable temperature ^1H and $^{31}P\{^1H\}$ NMR spectra of **2.26** is consistent with the presence of more than one isomer in solution, and also that these isomers interconvert with one another. The $SiMe_2$ resonances in the ^1H NMR spectrum were too broad to be interpreted. However, some of the resonances associated with the Cp ligand were informative. The appearance of two broad doublets at 6.05 and 4.65 ppm were assigned to the olefinic protons of an η^1-Cp ligand. The variable temperature ^1H NMR spectra show that the resonances associated with the η^1-Cp ligand decrease in intensity with a concomitant increase of the peak at 5.22 ppm. This spectral feature could be due to the Cp ring-slip between a η^1 and η^5 coordination, where the latter corresponds to the resonance at 5.22 ppm. Comparison of the ^1H NMR chemical shifts of the Cp ligand in zirconium(IV) PNP derivatives, which appear around 6 ppm, the peak at 5.22 ppm is significantly shifted to higher field. In fact, in the zirconium(II) dicarbonyl complex, $Zr(\eta^5\text{-}C_5H_5)(CO)_2[N(SiMe_2CH_2PPr^i_2)_2]$, the resonances due to Cp appear at 4.7 ppm.

The fluxional process shown in Scheme **2.13** can rationalize some of the spectral features of intermediate **2.26**. The species **2.26a** is generated by the addition of one BzBr unit across one of the zirconium-nitrogen bonds of the Zr_2N_2 core, which probably undergoes rapid isomerization to give other species. The species depicted as **2.26b**, **2.26c** and **2.26d** are generated by incorporating a zirconium(II) fragment, "$ZrCp[N(SiMe_2CH_2PPr^i_2)_2]$" into a benzyldiazinide $(PhCH_2N{=}N)^{-1}$ ligand of a zirconium(IV) monomer, "$ZrCpBr(N{=}NCH_2Ph)$-$[N(SiMe_2CH_2PPr^i_2)_2]$". All of the structural types associated with the benzyldiazinide ligand have precedence in the literature.[104,105] The intermediates **2.26a** and **2.26b** are formulated as Zr(IV)-Zr(IV) complexes whereas **2.26c** and **2.26d** are formulated as Zr(II)-Zr(IV) complexes. In **2.26b** one of the zirconium centers has a Cp ligand bound in an η^1 fashion and also interacts with the diazinide ligand in an η^2 fashion.[106] Of the two Zr(II)-Zr(IV) complexes **2.26d** is sterically more congested than **2.26c** and could dissociate into Zr(II), "$ZrCp[N(SiMe_2$-$CH_2PPr^i_2)_2]$" and zirconium(IV), "$ZrCpBr(N{=}NCH_2Ph)[N(SiMe_2CH_2PPr^i_2)_2]$" monomers. The former, in the presence of dinitrogen, may proceed to form the end-on dinitrogen complex **2.9** whereas the latter is probably unstable and undergoes decomposition. It is important to note

references on page 119

that in Scheme **2.13** all of the intermediates are drawn with phosphine donors coordinated, but each case can involve reversible dissociation of the phosphine donors. Such a process would explain the broad resonances observed in the $^{31}P\{^{1}H\}$ NMR spectrum.

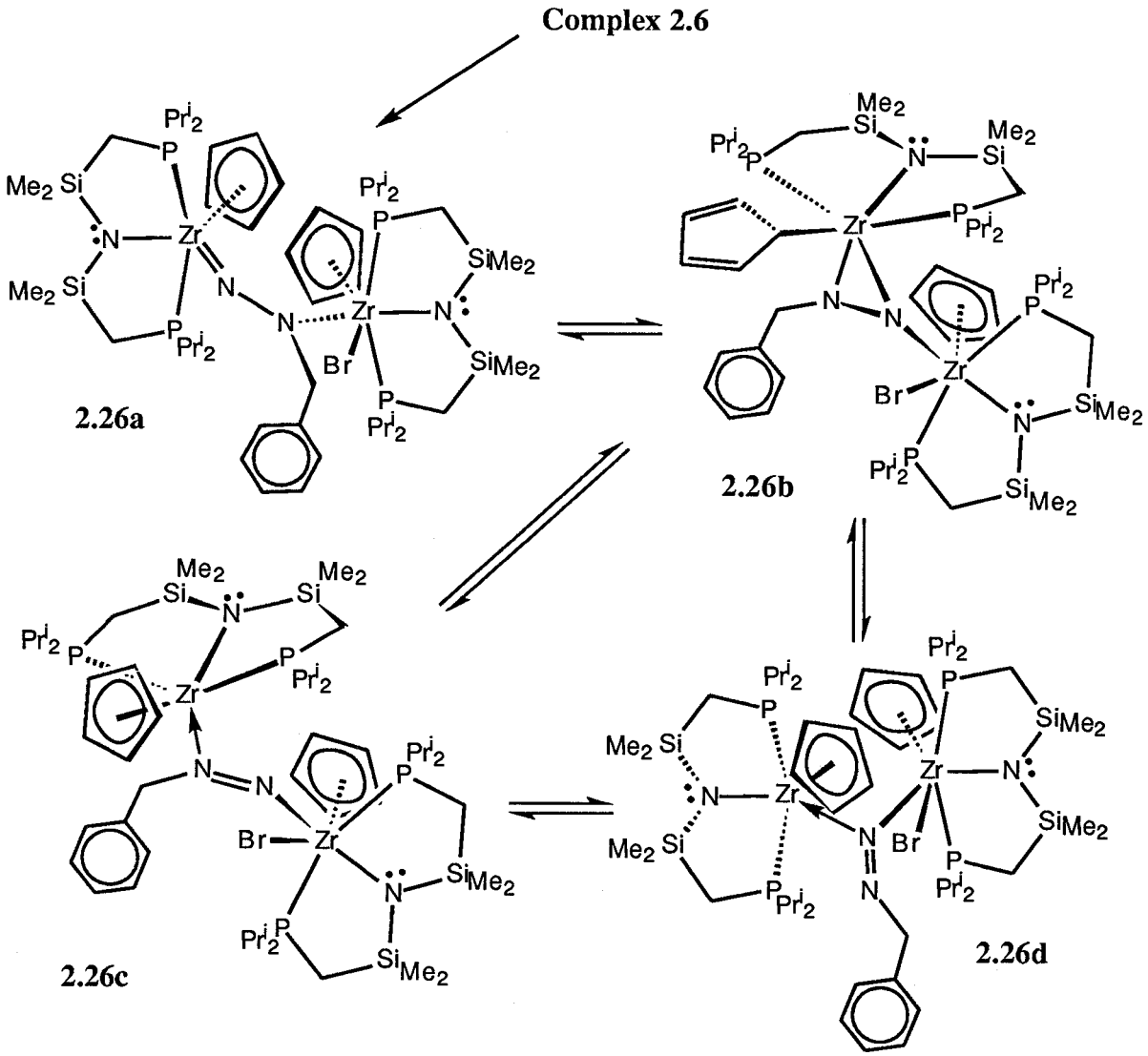

Scheme 2.13

2.8.4b Reactivity With Dihaloalkanes

Initial investigations involved the reaction of the simplest dihalo alkane dibromomethane, CH_2Br_2 and complexes **2.2** and **2.9**. It was envisaged that the reaction of 0.5 equivalents of CH_2Br_2 with **2.2** or **2.9** would lead to the formation of an isodiazomethane or a diazomethane complex respectively (Scheme **2.14**). It is also known that reactions involving

references on page 119

diazomethane and low valent metal complexes (e.g., $[Ru(NO)(PPh_3)_2Cl]$) lead to the formation of methylidene intermediates which then proceed to form ethylene complexes.[107]

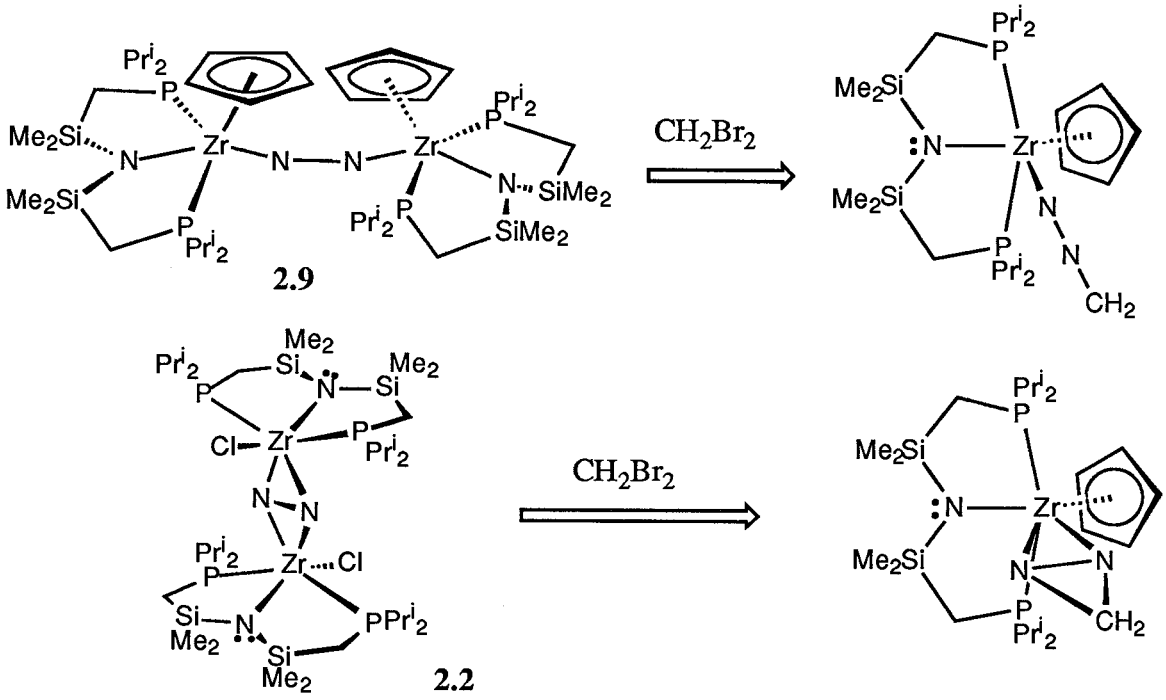

Scheme 2.14

Reacting the end-on complex **2.9** with approximately 0.5 equivalent of CH_2Br_2 inside a sealed NMR tube and monitoring by $^{31}P\{^1H\}$ NMR spectroscopy showed a clean conversion of the dinitrogen complex **2.9** to the zirconium(IV) derivative $ZrCpBr_2[N(SiMe_2CH_2PPr^i_2)_2]$, **2.7**. The only peak unaccounted for in the ^1H NMR spectrum was at 5.2 ppm, which is identical to the chemical shift of ethylene. Also, at the end of the reaction (i.e., when all the CH_2Br_2 was consumed) approximately 0.5 equivalent of the dinitrogen complex **2.9** was left unreacted and no NMR features that would correspond to an oxidative addition product (e.g., $ZrCpBr(CH_2Br)[N(SiMe_2CH_2PPr^i_2)_2]$) were observed.

The above results seems to suggest that the proposed diazomethane intermediate, $ZrCp(N_2CH_2)[N(SiMe_2CH_2PPr^i_2)_2]$ **2.27**, was formed during the course of the reaction. Low temperature NMR studies did not show any features that would correspond to free diazomethane CH_2N_2, or CH_2NNCH_2. Scheme **2.15** shows a possible mechanistic pathway to generate

references on page 119

ethylene from the proposed diazo intermediate. The diazomethane intermediate probably undergoes a bimolecular decomposition pathway to yield ethylene and 0.5 equivalent of dinitrogen complex. However, the literature precedence seems to suggest that the diazomethane complex could form a methylidene intermediate, $ZrCp(CH_2)[N(SiMe_2CH_2PPr^i_2)_2]$ which then proceeds to yield ethylene and the dinitrogen complex **2.9**.[104,107]

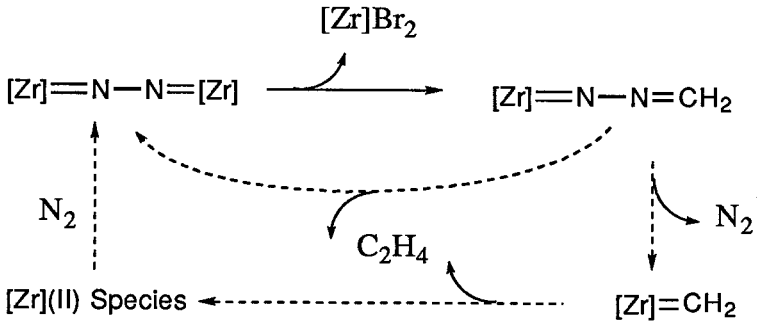

[Zr] = "$ZrCp[N(SiMe_2CH_2PPr^i_2)_2]$"

Scheme 2.15

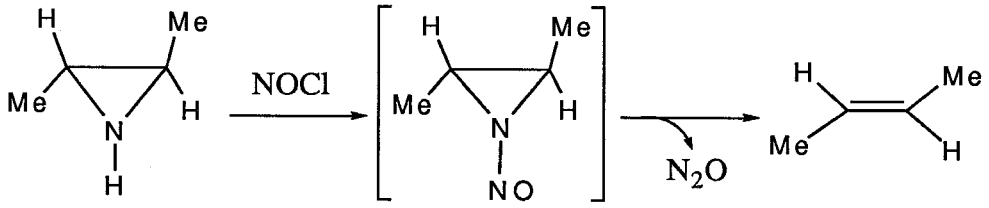

2.3

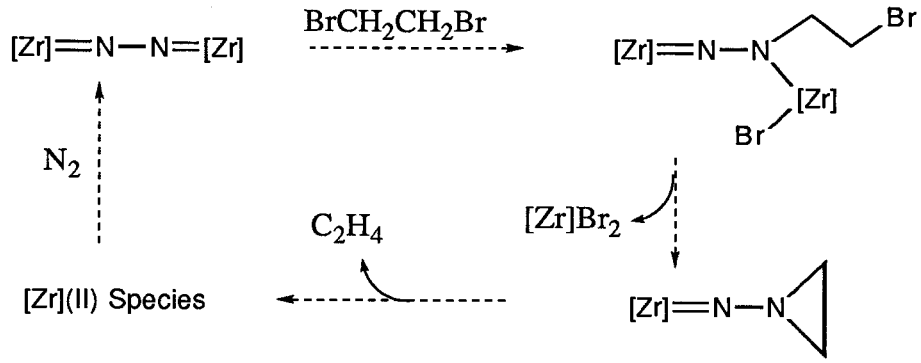

[Zr] = "$ZrCp[N(SiMe_2CH_2PPr^i_2)_2]$"

Scheme 2.16

references on page 119

The reaction involving 0.5 equivalents of 1,2-dibromoethane and the end-on derivative **2.9** also gave exclusively ethylene and the zirconium(IV) complex, $ZrCpBr_2[N(SiMe_2CH_2PPr^i_2)_2]$. In this case a three-membered azacyclic intermediate, $ZrCp[NN(CH_2)_2][N(SiMe_2CH_2PPr^i_2)_2]$ is probably formed during the reaction (Scheme **2.16**). The elimination of ethylene from this intermediate may be comparable to the reaction of some N-nitrosyl aziridine derivatives which decompose to give olefins and N_2O (Equation **2.3**).[108]

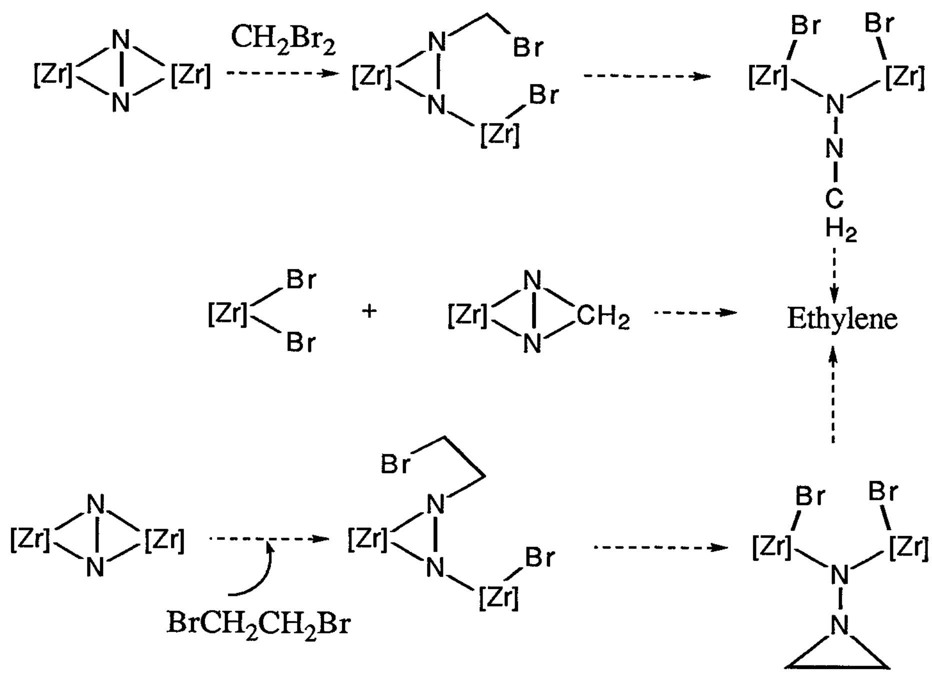

$[Zr] = $ "$ZrX[N(SiMe_2CH_2PPr^i_2)_2]$"

Scheme 2.17

The reactions involving side-on complexes **2.2** or **2.12** and CH_2Br_2 or $BrCH_2CH_2Br$ also gave ethylene and the zirconium(IV) trihalo derivative $ZrBr_2Cl[N(SiMe_2CH_2PPr^i_2)_2]$. Due to the poor solubility of the side-on dinitrogen complexes the solutions always contained an excess of the dihalo alkane and therefore hampered the NMR experiments to detect the intermediates involved in the reaction. The possible intermediates involved during the reactions with CH_2Br_2 could be either an η^2-diazirine complex or a bridging μ-η^1-diazomethane complex (Scheme **2.17**). For the reaction of the side-on derivatives with $BrCH_2CH_2Br$ the intermediate

$\{[(Pr^i_2PCH_2SiMe_2)_2N]ZrXBr\}_2[\mu\text{-}NN(CH_2)_2]$, where X = Cl or OAr^*, with a bridging $[NN(CH)_2]^{2-}$ ligand is possible, which is similar to the proposed intermediate for the end-on case (Scheme **2.17**).

2.9 Conclusions

The synthesis of dinitrogen complexes similar to $\{[(Pr^i_2PCH_2SiMe_2)_2N]ZrCl\}_2$-$(\mu\text{-}\eta^2\text{:}\eta^2\text{-}N_2)$ **2.2** was successful in two cases where the chloride ligand was replaced with the Cp or with an aryloxy ligand, $((OC_6H_3\text{-}2,6\text{-}Me_2)^{-1}$, $OAr^*)$. The complex with Cp ligands, $\{[(Pr^i_2PCH_2SiMe_2)_2N]ZrCp\}_2(\mu\text{-}\eta^1\text{:}\eta^1\text{-}N_2)$ **2.9** has a bridging end-on bound dinitrogen ligand whereas the complex with OAr^* ligands $\{[(Pr^i_2PCH_2SiMe_2)_2N]ZrOAr^*\}_2(\mu\text{-}\eta^2\text{:}\eta^2\text{-}N_2)$ **2.12** has a side-on bound dinitrogen ligand with a bent Zr_2N_2 core. However, attempts to incorporate allyl, alkyl or amide ligands or the incorporation of the less bulky tridentate ligand "Zr[N($SiMe_2CH_2PMe_2$)$_2$]" were not successful. The solid state X-ray structures of the two complexes show that in the end-on case **2.9**, the nitrogen-nitrogen bond distance of the dinitrogen ligand was 1.301(3) Å whereas in the side-on case **2.12**, the bond distance was 1.528(7) Å which was identical to the chloride analogue **2.2** (1.548(7) Å). The tert-butoxy analog of complex the **2.12**, $\{[(Pr^i_2PCH_2SiMe_2)_2N]ZrOBu^t\}_2(\mu\text{-}N_2)$, **2.14**, shows certain NMR spectroscopic features which tend to suggest that it is similar to other side-on derivatives, although the lack of suitable crystals hampered full charecterization.

Solid and solution state resonance Raman spectroscopic studies on the side-on **2.2** and on the end-on **2.9** derivatives show that the mode of dinitrogen coordination observed in the solid state X-ray structures of these complexes is also preserved in the solution state. The observed nitrogen-nitrogen stretching frequencies for the end-on and side-on derivatives were 1211 cm^{-1} and 731 cm^{-1} respectively, which correlate well with the observed bond distances associated with the same atoms. The ^{15}N NMR spectroscopic evidence also shows that the side-on derivative has the same mode of dinitrogen coordination in both the solid and the solution states. The mixed halogen derivative $\{[(Pr^i_2PCH_2SiMe_2)_2N]Zr\}_2ClBr(\mu\text{-}N_2)$ gives rise to a singlet in the ^{15}N NMR spectrum showing that nitrogens of the dinitrogen ligand are

references on page 119

chemically equivalent and therefore, it is inferred that the bonding mode of the N_2 ligand in the solution state is side-on, (μ-η^2:η^2-N_2).

The ML_4 fragment (C_{4v}) has three available orbitals that are suitable for dinitrogen bonding

⇓

In the case of $[(H_3P)_2(H_2N)ZrX]$, X = Cl, Cp or OAr^* the π-interactions leads to two cases

⇙ ⇘

π-interactions on the plane defined by the ligands

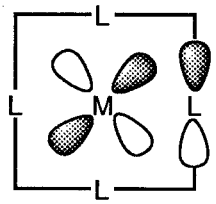

⇓

The remaining two metal based orbitals are perpendicular to the plane and can form only two π-type bonds with the dinitrogen π^*-orbitals

⇓

End-On Complex

π-interactions perpendicular to the plane defined by the ligands

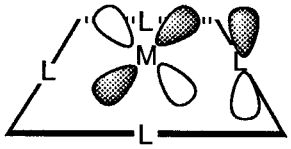

⇓

Of the remaining two metal based orbitals one is perpendicular to the plane and the other is on the plane and can form one π-type and one δ-type bond respectively with the dinitrogen π^*-orbitals

⇓

Side-On Complex

Scheme 2.18

The semi-empirical molecular orbital studies performed on the end-on derivative **2.9** and on the side-on derivatives **2.2** and **2.12** show that the π-acceptor interactions involving the π^*-orbitals of the dinitrogen ligand are significantly different. In the end-on case these interactions give rise to two π-MOs (HOMO and HOMO-1) whereas, the side-on cases gives rise to one δ-MO (HOMO) and one π-MO (HOMO-9 for **2.2** and HOMO-3 for **2.12**), which were found to be much lower in energy than the δ-MO. The Mulliken population analysis shows greater electron donation into the dinitrogen ligand in the side-on cases than in the end-on case, which

references on page 119

in turn is reflected in the formal charge on the dinitrogen ligand which was greater for the former than in the latter. The Wiberg indices suggest a weaker nitrogen-nitrogen bond for the side-on mode than the end-on mode, which is consistent with the observed nitrogen-nitrogen bond distances of these complexes.

An analysis of the fragment orbitals of the metal unit, $[(H_3P)_2(H_2N)ZrX]$, where X = Cl, Cp or OH, show that the metal-ligand d_π-p_π interactions influence the mode of dinitrogen coordination, i.e., end-on vs side-on. Scheme **2.18** summarizes how the metal-ligand π-interactions influence the mode of dinitrogen bonding.

An intramolecular rotation of the dinitrogen ligand within a dinuclear center was demonstrated by the conversion of the side-on complex **2.2** to the end-on complex **2.9** by the reaction of NaCp•DME. The reaction of the side-on derivative **2.2** and **2.12** with $LiBEt_4$ forms an unusual complex, $\{[(Pr^i_2PCH_2SiMe_2)_2N]ZrH\}\{[(Pr^i_2PCH_2SiMe_2)_2N]ZrEt\}(\mu\text{-}N_2\bullet BEt_3)$ where the dinitrogen ligand seems to be bonded to a BEt_3 unit. Reactions of the dinitrogen complex **2.9** with alkyl halides were very complex, but in the case of benzyl bromide it was found that the reaction proceeds through an intermediate containing a benzyl diazenido, $(NNBz)^{-1}$, ligand. The side-on and end-on derivatives react with methylene dibromide or with 1,2-dibromoethane to give ethylene.

2.10 Experimental

2.10a General Procedures All manipulations were performed under prepurified nitrogen in a Vacuum Atmospheres HE-553-2 work station equipped with a MO-40-2H purification system or in Schlenk-type glassware.[109,110] Pentane, diethyl ether and hexanes were dried and deoxygenated by distillation from sodium-benzophenone ketyl under argon. Toluene was predried by refluxing over CaH_2 and then distilled from sodium under argon. Tetrahydrofuran and hexanes were predried by refluxing over CaH_2 and then distilled from sodium-benzophenone ketyl under argon. Deuterated benzene (C_6D_6, 99.6 atom % D) and deuterated toluene (C_7D_8, 99.6 atom %D), purchased from MSD Isotopes, were dried over activated 4Å molecular sieves, vacuum transferred and freeze-pump-thawed three times before use.

references on page 119

Dinitrogen gas was purified by purging through a column containing manganese oxide, MnO, and activated 4Å molecular sieves. The 99% $^{15}N_2$ was obtained from Cambridge Isotopes Ltd., and was used as supplied.

The ^{1}H, ^{31}P and ^{13}C NMR spectra were recorded on a Varian XL-300, a Bruker AC 200, a Bruker WH-400 or a Bruker AM 500 spectrometer. Proton spectra were referenced using the partially deuterated solvent peak as the internal reference, C_6D_5H at 7.15 ppm and $C_6D_5CD_2H$ at 2.09 ppm relative to Me_4Si. The $^{31}P\{^{1}H\}$ NMR spectra were referenced to external $P(OMe)_3$ set at +141.00 ppm relative to 85% H_3PO_4. The $^{13}C\{^{1}H\}$ NMR spectra were referenced to the C_6D_6 signal at 128.0 ppm or to the $CD_3C_6D_5$ signal at 20.4 ppm. Solution $^{15}N\{^{1}H\}$ NMR spectra were recorded on the Varian XL-300, referenced to external formamide set at 0.00 ppm. Solid-state ^{15}N NMR spectra were run on a Bruker MSL-400, referenced to solid NH_4Cl set at -73.39 ppm with respect to neat formamide at 0.00 ppm. $^{11}B\{^{1}H\}$ NMR spectra were recorded in C_7D_8 on the Varian XL-300 referenced to external Et_3B set at 0.00 ppm. The final $^{11}B\{^{1}H\}$ NMR spectra were obtained by subtracting the spectra of glass obtained using identical acquisition parameters as those of the sample spectra. $^{1}H\{^{31}P\}$ NMR spectra were recorded on the Bruker AM 500 spectrometer.

Resonance Raman* spectra were recorded on a modified Jarrel-Ash model 25-300 Raman spectrometer. Excitation radiation was supplied by Spectra Physics Ar^+ and Kr^+ laser soperating at 514.5 nm and 647.1 nm respectively. Scattered radiation was collected by a back scattering geometry. Multiple scans were collected and calibrated against indene, toluene and THF as external standards for peak positions. All wave number assignments were estimated to be accurate within 2 cm^{-1}. Spectra for polarization studies of solution samples were collected in a 90° scattering geometry at 278 K on a Dilor Z-24 Raman spectrophotometer. Typical slit-width settings were between 5 cm^{-1} and 9 cm^{-1}. All samples were sealed under N_2 in 1.5 - 1.8×90 mm Kimax glass capillary tubes.

* The resonance Raman spectra were recorded at the Department of Chemistry, Biochemistry and Molecular Biology of the Oregon Graduate Institute of Science and Technology by Prof. Thomas M. Loehr and Jonathan D. Cohen.

references on page 119

UV-Vis spectra were recorded on a Perkin Elmer 5523 UV/Vis spectrophotometer stabilized at 20°C. Mass spectral studies were carried out on a Kratos MS 50 using an EI source. IR spectra were recorded on a Bomem MB-100 spectrometer. Solution samples were recorded in a 0.1mm KBr cell and solid samples were recorded as KBr pellets. Carbon, hydrogen and nitrogen analyses were performed by the microanalyst of this department.

The complexes $ZrCl_3[N(SiMe_2CH_2PR_2)_2]$ where R = Pr^i and Me, were prepared according to the published procedures.[11] NaCp•DME,[111] where DME = 1,2-dimethoxyethane, was prepared by the reaction of sodium metal with freshly cracked cyclopentadiene in dry DME and crystallized directly from the reaction mixture. Mercury was purchased from BDH and purified as follows:[112] in a separatory funnel mercury (500g) was washed with 2M HCl (2×25 mL) acid then with distilled water (2×50 mL) and finally rinsed a few times with Et_2O (25 mL) until no further gray colour was present in the ether washings. During washings a slag was formed on the surface of the Hg which was separated from the shiny Hg. Pure Hg was dried under vacuum for 12 hours. Amalgam was made under a nitrogen atmosphere and washed with toluene (2×25 mL) until the washings showed no gray coloration.

Sodium alkoxide, NaOR', where R' = $CHPh_2$ and aryloxides, NaOAr where Ar = Ph or $C_6H_3Me_2$-2,6 were prepared by reacting (3 hours at room temperature and then refluxed for 3 hours) a toluene solution of the alcohol with sodium. The resulting white solid was filtered, extracted with THF (to remove finely dispersed sodium) and stripping off THF under vacuum gave alcohol free NaOAr. Prior to the reaction the alcohol was dissolved in toluene and stirred with Mg turnings (0.1 equivalent) for 12h and then filtered. The above procedure is likely to minimize the presence of NaOH or unreacted alcohol in the final product. $KOBu^t$ was purchased from Aldrich and was sublimed prior to use. The sodium amide, $NaNPh_2$ was prepared by reacting the amine, $HNPh_2$ with $NaN(SiMe_3)_2$ in toluene. The $NaNPh_2$ precipitates out of toluene, which was then collected on a frit and washed with hexanes to obtain pure material.

references on page 119

CH_3I, CH_2Br_2, $C_2H_4Br_2$ and $C_6H_5CH_2Br$ were purchased from Aldrich and were dried over activated 4Å molecular sieves for 24h. $ZrBr_4$ was purchased from Strem and used as supplied.

2.10b Synthesis of Precursors

2.10b.1 $ZrBr_3[N(SiMe_2CH_2PPr^i_2)_2]$, 2.4. To a suspension of $ZrBr_4$ (2.03 g, 4.94 mmol) in toluene (50 mL) was added a solution of $Li[N(SiMe_2CH_2PPr^i_2)_2]$, (1.00 g, 2.50 mmol) in toluene (10 mL) at room temperature. The reaction mixture was stirred for 16 hours and then the salt (LiCl) was removed by filtering the solution through Celite. The filtrate was concentrated to 15 mL and hexanes was added until the solution turned turbid; cooling at -30 °C gave a colorless crystalline product (1.12 g, 73%). ^1H NMR (δ, 200.123 MHz, C_6D_6): 0.41 (s, 12H, $Si(CH_3)_2$); 1.11 (m, 28H, $P[CH(CH_3)_2]_2$, $SiCH_2P$); 2.07 (sept of triplets, 4H, $P[CH(CH_3)_2]_2$, $^2J_{H-P}$ = 2.7 Hz, $^3J_{H-H}$ = 7.2 Hz). $^{31}P\{^1H\}$ NMR (δ, 81.015 MHz, C_6D_6): 16.52 (s). $^{13}C\{^1H\}$ NMR (δ, 50.323 MHz, C_6D_6): 4.50 (s, $Si(CH_3)_2$); 11.93 (s, $SiCH_2P$); 18.85 (s, $P[CH(CH_3)_2]_2$); 19.12 (s, $P[CH(CH_3)_2]_2$); 25.14 (t, $P[CH(CH_3)_2]_2$, $^2J_{C-P}$ = 6.8 Hz). Anal. Calcd for $C_{18}H_{44}Br_3NP_2Si_2Zr$: C, 29.88; H, 6.13; N, 1.94. Found: C, 30.00; H, 6.30; N, 1.99.

2.10b.2 $Zr(\eta^5\text{-}C_5H_5)Cl_2[N(SiMe_2CH_2PPr^i_2)_2]$, 2.6. To a solution of $ZrCl_3[N(SiMe_2CH_2PPr^i_2)_2]$ **2.1**, (4.040 g, 6.84 mmol) in toluene (150 mL) was added solid NaCp•DME (1.340 g, 7.52 mmol) at room temperature. The reaction mixture was stirred for 16 hours and then the salt (NaCl) was removed by filtering through Celite. The filtrate was concentrated to 15 mL and hexanes was added until the solution turned turbid; cooling at -30 °C gave yellow hexagonal shaped crystals (3.16 g, 75%). ^1H NMR (δ, 300 MHz, C_6D_6): 0.64 (s, 12H, $Si(CH_3)_2$); 1.00 (m, 28H, $P[CH(CH_3)_2]_2$, $SiCH_2P$); 2.12 (m, 4H, $P[CH(CH_3)_2]_2$); 6.15 (t, ~5H, C_5H_5, $^3J_{H-P}$ = 1.4 Hz). $^{31}P\{^1H\}$ NMR (δ, 121.421 MHz, C_6D_6): 16.11 (s). $^{13}C\{^1H\}$ NMR (δ, 50.323 MHz, C_6D_6): 7.82 (s, $Si(CH_3)_2$); 8.71 (s, $SiCH_2P$); 18.74 (s, $P[CH(CH_3)_2]_2$); 18.96 (s, $P[CH(CH_3)_2]_2$); 24.72 (t, $P[CH(CH_3)_2]_2$, $^2J_{C-P}$ = 4.5 Hz); 116.00 (s, C_5H_5). Anal. Calcd for $C_{23}H_{49}Cl_2NP_2Si_2Zr$: C, 44.56; H, 7.97; N, 2.26. Found: C, 44.72; H, 8.20; N, 2.32.

references on page 119

2.10b.3 $Zr(\eta^5\text{-}C_5H_5)Br_2[N(SiMe_2CH_2PPr^i_2)_2]$, 2.7. This complex was synthesized by a procedure similar to the one described above in section **2.2b.2**, using $ZrBr_3[N(SiMe_2CH_2PR_2)_2]$ (0.180 g, 0.270 mmol) and NaCp•DME (0.053 g, 0.300 mmol). ^1H NMR spectrum of the crude reaction mixture showed the presence of **2.7** in greater than 90% yield. ^1H NMR (δ, 300 MHz, C_6D_6): 0.69 (s, 12H, $Si(CH_3)_2$); 0.98 (m, 24H, $P[CH(CH_3)_2]_2$); 1.06 (t, 4H, $SiCH_2P$, $^3J_{P\text{-}H}$ = 5.4 Hz); 2.13 (sept, 4H, $P[CH(CH_3)_2]_2$, $^3J_{H\text{-}H}$ = 7.2 Hz); 6.62 (br, 5H, C_5H_5). $^{31}P\{^1H\}$ NMR (δ, 121.421 MHz, C_6D_6): 16.57 (s). Anal. Calcd for $C_{23}H_{49}Br_2NP_2Si_2Zr$: C, 38.97; H, 6.97; N, 1.98. Found: C, 39.00; H, 7.08; N, 1.98.

2.10b.4 $Zr(\eta^5\text{-}C_5H_5)Cl_2[N(SiMe_2CH_2PMe_2)_2]$, 2.8. To a solution of $ZrCl_3[N(SiMe_2CH_2\text{-}PMe_2)_2]$ (1.45 g, 3.03 mmol) in toluene (150 mL) was added solid NaCp•DME (0.541 g, 3.04 mmol) in two portions at 1 hour interval at room temperature. The reaction mixture was stirred for 16 hours and then the salt (NaCl) was removed by filtering through Celite. The filtrate was concentrated to 20 mL and hexanes was added until the solution turned turbid; cooling at -30 °C gave a yellow crystalline material (1.08 g, 70%). ^1H NMR (δ, 300 MHz, C_6D_6): 0.58 (s, 12H, $Si(CH_3)_2$); 0.92 (br, 4H, $SiCH_2P$); 0.95 (t, 12H, $P(CH_3)_2$, $^2J_{H\text{-}P}$ = 3.6Hz); 6.33 (t, 5H, C_5H_5, $^3J_{H\text{-}P}$ = 1.5Hz). $^{31}P\{^1H\}$ NMR (δ, 121.421 MHz, C_6D_6): -21.73 (s). $^{13}C\{^1H\}$ NMR (δ, 50.323 MHz, C_6D_6): 7.24 (s, $Si(CH_3)_2$); 14.96 (t, $P(CH_3)_2$, $^1J_{C\text{-}P}$ = 7.8Hz); 20.64 (s, $SiCH_2P$); 115.50 (s, C_5H_5). Anal. Calcd for $C_{15}H_{33}Cl_2NP_2Si_2Zr$: C, 35.49; H, 6.55; N, 2.76; Cl, 13.98. Found: C, 35.53; H, 6.38; N, 2.76; Cl, 14.20.

2.10b.5 $Zr(\eta^3\text{-}C_3H_5)Cl_2[N(SiMe_2CH_2PPr^i_2)_2]$, 2.10. To a cooled solution (-78 °C) of $ZrCl_3\text{-}[N(SiMe_2CH_2PPr^i_2)_2]$ (2.50 g, 4.24 mmol) in THF (70 mL) was added a THF solution of C_3H_5MgCl (23.3 mL of 0.2 M solution, 4.66 mmol) and stirred at -78 °C for 10 minutes. After allowing the reaction mixture to warm to room temperature, dioxane (4.5 mL, 50 mmol) was added and stirred for 3 hours. A copious white precipitate of $MgCl_2$•xTHF was removed by filtering through Celite. Solvent was stripped under vacuum and redissolved the crude product in hexanes and cooled to -30 °C to give a bright yellow crystalline product. (1.62 g, 64%). ^1H NMR (δ, 300 MHz, C_6D_6)*: 0.58 (s, 6H, $Si(CH_3)_2$); 0.59 (s, 6H, $Si(CH_3)_2$); 0.96 (m, 4H,

* H_c, H_a and H_s refer to central, anti and syn protons of the allylic ligand respectivly.

references on page 119

SiCH_2P);1.08 (m, 24H, P[CH(CH_3)2]2); 2.18 (sept, 2H, P[CH(CH$_3$)2]2); 2.25 (sept, 2H, P[CH(CH$_3$)2]2); 3.32 (d of triplets, 2H$_a$, C$_5H_3$, $^3J_{Ha-Hc}$ = 15.2 Hz, $^3J_{Ha-P}$ = 3.4 Hz); 4.46 (d of triplets, 2H$_s$, C$_5H_3$, $^3J_{Hs-Hc}$ = 8.8 Hz, $^3J_{Hs-P}$ = 4.4 Hz); 6.08 (t of t, 1H$_c$, C$_5H_3$, $^3J_{Hc-Ha}$ = 15.2 Hz, $^3J_{Hc-Hs}$ = 8.8 Hz). $^{31}P\{^1H\}$ NMR (δ, 121.421 MHz, C_6D_6): 21.13 (s). $^{13}C\{^1H\}$ NMR (δ, 50.323 MHz, C_6D_6): 78.20 (s, CH$_2$*C*HCH$_2$); 139.25 (s, *C*H$_2$CH*C*H$_2$). NOEDIFF Experiments (δ, 400 MHz, C_6D_6): Irradiating the resonance at 6.08 ppm resulted in the enhancement of peaks at 3.32 and 4.46 ppm. Attempts to radiate peaks at 3.32 or 4.46 ppm resulted in spin saturation of both resonances and enhanced the peak at 6.08 ppm. Anal. Calcd for $C_{21}H_{49}Cl_2NP_2Si_2Zr$: C, 42.33; H, 8.29; N, 2.35. Found: C, 42.67; H, 8.47; N, 2.34.

The $^{31}P\{^1H\}$ NMR (δ, 81.015 MHz, C_6D_6) data for **Zr(η^3-C$_3$H$_5$)ClBr[N(SiMe$_2$CH$_2$-PPr$^i_2$)$_2$] 2.10a**, an AB quartet, 21.08 (1P, $^2J_{P-P}$ = 7.9 Hz) and 21.65 (1P, $^2J_{P-P}$ = 7.9 Hz). Anal. Calcd for $C_{21}H_{49}ClBrNP_2Si_2Zr$: C, 39.39; H, 7.71; N, 2.19. Found: C, 38.90; H, 7.58; N, 2.10.

2.10b.6 Zr(OAr*)Cl$_2$[N(SiMe$_2$CH$_2$PPr$^i_2$)$_2$], 2.11. To a solution of ZrCl$_3$[N(SiMe$_2$CH$_2$-PPr$^i_2$)$_2$] **2.1**, (4.00 g, 5.08 mmol) in toluene (150 mL) was added solid Na(OAr*) (1.03 g, 6.35 mmol) in three portions at 1 hour intervals at room temperature. The reaction mixture was stirred for 16 hours and then the salt (NaCl) was removed by filtering through Celite. The filtrate was concentrated to 25 mL, an equal volume of hexanes added, and the mixture allowed to stand at room temperature for 24 hours. A colorless crystalline product slowly separated from the solution (2.41 g, 70%). ^1H NMR (δ, 300 MHz, C_6D_6): 0.48 (s, 12H, Si(CH_3)$_2$); 0.96 (d of d, 16H, 12H of P[CH(CH_3)2]2 and 4H of SiCH_2P, $^3J_{H-H}$ = 6.1 Hz, $^3J_{P-H}$ = 14.0 Hz); 1.06 (d of d, 12H, P[CH(CH_3)2]$_2$, $^3J_{H-H}$ = 6.1 Hz, $^3J_{P-H}$ = 14.0 Hz); 2.00 (sept, of t, 4H, P[CH(CH$_3$)2]$_2$ $^3J_{H-H}$ = 6.1 Hz, $^2J_{P-H}$ = 2.0 Hz); 2.80 (s, 6H, 2, 6-*Me*$_2$Ph); 6.82 (t, 1H, *p*-Ph, $^3J_{H-H}$ = 7.4 Hz); 7.05 (d, 2H, *m*-Ph, $^3J_{H-H}$ = 7.4 Hz). $^{31}P\{^1H\}$ NMR (δ, 121.421 MHz, C_6D_6): 14.98 (s). $^{13}C\{^1H\}$ NMR (δ, 50.323 MHz, C_6D_6): 5.41 (s, Si(*C*H$_3$)$_2$); 10.70 (s, Si*C*H$_2$P); 19.07 (s, P[CH(*C*H$_3$)2]$_2$); 19.15 (s, P[CH(*C*H$_3$)2]$_2$); 19.86 (s, 2, 6-*Me*$_2$-Ph); 24.09 (t, P[*C*H(CH$_3$)2]$_2$, $^2J_{C-P}$ = 6.2 Hz); 120.94 (s, *p*-Ph); 128.79 (s, *m*-Ph). Anal. Calcd for $C_{26}H_{53}Cl_2NOP_2Si_2Zr$: C, 46.20; H, 7.90; N, 2.07. Found: C, 46.07; H, 8.10; N, 2.03.

references on page 119

2.10b.7 $Zr(OBu^t)Cl_2[N(SiMe_2CH_2PPr^i_2)_2]$, 2.11. To a solution of $ZrCl_3[N(SiMe_2CH_2PPr^i_2)_2]$ (1.50 g, 2.54 mmol) in Et_2O (60 mL) was added a solution of $KOBu^t$ (285 mg, 2.54 mmol) in Et_2O (10 mL) at room temperature and stirred for 3 hours. The solvent was stripped under vacuum and the residues were extracted with pentane (40 mL) and then filtered through a layer of Celite. Stripping off the solvent gave a colorless oil containing >80% (by ^1H NMR spectroscopy) of the desired product. ^1H NMR (δ, 300 MHz, C_6D_6): 0.45 (s, 12H, $Si(CH_3)_2$); 1.05 (d, 4H, $SiCH_2P$ $^2J_{P-H}$ = 5.7 Hz); 1.32 and 1.35 (each d of d, 24H, $P[CH(CH_3)_2]_2$, $^3J_{P-H}$ = 2.9 Hz, $^3J_{H-H}$ = 7.6 Hz); 1.50 (s, 9H, $OC(CH_3)_3$); 2.04 (t of sept, 4H, $P[CH(CH_3)_2]_2$, $^2J_{P-H}$ = 1.9 Hz, $^3J_{H-H}$ = 7.6 Hz). $^{31}P\{^1H\}$ NMR (δ, 81.015 MHz, C_6D_6): 11.60 (s).

2.10b.8 $Zr(OBu^t)Cl_2[N(SiMe_2CH_2PMe_2)_2]$, 2.13. The complex was prepared by a procedure similar to the one described above in section **2.10b.7**, using $ZrCl_3[N(SiMe_2CH_2PMe_2)_2]$ (440 mg, 0.92 mmol) and $KOBu^t$ (114 mg, 1.01 mmol). The product was crystallized from a solvent mixture containing Et_2O and pentane (0.38 g, 71%). ^1H NMR (δ, 300 MHz, C_6D_6): 0.26 (s, 12H, $Si(CH_3)_2$); 0.87 (d, 4H, $SiCH_2P$, $^2J_{P-H}$ = 9.6 Hz); 1.01 (d, 12H, $P(CH_3)_2$, $^2J_{P-H}$ = 6.3 Hz); 1.50 (s, 9H, $OC(CH_3)_3$). $^{31}P\{^1H\}$ NMR (δ, 121.421 MHz, C_6D_6): -32.33 (s). $^{13}C\{^1H\}$ NMR (δ, 50.323 MHz, C_6D_6): 5.92 (s, $Si(CH_3)_2$); 12.53 (d, $P(CH_3)_2$, $^1J_{C-P}$ = 10.6 Hz); 17.48 (s, $SiCH_2P$); 32.14 (s, $OC(CH_3)_3$). Anal. Calcd for $C_{14}H_{37}Cl_2NOP_2Si_2Zr$: C, 32.61; H, 7.23; N, 2.72. Found: C, 32.72; H, 7.13; N, 2.80.

2.10b.9 $Zr(OCHPh_2)Cl_2[N(SiMe_2CH_2PPr^i_2)_2]$, 2.16. The complex was prepared by a procedure similar to the one described above in section **2.10b.6**, using $ZrCl_3[N(SiMe_2CH_2PPr^i_2)_2]$ (1.25 g, 2.12 mmol) and Ph_2CHONa•THF (589 mg, 2.12 mmol). The product was crystallized from a solvent mixture containing Et_2O and pentane (1.23 g, 78%). ^1H NMR (δ, 200.132 MHz, C_6D_6): 0.50 (s, 12H, $Si(CH_3)_2$); 0.94 (m, 28H, $SiCH_2P$ and $P[CH(CH_3)_2]_2$); 1.73 (sept, 4H, $P[CH(CH_3)_2]_2$, $^3J_{H-H}$ = 6.8 Hz); 6.82 (s, 1H, CHPh); 7.00 (2H, t, *p*-Ph, $^3J_{H-H}$ = 7.6 Hz); 7.16 (4H, t, *m*-Ph, $^3J_{H-H}$ = 7.6 Hz); 7.71 (4H, d, *o*-Ph, $^3J_{H-H}$ = 7.6 Hz). $^{31}P\{^1H\}$ NMR (δ, 81.015 MHz, C_6D_6): 13.53 (s). Anal. Calcd for $C_{31}H_{55}Cl_2ONP_2Si_2Zr$: C, 50.45; H, 7.51; N, 1.90. Found: C, 51.25; H, 7.67; N, 1.76.

references on page 119

2.10b.10 $Zr(NPh_2)Cl_2[N(SiMe_2CH_2PPr^i_2)_2]$, 2.17. To a solution of $ZrCl_3[N(SiMe_2CH_2PPr^i_2)_2]$ (1.25 g, 2.12 mmol) in THF (60 mL) was added a solution of $NaNPh_2$ (199 mg, 2.12 mmol) in THF (20 mL), at room temperature and stirred for 2 hours. The solvent was stripped under vacuum and the residues were extracted with toluene (20 mL) and then filtered through a layer of Celite. The product was crystallized from a solvent mixture containing toluene and hexanes (1.15 g, 75%). ^1H NMR (δ, 400 MHz, C_6D_6): 0.47 (s, 12H, $Si(CH_3)_2$); 1.16 and 1.10 (m, 28H, $SiCH_2P$ and $P[CH(CH_3)_2]_2$); 2.12 (sept, 4H, $P[CH(CH_3)_2]_2$, $^3J_{H-H}$ = 4.0 Hz); 6.96 (2H, t, *p*-Ph, $^3J_{H-H}$ = 8.0 Hz); 7.23 (4H, t, *m*-Ph, $^3J_{H-H}$ = 8.0 Hz); 7.30 (4H, d, *o*-Ph, $^3J_{H-H}$ = 8.0 Hz). $^{31}P\{^1H\}$ NMR (δ, 81.015 MHz, C_6D_6): 15.58 (s); in a solvent mixture containing THF and C_6D_6: 2.70 (br.); -1.20 (br.). $^{13}C\{^1H\}$ NMR (δ, 50.323 MHz, C_6D_6): 5.04 (s, $SiCMe_2$); 9.69 (s, CH_2Si); 18.85 and 19.59 (s, $CH(CH_3)_2$); 24.28 (t, $CH(CH_3)_2$, $^1J_{P-C}$ = 5.6 Hz); 123.41 (s, Ph); 126.98 (s, Ph); 128.26 (s, Ph). Anal. Calcd for $C_{30}H_{54}Cl_2N_2P_2Si_2Zr$: C, 49.83; H, 7.53; N, 3.88. Found: C, 50.09; H, 7.56; N, 4.00.

2.10b.11 $Zr(CH_2SiMe_3)Cl_2[N(SiMe_2CH_2PPr^i_2)_2]$, 2.18. To a cooled (-78 °C) solution of $ZrCl_3[N(SiMe_2CH_2PPr^i_2)_2]$, (1.25 g, 2.12 mmol) in THF (60 mL) was added a solution of $LiCH_2SiMe_3$ (199 mg, 2.10 mmol) in toluene (15 mL) over a period of 30 minutes. The resulting yellow colored reaction mixture was stirred at -78 °C for 1h, warmed to room temperature and stirred for another 1 hour. The solvent was stripped off under vacuum and extracted with pentane (20 mL) and then filtered through a layer of Celite. It is important to remove THF as completely as possible to ensure complete precipitation of LiCl. Gradual stripping of pentane (5 mL at a time) and cooling at -30 °C gave yellow solid (960 mg, 71%). ^1H NMR (δ, 300 MHz, C_6D_6): 0.33 (s, 12H, $CH_2Si(CH_3)_2$); 0.52 (s, 9H, $Si(CH_3)_3$); 0.97 (d, 2H, $SiCH_2P$, $^2J_{P-H}$ = 9.2 Hz); 1.10 (d of d, 12H, $P[CH(CH_3)_2]_2$, $^3J_{P-H}$ = 13.0 Hz, $^3J_{H-H}$ = 7.3 Hz); 1.18 (d of d, 12H, $P[CH(CH_3)_2]_2$, $^3J_{P-H}$ = 13.4 Hz, $^3J_{H-H}$ = 7.3 Hz); 1.35 (br s, 2H, $CH_2Si(CH_3)_2$); 2.01 (d of sept, 4H, $P[CH(CH_3)_2]_2$, $^2J_{P-H}$ = 4.1 Hz, $^3J_{H-H}$ = 7.3 Hz). $^{31}P\{^1H\}$ NMR (δ, 121.421 MHz, C_6D_6): 8.48 (s).

references on page 119

2.10c Synthesis of Dinitrogen Complexes

2.10c.1 {[(Pr$^i_2$PCH$_2$SiMe$_2$)$_2$N]ZrCl}$_2$(μ-η^2:η^{2}-^{14}N$_2$), 2.2. This complex was made according to the published procedure.[8] Resonance Raman (cm^{-1}): Solid, 258, 317, 393, 518, 579, 636, 731, 991, 1046; Solution (THF), 262, 321, 331, 585, 733, 745, 1030. MS (EI) *m/z*: 1066 (M$^+$), 1023, 981, 935, 803, 350, 262.

2.10c.2 {[(Pr$^i_2$PCH$_2$SiMe$_2$)$_2$N]ZrCl}$_2$(μ-η^2:η^{2}-^{15}N$_2$), 2.2. The nitrogen-15 analogue of **2.2** was prepared by introducing ^{15}N$_2$ gas into the flask containing the degassed reaction mixture. Workup was carried out under normal N$_2$. ^{15}N{^{1}H} NMR (δ, 30.406 MHz, C$_7$D$_8$): 350.92 (s). ^{15}N MAS NMR (δ, 40.60 MHz): 345 (s). Resonance Raman (cm^{-1}): Solid, 258, 317, 339, 518, 579, 636, 709, 968, 1024; Solution (THF), 260, 318, 327, 710, 718, 1028. MS (EI) *m/z*: 1068 (M$^+$), 1025, 983, 937, 805, 350, 262.

2.10c.3 {[(Pr$^i_2$PCH$_2$SiMe$_2$)$_2$N]Zr(η^5-C$_5$H$_5$)}$_2$(μ-η^1:η^1-N$_2$), 2.9. A solution of Zr(η^5-C$_5$H$_5$)-Cl$_2$[N(SiMe$_2$CH$_2$PPr$^i_2$)$_2$] (0.980 g, 1.58 mmol) in toluene (60 mL) was transferred into a thick-walled reaction flask (300 mL) containing Na/Hg (85 g of 0.33% amalgam, 12.17 mmol of Na). The flask was then cooled to –196 °C, filled with 1 atmosphere of N$_2$, sealed, and allowed to warm slowly to room temperature with stirring. Upon warming up to room temperature the reaction mixture quickly turned green (1 hour) and then slowly turned deep brown. After the disappearance of the green colour (3 days) the solution was decanted from the amalgam and filtered through a layer of Celite. The amalgam was extracted with 15 mL portions of toluene (total of 60 mL), until the extracts showed no brown colour. The filtrate and the extracts were combined and stripping off the solvent gave a dark brown powder (0.860 g, 96%) in high purity (>95% by NMR spectroscopy). The product was crystallized from a 1:1 mixture of toluene and pentane. ^{1}H NMR (δ, 300 MHz, C$_6$D$_6$): 0.28 (s, 12H, Si(C*H*$_3$)$_2$); 0.33 (s, 12H, Si(C*H*$_3$)$_2$); 1.18 (m, 48H, P[CH(C*H*$_3$)$_2$]$_2$); 1.54 (broad, 8H, SiC*H*$_2$P); 1.88 (m, 4H, P[C*H*(CH$_3$)$_2$]$_2$); 2.54 (m, 4H, P[C*H*(CH$_3$)$_2$]$_2$); 6.11 (broad, ~10H, C$_5$*H*$_5$). ^{31}P{^{1}H} NMR (δ, 121.421 MHz, C$_7$D$_8$): at 20 °C 20.26 (s); at -40 °C, AB quartet at 19.95 (d, ^{2}J$_{P\text{-}P}$ = 80.7Hz) and 20.57 (d, ^{2}J$_{P\text{-}P}$ = 80.7Hz). ^{13}C{^{1}H} NMR (δ, 50.323 MHz, C$_6$D$_6$): 6.46 (s, Si(*C*H$_3$)$_2$); 6.71 (s, Si(*C*H$_3$)$_2$); 11.63 (s, Si*C*H$_2$P); 18.40 (s, P[*C*H(CH$_3$)$_2$]$_2$); 20.94 (s, P[CH(*C*H$_3$)$_2$]$_2$); 21.35 (s, P[CH(*C*H$_3$)$_2$]$_2$); 101,37

references on page 119

(s, C_5H_5). Anal. Calcd for $C_{46}H_{98}N_4P_4Si_4Zr_2 \cdot 0.5C_5H_{12}$: C, 50.13; H, 9.02; N, 4.82. Found: C, 50.11; H, 8.94; N, 4.90. Resonance Raman (cm^{-1}): Solid, 226, 277, 295, 325, 1126, 1211; Solution (toluene), 225, 290, 320, 1125, 1201. MS (EI) *m/z*: 1124 (M^+), 1081, 993, 949, 732, 688, 562, 519, 497, 475, 445, 431, 350, 262.

2.10c.4 $\{[(Pr^i_2PCH_2SiMe_2)_2N]Zr(\eta^5\text{-}C_5H_5)\}_2(\mu\text{-}\eta^1\text{:}\eta^1\text{-}^{15}N_2)$, **2.9**. The nitrogen-15 analogue was prepared by a procedure similar to the one described in section **2.10c.3**, by introducing $^{15}N_2$ gas into the flask containing the degassed reaction mixture. Workup was carried out under unlabelled N_2. $^{15}N\{^1H\}$ NMR (δ, 30.406 MHz, C_7D_8): 353.95 (s). Resonance Raman (cm^{-1}): Solid, 228, 277, 294, 323, 1125, 1172; Solution (toluene), 227, 290, 319, 1124, 1165. MS (EI) *m/z*: 1126 (M^+), 1083, 995, 951, 734, 690, 563, 520, 498, 476, 446, 432, 350, 262.

2.10c.5 $\{[(Pr^i_2PCH_2SiMe_2)_2N]Zr(OAr^*)\}_2(\mu\text{-}\eta^1\text{:}\eta^1\text{-}^{14}N_2)$, **2.12**. A solution of $Zr(OAr^*)Cl_2$-$[N(SiMe_2CH_2PPr^i_2)_2]$ (1.05 g, 1.48 mmol) in toluene (100 mL) was transferred into a thick-walled reaction flask (300 mL) containing Na/Hg (80 g of 0.17% amalgam, 5.74 mmol of Na). The flask was then cooled to –196 °C, filled with 1 atmosphere of N_2, sealed, and allowed to warm slowly to room temperature with stirring. The colorless solution slowly takes on the deep blue colour of the product. The reaction mixture was stirred for 5 days the solution was decanted from the amalgam and then filtered through a layer of Celite. The amalgam-containing residue was extracted with several 50 mL portions (approx. 400 mL) of toluene, until the extracts showed no blue colour. The filtrate and the extracts were combined and stripping off the solvent gave a deep blue solid which was washed with hexanes (2x25 mL). Pure product was obtained by slow evaporation of a toluene solution of the crude product at room temperature (0.36 g, 40%). $^1H\{^{31}P\}$ NMR (δ, 500 MHz, C_7D_8): See Table **2.20**

$^{31}P\{^1H\}$ NMR (δ, 121.421 MHz, C_7D_8): at 20 °C, major isomer 8.69 (s); minor isomer 8.85 (s) and 11.26 (s). NOEDIFF experiments (δ, 400 MHz, C_7D_8): radiating the resonances at 7.00 or 6.98 ppm showed enhancements at 2.34 and 2.32. Variable temperature $^{31}P\{^1H\}$ NMR (δ, 121.42 MHz, C_7D_8): upon cooling a sample of pure major isomer, the resonance at 8.69 ppm broadens and below -40 °C begins to show shoulders at 7.60 ppm and 9.10 ppm. Below -78 °C a broad peak begins to appear at 4.00 ppm which increases in intensity with decreasing

references on page 119

temperature (up to -93 °C). Anal. Calcd for a sample containing only the major isomer, $C_{26}H_{53}ON_2P_2Si_2Zr$: C, 50.44; H, 8.63; N, 4.53. Found: C, 50.70; H, 8.87; N, 4.33. Anal. Calcd for a sample containing a mixture of major isomer and minor isomer (major:minor = 2:1), $C_{26}H_{53}ON_2P_2Si_2Zr$: C, 50.44; H, 8.63; N, 4.53. Found: C, 50.24; H, 8.71; N, 4.29. Resonance Raman (cm^{-1}): Solid, 258, 278, 314, 350, 595, 732, 751, 1046. MS (EI) *m/z*: 1236, 1193, 1107, 1063, 1007, 975, 695, 350, 262.

Table 2.20 ^1H $\{^{31}P\}$ NMR data for complexes **2.12** and **2.12a**.

Groups	Major isomer (δ)	Minor isomer(δ)
$Si(CH_3)_2$	0.37 (s, 12H)	0.29 (s, 6H), 0.32 (s. 6H)
	0.41 (s, 12H)	0.32 (s, 6H), 0.35 (s, 6H)
$SiCH_2P$	1.30 (d, 4H, $^2J_{H-H}$ = 1.6 Hz)	obscured
	1.32 (d, 4H, $^2J_{H-H}$ = 1.6 Hz)	
$P[CH(CH_3)_2]_2$	1.04 (d, 12H, $^3J_{H-H}$ = 6.7 Hz)	1.13 (d, 6H), 1.26 (d, 6H)
	1.05 (d, 12H, $^3J_{H-H}$ = 6.7 Hz)	1.34 (d, 6H), 1.44 (d, 6H)
	1.17 (d, 12H, $^3J_{H-H}$ = 7.3 Hz)	rest of the resonances were
	1.23 (d, 12H, $^3J_{H-H}$ = 7.3 Hz)	obscured
$P[CH(CH_3)_2]_2$	2.03 (sept. 4H, $^3J_{H-H}$ = 7.3 Hz)	2.04 (sept. 2H, $^3J_{H-H}$ = 7.4 Hz)
	2.39 (sept. 4H, $^3J_{H-H}$ = 6.7 Hz)	2.20 (sept. 2H, $^3J_{H-H}$ = 7.4 Hz)
		2.48 (sept. 2H, $^3J_{H-H}$ = 7.4 Hz)
		2.53 (sept. 2H, $^3J_{H-H}$ = 7.4 Hz)
2, 6-Me_2Ph	2.34 (s, 12H)	only assignable resonance was a broad peak at 2.32
p-Ph	6.66 (t, 2H, $^3J_{H-H}$ = 7.1 Hz)	6.62 (t, 2H, $^3J_{H-H}$ = 6.9 Hz)
m-Ph	7.00 (t, 4H, $^3J_{H-H}$ = 7.1 Hz)	6.98 (t, 4H, $^3J_{H-H}$ = 6.9 Hz)

references on page 119

2.10c.6 **{[(Pr$^i_2$PCH$_2$SiMe$_2$)$_2$N]Zr(OAr*}$_2$(μ-η^2:η^2-^{15}N$_2$), 2.12.** The nitrogen-15 analogue was prepared by a procedure similar to the one described in section **2.10c.5**, but by introducing $^{15}N_2$ gas into the flask containing the degassed reaction mixture. Workup was carried out under unlabelled N_2. $^{15}N\{^1H\}$ NMR (δ, 30.406 MHz, C_7D_8): minor isomer, 342.91 (s); major isomer, 339.06 (s). Resonance Raman (cm^{-1}): Solid, 278, 310, 350, 577, 595, 725, 751, 1046. MS (EI) *m/z*: 1238, 1195, 1111, 977, 696, 350, 262.

2.10c.7 **{[(Pr$^i_2$PCH$_2$SiMe$_2$)$_2$N]Zr(OBu^t)}$_2$(μ-η^2:η^2-N$_2$), 2.12.** A solution of crude Zr(OBu^t)-Cl$_2$[N(SiMe$_2$CH$_2$PPr$^i_2$)$_2$] (approx. 1.05 g, 1.48 mmol) from the reaction described in section **2.10b.7** was dissolved in toluene (100 mL) and transferred into a thickwalled reaction flask (300 mL) containing Na/Hg (80 g of 0.30% amalgam, 10.4 mmol of Na). The flask was then cooled to –196 °C, filled with 1 atmosphere of N_2, sealed, and allowed to warm slowly to room temperature with stirring. The colorless solution slowly takes on a deep purple colour of the product. The reaction mixture was stirred for 5 days and the solution was decanted and filtered through a layer of Celite. Stripping off the solvent from the filtrate gave a dark purple oil. Attempts to crystallize the product were not successful. ^1H NMR (δ, 300 MHz, C_6D_6): 0.46 and 0.42 (s, 12H, Si(C*H*$_3$)$_2$); 1.24 (br m, 28H, SiC*H*$_2$P and P[CH(C*H*$_3$)$_2$]$_2$); 1.42 (s, 9H, OC(C*H*$_3$)$_3$); 1.97 (br sept. 2H, P[C*H*(CH$_3$)$_2$]$_2$, $^3J_{H\text{-}H}$ = 7.2 Hz); 2.25 (br sept. 2H, P[C*H*(CH$_3$)$_2$]$_2$, $^3J_{H\text{-}H}$ = 6.6 Hz). $^{31}P\{^1H\}$ NMR (δ, 81.015 MHz, C_6D_6): 8.16 (s). $^{15}N\{^1H\}$ NMR (δ, 30.406 MHz, C_7D_8): 346.41 (s); 334.35 (s); 319.64 (s); 254.87 (s); 248.86 (s).

2.10c.8 **{[(Pr$^i_2$PCH$_2$SiMe$_2$)$_2$N]ZrBr}$_2$(μ-η^2:η^2-^{14}N$_2$), 2.19.** A solution of ZrBr$_3$[N(SiMe$_2$CH$_2$-PPr$^i_2$)$_2$] (0.628 g, 0.943 mmol) in toluene (80 mL) was transferred into a thick-walled reaction flask (300 mL) containing 0.35% Na/Hg (24 g, 3.59 mmol). The flask was then cooled to –196 °C, filled with 1 atmosphere of N_2, sealed, and allowed to warm slowly to room temperature with stirring. The colorless solution slowly takes on the deep blue colour of the product. The reaction mixture was stirred for 7 days and the solution was decanted and filtered through a layer of Celite. The amalgam-containing residue was extracted with 80 mL portions (approx. 1L) of toluene, until the extracts showed no blue colour. Stripping off the solvent from the combined filtrate and extracts gives a dark blue crystalline material (0.23g

references on page 119

42%). ^{1}H NMR (δ, 300 MHz, C_7D_8): 0.30 (s, 12H, Si(CH_3)$_2$); 0.34 (s, 12H, Si(CH_3)$_2$); 1.02 (m, 8H, SiCH_2P); 1.44 (d of d, 12H, P[CH(CH_3)$_2$]$_2$, $^3J_{H-H}$ = 7.3 Hz, $^2J_{H-P}$ = 13.7 Hz); 1.24 (m, 36H, P[CH(CH_3)$_2$]$_2$); 2.18 (d of sept, 4H, P[CH(CH_3)$_2$]$_2$, $^3J_{H-H}$ = 7.5 Hz, $^2J_{H-P}$ = 4.2 Hz); 2.42 (d of sept, 4H, P[CH(CH_3)$_2$]$_2$, $^3J_{H-H}$ = 7.6 Hz, $^2J_{H-P}$ = 3.9 Hz). ^{31}P{^{1}H} NMR (δ, 121.4 MHz, C_7D_8): 9.96 (s). Anal. Calcd for $C_{18}H_{44}BrN_2P_2Si_2Zr$: C, 37.42; H, 7.68; N, 4.85. Found: C, 37.84; H, 7.84; N, 3.89. According to the microanalysts comments, the complex shows lower nitrogen content than expected due to the formation of nitrides during the combustion.

2.10c.9 {[(Pr$^i_2$PCH$_2$SiMe$_2$)$_2$N]ZrBr}$_2$(μ-η^2:η^2-^{15}N$_2$), 2.19. The nitrogen-15 analogue was prepared by a procedure similar to the one described in section **2.10c.8**, but by introducing $^{15}N_2$ gas into the flask containing the degassed reaction mixture. Workup was carried out under unlabelled N_2. ^{15}N{^{1}H} NMR (δ, 30.406 MHz, THF / C_6D_6): 345.75 (s). Resonance Raman (cm^{-1}): Solid, 295, 589, 709, 880, 1009, 1167, 1293. MS (EI) *m/z*: 1158, 1113, 1025, 941, 895, 350, 262.

2.10c.10 {[(Pr$^i_2$PCH$_2$SiMe$_2$)$_2$N]Zr}$_2$ClBr(μ-η^2:η^2-N$_2$), 2.20. A solution containing a mixture of ZrBr$_3$[N(SiMe$_2$CH$_2$PPr$^i_2$)$_2$] (0.160 g, 0.221 mmol) and ZrCl$_3$[N(SiMe$_2$CH$_2$PPr$^i_2$)$_2$] (0.131g, 0.222 mmol) was treated with 0.34% Na amalgam (12.2 g, 1.79 mmol) as described in the synthesis of {[(Pr$^i_2$PCH$_2$SiMe$_2$)$_2$N]ZrBr}$_2$(μ-η^2:η^2-N$_2$). ^{1}H {^{31}P} NMR (δ, 500 MHz, C_7D_8): 0.28 (s, Si(CH_3)$_2$); 0.29 (s, Si(CH_3)$_2$); 0.31 (s, Si(CH_3)$_2$); 0.32 (s, Si(CH_3)$_2$); 0.33 (s, Si(CH_3)$_2$); 0.34 (s, Si(CH_3)$_2$); 0.65 (m, SiCH_2P); 1.00 (m, SiCH_2P); 1.28 (m, P[CH(CH_3)$_2$]$_2$); 1.41 (m, P[CH(CH_3)$_2$]$_2$); 2.40 (m, P[CH(CH_3)$_2$]$_2$). ^{1}P{^{1}H} NMR (δ, 121.4 MHz, C_7D_8): 10.30 (s); 10.06 (s); 9.96 (s); 9.89 (s). MS (EI) *m/z*: 1111, 1067, 1023, 979, 262.

2.10c.11 {[(Pr$^i_2$PCH$_2$SiMe$_2$)$_2$N]Zr}$_2$ClBr(μ-η^2:η^2-^{15}N$_2$) 2.20. The nitrogen-15 analogue was prepared by a procedure similar to the one described in **2.10c.10**, but by introducing $^{15}N_2$ gas into the flask containing the degassed reaction mixture. Workup was carried out under unlabelled N_2. ^{15}N{^{1}H} NMR (δ, 30.406 MHz, C_4H_8O / C_6D_6): 352.50 (s, approx. 1N); 349.26 (s, approx. 2N); 345.75 (s, approx. 1N). Resonance Raman (cm^{-1}): Solid, 264, 300, 313, 579, 709, 884, 976, 1021. MS (EI) *m/z*: 1113, 1069, 1025, 981, 895, 849, 350, 262.

references on page 119

2.10d Reactions Involving Dinitrogen Complexes

2.10d.1 {[(Pr$^i_2$PCH$_2$SiMe$_2$)$_2$N]ZrCl}$_2$(μ-η^2:$\eta^{2\text{-}15}$N$_2$) and NaCp•DME. To a solution of {[(Pr$^i_2$PCH$_2$SiMe$_2$)$_2$N]ZrCl}$_2$(μ-η^2:$\eta^{2\text{-}15}$N$_2$) (30 mg, 0.028 mmol) in THF (4 mL) was added a solution of NaCp•DME (11 mg, 0.062 mmol) dissolved in THF (2 mL), under an atmosphere of unlabelled dinitrogen. A control experiment was set up under an atmosphere of argon. Both reactions were stirred at room temperature until they turned brown (6 days). The solvent was removed *in vacuo*, and extraction of the crude product with pentane and striping off the solvent gave a brown powder. The brown powder was shown to be {[(Pr$^i_2$PCH$_2$SiMe$_2$)N]Zr-(η^5-C$_5$H$_5$)}$_2$(μ-N$_2$) by NMR. A similar reaction carried out in an NMR tube showed clean conversion of the side-on complex to the end-on complex. MS (EI) *m/z*: 1126 M$^+$, 1083, 995, 951, 734, 690.

2.10d.2 Protonation Reactions. The zirconium dinitrogen complex {[(Pr$^i_2$PCH$_2$SiMe$_2$)$_2$N]Zr-(η^5-C$_5$H$_5$)}$_2$(μ-η^1:η^1-N$_2$), **2.9** was protonated by the addition of excess dry HCl gas to a toluene solution of the complex. Extraction of the organic phase with distilled water and calorimetric analysis to determine the amount of hydrazine produced by the method of Watt and Chrisp[113] gave the following results:

Table 2.21 Moles of hydrazine measured from the reaction of {[(Pr$^i_2$PCH$_2$SiMe$_2$)$_2$N]Zr-(η^5-C$_5$H$_5$)}$_2$(μ-η^1:η^1-N) complex in toluene with anhydrous HCl gas. * Expected concentration was calculated by taking into account the amount of pentane present in the complex.

Sample Weight	*Expected Concentration of NH$_2$—NH$_2$	Measured Concentration of NH$_2$—NH$_2$	Ratio Measured/Expected
0.023 g	5.09·10^{-6} M	5.43·10^{-6} M	1.07
0.037 g	6.33·10^{-6} M	7.08·10^{-6} M	1.12

references on page 119

The reactions with 1M HCl solution and with water were carried out with a gas uptake apparatus. An appropriate amount of sample was weighed into the glass bucket and was covered with KBr. The proton source ($HCl_{(aq)}$ or water) was syringed into the flask and allowed to equilibrate at a known pressure of dinitrogen. Then the bucket was dropped and the flask was vigorously shaken and the pressure change was measured after 15 minutes. A qualitative test with the colour developer used in the Watt and Chrisp method showed the presence of hydrazine.

Table 2.22 Mole percent gas evolved during the reaction of $\{[(Pr^i_2PCH_2SiMe_2)_2N]Zr(\eta^5\text{-}C_5H_5)\}_2(\mu\text{-}\eta^1\text{:}\eta^1\text{-}N)$ complex with H_2O and HCl solution. * Percent gas evolutions were calculated by taking into account the amount of pentane present in the complex. ** The data in parenthesis was obtained after 30 minutes.

Sample Weight	Proton Source	Measured Pressure	% Gas evolution*
0.066 g	1 M HCl	351 mmHg	90%
0.037 g	H_2O	349 mmHg	81% (114%)**

Protonation reactions with pyridinium hydrochloride were carried out inside a NMR tube. Complex **2.6** or **2.2** (approx. 30 mg) was dissolved in C_7D_8 (1 mL) and added an excess of $C_5H_5N{\bullet}HCl$ (5 mg) and shaken occasionally until the colour of the N_2 complex dissappeared. ^1H NMR data for complex **2.25**: 0.40 and 0.55 (s, $Si(CH_3)_2$), 1.48 and 2.35 (m, $P[CH(CH_3)_2]$), 4.99 (s, NNH_2). $^{31}P\{^1H\}$ NMR has a broad peak centered at 14 ppm.

2.10d.3 $\{[(Pr^i_2PCH_2SiMe_2)_2N]ZrX\}_2(\mu\text{-}\eta^2\text{:}\eta^2\text{-}N_2)$ where X = Cl, Br or OAr*, and $LiBEt_4$. The side-on dinitrogen complexes were reacted with $LiBEt_4$ in an approximately 1:2 mole ratio in toluene. The deep blue colour of the reaction mixture slowly decreased in intensity to give a yellow solution over a period of 7 days. Stripping off the toluene and extracting the residue with pentane and subsequent stripping off pentane gave a yellow oily substance which seemed to consist of a single complex. Monitoring the reaction by NMR spectroscopy suggested an

references on page 119

almost quantitative conversion of the N_2 complex to the product. The following spectroscopic data is for a reaction carried out in a sealed NMR tube.

^1H {^{31}P} NMR (δ, 500 MHz, C_7D_8): 0.05 (d of quartet, 1H, $^2J_{H-H}$ = 10.2 Hz, $^3J_{H-H}$ = 7.1 Hz); 4.81 (s, 1H); 0.19, 0.31, 0.33, 0.44, 0.48, 0.52, 0.54 and 0.95 (s, each 3H, $Si(CH_3)_2$); 1.62, 1.70, 1.78, 1.82, 1.85, 1.95, 2.15 and 2.25 (sept, $P[CH(CH_3)_2]_2$, each 1H, $^3J_{H-H}$ = 7.0 Hz); 1.51, 1.37 and 1.31 (t, $B(CH_2CH_3)_3$, $^3J_{H-H}$ = 8.3 Hz); 0.6 to 0.85 (overlapping singlets, $SiCH_2$); 0.9 to 1.3 ($P[CH(CH_3)_2]_2$ and $B(CH_2CH_3)_3$). $^{31}P\{^1H\}$ NMR (δ, 121.4 MHz, C_7D_8): Spectrum consisted of an ABMX spin system; 22.28 (d, 1P, $^2J_{P-P}$ = 71.7 Hz); 18. 56 (d, 1P, $^2J_{P-P}$ = 71.7 Hz); 12.56 (s, 1P); 0.06 (s, 1P). $^{15}N\{^1H\}$ NMR (δ, 30.406 MHz, C_7D_8): 250.5 (d, approx. 1N, $^2J_{N-N}$ = 12 Hz); 185.9 (d, approx. 1N, $^2J_{N-N}$ = 12 Hz). $^{11}B\{^1H\}$ NMR (δ, 96.2 MHz C_7D_8): 0.00 (s, free BEt_3); -41.6 (br., coordinated BEt_3); -104.1 (s, unreacted $LiBEt_4$).

2.10d.4 {[($Pr^i_2PCH_2SiMe_2)_2N$]ZrX}$_2$(μ-N_2) Where X = Cp, Cl or OAr*, and Alkyl Halides. A typical reaction involved a toluene solution of the dinitrogen complex and varying equivalents of the alkyl halides. Appropriate equivalents of the volatile alkyl halides MeI, CH_2Br_2 and $BrCH_2CH_2Br$ were transfered into the reaction flask by using a constant volume gas bulb. The constant volume bulbs were filled with the vapor of the alkyl halide at room temperature at the vapor pressure of the pure alkyl halide and then condensed into the reaction flask. Benzyl bromide was made up into a standard toluene solution and then an appropriate volume of the solution was used.

The isolation of {[($Pr^i_2PCH_2SiMe_2)_2N$]ZrCp}$_2$(N_2)•C_7H_7Br, **2.26**. Anal. Calcd for $C_{53}H_{105}BrN_4P_4Si_4Zr_2$: C, 49.08; H, 8.16; N, 4.32. Found: C, 49.44; H, 8.19; N, 4.21.

2.10e Molecular Orbital Calculations. All molecular orbital calculations were performed on the CAChe Worksystem, a product developed by Tektronix. The parameters used in the INDO/1 and Extended Huckel semi-empirical molecular orbital calculations were used as provided by the CAChe Work system, which in turn were taken from the literature.[45,93,94] The structural parameters for the model $[(H_3P)_2(NH_2)ZrCl]_2(\mu\text{-}\eta^2\text{:}\eta^2\text{-}N_2)$, **F** were taken from the literature.[8] The structural parameters for the models $[(H_3P)_2(NH_2)ZrCp]_2(\mu\text{-}\eta^1\text{:}\eta^1\text{-}N_2)$, **A** and

references on page 119

$[(H_3P)_2(NH_2)Zr(OAr^*)]_2(\mu\text{-}\eta^2\text{:}\eta^2\text{-}N_2)$, **H** were obtained from the X-ray crystal structure analysis of complexes $\{[(Pr^i_2PCH_2SiMe_2)_2N]Zr(\eta^5\text{-}C_5H_5)\}_2(\mu\text{-}\eta^1\text{:}\eta^1\text{-}N_2)$, **2.9** and $\{[(Pr^i_2PCH_2SiMe_2)_2N]Zr(OAr^*)\}_2(\mu\text{-}\eta^2\text{:}\eta^2\text{-}N_2)$, **2.12a**. The symmetry of the models **H** and **A** were restricted to C_{2v} and C_2 respectively. The hydrogen atoms were aligned to satisfy the overall symmetry of the model. For all the models the following standard bond lengths were used: P–H = 1.38 Å, C–H = 1.09 Å, N–H = 1.07 Å. The fragment model $(H_3P)_2(NH_2)ZrCl$, **G** was obtained from the literature,[45] and the model $(H_3P)_2(NH_2)ZrCp$, **B** was constructed from the model **A**.

The model **O** was used to obtain the intermediate cases for the rotation of the side-on bound dinitrogen to the end-on bonding mode. The dinitrogen ligand was rotated in the plane defined by the Zr_2N_2 core (which also contains the phosphine ligands) without altering the relative positions of the ligands on the metal centers. A phantom atom "A" was placed in the centre of the dinitrogen ligand and the rotation angle was measured as showed in Figure **2.16**. The shortest zirconium-nitrogen bond distance between the zirconium and dinitrogen was kept identical to that in model **F**.

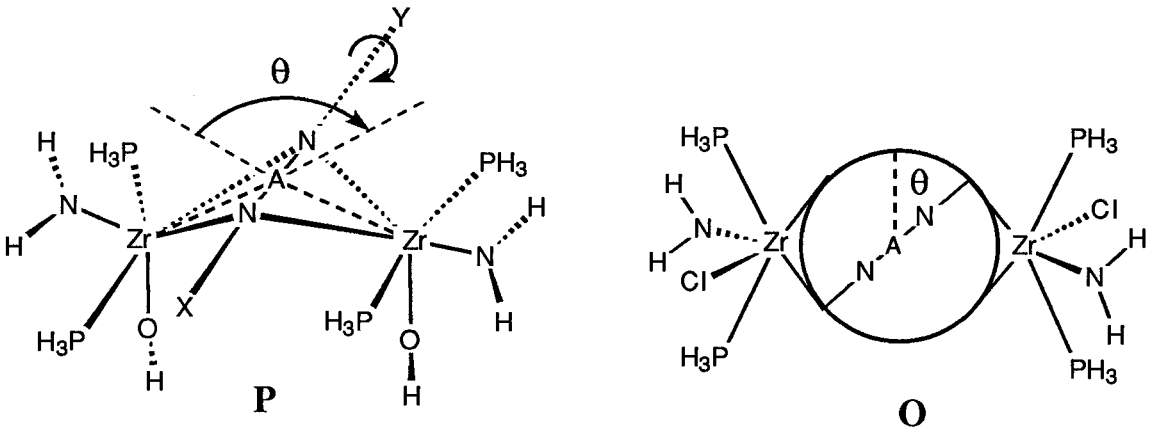

Figure 2.25 The models used to generate the intermediate structures for the bending **P**, and rotation **O**, of side-on bound dinitrogen complexes. The phantom atom "A" is placed in the middle of the N–N bond. The line X–Y in model **P** refers to the axis of the hinge about which the Zr_2N_2 plane was bent.

references on page 119

The model **P** was used to obtain the intermediate cases for the bending of the side-on bound dinitrogen complex. The bending was carried out by moving the dinitrogen ligand on a plane perpendicular to the zirconium-zirconium axis while having the zirconium-"A" distance constant. Also the dihedral angle H–N–Zr–O, where the hydrogen and nitrogen corresponds to the amide, was set to 90°. The angle θ was measured by taking Zr–"A"–Zr bond angles. The bond angle parameters associated with "A"–Zr–Z, where Z = P, N or Cl were maintained constant. The process can be imagined as bending of the Zr_2N_2 core using the nitrogen-nitrogen axis as a hinge.

2.11 References.

(1) Fryzuk, M. D. *Can. J. Chem.* **1992**, *70*, 2849.

(2) Fryzuk, M. D.; MacNeil, P. A. *J. Am. Chem. Soc.* **1981**, *103*, 3592.

(3) Fryzuk, M. D.; MacNeil, P. A.; Rettig, S. J.; Secco, A. S.; Trotter, J. *Organometallics* **1982**, *1*, 918.

(4) Fryzuk, M. D.; Montgomery, C. D. *Coord. Chem. Rev.* **1989**, *95*, 1.

(5) Fryzuk, M. D.; Haddad, T. S.; Berg, D. J.; Rettig, S. J. *Pure Appl. Chem.* **1991**, *63*, 845.

(6) Pearson, R. G. *J. Chem. Ed.* **1968**, *45*, 581.

(7) Pearson, R. G. *J. Chem. Ed.* **1986**, *45*, 643.

(8) Fryzuk, M. D.; Haddad, T. S.; Rettig, S. J. *J. Am. Chem. Soc.* **1990**, *112*, 8185.

(9) Fryzuk, M. D.; McManus, N. T.; Rettig, S. J.; White, G. S. *Angew. Chem., Int. Ed. Engl.* **1990**, *29*, 73.

(10) Fryzuk, M. D.; MacNeil, P. A.; Rettig, S. J. *J. Am. Chem. Soc.* **1987**, *109*, 2803.

(11) Fryzuk, M. D.; Carter, A.; Westerhaus, A. *Inorg. Chem.* **1985**, *24*, 642.

(12) Fryzuk, M. D.; Gao, X.; Joshi, K.; MacNeil, P. A.; Massey, R. L. *J. Am. Chem. Soc.* **1993**, *115*, 10581.

(13) Fryzuk, M. D.; Gao, X. **1993**, Unpublished work.

(14) Fryzuk, M. D.; Haddad, T. S.; Rettig, S. J. *Organometallics* **1988**, *7*, 1224.

(15) Fryzuk, M. D.; Haddad, T. S.; Rettig, S. J. *Organometallics* **1989**, *8*, 1723.

(16) Fryzuk, M. D.; Carter, A.; Rettig, S. J. *Organometallics* **1992**, *11*, 469.

(17) Sutton, L. E. *Tables of Interatomic Distances and Configurations in Molecules and Ions*; Chemical Society: London, 1958; Vol. No. 11.

(18) Manriquez, J. M.; Bercaw, J. E. *J. Am. Chem. Soc.* **1974**, *96*, 6229.

(19) Manriquez, J. M.; Sanner, R. D.; Marsh, R. E.; Bercaw, J. E. *J. Am. Chem. Soc.* **1976**, *98*, 3042.

(20) Manriquez, J. M.; McAlister, D. R.; Sanner, R. D.; Bercaw, J. E. *J. Am. Chem. Soc.* **1976**, *98*, 6734.

(21) Sanner, R. D.; Manriquez, J. M.; Marsh, R. E.; Bercaw, J. E. *J. Am. Chem. Soc.* **1976**, *98*, 8351.

(22) Bush, M. A.; Sim, G. A. *J. Chem. Soc. (A)* **1971**, 2225.

(23) Engelhardt, L. M.; Papasergio, R. I.; Raston, C. L.; White, A. H. *Organometallics* **1984**, *3*, 18.

(24) Cardin, D. J.; Lappert, M. F.; Raston, C. L. *Chemistry of Organo-Zirconium and Hafnium Compounds;* 1 ed.; Ellis Horwood Limited: Toronto, 1986.

(25) Buchwald, S. L.; King, S. M. *J. Am. Chem. Soc.* **1991**, *113*, 258.

(26) Grossman, R. B.; Davis, W. M.; Buchwald, S. L. *J. Am. Chem. Soc.* **1991**, *113*, 2321.

(27) Houri, A. F.; Didiuk, M. T.; Zu, X.; Horan, N. R.; Hoveyda, A. M. *J. Am. Chem. Soc.* **1991**, *1993*, 6614.

(28) Lipshutz, B. H.; Ellsworth, E. L. *J. Am. Chem. Soc.* **1991**, *112*, 7441.

(29) Negishi, E. *Pure Appl. Chem.* **1981**, *53*, 2333.

(30) Negishi, E.; Takahashi, T. *Aldrichimica Acta* **1985**, *18*, 31.

(31) Nigishi, E.; Takahashi, T. *Synthesis* **1988**, 1.

(32) Takagi, K.; Rousset, C. J.; Negishi, E. *J. Am. Chem. Soc.* **1991**, *113*, 1440.

(33) Takahashi, T.; Hasegawa, M.; Suzuki, N.; Subari, M.; Rousset, C. J.; Fanwick, P. E.; Negishi, E. *J. Am. Chem. Soc.* **1991**, *113*, 8564.

(34) Takahashi, T.; Seki, T.; Nitto, Y.; Saburi, M.; Rousset, C. J.; Negishi, E. *J. Am. Chem. Soc.* **1991**, *113*, 6266.

(35) Tidwell, J. H.; Senn, D. R.; Buchwald, S. L. *J. Am. Chem. Soc.* **1991**, *113*, 4685.

(36) Yoshida, T.; NIgishi, E. *J. Am. Chem. Soc.* **1981**, *103*, 4985.

(37) Fryzuk, M. D.; Erker, G.; Mylvaganam, M. Private Communication.

(38) Erker, G.; Wilker, S.; Kruger, C.; Goddard, R. *J. Am. Chem. Soc.* **1992**, *114*, 10983.

(39) Erker, G.; Temme, B. *J. Am. Chem. Soc.* **1992**, *114*, 4004.

(40) Burk, M. J. *J. Am. Chem. Soc.* **1991**, *113*, 8518.

(41) Peterson, E. J.; Dreele, R. B. v.; Brown, T. M. *Inorg. Chem.* **1979**, *15*, 309.

(42) Archer, R. D.; Day, R. O.; Illingsworth, M. L. *Inorg. Chem.* **1976**, *18*, 2908.

(43) Wilkinson, P. G.; Hounk, N. B. *J. Chem. Phys.* **1956**, *24*, 528.

(44) Allen, F. H.; Kennard, O.; Watson, D. G.; Brammer, L.; Orpen, A. G.; Taylor, R. *J. Chem. Soc., Perkin Trans.* **1987**, *II*, S1.

(45) Fryzuk, M. D.; Haddad, T. S.; Mylvaganam, M.; McConville, D. H.; Rettig, S. J. *J. Am. Chem. Soc.* **1993**, *115*, 2782.

(46) Evans, W. J.; Ulibarri, T. A.; Ziller, J. W. *J. Am. Chem. Soc.* **1988**, *110*, 6877.

(47) Blum, L.; Williams, I. D.; Schrock, R. R. *J. Am. Chem. Soc.* **1984**, *106*, 8316.

(48) Chow, P. C. Ph. D. Thesis, UBC, 1993.

(49) Turner, H. W.; Fellmann, J. D.; Rocklage, S. M.; Schrock, R. R.; Churchill, M. R.; Wasserman, H. J. *J. Am. Chem. Soc.* **1980**, *91*, 6512.

(50) Fryzuk, M. D.; Haddad, T. S.; Berg, D. J. *Coord. Chem. Rev.* **1990**, *99*, 137.

(51) Walsh, P. J.; Hollander, F. J.; Bergman, R. G. *J. Am. Chem. Soc.* **1988**, *110*, 8729.

(52) Archer, R. D.; Day, R. O.; Illingsworth, M. L. *Inorg. Chem.* **1976**, *18*, 2908.

(53) Lubben, T. V.; Wolczanski, P. T.; vanDuyne, G. D. *Organometallics* **1984**, *3*, 977.

(54) Hunter, W. E.; Hrncir, D. C.; Bynum, R. V.; Penttila, R. A.; Atwood, J. L. *Organometallics* **1983**, *2*, 750.

(55) Mason, J. *Chem. Rev.* **1981**, *81*, 205.

(56) Sanner, R. D.; Duggan, D. M.; McKenzie, T. C.; Marsh, R. E.; Bercaw, J. E. *J. Am. Chem. Soc.* **1976**, *98*, 8358.

(57) Duchateau, R.; Gambarotta, S.; Beydoun, N.; Bensimon, C. *J. Am. Chem. Soc.* **1991**, *113*, 8986.

(58) Beydoun, N.; Duchateau, R.; Gambarotta, S. *J. Chem. Soc., Chem. Commun.* **1992**, 244.

(59) Mtunzi, S. D.; Richards, R. L. *J. Chem. Soc., Dalton Trans.* **1984**, 469.

(60) Lazarowych, N. J.; Morris, R. H.; Ressner, J. M. *Inorg. Chem.* **1986**, *25*, 3926.

(61) Manriquez, J. M.; McAlister, D. R.; Rosenberg, E.; Shiller, A. M.; Williamson, K. L.; Chan, S. I.; Bercaw, J. E. *J. Am. Chem. Soc.* **1978**, *100*, 3078.

(62) McConville, D. H. Ph. D. Thesis, UBC, 1991.

(63) Rocklage, S. M.; Turner, H. W.; Fellmann, J. D.; Schrock, R. R. *Organometallics* **1982**, *1*, 703.

(64) O'Regan, M. B.; Liu, A. H.; Finch, W. C.; Schrock, R. R.; Davis, W. M. *J. Am. Chem. Soc.* **1990**, *112*, 4331.

(65) Haddad, T. S. Unpublished results.

(66) Mylvaganam, M. Unpublished results.

(67) *Resonance Raman Spectroscopy As An Analytical Tool*; Melveger, A. J., Ed.; The Franklin Institute Press: Philadelphia, 1977.

(68) Baldwin, M. J.; Root, D. F.; Pate, J. E.; Fujisawa, K.; Kitajima, N.; Solomon, E. I. *J. Am. Chem. Soc.* **1992**, *114*, 10421.

(69) Jolly, W. L. *The Inorganic Chemistry Of Nitrogen*; W A Benjamin, Inc.: New York, 1964.

(70) Durig, J. R.; Pate, C. B.; Harris, W. C. *J. Chem. Phys.* **1972**, *52*, 5652.

(71) Dollish, F. R.; Fateley, W. G.; Bentley, F. F. *Characteristic Raman Frequencies of Organic Compounds*; John Wiley and Sons: Toronto, 1974.

(72) Treitel, I. M.; Flood, M. T.; Marsh, R. E.; Gray, H. B. *J. Am. Chem. Soc.* **1969**, *91*, 6512.

(73) Chatt, J.; Duncanson, L. A. *J. Chem. Soc.* **1953**, 2939.

(74) Dewar, M. J. S. *Bull. Soc. Chim. Fr.* **1951**, 79.

(75) Chatt, J. *Pure Appl. Chem.* **1970**, *24*, 425.

(76) Rosi, M.; Sgamellotti, A.; Tarantelli, F.; Floriani, C.; Cederbaum, L. S. *J. Chem. Soc., Dalton Trans.* **1989**, 33.

(77) Sellmann, D. *Angew. Chem., Int. Ed. Engl.* **1974**, *13*, 639.

(78) Chatt, J.; Leigh, G. J. *Chem. Soc. Rev.* **1972**, *1*, 121.

(79) Powell, C. B.; Hall, M. B. *Inorg. Chem.* **1984**, *23*, 4619.

(80) Albright, T. A.; Burdett, J. K.; Whangbo, M. H. *Orbital Interactions in Chemistry*; A Wiley-Interscience Publication: New York, 1985.

(81) Kubacek, P.; Hoffmann, R.; Havlas, Z. *Organometallics* **1982**, *1*, 180.

(82) Schleyer, P. R.; Maslak, P.; Chandrasekhar, J.; Grev, R. S. *Tetrahedron Lett.* **1993**, *34*, 6387.

(83) Sannigrahi, A. B.; Kar, T. *J. Chem. Ed.* **1988**, *65*, 674.

(84) Wiberg, K. A. *Tetrahedron* **1968**, *24*, 1083.

(85) Boca, R.; Pelikan, P.; Haring, M. *J. Mol. Cat.* **1981**, *11*, 41.

(86) Pelikan, P.; Boca, R. *Coord. Chem. Rev.* **1984**, *55*, 55.

(87) Yamabe, T.; Hori, K.; MInato, T.; Fukui, K. *Inorg. Chem.* **1980**, *19*, 2154.

(88) Hori, K.; Asai, Y.; Yamabe, T. *Inorg. Chem.* **1983**, *22*, 3218.

(89) Goldberg, K. I.; Hoffmann, D. M.; Hoffmann, R. *Inorg. Chem.* **1982**, *21*, 3863.

(90) Hoffmann, R.; Chen, M. M. L.; Thorn, D. L. *Inorg. Chem.* **1977**, *16*, 503.

(91) Blomberg, M. R. A.; Siegbahn, P. E. M. *J. Am. Chem. Soc.* **1993**, *115*, 6908.

(92) Richardson, D. E. *J. Chem. Ed.* **1993**, *70*, 372.

(93) Evans, W. J.; Ulibarri, T. A.; Ziller, J. W. *J. Am. Chem. Soc.* **1988**, *110*, 6877.

(94) Ho, J.; Drake, R. J.; Stephan, D. W. *J. Am. Chem. Soc.* **1993**, *115*, 3792.

(95) Morokuma, K. *Acc. Chem. Ses.* **1977**, *10*, 294.

(96) Fryzuk, M. D.; Lloyd, B. R.; Clentsmith, G. K. B.; Rettig, S. J. *J. Am. Chem. Soc.* **1991**, *113*, 4332.

(97) Henderson, R. A.; Oglieve, K. E. *J. Chem. Soc., Dalton Trans.* **1990**, 1093.

(98) Glassman, T. E.; Liu, A. H.; Schrock, R. *Inorg. Chem.* **1991**, *30*, 4723.

(99) SmithIII, M. R.; Cheng, T. Y.; Hillhouse, G. L. *J. Am. Chem. Soc.* **1993**, *115*, 8638.

(100) Churchill, M. R.; Li, Y. J.; Blum, L.; Schrock, R. *Organometallics* **1984**, *3*, 109.

(101) vanTamelan, E. E. *Acc. Chem. Res.* **1970**, *11*, 361.

(102) Colquhoun, H. M. *Acc. Chem. Res.* **1984**, *17*, 23.

(103) Kawaguchi, M.; Hamaoka, S.; Mori, M. *Tetrahedron Lett.* **1993**, *34*, 6907.

(104) Collman, J. P.; Hegedus, L. S.; Norton, J. R.; Finke, R. G. *Principles and Applications of Organotranstion Metal Chemistry;* second edition ed.; University Science Books: Mill Valley, CA., 1987.

(105) Henderson, R. A.; Leigh, G. J.; Pickett, C. J. *Adv. Inorg. Chem. Radiochem.* **1983**, *27*, 197.

(106) Nakamura, A.; Yoshida, T.; Cowie, M.; Ibers, S. O. A. *J. Am. Chem. Soc.* **1977**, *99*, 2108.

(107) Burrell, A. K.; Clark, G. R.; Rickard, C. E. F.; Roper, W. R. *J. Chem. Soc., Dalton Trans.* **1991**, 609.

(108) Joule, J. A.; Smith, G. F. *Heterocyclic Chemistry;* second ed.; Van Nostrand Reinhold (UK) Co.Ltd: Cambridge, 1984, pp 345.

(109) Wayda, A. L.; Darensbourg, M. Y. In *ACS Symp. Ser. Vol. 357: Experimental Organometallic Chemistry;* American Chemical Society: Washington, D. C; **1987**.

(110) Shriver, D. F.; Drezdzon, M. A. *The Manipulation of Air-Sensitive Compounds;* 2nd ed.; John Wiley and Sons: New York, 1986.

(111) Smart, J. C.; Curtis, C. J. *Inorg. Chem.* **1977**, *16*, 1788.

(112) Perrin, D. D.; Armarego, W. L. F. *Purification of Laboratory Chemicals;* 3 ed.; Pergoman Press: Toronto, 1988.

(113) Watt, G. W.; Chrisp, J. D. *Anal. Chem.*, **1954**, 24, 2006.

(114) Wang, C; Bodenbinder, M; Willner, H; Rettig, S; Trotter, J; Aubke, F. *Inorg. Chem.* **1994**, 33, 779.

(115) Rasetti, F. *Proc. Natl. Acad. Sci. U. S. A.* **1929**, 15, 431.

Chapter 3

Introduction to Zirconium(III) Chemistry

3.1 General

It is well established in transition metal chemistry that the first row elements show some deviations from their second and third row counterparts.[1,2] For example, if one considers formal oxidation states, then for complexes of the group 4 elements, titanium exhibits +3 and +4 formal oxidation states predominantly,[2] which is in stark contrast to the heavier members of the group, namely zirconium and hafnium, for which the +4 formal oxidation state dominates.[3] In fact, organometallic and coordination compounds of zirconium(III) and hafnium(III) are very poorly documented in the literature and still remain a scarcity.[3]

The rarity of the +3 formal oxidation state in zirconium is partly attributed to the relatively low potential at which it is reduced from the +4 to the +3 state. Reduction potentials for various zirconocene derivatives range from E^0 = -1.6 V to E^0 = -2.1 V.[3,4] In comparison to their titanium counterparts, for example the first reduction potential for Cp_2TiCl_2 is E^0 = -0.75 V, zirconium derivatives are reduced approximately 1 V more negative.[3,4] This large difference in reduction potential is in part due to the coordinative solvation (by THF) of the zirconium center.[3,4] Electrochemical studies involving complexes containing bulky ligands, for example complexes of the type $Cp_2M[C_6H_4(CHSiMe_3)_2$-1,2], gave E^0 values of -1.46, -2.02 and -2.26 V for M = titanium, zirconium and hafnium respectively, where the differences between the reduction potentials of titanium and zirconium are only 0.56 V.[5,6]

A comparison of the ionic radius of titanium (for 4, 5, 6 and 8 coordination numbers the effective ionic radii are 56, 65, 74.5 and 88 ppm respectivly)[7] and zirconium (for 4, 5, 6, 7, 8 and 9 coordination numbers the effective ionic radii are 73, 80, 86, 92, 98 and 103 ppm respectivly)[7] in their +4 formal oxidation state suggests that for complexes with same coordination number and identical ligands, a titanium center in +3 formal oxidation state will be more effectively shielded than the a zirconium(III) center. Therefore, it has been suggested that the zirconium(III) centers could be kinetically activated to undergo further reactions.[3,4]

references on page 133

3.2 Coordination Complexes of Zirconium(III)

A number of adducts of ZrX_3 (X = Cl, Br and I) with nitrogen containing donor ligands such as ammonia, pyridine, acetonitrile, bipyridyl and phenanthroline have been prepared. Although these can be considered as zirconium(III) derivatives the evidence is circumstantial. These compounds are highly colored and have unusual stoichiometries; for example, the metal-to-ligand ratio is 1:2 for $ZrCl_3(py)_2$, 1:1.5 for $Zr_2Cl_6(bipy)_3$ and 1:2.5 for $Zr_2Cl_6(MeCN)_5$.[8-11] The magnetic properties of these complexes are lower than what would be expected for a d^1 complex, and suggest dinuclear or oligonuclear structures with some magnetic exchange between neighboring zirconium atoms. Due to the low solubility of these complexes molecular weight measurements were not possible and therefore any structural proposals are necessarily speculative.

$$ZrCl_4 + 2PR_3 \xrightarrow[Na/Hg]{\text{toluene}} [Zr_2Cl_6(PR_3)_4] \qquad \textbf{3.1}$$

$$PR_3 = PMe_3, PEt_3, PPr_3, PBu^n_3$$

$$[Zr_2Cl_6(PR_3)_4] \rightleftharpoons [Zr_2Cl_6(PR_3)_3] + PR_3 \qquad \textbf{3.2}$$

$$0.5\,[Zr_2Cl_6(PR_3)_4] \rightleftharpoons [ZrCl_3(PR_3)_2] \underset{-\,PR_3}{\overset{+\,PR_3}{\rightleftharpoons}} [ZrCl_3(PR_3)_3] \qquad \textbf{3.3}$$

The class of complexes $[ZrCl_2(\mu\text{-}Cl)(PR_3)_2]_2$, (R = Me, Et, Pr or Bu^n) prepared by the reduction of $ZrCl_4$ in the presence of an alkyl phosphine was the first well characterized coordination complexes of zirconium(III), with complex $[ZrCl_2(\mu\text{-}Cl)(PBu^n_3)_2]_2$ **3.1**, being structurally characterized.[12,13] The solid state structure of $[ZrCl_2(\mu\text{-}Cl)(PBu^n_3)_2]_2$, **3.1**, is centrosymmetric with the zirconium atoms positioned in a pseudo octahedral environment. The short zirconium-zirconium separation of 3.182(1) Å in **3.1** is attributed to a metal-metal bond and is close to that of zirconium metal, 3.1789 Å. The NMR spectroscopic studies with the complexes analogous to **3.1**, $[ZrCl_2(\mu\text{-}Cl)(PR_3)_2]_2$, indicate that they undergo reversible

references on page 133

phosphine dissociation (Equation **3.2**). Also the ESR spectra of a toluene solution of these complexes show a weak signal which becomes more intense when excess phosphine is added, implying the break-down of the dimer into monomers (Equation **3.3**).

Recently, complexes analogous to **3.1** have been synthesized; addition of 4-*tert*-butyl-pyridine to complex **3.1** gave $[ZrCl_2(\mu\text{-}Cl)(C_5H_4NBu^t\text{-}4)_2]_2$, which upon reaction with Bu^tCN gave a dinuclear complex containing a bridging Bu^tCN ligand where the bonding of the nitrile ligand could be described as $(\mu\text{-}\eta^2\text{:}\eta^1)$, **3.2**.[14]

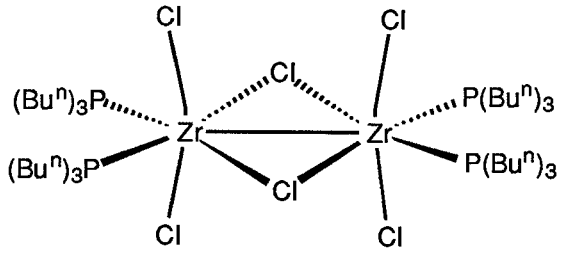

3.1

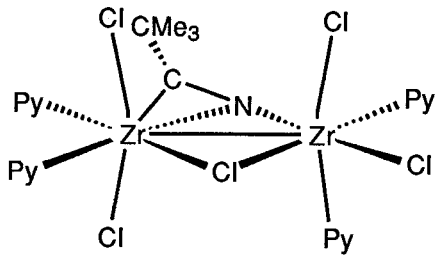

3.2

3.3 Organometallic Complexes of Zirconium(III)

3.3.1 Dinuclear Organometallic Complexes of Zirconium(III)

Most of the attempted syntheses of organometallic zirconium(III) derivatives have resulted in the formation of dinuclear and diamagnetic complexes.[13-26] One class of dinuclear zirconium(III) complexes that contain fulvalene type ligands were synthesized by the reduction of dihalozirconocene derivatives[17,20] or by disproportionation reactions involving Zr(II) and zirconium(IV) precursors (Scheme **3.1**). During the course of the reaction, coupling of two Cp ligands leads to the formation of the fulvalene ligand which bridges the two metal centers. The second class of complexes are of the type $(Cp'_2Zr)_2(\mu\text{-}X_2)$, where Cp' = C_5H_5 or C_5H_4Me and the bridging ligands are either halide groups[19] or dialkyl phosphide[21] groups. The bridging halide derivatives are prepared by the photochemical reaction of the monoalkyl derivatives, Cp'_2ZrXBu^i (Cp' = C_5H_4Me) and the corresponding phosphide derivatives were prepared by the

references on page 133

reduction of Cp_2ZrCl_2 (Cp' = C_5H_5) in the presence of Me_2P—PMe_2. The hafnium derivatives of the latter case (i.e., with bridging phosphides) have also been synthesized.

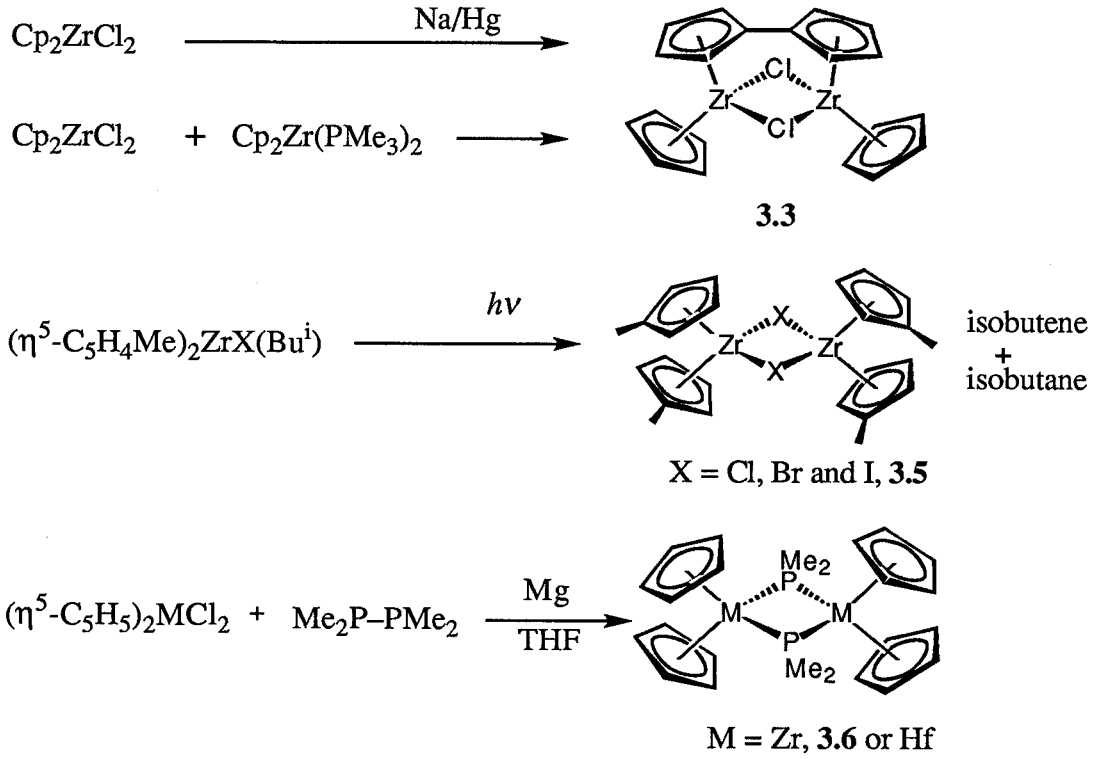

Scheme 3.1

Considerable attention has been focused on the metal-metal separations in the dinuclear zirconium(III) derivatives and their relationship to the possible existence of metal-metal bonding.[29] In fact, the incorporation of a fulvalene dianion as a bridging ligand allows one to constrain the two metal centers within short distances i.e., in the range of zirconium-zirconium bonds.[29] The compilation of metal-metal separations given in Table **3.1** shows that the zirconium-zirconium separations range from 3.099 Å to 4.171 Å. Of all the known dimers, only the complexes of the type $[C_5H_3(SiMe_3)\text{-}1,3]_2Zr(\mu\text{-}X)]_2$ where X = Cl, **3.7** (Scheme **3.4**), Br and I, show paramagnetic behavior.[26] The diamagnetic behaviour of the complexes with metal-metal separations less than 3.4 Å is attributed to metal-metal bonding, whereas for the cases with metal-metal separations greater than 3.4 Å ligand mediated superexchange is invoked. However, *ab initio* calculations done with zirconium dimers having metal-metal separation ranging from 3.6 Å to 4.0 Å, for example, $[(C_5H_5)_2Zr(\mu\text{-}PMe_2)]_2$, **3.6**, have shown that there is

references on page 133

significant d-orbital interactions between the two zirconium centers of the zirconocene fragments (i.e., up to 4 Å separation between "Cp_2Zr"), suggesting the existence of the "super-long" metal-metal bonds.[30]

Table 3.1 Selected zirconium-zirconium distances. ($C_{10}H_8$ refers to the fulvalene ligand).

Complex	metal-metal separation	reference
β-Zr	3.1789 Å	27
β-$ZrCl_3$	3.07 Å	28
$ZrBr_3$	3.16 Å	28
ZrI_3	3.32 Å	28
$[Zr(\mu\text{-}Cl)(Cl_2)(dppe)]_2$	3.099(2) Å	16
$[Zr(\mu\text{-}Cl)Cl_2(PBu^n{}_3)_2]_2$, **3.1**	3.182 Å	13
$[(C_{10}H_8)(C_5H_5)_2Zr_2(\mu\text{-}Cl)_2$, **3.3**	3.233(1) Å	23
$[(C_{10}H_8)(C_5H_5)_2Zr_2(\mu\text{-}I)_2$, **3.4**	3.472(1) Å	19
$[(C_5H_4Me)_2Zr(\mu\text{-}I)]_2$, **3.5**	3.649 (1) Å	19
$[(C_5H_5)_2Zr(\mu\text{-}PMe_2)]_2$, **3.6**	3.653 (2) Å	21
$[C_5H_3(SiMe_3)\text{-}1,3]_2Zr(\mu\text{-}X)]_2$		
X = Cl, **3.7**	3.90 Å	26
X = Br	4.101(1) Å	
X = I	4.171(2) Å	

Most of the chemistry associated with the dinuclear zirconium(III) complexes has been restricted to their synthesis and X-ray structure elucidation. The oxidation of the fulvalene derivatives (e.g., complex **3.3** in Scheme **3.1**) gives Zr(IV)-Zr(IV) dimers having cis (i.e., both zirconium centers on the some side of the fulvalene ligand) or trans geometries.[29] It was expected that during the oxidation of the fulvalene bridged Zr(III)-Zr(III) dimers to Zr(IV)-Zr(IV) dimers the cis geometry would be retained, however, experimental evidence

references on page 133

shows that the cis geometry is retained only when good bridging ligands (e.g., S^{2-} or O^{2-}) are present, whereas trans geometry was found for poorly bridging ligands (e.g., methyl group).

The thermal or photochemical disproportionation reactions of the complexes of the type $[Cp_2Zr(\mu\text{-}X)]_2$, where X = Cl, Br and I, giving zirconium(IV), (Cp_2ZrX_2) and Zr(II), ("Cp_2Zr") species is probably the only reactivity know for bimetallic zirconium(III) complexes.[19] Studies show that the complexes with bridging chloride ligands were the most susceptible towards disproportionation whereas the iodide and bromide analogues were significantly slower. An important feature of these reactions is that their disproportionation was accelerated in the presence of coordinating solvents and in the presence of ligands such as CO and butadiene. For example, reacting $[Cp_2Zr(\mu\text{-}I)]_2$ with CO gives an equimolar ratio of Cp_2ZrI_2 and $Cp_2Zr(CO)_2$.[19]

3.3.2 Mononuclear Organometallic Complexes of Zirconium(III)

In most instances mononuclear zirconium(III) species were generated in situ under photochemical or reducing conditions; typically a common synthetic procedure involved performing reactions inside the cavity of an ESR spectrometer.[31-42] Photochemical reactions of zirconium(IV) zirconocene derivatives leads to the homolysis of a zirconium-carbon bond, forming the corresponding organic radical and the zirconium(III) species. The photolysis of Cp_2ZrCl_2 led to the formation of $CpZrCl_2$ and a $Cp^{\bullet}$ radical, whereas the photolysis of $Cp_2ZrMeCl$ gave Cp_2ZrCl and a $Me^{\bullet}$ radical.[41] When the dialkyl or diaryl derivatives, Cp_2ZrR_2 (where R = alkyl or Ph) were irradiated, the ESR spectral features consisted of a doublet which has been attributed to the formation of a mononuclear hydride species.[38]

The reduction of dialkyl zirconocene derivatives with sodium dihydronaphthylide have shown the formation of an anionic zirconium(III) species, some of which were stable up to 12 hours at room temperature. The anionic species, formed by the reduction of $Cp_2Zr(CH_2SiMe_3)_2$, gave a binomial quintet, coupling due to the methylene protons of the two alkyl groups, suggesting that it is a mononuclear species formulated as $[Cp_2Zr(CH_2SiMe_3)_2]^-[Na(THF)x]^+$.[4] By comparison, the ESR spectrum of a similar titanium species, for example,

references on page 133

$[Cp_2TiCl_2]^-[Na(THF)_x]^+$, shows coupling due to the interaction of the d^1 metal center with a solvated sodium ion (^{23}Na, I = 3/2, 100%).[43,44] The absence of such features in the ESR spectrum of the zirconium species is attributed to the steric bulk of the alkyl groups which probably hinders the formation of ion pairs.

Mononuclear neutral zirconium(III) intermediates have been synthesized by the reduction of the corresponding monoalkyl zirconocene derivatives, Cp_2ZrClR, with sodium amalgam. Among these neutral zirconium(III) derivatives, complexes containing a diphenylphosphinomethyl group, CH_2PPh_2, are particularly interesting because of their ability to form a three membered chelate ring upon formation of the zirconium(III) species (Scheme **3.2**).[37,40,45] The complex **3.7** was formed by reducing the precursor, $Cp_2Zr(CH_2PPh_2)Cl$, with Na/Hg whereas, complexes **3.8** and **3.9** were formed by electrochemical reduction (Scheme **3.2**).[37,40,46]

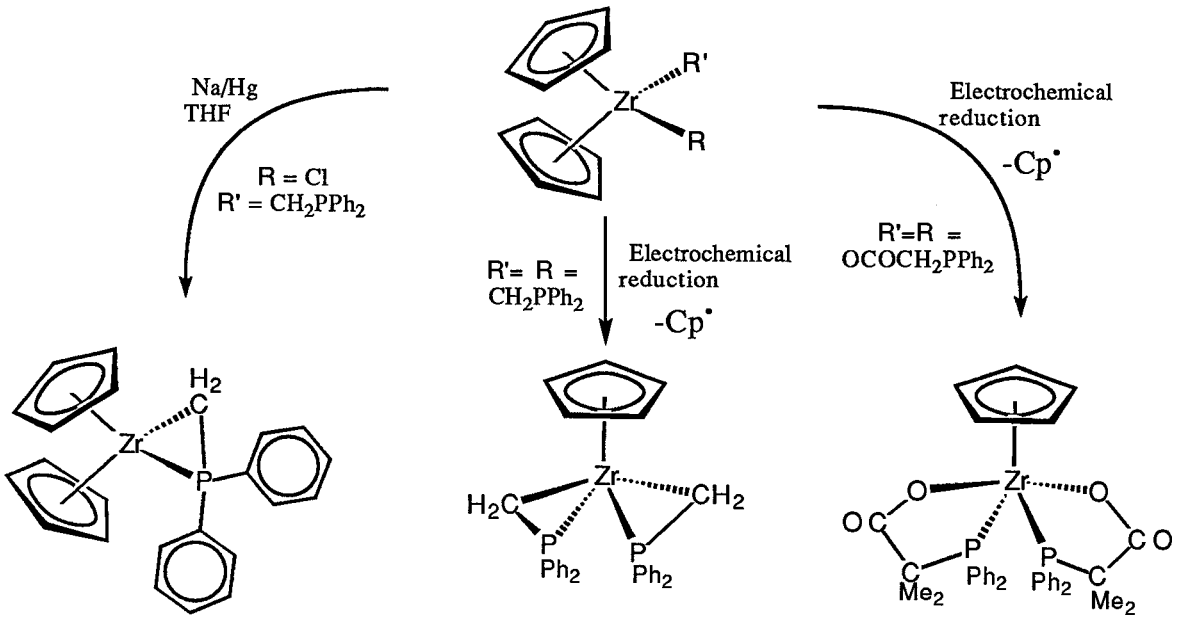

Scheme 3.2

It was found that a toluene solution of $Cp_2Zr(CH_2PPh_2)$ **3.7** slowly decomposes to give a diamagnetic dinuclear species, the formation of which is accelerated in THF solvent. On the basis of NMR spectroscopy, the mechanistic pathway shown in Scheme **3.3** is proposed for the

references on page 133

decomposition of **3.7**.[42,47] This study is important because it shows that the instability of the zirconium(III) complexes is at least partly due to their ability to undergo bimolecular disproportionation reactions which in turn sets off a series of other reactions.

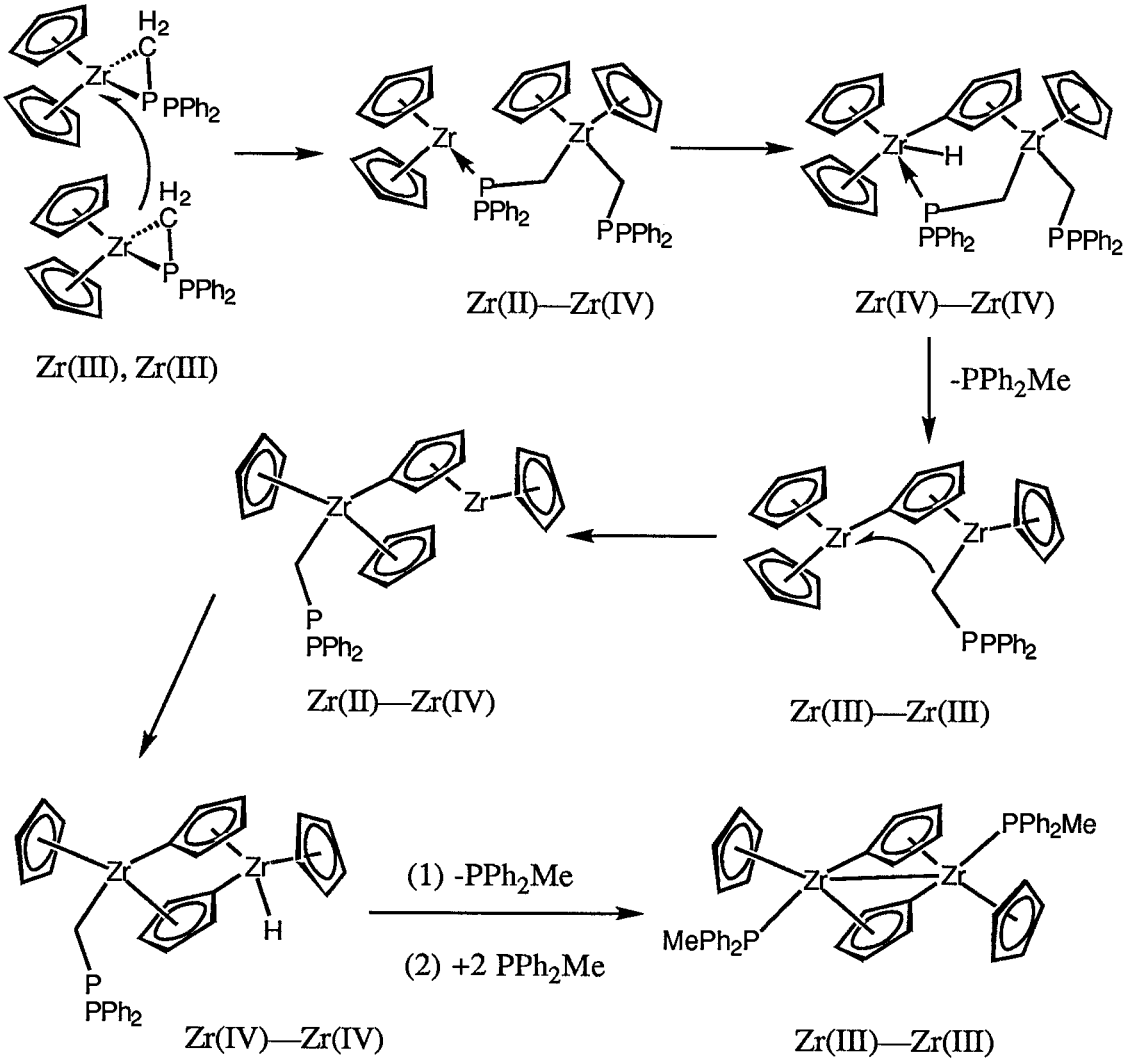

Scheme 3.3

The first step involves a bimolecular disproportionation of **3.7** to form a Zr(II)–Zr(IV) dimeric intermediate, where the zirconium(II) center oxidatively adds a C-H bond of a Cp ligand to give a Zr(IV)–Zr(IV) intermediate with one bridging (μ-η^1:η^5) Cp ligand.[22,31] This Zr(IV)–Zr(IV) intermediate reductively eliminates one $MePPh_2$ unit to form a Zr(III)–Zr(III) species which in turn disproportionates to give another Zr(II)–Zr(IV) intermediate. The Zr(II)

references on page 133

center of this intermediate can C–H activate a second Cp ring and eventually lead to the formation of a second Zr(IV)–Zr(IV) dimer with two bridging (μ-η^1:η^5) Cp ligands. The reductive elimination of the second mole of $MePPh_2$ gives the final product which is a Zr(III)-Zr(III) dimer.

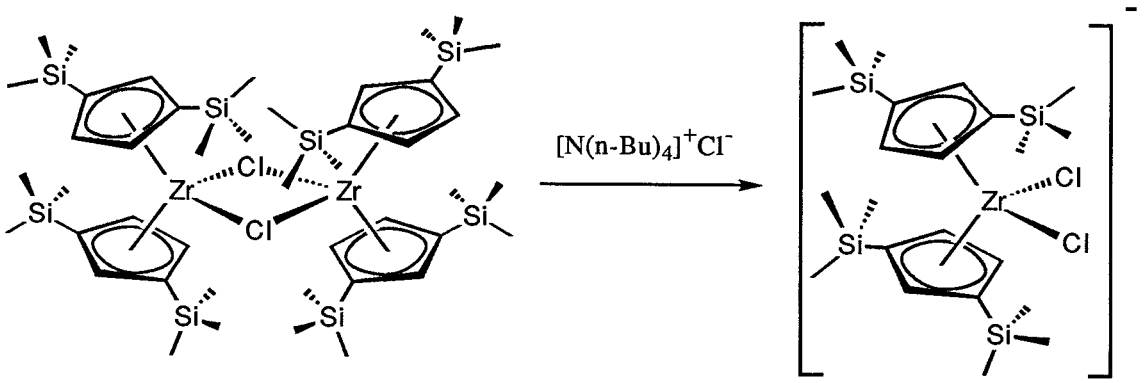

3.7 **3.12** $[N(n\text{-}Bu)_4]^+$

Scheme 3.4

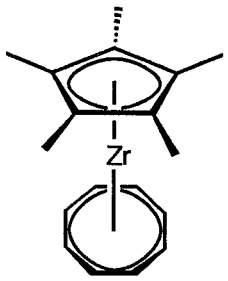

3.10

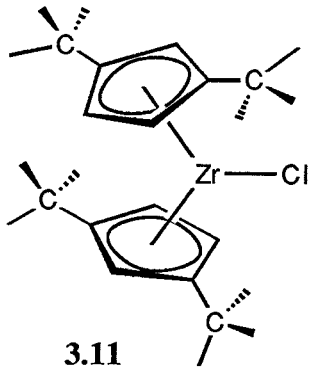

3.11

To our knowledge there are only four mononuclear zirconium(III) complexes that have been well characterized (i.e., including elemental analysis): (η^5-C_5Me_5)Zr(η^8-C_8H_8),[48] **3.10**, (η^5-$C_5H_3Bu^t_2$-1,3)$_2$ZrCl,[49] **3.11**, [Bu_4N][{(η^5-$C_5H_3(SiMe_3)_2$-1,3}$_2$$ZrCl_2$],[26] **3.12**, and Zr($\eta^5$-$C_5H_5$)$_2$($\eta^2$-$N_2$)[$CH(SiMe_3)_2$];[36] of these, only three, **3.10**, **3.11** and **3.12**, have been characterized by X-ray crystallography. The anionic complex **3.12** was prepared by reacting the dinuclear Zr(III)–Zr(III) dimer **3.7**, with a tetraalkyl ammonium salt (Scheme **3.4**), whereas the other three were made by the reduction of the corresponding zirconium(IV) halide precursor.

references on page 133

These examples illustrate that with sufficiently sterically demanding ligands, the tendency of the zirconium(III) state to dimerize and possibly disproportionate[42] can be avoided. However, the chemistry of these complexes has not been explored. In fact, there are no examples of simple, well characterized hydrocarbyl or hydride complexes of zirconium(III) known.

3.4 Summary

The chemistry of zirconium(III) complexes is rather poorly developed, with most of the attention being focused on the synthesis of such complexes. The dinuclear Zr(III)–Zr(III) complexes seem to be favored over the corresponding mononuclear counterparts. It appears that the disproportionation of zirconium(III) complexes to give Zr(II) and zirconium(IV) species is thermodynamically favored, which in part can be attributed to the stability of the zirconium(IV) complexes. The incorporation of bulky ligands around zirconium(III) centers can provide kinetic stability, which in turn has led to the isolation of some mononuclear zirconium(III) complexes.

In the following chapter the preparation of a series of mononuclear zirconium(III) complexes which also incorporate hydrocarbyl and hydride ligands will be discussed. These paramagnetic zirconium(III) derivatives provide the first opportunity to examine the reactivity of Zr–C and Zr–H bonds in d^1 complexes.

3.5 References

(1) Cotton, F. A.; Wilkinson, G. *Advanced Inorganic Chemistry;* Third Edition ed.; Wiley Interscience: New York, 1972.

(2) Greenwood, N. N.; Earnshaw, A. *Chemistry of the Elements*; Pergamon Press: Oxford, 1984; Vol. p. 1116.

(3) Cardin, D. J.; Lappert, M. F.; Raston, C. L. *Chemistry of Organo-Zirconium and Hafnium Compounds;* 1 ed.; Ellis Horwood Limited: Toronto, 1986.

(4) Lappert, M. F.; Pickett, C. J.; Riley, P. I.; Yarrow, P. I. W. *J. Chem. Soc., Dalton Trans.* **1981**, 805.

(5) Dumond, D. S.; Richmond, M. G. *J. Am. Chem. Soc.* **1988**, *110*, 7547.

(6) Gladysz, J. A.; Tam, W. *J. Am. Chem. Soc.* **1978**, *100*, 2545.

(7) Shannon, R. D. *Acta Crystallogr.* **1976**, A32, 751.

(8) Fowles, G. W. A.; Russ, B. J.; Willy, G. R. *Chem. Commun.* **1967**, 646.

(9) Fowles, G. W. A.; Willey, G. R. *J. Chem. Soc. (A)* **1968**, 1435.

(10) Larsen, E. N.; Hehzler, T. E. *Inorg. Chem.* **1974**, *13*, 581.

(11) Nicholls, D.; Ryan, T. A. *Inorg. Chim. Acta* **1977**, *21*, L17.

(12) Wengrovius, J. H.; Schrock, R. R. *J. Organomet. Chem.*, **1981**, *205*, 319.

(13) Wengrovius, J. H.; Schrock, R. R.; Day, C. S. *Inorg. Chem.* **1981**, *20*, 1844.

(14) Hoffman, D. M.; Lee, S. *Inorg. Chem.* **1992**, *31*, 2675.

(15) Ho, J.; Drake, R. J.; Stephan, D. W. *J. Am. Chem. Soc.* **1993**, *115*, 3792.

(16) Cotton, F. A.; Diebold, M. P.; Kibala, P. A. *Inorg. Chem.* **1988**, *27*, 799.

(17) Ashworth, T. V.; Agreda, T. C.; Herdtweck, E.; Herrmann, W. A. *Angew. Chem.., Int. Ed. Engl.* **1986**, *25*, 289.

(18) Wielstra, Y.; Gambarotta, S.; Meetsma, A.; Boer, J. L. d. *Organometallics* **1989**, *8*, 250.

(19) Wielstra, Y.; Gambarotta, S.; Meetsma, A. *Organometallics* **1989**, *8*, 2948.

(20) Cuenca, T.; Herrmann, W. A.; Ashworth, T. V. *Organometallics* **1986**, *5*, 2514.

(21) Chiang, M. Y.; Gambarotta, S.; Boihuis, F. v. *Organometallics* **1988**, *7*, 1864.

(22) Gell, K. I.; Harris, T. V.; Schwartz, J. *Inorg. Chem.* **1981**, *20*, 481.

(23) Gambarotta, S.; Chiang, M. Y. *Organometallics* **1987**, *6*, 897.

(24) Gambarotta, S.; Wielstra, Y.; Spek, A. L.; Smeets, W. J. J. *Organometallics* **1990**, *9*, 2142.

(25) Edwards, P. G.; Howard, J. A. K.; Perry, J. S.; Al-Soudani, A. R. *J. Chem. Soc., Chem. Commun.* **1991**, 1385.

(26) Hitchcock, P. B.; Lappert, M. F.; Lawless, G. A.; Olivier, H.; Rayn, E. J. *J. Chem. Soc. Chem. Commun.* **1992**, 474.

(27) Pearson, W. B. *Handbook of Lattice Spacing Structures of Metals and Alloys*; Pergomon: New York, 1976; Vol. 2, p 90.

(28) Dahl, L. F.; Chiang, T.; Seabaugh, P. W.; Larsen, E. M. *Inorg. Chem.* **1964**, *3*, 1236.

(29) Wielstra, Y.; Gambarotta, S.; Spek, A. L.; Smeets, W. J. J. *Organometallics* **1990**, *9*, 2142.

(30) Benard, M.; Rohmer, M. M. *J. Am. Chem. Soc.* **1992**, *114*, 4785.

(31) Choukroun, R.; Gervais, D. *J. Chem. Soc., Chem. Commun.* **1985**, 224.

(32) Choukroun, R.; Basso-Bert, M.; Gervais, D. *J. Chem. Soc., Chem. Commun.* **1986**, 1317.

(33) Choukroun, R.; Dahan, F.; Larsonneur, A. M.; Samuel, E.; Peterson, J.; Meunier, P.; Sornay, C. *Organometallics* **1991**, *10*, 374.

(34) Jones, C. B.; Petersen, J. F. *J. Am. Chem. Soc.* **1983**, *105*, 5503.

(35) Jones, C. B.; Petersen, J. F. *Inorg. Chem.* **1981**, *20*, 2889.

(36) Samuel, E. *Inorg. Chem.* **1983**, *22*, 2967.

(37) Schore, N. E.; Hope, H. *J. Am. Chem. Soc.* **1980**, *102*, 4251.

(38) Hudson, A.; Lappert, M. F.; Pichon, R. *J. Chem. Soc., Chem. Commun.* **1983**, 374.

(39) Gynane, M. J. S.; Jeffery, J.; Lappert, M. F. *J. Chem. Soc., Chem. Commun.* **1978**, 34.

(40) Etienne, M.; Choukroun, R.; Gervais, D. *J. Chem. Soc., Dalton Trans.* **1984**, 915.

(41) Atkinson, J. M.; Brindley, P. B.; Davis, A. G.; Hawari, J. A. A. *J. Organomet. Chem.* **1984**, *264*, 253.

(42) Blandy, C.; Locke, S. A.; Young, S. J.; Schore, N. E. *J. Am. Chem. Soc.* **1988**, *110*, 7540.

(43) Kenworthy, J. G.; Myatt, J.; Todd, P. F. *Chem. Commun.* **1969**, 263.

(44) Olive, H.; Olive, S. *Angew. Chem., Int. Ed. Engl.* **1968**, *7*, 386.

(45) Manzer, L. E. *J. Am. Chem. Soc.* **1978**, *100*, 8068.

(46) Raoult, Y.; Choukroun, R.; blandy, C. *Organometallics* **1992**, *11*, 2443-2446.

(47) Schore, N. E.; Young, S. J.; Olmstead, M. M. *Organometallics* **1983**, *2*, 1769.

(48) Rogers, R. D.; Teuben, J. H. *J. Organomet. Chem.* **1989**, *359*, 41.

(49) Urazowski, I. F.; Ponomaryev, V. I.; Nifantev, I. E.; Lemenovskii, D. A. *J. Organomet. Chem.* **1989**, *368*, 287.

Chapter 4

Zirconium(III) Complexes: Synthesis and Reactivity

4.1 General

A survey of the literature on zirconium(III) complexes in Chapter **3** has shown that almost all of the stable mononuclear organometallic derivatives contain bulky ligands such as $[\eta^5\text{-}C_5H_3(CMe_3)_2\text{-}1,3]^{-1}$, $[\eta^5\text{-}C_5H_3(SiMe_3)_2\text{-}1,3]^{-1}$ or cyclooctatetraenyl ligand, $[\eta^8\text{-}C_8H_8]^{2-}$ (Chapter **3**). By comparison the tridentate ligand $[N(SiMe_2CH_2PR_2)_2]^{-1}$, PNP is somewhat isoelectronic to the Cp ligand and, in addition, the steric bulk of PNP can be considerably altered by changing the substituents on the phosphorus, for example R = Me, Ph, Pr^i or Bu^t. Therefore by incorporating bulky PNP ligand systems that are comparable to the bulky Cp based ligands such as $[\eta^5\text{-}C_5H_3(CMe_3)_2\text{-}1,3]^{-1}$, it should be possible to stabilize mononuclear zirconium(III) complexes. It is also important to note that the syntheses of dinitrogen complexes (e.g., **2.2**, **2.9**, **2.12** etc.) were only successful with the isopropyl version of the PNP ligand, $[N(SiMe_2CH_2PPr^i_2)_2]^{-1}$ whereas reactions involving complexes containing the less bulky PNP ligand $[N(SiMe_2CH_2PMe_2)_2]^{-1}$, gave intractable material (Chapter **2**). This last result seems to suggest that incorporating the isopropyl substituents on PNP could provide adequate kinetic stability for stabilizing reactive intermediates.

4.2 Synthesis of Zirconium(III) and Hafnium(III) Complexes

It has been previously shown (Section **2.2.2**) that the reduction of the zirconium(IV) complex $Zr(\eta^5\text{-}C_5H_5)Cl_2[N(SiMe_2CH_2PPr^i_2)_2]$, **2.6** with excess Na/Hg under dinitrogen leads to the formation of the dinuclear dinitrogen complex $\{[(PPr^i_2CH_2SiMe_2)_2N]Zr(\eta^5\text{-}C_5H_5)\}_2\text{-}(\mu\text{-}N_2)$, **2.9**. During this process there is a color change from yellow to deep green which persists for hours followed by a slow change to deep brown, the color of the dinuclear dinitrogen derivative. By control of reaction times, the intermediate was intercepted in high yield (88%) as dark green crystals having the formula $Zr(\eta^5\text{-}C_5H_5)Cl[N(SiMe_2CH_2PPr^i_2)_2]$, **4.1** (Scheme **4.1**). This highly colored (λ_{max} = 324 nm, ε_{max} = 2600 $M^{-1}cm^{-1}$) zirconium(III)

references on page 199

chloro derivative, in contrast to other unstable (see Chapter 3) zirconium(III) derivatives, exhibits high thermal stability.[1,2]

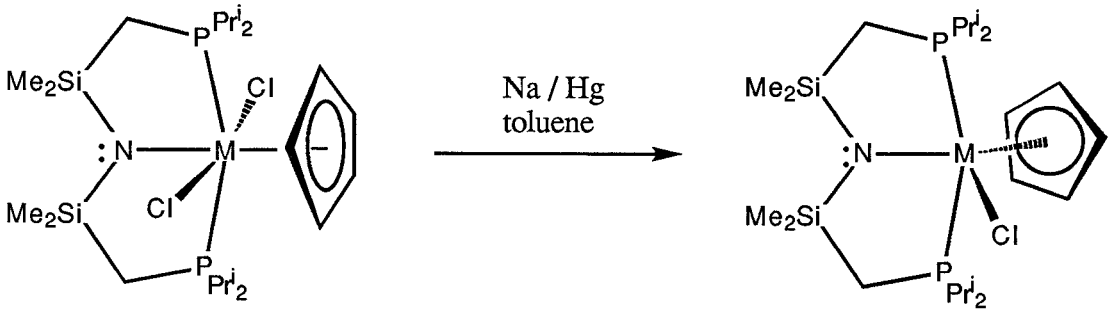

M = Zr, **2.6**
M = Hf, **4.2**

M = Zr, **4.1**
M = Hf, **4.3**

Scheme 4.1

The ^{1}H NMR spectrum of **4.1** is consistent with it being a paramagnetic system since only a broad resonance is observed and no signals were observed in the $^{31}P\{^{1}H\}$ NMR spectrum. Moreover, the solution (in toluene) ESR spectrum recorded at room temperature shows a binomial triplet at g = 1.955 with coupling to two phosphorus-31 nuclei and satellites due to one magnetically dilute zirconium nucleus (a(^{91}Zr) = 37.2 G, ^{91}Zr, 11.23%, I = 5/2), which is consistent with a mononuclear species in solution. The ESR spectrum of **4.1** was simulated using the following parameters: a(^{31}P) = 21.1 G, 2P; a(^{14}N) = 2.9 G, 1N; a(^{1}H) = 1.8 G, 5H; linewidth = 2.3 G. The solution magnetic measurements of **4.1** gave a value of $\mu_{eff.}$ = 1.57 B. M.*

The reduction of the hafnium(IV) precursor $Hf(\eta^5\text{-}C_5H_5)Cl_2[N(SiMe_2CH_2PPr^i_2)_2]$ **4.2,** with Na/Hg gave a brown material, from which deep brown crystalline cubes were isolated by recrystallization. The ESR spectrum of the recrystallized material consisted of a triplet and a broad singlet, where the triplet resonance was identical to the resonance of the zirconium(III) complex **4.1** (Figure **4.1**). The broad signal is assigned to the hafnium(III) species $Hf(\eta^5\text{-}C_5H_5)Cl[N(SiMe_2CH_2PPr^i_2)_2]$, **4.3**. An intriguing feature of the spectrum shown in

* This value is lower than the spin only value of 1.73 B. M. The lower magnetic moment could be attributed to magnetic exchange, i.e., some degree of association between mononuclear species; or to spin-orbit coupling. The calculated spin-orbit coupling constant of Zr^{3+}, 500 cm^{-1}, should give a magnetic moment of about 1.2 B.M.[74]

references on page 199

Figure **4.1** is that the signals due to the zirconium(III) and the hafnium(III) species have approximately equal intensity. However, it will be shown later that the sample consists mainly of hafnium(III) complex in approximately 10:1 ratio. This suggests that the ESR sensitivity of the zirconium(III) complex is approximately ten times greater than that of hafnium(III).

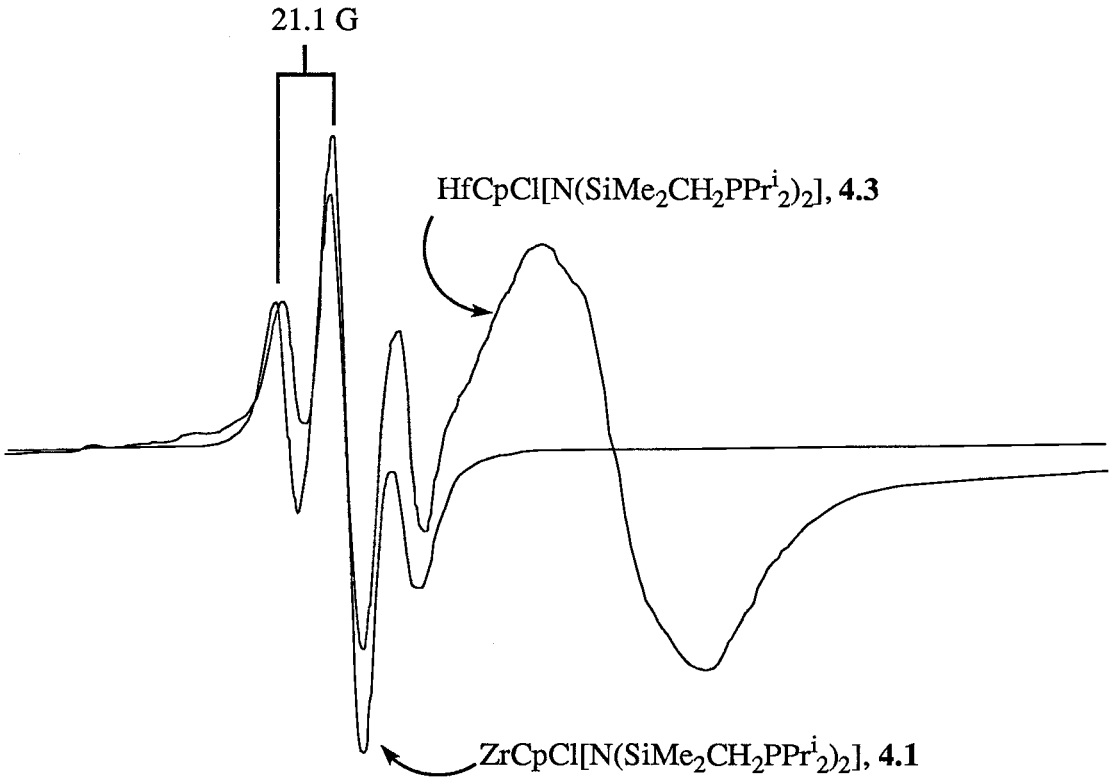

Figure 4.1 Overlapping room temperature ESR spectra of a solution (toluene) sample of $HfCpCl[N(SiMe_2CH_2PPr^i_2)_2]$ **4.3**, and $ZrCpCl[N(SiMe_2CH_2PPr^i_2)_2]$, **4.1**.

Commercially available hafnium precursors (e.g., $HfCl_4$) contain zirconium impurities in the range of 1 to 4%. Therefore, most organometallic complexes of hafnium are likely to have a very small percentage of the zirconium analogue as an impurity. During the reduction of the hafnium(IV) derivatives the hafnium intermediates possibly undergo decomposition at a higher rate than the zirconium counterparts, which would eventually lead to the enrichment of zirconium analogue in the product. The presence of zirconium impurities would also hamper the isolation of analytically pure hafnium(III) samples (Table **4.1**).[3] To our knowledge the

references on page 199

hafnium(III) complex **4.3** is the only complex that has been characterized by satisfactory microanalysis.

Table 4.1 Elemental composition found for some hafnium(III) derivatives.

Complex	C	H	Other	references
$HfCpCl[N(SiMe_2CH_2PPr^i_2)]$, **4.3**			N	
Calculated	41.13	7.35	2.09	this work
Found	41.49	7.49	1.96	
$[HfCl_3(dippe)_2]_2$			Cl	
Calculated	30.7	5.89	19.4	4
Found	31.7	6.05	18.3	
$Hf(\eta^5\text{-}C_5Me_5)(\eta^7\text{-}C_7H_7)$			Hf	
Calculated	50.43	5.48	44.09	3
Found	51.86	5.63	44.55	

4.3 Synthesis of Zirconium(III) Hydrocarbyl Complexes

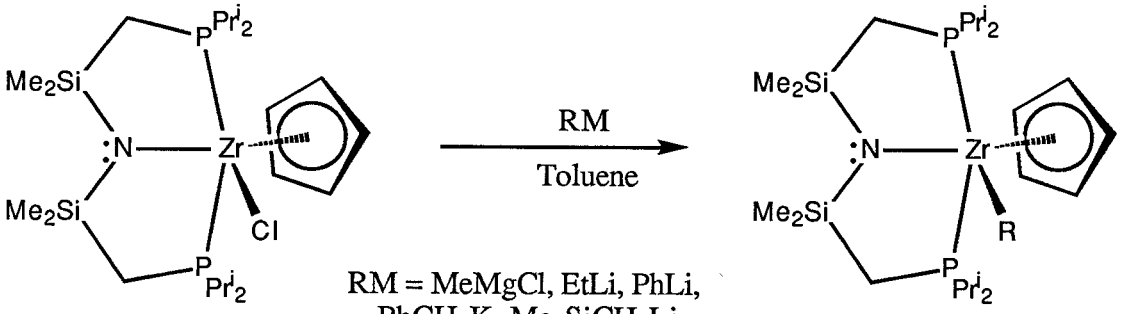

4.1

R = Me **4.5**, Et **4.6**, Ph **4.4**, CH_2Ph **4.7**, CH_2SiMe_3 **4.8**

Scheme 4.2

The metathesis reaction of $Zr(\eta^5\text{-}C_5H_5)Cl[N(SiMe_2CH_2PPr^i_2)_2]$, **4.1** with PhLi at -78 °C in toluene gives an instantaneous color change from a green to a deep red solution. Recrystallization from the crude product gave diamond shaped crystals; these were shown to be

references on page 199

$Zr(\eta^5\text{-}C_5H_5)Ph[N(SiMe_2CH_2PPr^i_2)_2]$, **4.4**. The solution (in toluene) ESR spectrum of complex **4.4** recorded at room temperature shows a broad binomial triplet at g = 1.981 indicating coupling to two phosphorus-31 ($a(^{31}P)$ = 20.3 G) nuclei, however no satellites due to the coupling of the zirconium-91 nucleus were observed.

The zirconium(III) alkyl complexes $Zr(\eta^5\text{-}C_5H_5)R[N(SiMe_2CH_2PPr^i_2)_2]$ where R = Me, **4.5**; Et, **4.6**; $PhCH_2$, **4.7** and Me_3SiCH_2, **4.8**, were synthesized using different alkyl transfer reagents (Scheme **4.2**). A typical reaction was carried out with a toluene solution of the chloro derivative **4.1** and an alkyl transfer reagent, usually at room temperature. Unlike the phenyl derivative, all of the alkyl derivatives are deep green in colour. Isolation of micro-analytically pure samples of the complexes with small alkyl groups, for example methyl, **4.5** and ethyl, **4.6** was hampered by the incorporation of LiCl or $MgCl_2$ in the samples. Table **4.2** gives the elemental compositions found for the hydrocarbyl derivatives of **4.1** and it can be noted that the values for complexes **4.5** and **4.6** are lower than expected. For the ethyl derivative, **4.6** the analytical data for the crystals from the first recrystallization and from the second recrystallization seem to fit for 0.6 and 0.2 equivalents of LiCl respectively. Also, for the methyl derivative **4.5** the crystals from the first recrystallization seem to contain 0.2 equivalents of $MgCl_2$, which is further corroborated by the determination of the chloride content of the sample.

It has been established that some zirconium(IV) complexes form adducts with LiCl,[5] a phenomenon that could be attributed to the Lewis acidity and to the coordinative unsaturation of the zirconium(IV) center. Similar factors may be responsible for the incorporation of LiCl and $MgCl_2$ into the zirconium(III) complexes **4.6** and **4.5** respectively. However, in these zirconium(III) derivatives, the interactions between the zirconium and the halide ion of the salts (i.e., LiCl or $MgCl_2$) are probably weaker and become insignificant as the steric bulk of the alkyl group is increased. The room temperature solution ESR spectra of the samples formulated as **4.6**•$(LiCl)_{0.6}$ and **4.6**•$(LiCl)_{0.2}$ were virtually identical. It is noteworthy that the ESR spectrum of the anionic zirconium species $[Cp_2Zr(CH_2SiMe_3)_2]^-[Na(THF)_x]^+$ did not show

references on page 199

hyperfine interaction due to sodium;[2] in contrast, the phosphide derivative $[Cp_2Zr(PEt_2)_2]^-[Na(THF)_x]^+$ shows hyperfine features due to the coupling of one sodium nucleus.[6]

Table 4.2 Micro-analytical data for the hydrocarbyl derivatives of $Zr(\eta^5\text{-}C_5H_5)Cl[N(SiMe_2CH_2PPr^i_2)_2]$.

Complex	C	H	N	Cl
$Zr(\eta^5\text{-}C_5H_5)Me[N(SiMe_2CH_2PPr^i_2)_2]$, **.4.5**				
Calculated for **4.5**	51.11	9.29	2.48	
Calculated for **4.5**•$(MgCl_2)_{0.22}$	49.28	8.96	2.39	2.67
Found	48.90	9.08	2.39	2.52
$Zr(\eta^5\text{-}C_5H_5)Et[N(SiMe_2CH_2PPr^i_2)_2]$, **4.6**				
Calculated for **4.6**	51.95	9.42	2.42	
Calculated for **4.6**•$(LiCl)_{0.6}$	49.76	9.02	2.32	
found for 1st recrystallization	49.81	9.14	2.30	
Calculated for **4.6**•$(LiCl)_{0.2}$	51.20	9.28	2.39	
found for 2nd recrystallization	51.21	9.27	2.40	
$Zr(\eta^5\text{-}C_5H_5)Ph[N(SiMe_2CH_2PPr^i_2)_2]$, **4.4**				
Calculated	55.63	8.69	2.24	
Found	55.51	8.68	2.35	
$Zr(\eta^5\text{-}C_5H_5)CH_2Ph[N(SiMe_2CH_2PPr^i_2)_2]$, **4.7**				
Calculated	56.29	8.82	2.19	
Found	56.58	8.86	2.25	
$Zr(\eta^5\text{-}C_5H_5)CH_2SiMe_3[N(SiMe_2CH_2PPr^i_2)_2]$, **4.8**				
Calculated	50.97	9.51	2.20	
Found	50.68	9.46	2.21	

Figure **4.2** shows the X-ray structures of the phenyl derivative $Zr(\eta^5\text{-}C_5H_5)Ph[N(SiMe_2\text{-}CH_2PPr^i_2)_2]$ **4.4**, and the alkyl derivative $Zr(\eta^5\text{-}C_5H_5)CH_2SiMe_3[N(SiMe_2CH_2PPr^i_2)_2]$, **4.8**. These two examples are the first structurally characterized, mononuclear hydrocarbyl derivatives of zirconium(III).

references on page 199

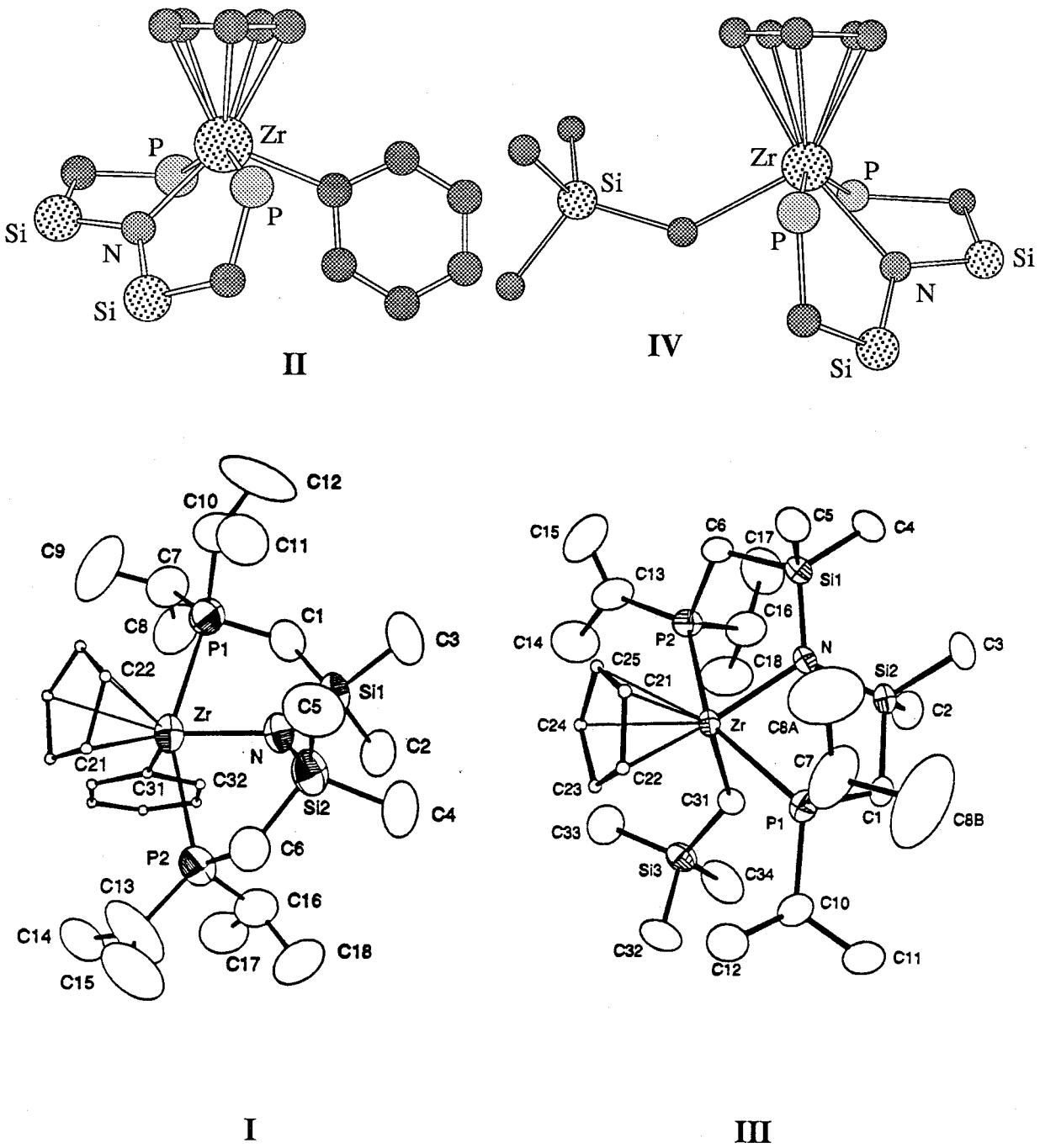

Figure 4.2 **I** and **III** are ORTEP views showing the complete atom labeling scheme for complexes $Zr(\eta^5\text{-}C_5H_5)Ph[N(SiMe_2CH_2PPr^i_2)_2]$ **4.4**, and $Zr(\eta^5\text{-}C_5H_5)CH_2SiMe_3\text{-}[N(SiMe_2CH_2PPr^i_2)_2]$ **4.8**, respectively. **II** and **IV** are Chem 3D® views showing the arrangements of ligands around the zirconium in complexes $Zr(\eta^5\text{-}C_5H_5)Ph\text{-}[N(SiMe_2CH_2PPr^i_2)_2]$ **4.4**, and $Zr(\eta^5\text{-}C_5H_5)CH_2SiMe_3[N(SiMe_2CH_2PPr^i_2)_2]$ **4.8**, respectively.

references on page 199

Table 4.3 Selected bond lengths of complexes $Zr(\eta^5\text{-}C_5H_5)Ph[N(SiMe_2CH_2PPr^i_2)_2]$ **4.4**, and $Zr(\eta^5\text{-}C_5H_5)CH_2SiMe_3[N(SiMe_2CH_2PPr^i_2)_2]$, **4.8**.

$Zr(\eta^5\text{-}C_5H_5)Ph[N(SiMe_2CH_2PPr^i_2)_2]$ **4.4**			$Zr(\eta^5\text{-}C_5H_5)CH_2SiMe_3[N(SiMe_2CH_2PPr^i_2)_2]$ **4.8**		
Atom	Atom	Distance (Å)	Atom	Atom	Distance (Å)
Zr	P(1)	2.7819 (14)	Zr	P(1)	2.7923 (16)
Zr	P(2)	2.7843 (16)	Zr	P(2)	2.8563 (17)
Zr	N	2.231 (3)	Zr	N	2.216 (4)
Zr	C(31)	2.272 (4)	Zr	C(31)	2.337 (5)
Zr	Cp	2.225	Zr	Cp	2.2162 (5)

The structural parameters (Table **4.3** and **4.4**) associated with the PNP ligand in both complexes are similar to other zirconium(IV) derivatives.[7-9] A comparison of bond angles around the zirconium centers suggests that the coordination environment can be envisaged as a distorted trigonal bipyramid with the phosphine donors of the meridionally coordinated PNP ligand occupying the axial positions. The distances from the zirconium to the centroid of the Cp ligand in the phenyl, **4.4** (2.225 Å) and the alkyl, **4.8** (2.2162 (5) Å) derivatives are slightly shorter (the difference is greater than 0.05 Å) than the distances observed for the zirconium(IV) derivatives **2.7** (2.286 Å) and **2.9** (2.286 and 2.294 Å). Shorter zirconium–Cp distances reflect the decreased steric constrains around the zirconium(III) centers of **4.4** and **4.8** than the zirconium centers of **2.7** and **2.9**.

The zirconium-carbon bond distances associated with the phenyl, **4.4** (2.272 (3) Å) and the alkyl, **4.8** (2.337 (5) Å) derivatives are within the observed range for zirconium complexes containing bulky alkyl groups, for example in $Cp_2ZrPh[CH(SiMe_3)_2]$ the zirconium-C_{ipso} and zirconium-C(alkyl) distances are 2.324 (7) and 2.329 (6) Å respectively.[10] For zirconocene derivatives the zirconium-C(sp^3) bond distances range from 2.251 (6) Å to 2.388 (12) Å where the longer distances are associated with larger alkyl groups.[2,10-12] In the PNP derivative $Zr(\eta^4\text{-}C_4H_6)Ph[N(SiMe_2CH_2PPr^i_2)_2]$, the zirconium-$C_{ipso}$ distance of 2.317 (7) Å is slightly longer than what was observed in the zirconium(III) phenyl derivative, **4.4**.

references on page 199

Table 4.4 Selected bond angles of complexes $Zr(\eta^5\text{-}C_5H_5)Ph[N(SiMe_2CH_2PPr^i_2)_2]$ **4.4**, and $Zr(\eta^5\text{-}C_5H_5)CH_2SiMe_3[N(SiMe_2CH_2PPr^i_2)_2]$, **4.8**.

$Zr(\eta^5\text{-}C_5H_5)Ph[N(SiMe_2CH_2PPr^i_2)_2]$ **4.4**				$Zr(\eta^5\text{-}C_5H_5)CH_2SiMe_3[N(SiMe_2CH_2PPr^i_2)_2]$ **4.8**			
Atom	Atom	Atom	Angle (°)	Atom	Atom	Atom	Angle (°)
P(1)	Zr	P(2)	150.09 (4)	P(1)	Zr	P(2)	151.17 (5)
P(1)	Zr	N	79.47 (9)	P(1)	Zr	N	77.83 (11)
P(2)	Zr	N	75.01 (10)	P(2)	Zr	N	74.37 (11)
P(1)	Zr	C(31)	87.04 (11)	P(1)	Zr	C(31)	85.13 (13)
P(2)	Zr	C(31)	88.57 (11)	P(2)	Zr	C(31)	93.47 (13)
P(1)	Zr	Cp	104.27	P(1)	Zr	Cp	103.95 (4)
P(2)	Zr	Cp	104.82	P(2)	Zr	Cp	102.08 (4)
N	Zr	C(31)	112.60 (13)	N	Zr	C(31)	102.47 (16)
N	Zr	Cp	135.57	N	Zr	Cp	139.47 (10)
C(31)	Zr	Cp	111.81	C(31)	Zr	Cp	118.05 (13)
Zr	C(31)	C(36)	132.5 (5)	Zr	C(31)	Si(3)	134.0 (3)
Zr	C(31)	C(32)	114.9 (3)	Si(3)	C(31)	C(33)	114.9 (3)
Si(1)	N	Si(2)	119.15 (17)	Si(1)	N	Si(2)	120.18 (23)

Cp refers to the centroid of the Cp ligand. All structural parameters associated with the Cp ligand for the complex **4.4** were taken from the Chem 3D® structure.

The bond angles between the zirconium, ipso-carbon and the ortho-carbons in $Zr(\eta^4\text{-}C_4H_6)Ph[N(SiMe_2CH_2PPr^i_2)_2]$ are 121.1° (6) and 125.3° (6)[13]; however, the comparable angles in the zirconium(III) phenyl complex **4.4**, Zr–C(31)–C(36) and Zr–C(31)–C(32) are 132.5° (5) and 114.9° (3) Å respectively. These angle parameters seems to suggest that in **4.4** the phenyl ligand is twisted about the ipso-carbon towards the nitrogen of the PNP. The phenyl group in complex **4.4** is coplanar with the equatorial plane and therefore is expected to

references on page 199

experience significant steric interactions with the Cp ligand, where the centroid of the Cp ligand also lies on the equatorial plane.

It is noteworthy that attempts to metathesize the zirconium-chloride bond of **4.1** with the Grignard reagent BzMgCl gave a diamagnetic compound (in approximately 20% isolated yield) as one of the products. Spectroscopic and elemental analysis of this compound are consistent with the formula $ZrBz_2Cl[N(SiMe_2CH_2PPr^i_2)_2]$, **4.9**. It seems that the reaction of **4.1** with BzMgCl or BzK involves more than one reaction pathway, one of which being the exchange of the Cp ligand of **4.1** with the benzyl group. This exchange reaction is less significant when BzK was used, where the zirconium(III) benzyl derivative was the main product. It is noteworthy that the $^{31}P\{^1H\}$ NMR spectrum of the mother liquor of the aforementioned reactions shows that one of the diamagnetic impurities is the end-on dinitrogen complex **2.9**. This observation seems to suggest the formation of a zirconium(II) species (which subsequently binds dinitrogen) during the reaction of **4.1** with benzyl transfer reagents.

A possible mechanism to rationalize the formation of the zirconium(IV) dibenzyl derivative **4.9** could involve the formation of the zirconium(III) benzyl intermediate $ZrBzCl[N(SiMe_2CH_2PPr^i_2)_2]$ by the exchange of the Cp ligand of **4.1** rather than the replacement of the chloride ligand. This intermediate, by comparison with the stable zirconium(III) complex $ZrCpCl[N(SiMe_2CH_2PPr^i_2)_2]$ **4.1**, is sterically less crowded. Therefore, $ZrBzCl[N(SiMe_2CH_2PPr^i_2)_2]$ is likely to be kinetically labile towards disproportionation to give the zirconium(IV) complex **4.9** and some unknown zirconium(II) species.

Solution magnetic studies (Evans Method) on the CH_2SiMe_3 derivative gave a value of $\mu_{eff.}$ = 1.73 B.M., which is close to the calculated spin only value of a d^1 zirconium(III) center. The room temperature solution ESR spectra of the alkyl derivatives are more complicated than the spectrum of the phenyl derivative **4.4**. With the exception of the benzyl derivative, the hyperfine interaction of the unpaired electron with the two phosphorus nuclei are in the range of 20 to 21 G. In the case of the Et and the Bz derivatives, the satellites due to zirconium-91 nuclei were not observed.

references on page 199

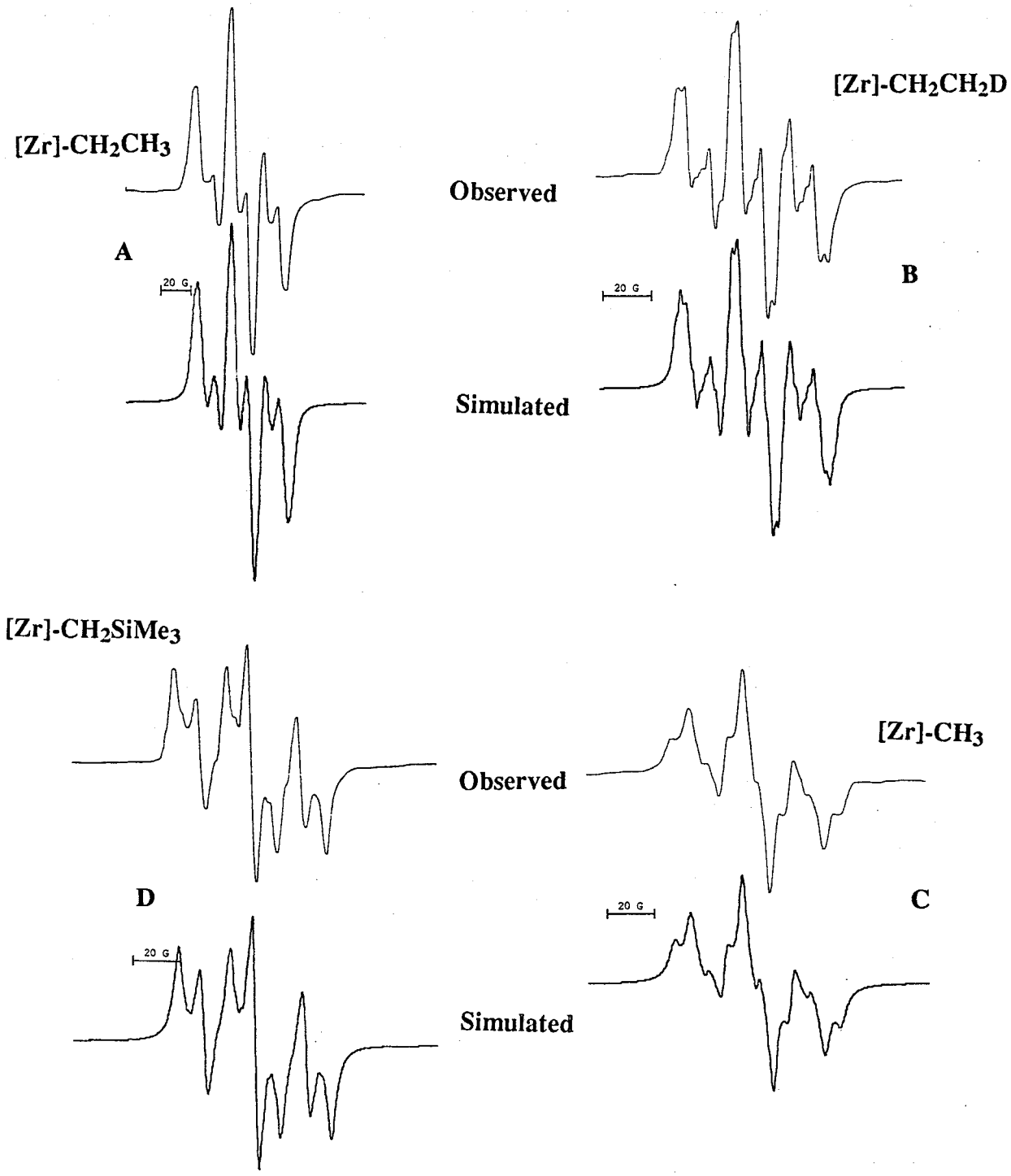

[Zr] = "ZrCp[N(SiMe$_2$CH$_2$PPr$^i_2$)$_2$]"

Figure 4.3 The ESR spectra of the alkyl complexes **A 4.6**, **B 4.6**-d_1, **C 4.5** and **D 4.8**. For each case the observed spectrum is shown on the top and the simulated spectrum is shown below.

references on page 199

Table 4.5 Hyperfine coupling constants (G) for the chloro and the hydrocarbyl derivatives of $ZrCpR[N(SiMe_2CH_2PPr^i_2)_2]$. All the values were obtained from simulations.

R	g	a(^{91}Zr)	a(^{31}P)	a(^{14}N)	a($^1H_\alpha$)	a($^1H_\beta$)	a($^1H_{Cp}$)
Cl	1.955	37.2	21.1	2.9			1.8
C_6H_5	1.981	20.7	20.3	1.8			1.1
CH_3	1.963	28.0	21.1	2.1	6.6		
CH_2CH_3	1.962		20.9	2.6	9.3 3.2	1.8	
$CH_2C_6H_5$*	1.956		18.6	3.4	3.2		1.2
$CH_2Si(CH_3)_3$	1.973	30.5	21.4	2.0	9.3 6.2		

* The hyperfine values given for the benzyl derivative are only an approximate value.

Simulation studies of the room temperature solution (toluene) ESR spectrum of the methyl derivative **4.5** suggest that the three α-hydrogens of the methyl group attached to zirconium are isotropic. It is important to note that the minor features of the simulated ESR spectrum of the methyl complex **4.5** (Figure **4.3**) using the values given in Table **4.5** are slightly different from that of the actual spectrum. It is believed that this could be a result of the unsophisticated ESR simulation program, where only one overall line broadening value could be used. It is possible that a more accurate spectral simulation could be obtained using different values of line broadening for each type of spin system, for example, a different line broadening value for the two phosphorus nuclei and a different value for the three α-hydrogens.

An intriguing feature in the ESR spectra of the ethyl and CH_2SiMe_3 derivatives is that the α-hydrogens have different hyperfine coupling constants. This difference in hyperfine interaction could be due to restricted rotation about the zirconium-carbon bond associated with the alkyl substitution. If the rotation is slow on the ESR time scale, some rotational isomers

references on page 199

would have a longer lifetimes that the others.[14,15] Scheme **4.3** shows the two types of conformational isomers for the ethyl and the CH_2SiMe_3 derivatives, where type **A** has diastereotopic α-hydrogens, and type **B** has enantiotopic α-hydrogens. The diastereotopic α-hydrogens of conformer **A** will have different hyperfine coupling constants.[14,15]

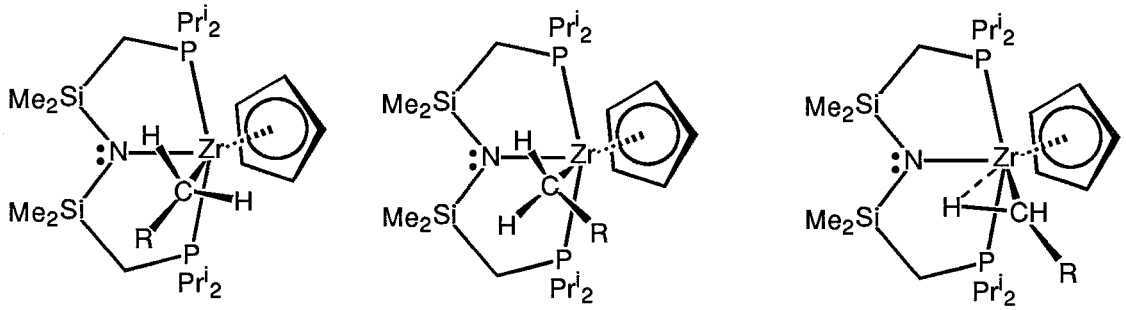

R = Me, $SiMe_3$

Scheme 4.3

An alternate explanation for the different coupling constants for the α-hydrogens would be that, in solution, one of the α-hydrogens weakly interacts with the metal center, **C** (Scheme **4.3**). Infrared spectroscopic experiments were carried out to elucidate the presence of agostic C–H bond interactions. Any such bonding interactions of the α-hydrogens should be reflected in the stretching frequencies associated with the carbon-hydrogen bonds of the α-hydrogens. The carbon-hydrogen stretching frequencies associated with the PNP ligand give rise to a very complicated pattern from 3000 to 2700 cm^{-1}. Therefore the solution infrared spectra of deuteride derivatives of the ethyl complex, $Zr(\eta^5\text{-}C_5H_5)CH_2CH_2D[N(SiMe_2CH_2PPr^i_2)_2]$, **4.6**-$d_1$ and $Zr(\eta^5\text{-}C_5H_5)CD_2CD_3[N(SiMe_2CH_2PPr^i_2)_2]$, **4.6**-$d_5$ were analyzed. The infrared spectra of the monodeuterio derivative **4.6**-d_1 enabled the assignment the stretching frequencies associated with the β-deuterides of the ethyl group and then comparison with the infrared spectra of the perdeuterio ethyl derivative **4.6**-d_5 enabled to assign the stretching bands associated with the α-deuterides.

references on page 199

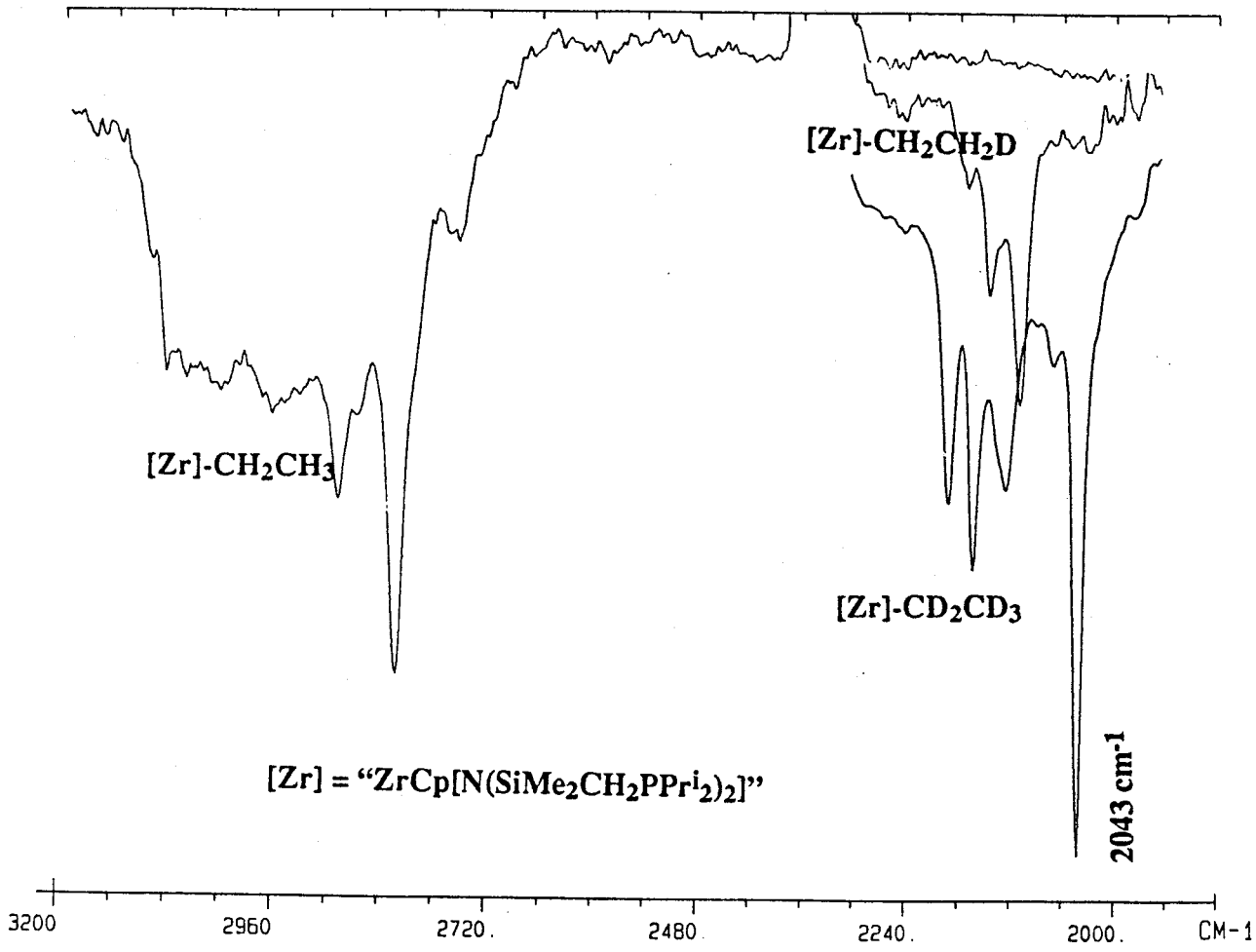

Figure 4.4 The solution infrared spectra of complexes **4.6**, **4.6**-d_1 and **4.6**-d_5.

A comparison of the infrared spectra of complexes **4.6**-d_1 and **4.6**-d_5 show that the latter has an absorption band at 2043 cm^{-1} which can be assigned as an α-deuterium stretch. Also, this band is 85 cm^{-1} lower than the next nearest carbon-deuterium stretching band, suggesting some weakening of the C–D bond associated with the band at 2043 cm^{-1}. The carbon-deuterium stretching band at 2043 cm^{-1} will correspond to a carbon-hydrogen stretching band around 2783 cm^{-1}. For comparison, the agostic carbon-hydrogen stretching frequencies of various transition metal complexes range between 2700 cm^{-1} and 2350 cm^{-1}.[16-18] However, in some rarer occasions higher C–H stretches have been reported for agostic C-H bonds. For example in the cationic complex $[IrH_2(PPh_3)_2L]^+$, where L = 8-methylquinoline, an agostic bond is formed between the iridium and the one of the C–H bonds of the methyl group, and an

references on page 199

infrared band at 2848 cm^{-1} has been assign to the agostic C–H stretch.[19] Therefore it is possible that one of the α-hydrogen of the ethyl derivative could be weakly interacting with the metal center which in turn could be attributed to different coupling constants observed for the α-hydrogens in the ESR spectra of the alkyl derivatives.

The solution ESR spectrum of the benzyl zirconium(III) derivative **4.7**, does not have a center of symmetry, suggests that more than one species exist in solution. It is possible that the benzyl ligand is coordinated in an η^2 fashion, with a geometry similar to **C** shown in Scheme **4.3**. Such a geometry would make the two benzylic protons enantiotopic, and this proposal is consistent with the hyperfine values obtained (by simulation) for the α-hydrogens.

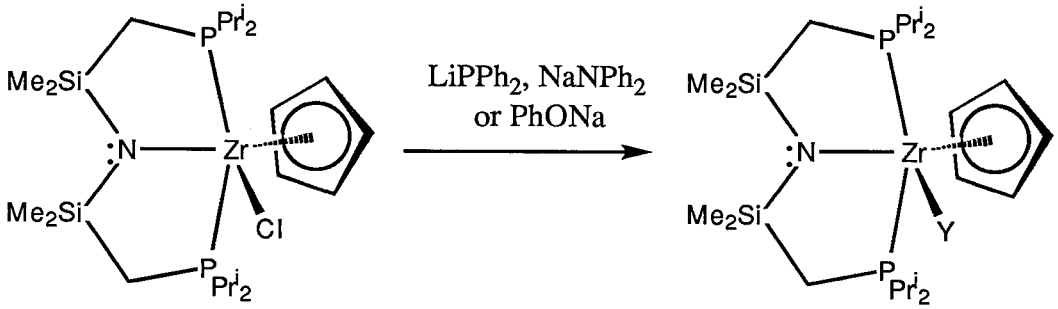

4.1 Y = OPh **4.10**, NPh_2 **4.11** or PPh_2 **4.12**

Scheme 4.4

Metathesis reactions with the zirconium(III) chloride complex **4.1** with one equivalent of NaOPh, $NaNPh_2$ or $LiPPh_2$ led to the synthesis of $Zr(\eta^5\text{-}C_5H_5)OPh[N(SiMe_2CH_2PPr^i_2)_2]$ **4.10**, $Zr(\eta^5\text{-}C_5H_5)NPh_2[N(SiMe_2CH_2PPr^i_2)_2]$ **4.11**, and $Zr(\eta^5\text{-}C_5H_5)PPh_2[N(SiMe_2CH_2PPr^i_2)_2]$ **4.12**, respectively (Scheme **4.4**). The phenoxy derivative was deep green in colour whereas the amido and the phosphido derivatives gave dark brown solutions. These complexes were extremely soluble in hydrocarbon solvents and only the phenoxy derivative was isolated in a solid form amenable to elemental analysis. However, the ESR spectra of the crude samples were symmetric, and the ^1H NMR spectra showed only broad peaks, suggesting that the synthesis of these complexes proceeds in virtually quantitative yields. The room temperature solution ESR spectra of the amido derivative, **4.11** (g = 1.953, $a(^{31}P)$ = 11.2 G), and the phenoxy derivative, **4.10** (g = 1.955, $a(^{31}P)$ = 18.7 G), consist of a broad binomial triplet

references on page 199

indicating coupling of two equivalent phosphorus nuclei. The phosphido derivative, **4.12** displays of a doublet of triplets (g = 1.965; a(^{31}P) = 29.8 G, 1P; a(^{31}P) = 18.6 G, 2P) which is consistent with a mononuclear zirconium species (Figure **4.5**). It is important to note that other phosphido derivatives of zirconium(III) cited in the literature are reported to be binuclear and diamagnetic containing bridging phosphido ligands (e.g., **3.6**).

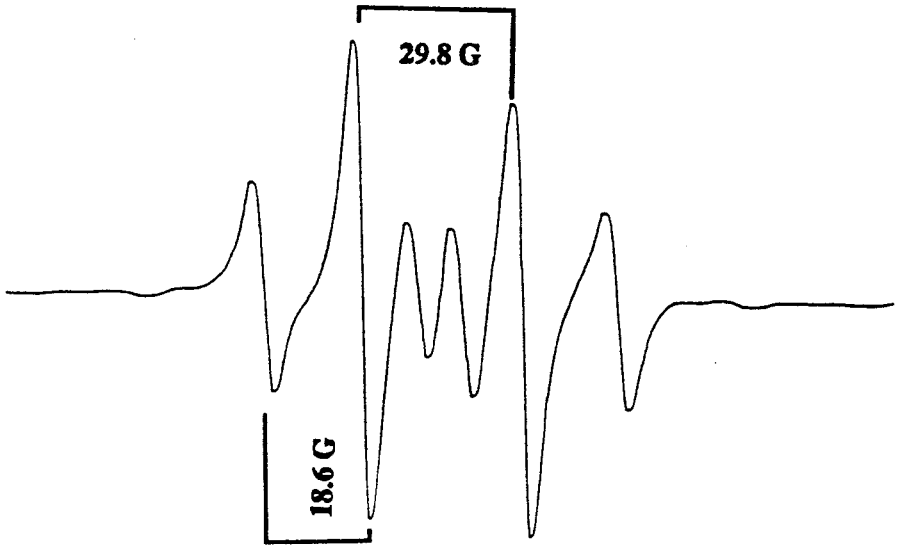

Figure 4.5 The room temperature solution (toluene) ESR spectrum of the phosphide complex $Zr(\eta^5\text{-}C_5H_5)PPh_2[N(SiMe_2CH_2PPr^i_2)_2]$, **4.12**.

4.4 Oxidation of Zirconium(III) Complexes

Treating a solution of zirconium(III) chloro derivative **4.1** with solid $TiCl_3$ or $PbCl_2$ led to the oxidation of the zirconium complex to give the dichloro zirconium(IV) complex **2.6** in almost quantitative yield. Also, 0.5 equivalents of Ph_2S_2 react with complex **4.1** to give the zirconium(IV) thiolate derivative, $Zr(\eta^5\text{-}C_5H_5)(SPh)Cl[N(SiMe_2CH_2PPr^i_2)_2]$, **4.13** in quantitative yields (Scheme **4.5**). These reactions have been useful in quantifying the purity of some zirconium(III) derivatives. For example, during the synthesis of the alkyl complex $Zr(\eta^5\text{-}C_5H_5)CH_2SiMe_3[N(SiMe_2CH_2PPr^i_2)_2]$, **4.8** an aliquot of the crude reaction mixture was titrated against a solution of Ph_2S_2, where a color change occurs from deep green to yellow. The resulting solution is then analyzed by $^{31}P\{^1H\}$ NMR spectroscopy. Such analyses have

references on page 199

shown that the metathesis reactions involving **4.1** and alkyl transfer reagents proceed in almost quantitative (> 95%) yields.

Oxidation of a crude sample of the hafnium(III) chloro derivative, **4.3** with $TiCl_3$ showed the presence of hafnium(IV) and zirconium(IV) species in approximately 10:1 ratio. This result is consistent with the previous suggestion that during the reduction of the hafnium(IV) precursor the ratio of the zirconium impurity increases.

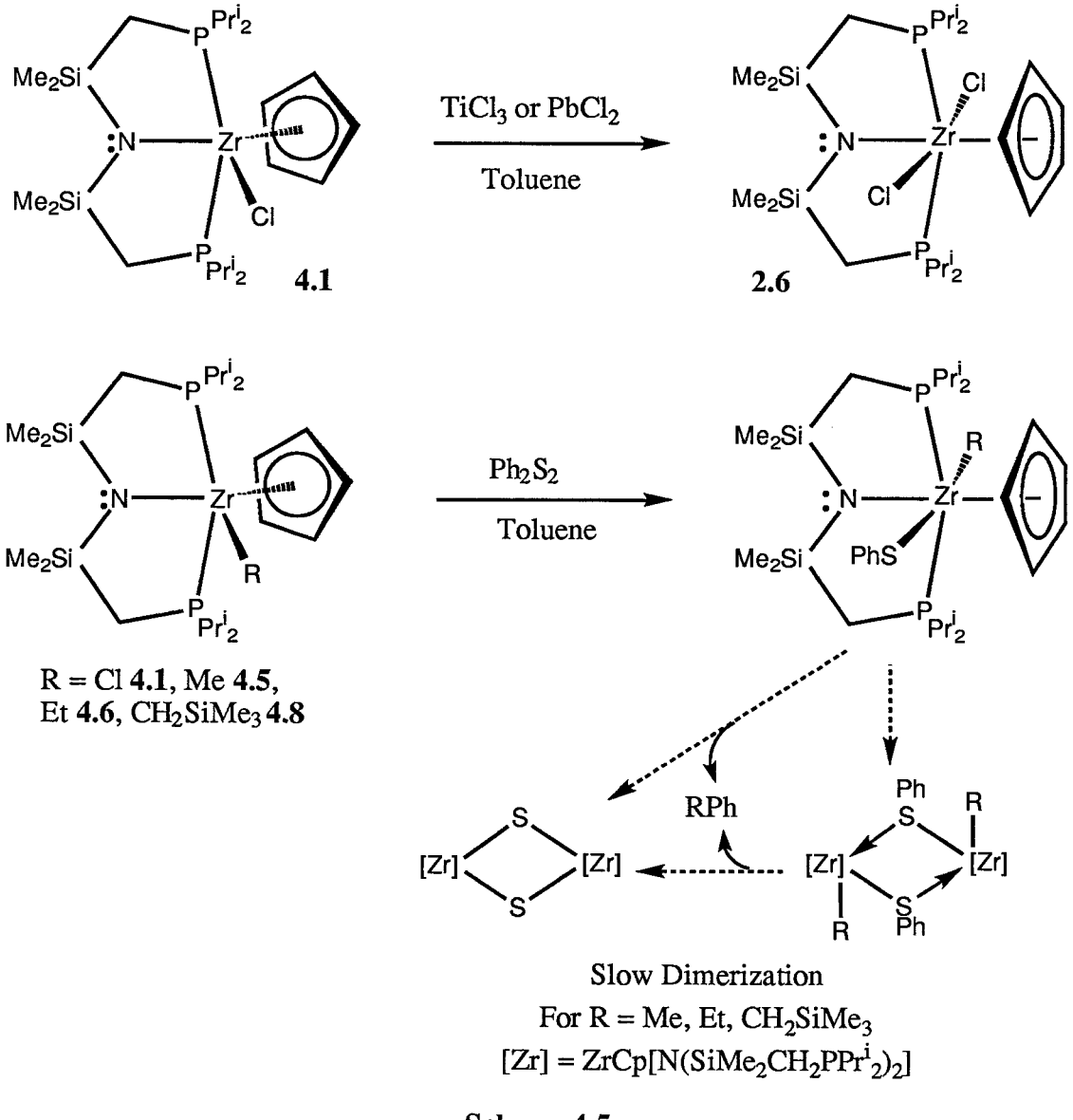

Scheme 4.5

references on page 199

It is noteworthy that the oxidized monoalkyl derivatives, i. e., alkylthiolate and the alkylchloro complexes, $Zr(\eta^5\text{-}C_5H_5)XR[N(SiMe_2CH_2PPr^i_2)_2]$, where X = SPh and R = Me, Et or CH_2SiMe_3 or X = Cl and R = Me, Et or Bz, show broad resonances in their NMR spectra, suggesting the molecules are fluxional. The alkylchloro derivatives could be isolated as solid materials and were found to be thermally labile. The alkylthiolate derivatives are oils at room temperature and undergo further reaction to give a material which has complex ^1H NMR spectra. Also, the $^{31}P\{^1H\}$ NMR spectra of this materials were virtually identical for all three derivatives, consisting of two low field and two high field singlets around 19 and -2 ppm respectively. The NMR spectral features are possibly a result of an unsymmetrical dimeric species, containing bridging sulfido ligands (Scheme **4.5**).[20] However, more investigation is required to comfirm the nature of this diamagnetic complex.

4.5 Hydride Complexes of Zirconium(III)

4.5.1 General

Hydride derivatives of zirconocene dihalides; for example Schwartz's reagent, Cp_2ZrHCl, are among the transition metal hydrides that have been found useful in stoichiometric and catalytic reactions.[21] Although there are a number of reports of zirconium(III) hydride derivatives, they are all poorly characterized (only by ESR) and all of these hydride complexes have been generated in situ by different reduction methods (Scheme **4.5**).[22-28] Also, there are no unambiguously understood reactions of zirconium(III) hydrides, even the migratory insertion of the hydride into an unsaturated organic functionality such as olefin is not well established.[23,26,28]

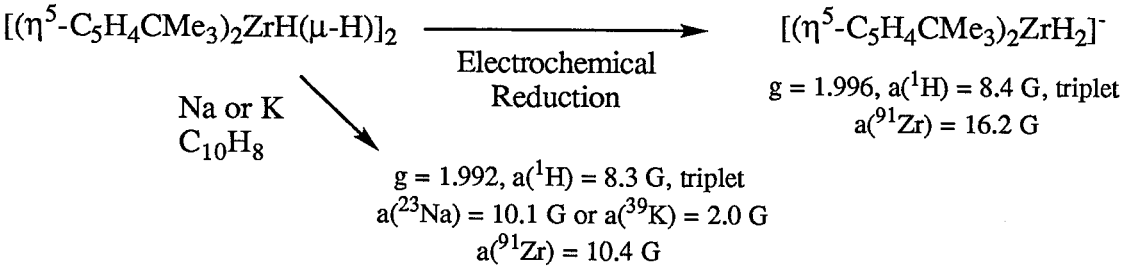

Scheme 4.6 continued

references on page 199

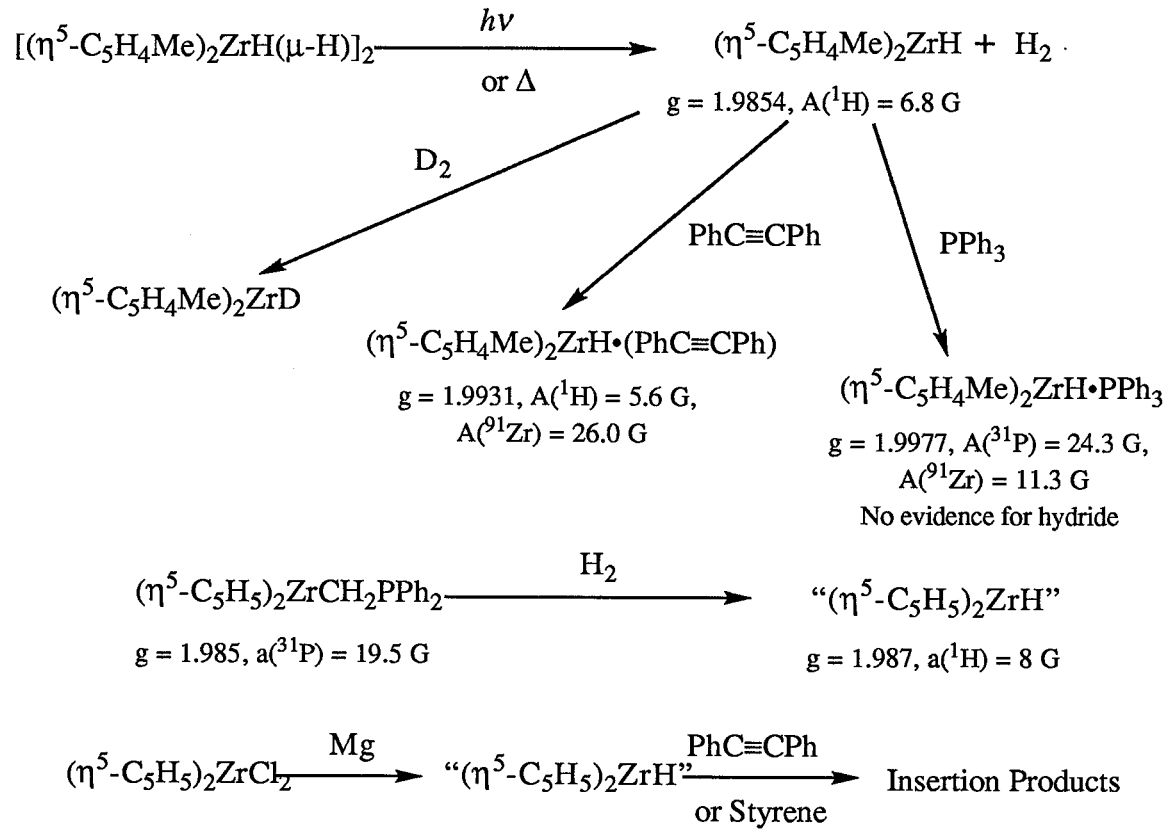

Scheme 4.6

The hydride species $(\eta^5\text{-}C_5H_4Me)_2ZrH$, generated by thermolysis or photolysis of $[(\eta^5\text{-}C_5H_4Me)_2ZrH]_2(\mu\text{-}H)_2$, is suggested to form an adduct with diphenyl acetylene; however, there is no evidence for the insertion of the triple bond into the zirconium-hydrogen bond.[22,26] However, the zirconocene monohydride, Cp_2ZrH, generated either by magnesium reduction[28] of Cp_2ZrCl_2 or by the hydrogenolysis[24] of $Cp_2ZrCH_2PPh_2$, is suggested to insert carbon-carbon triple and double bonds into the zirconium-hydrogen bond. In an experiment monitored by ESR spectroscopy, Cp_2ZrH was generated in situ by magnesium reduction and then, upon addition of styrene or diphenyl acetylene, there was a disappearance of the doublet resonance due to the hydride species and the formation of a singlet resonance, which has been attributed to the formation of the insertion product.[28] Also, hydrolysis of the reaction mixture shows the presence of hydrogenated products.[28] However, it is important to note that ESR spectra of the adduct formed from the reaction of $(\eta^5\text{-}C_5H_4Me)_2ZrH$ and PPh_3 consists only of a doublet,

references on page 199

coupling that has been attributed to one phosphorus-31 nucleus; no coupling was observed due to the hydride ligand.[26]

Hydrogenolysis of $Cp_2ZrCH_2PPh_2$ in the presence of a substrate shows catalytic hydrogenation of the substrate. For example, 1-hexene was hydrogenated to hexane at 80 °C and 40 bar hydrogen pressure in THF using a catalyst/substrate/solvent ratio of 1:300:1000 where 100% conversion was observed in 20 minutes. However, when the reaction mixture was analyzed by ESR spectroscopy only two doublets were observed, one of which corresponded to $Cp_2ZrCH_2PPh_2$ and the other to the hydride species Cp_2ZrH; no evidence for the zirconium(III) alkyl intermediate was found.[24]

4.5.2 Synthesis of $Zr(\eta^5\text{-}C_5H_5)H[N(SiMe_2CH_2PPr^i_2)_2]$

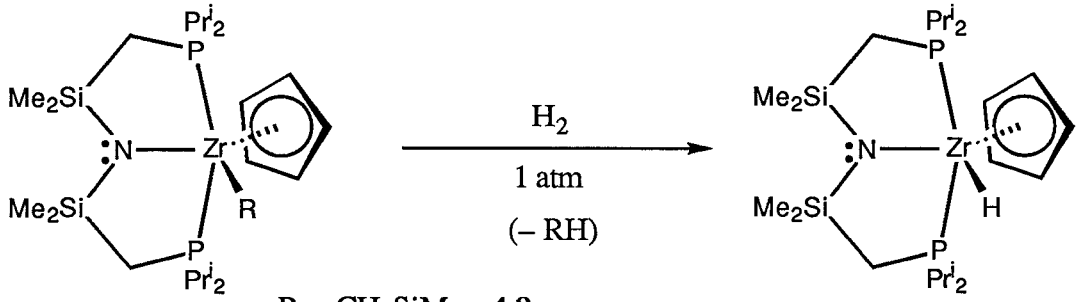

R = CH_2SiMe_3, **4.8**
R = CH_3, **4.5**

4.14

Scheme 4.7

The reaction of the zirconium(III) alkyl complexes such as the methyl **4.5** or the CH_2SiMe_3 **4.8** derivatives with one atmosphere of dihydrogen at room temperature proceeds smoothly over a period of 10 to 12 hours to generate the mononuclear zirconium(III) hydride complex $Zr(\eta^5\text{-}C_5H_5)H[N(SiMe_2CH_2PPr^i_2)_2]$, **4.14** (Scheme **4.7**). The ESR spectrum of the hydride complex consists of a 1:1:2:2:1:1 doublet of triplets centred at g = 1.988, due to the coupling to two phosphorus-31 nuclei ($a(^{31}P)$ = 21.7 G) and one hydride ($a(^1H)$ = 8.7 G) ligand. The same reaction with molecular deuterium gas produces the corresponding deuteride $Zr(\eta^5\text{-}C_5H_5)D[N(SiMe_2CH_2PPr^i_2)_2]$, **4.14**-$d_1$; the triplet observed in the ESR spectrum of this

references on page 199

material is consistent with the expected deuterium hyperfine interaction of approximately one seventh of a(^{1}H) (Figure **4.6**). For comparison, ESR data reported for other d^1 hydride complexes are as follows: (g, a(^{1}H)); Cp_2NbH_2, (2.0097, 11.7 G);[29] [Cp_2TiH_2], (1.992, 7 G (approximate));[30-32] $TaCl_2H_2(PMe_3)_2$, (1.960, 6 to7 G (estimated)).[33]

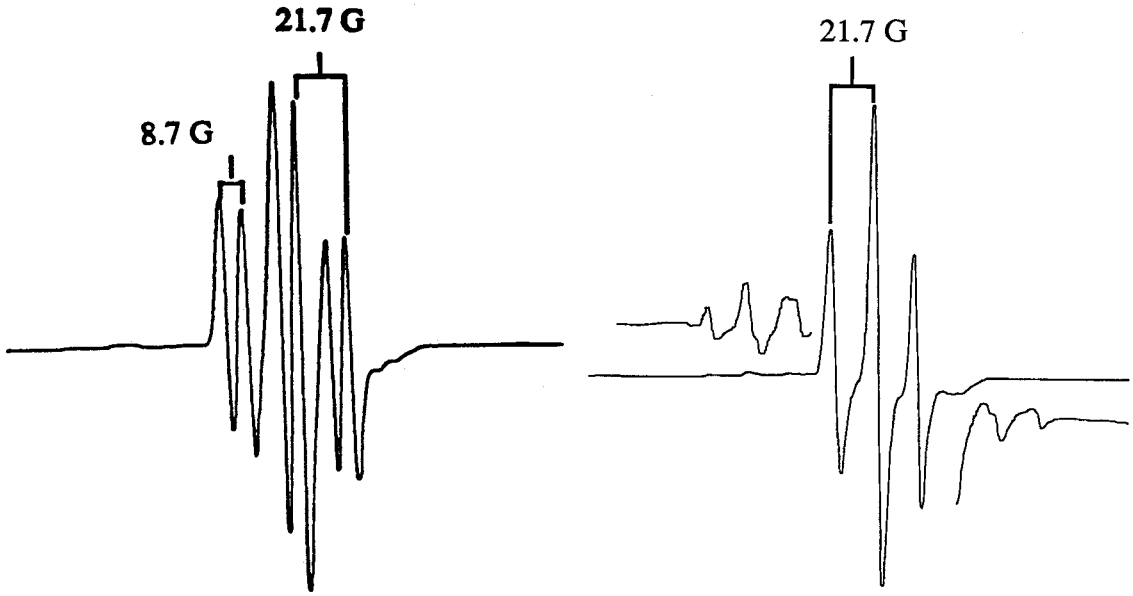

$ZrCpH[(NSiMe_2CH_2PP^iPr_2)_2]$ $ZrCpD[(NSiMe_2CH_2PP^iPr_2)_2]$

A **B**

Figure 4.6 The X-band room temperature solution (toluene) ESR spectrum of,
(**A**) $Zr(\eta^5\text{-}C_5H_5)H[N(SiMe_2CH_2PPr^i_2)_2]$ **4.14**, and
(**B**) $Zr(\eta^5\text{-}C_5H_5)D[N(SiMe_2CH_2PPr^i_2)_2]$, **4.14**-$d_1$.

Monitoring the hydrogenolysis reaction of the CH_2SiMe_3 derivative **4.8** by ESR and ^{1}H NMR spectroscopy shows a clean conversion to the hydride complex with concomitant formation of tetramethyl silane. Also, the reaction of the methyl derivative **4.5** with molecular deuterium shows the formation of CH_3D. However, we have not been able to isolate the hydride complex as a solid due to its high solubility in hydrocarbon solvents. In the absence of dihydrogen, complex **4.14** is thermally stable for 48 hours at RT as evidenced by monitoring a toluene solution of **4.14** by ESR spectroscopy. The hydrogenolysis of the benzyl derivative,

references on page 199

4.12 was very slow at room temperature whereas the phenyl derivative was inert under dihydrogen.

An attempted one-pot synthesis of the zirconium(III) hydride by reacting the zirconium chloro derivative **4.1** with $LiCH_2SiMe_3$ and then, without removing the LiCl, stirring under an atmosphere of dihydrogen resulted in the formation of a diamagnetic zirconium species **4.15**. This reaction reaches completion in approximately 5 hours. However, when a pure sample of the alkyl derivative was sealed under 4 atmospheres of dihydrogen and monitored by ^1H and $^{31}P\{^1H\}$ NMR spectroscopy, there was observed a slow formation (approximately 5 days) of a diamagnetic species, **4.15**. Also, the reduction of the zirconium(IV) dichloro derivative $Zr(\eta^5\text{-}C_5H_5)Cl_2[N(SiMe_2CH_2PPr^i_2)_2]$ **2.6**, under dihydrogen gave the identical diamagnetic species, **4.15**. The micro-analytical data of this compound was consistent with the formula $Zr(\eta^5\text{-}C_5H_5)H_2[N(SiMe_2CH_2PPr^i_2)_2]$.

The NMR and infrared spectroscopic data strongly suggest that this diamagnetic hydride complex is not a mononuclear species. The solid state infrared spectra of **4.15** show a broad band at 1435 cm^{-1} which shifts to 1160 cm^{-1} upon substitution of the hydrides with deuterium, **4.15**-d_4.* Although, this infrared spectral feature could be assigned to a Zr–H bond stretch, by comparison with other known zirconium hydride complexes it is difficult to assign whether it is due to a terminal or a bridging hydride ligand. For example, in $(Cp'_2ZrH)_2(\mu\text{-}H)_2$ the terminal and the bridging hydrides give rise to absorptions at 1565 and 1330 cm^{-1} respectively.[34]

The $^1H\{^{31}P\}$ and $^{31}P\{^1H\}$ NMR (Figure **4.7**) data suggest that the complex is an unsymmetrical dinuclear species and in solution it exists in two isomeric forms in approximately a 9:1 ratio. The ^1H NMR spectrum shows 7 separate resonances for the $SiMe_2$ protons of the major isomer and two resonances, 6.15 (triplet) and 6.57 (singlet) ppm corresponding to the Cp ligand. Occasionally, when the hydride complex was precipitated from a Et_2O solution it gave only the major isomer, which within a few hours isomerized to give the mixture of isomers.

* It will be more appropriate to designate the deuteride as **4.15**-d_n.

references on page 199

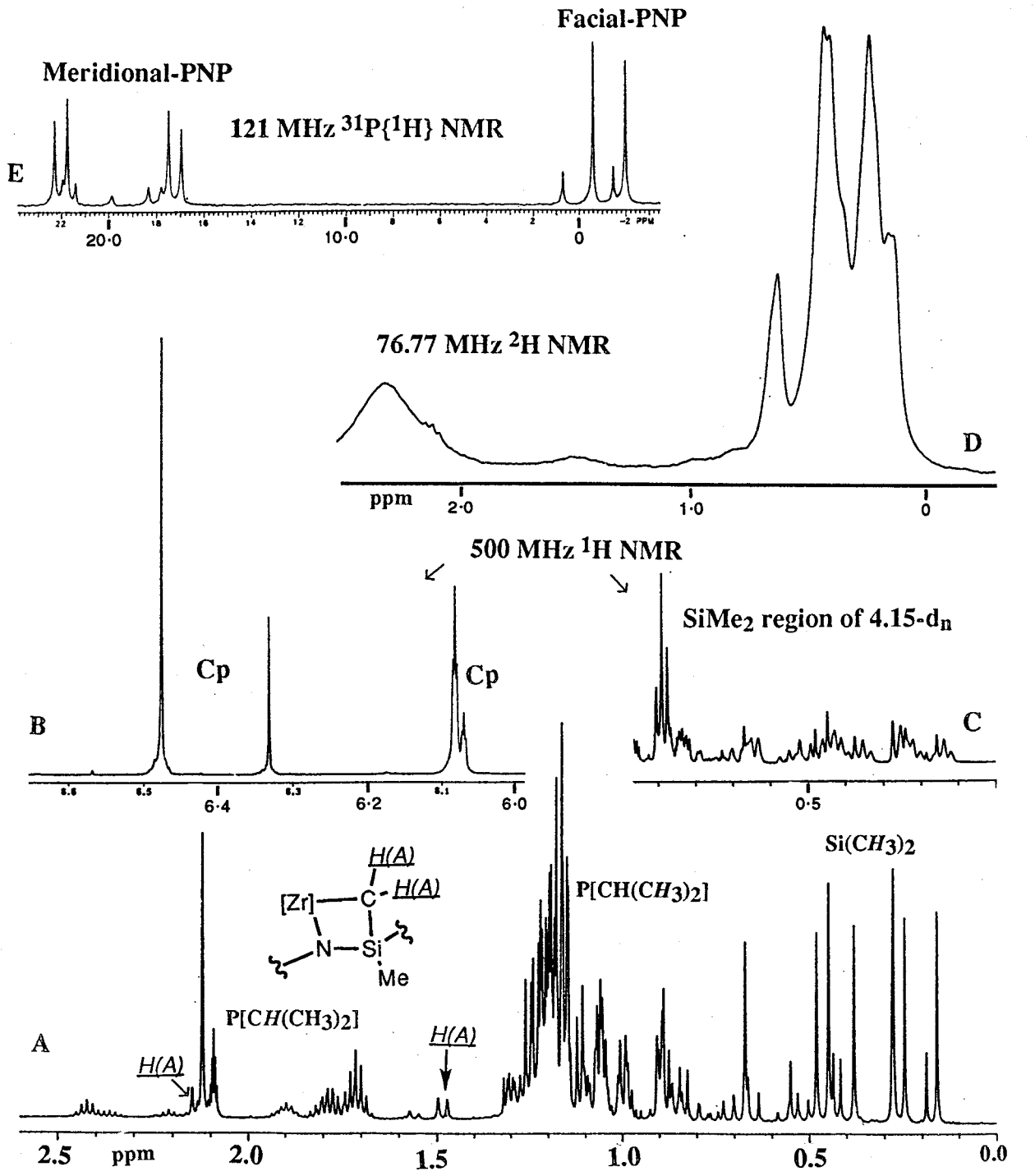

Figure 4.7 **A** 500 MHz $^{1}H\{^{31}P\}$ NMR spectrum of **4.15** showing the resonances associated with the PNP ligand. **B** 500 MHz ^{1}H NMR spectrum of **4.15** showing the resonances associated with the Cp ligand. **C** 500 MHz $^{1}H\{^{31}P\}$ NMR spectrum of the deuteride analogue **4.15**-d_n showing the resonances associated with the $SiMe_2$ groups. **D** 76.77 MHz ^{2}H NMR spectrum of **4.15**-d_n showing the resonances associated with the PNP ligand. **E** 121.4 MHz $^{31}P\{^{1}H\}$ NMR spectrum of **4.15**.

references on page 199

The $^{1}H\{^{31}P\}$ NMR spectrum of the major isomer seems to suggest that the hydride resonances are probably obscured by the resonances due to the ligand. Also, the two doublets ($^{2}J_{H\text{-}H}$ = 10.7 Hz) around 1.48 and 2.18 ppm may correspond to a cyclometalated CH_2 unit of the missing methyl of the $SiMe_2$ unit. The $^{31}P\{^{1}H\}$ NMR spectrum consist of an ABMX spin system where the AB spins appear at lower field and the MX spins appear at higher fields. In fact the $^{31}P\{^{1}H\}$ NMR spectral pattern of complex **4.15** was very similar to the product **2.24**, obtained from the reaction of the side-on dinitrogen complexes with $LiBEt_4$. It is possible that the low field phosphorus resonances, that is the AB spins, correspond to the meridionally bound PNP ligand of one zirconium center and the high field resonances, that is the MX spins, correspond to a facially bound PNP ligand of the second zirconium center. Selective ^{31}P decoupled ^{1}H NMR spectra show that the triplet resonance of the Cp ligand at 6.15 ppm is due to the coupling of the two low field ^{31}P nuclei.

To locate the resonances due to the hydride ligands, the deuteride analogue **4.15**-d_4 was synthesized by reducing the zirconium(IV) precursor **2.6** under molecular deuterium. However, the ^{1}H NMR spectrum of this material was more complicated than the spectrum of the hydride analogue; in particular, the $SiMe_2$ region showed numerous broad peaks. Also, the ^{2}H NMR spectrum showed overlapping resonances between 0.0 and 0.7 ppm, which clearly indicate that some of the protons of the $SiMe_2$ moieties are replaced by deuterium. The ^{2}H NMR showed no evidence for the incorporation of deuterium into the isopropyl groups of PNP.

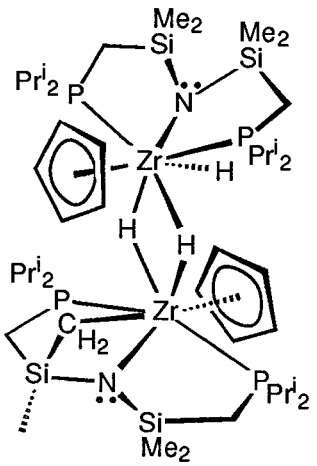

4.15

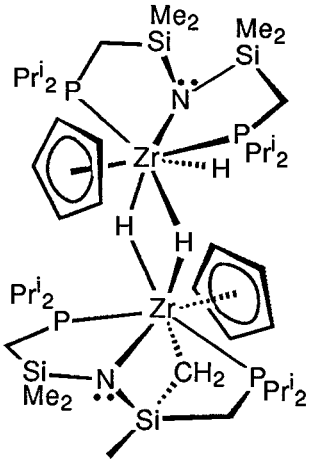

4.15a

references on page 199

On the basis of the available NMR spectroscopic data the structures depicted as **4.15** and **4.15a** have been proposed for the diamagnetic dinuclear hydride complex. Because the major and the minor isomers show similar spectroscopic features they are likely to have closely related structures; for example **4.15a** could be the minor isomer.

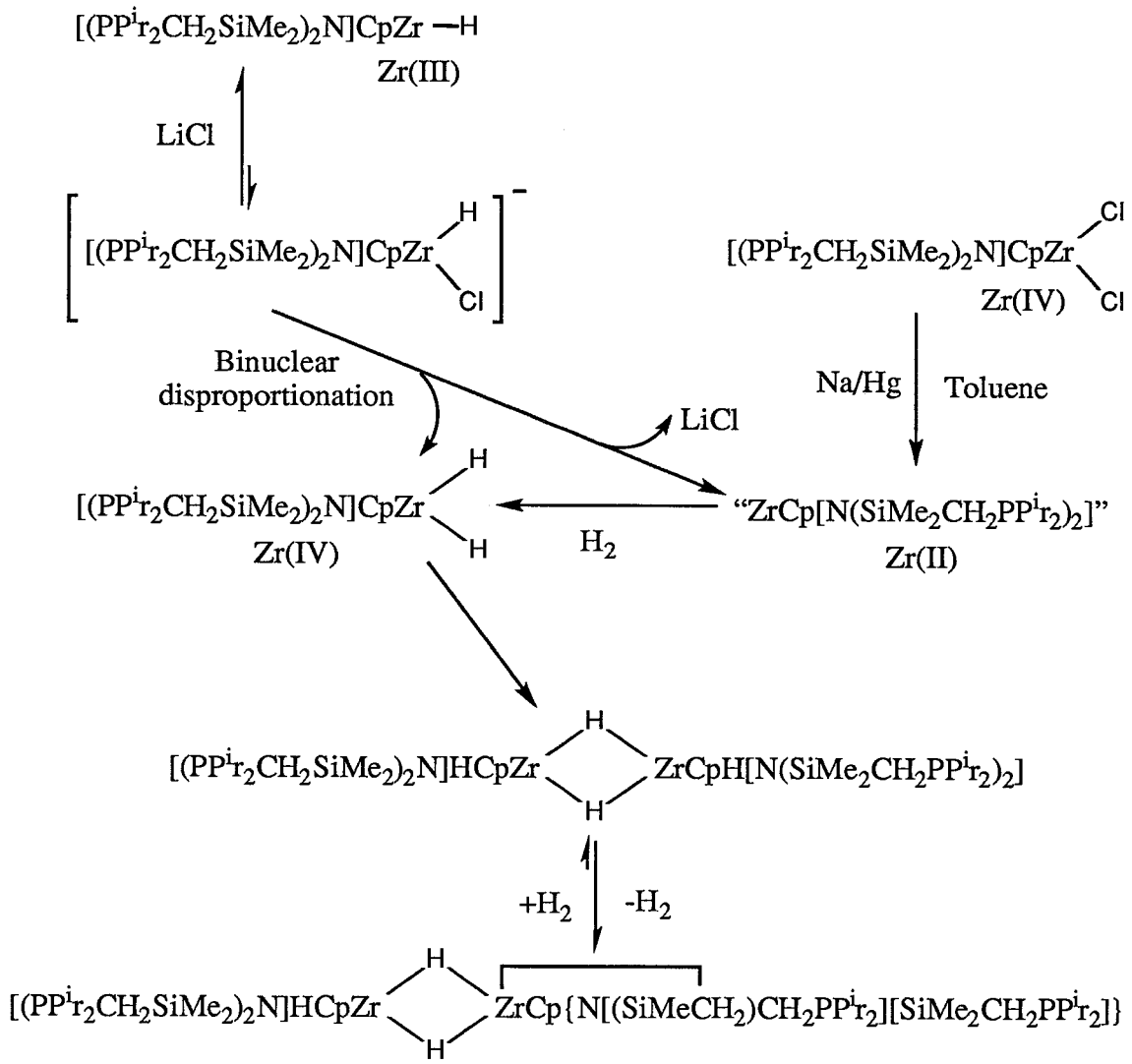

Scheme 4.8

With regard to the mechanism of formation of the diamagnetic hydride complex, the reduction of the zirconium(IV) complex **2.6** could possibly generate the zirconium(II) species, "$Zr(\eta^5\text{-}C_5H_5)[N(SiMe_2CH_2PPr^i_2)_2]$" which then oxidatively adds dihydrogen and forms the dihydride intermediate, $Zr(\eta^5\text{-}C_5H_5)H_2[N(SiMe_2CH_2PPr^i_2)_2]$ (Scheme **4.8**). Dimerization of

references on page 199

this intermediate and a σ-bond metathesis reaction with one of the carbon-hydrogen bonds of the $SiMe_2$ unit would lead to the formation of complex **4.15**. In the presence of dihydrogen the zirconium-carbon bond of the metallacycle could undergo reversible hydrogenolysis and σ-bond metathesis; such a process, under molecular deuterium would lead to the exchange of hydrogens of the $SiMe_2$ unit with deuterium.

As mentioned before the formation of the diamagnetic hydride **4.15** from the zirconium(III) hydride **4.14** under dihydrogen is influenced by the presence of LiCl. On the basis of the discussion presented for the alkyl derivatives, particularly the methyl and ethyl derivatives, it is reasonable to presume that the hydride derivative could also interact with LiCl (Scheme **4.8**). In the presence of LiCl the neutral hydride complex **4.14** may establish an equilibrium with an anionic zirconium(III) hydride species. This anionic species could interact with a neutral zirconium(III) hydride species, for example formation of a dimeric species having bridging hydride ligands. Such a species could undergo disproportionation to give a zirconium(II) and a zirconium(IV) dihydride species (Scheme **4.8**). It is possible that even a pure sample of the zirconium(III) alkyl precursor **4.8**, may contain small amounts of LiCl which could be catalyzing the formation of the zirconium(IV) hydride, **4.15** during hydrogenolysis.

4.5.3 Reactions of $Zr(\eta^5\text{-}C_5H_5)H[N(SiMe_2CH_2PPr^i_2)_2]$

The paramagnetic hydride **4.14** reacts almost instantaneously with 1 atmosphere of ethylene at room temperature. The ESR spectrum of the product was identical to the zirconium(III) ethyl derivative **4.6**, generated by the metathesis reaction of EtLi and **4.1**. Reacting the hydride complex with ethylene-d_4 gave $Zr(\eta^5\text{-}C_5H_5)CD_2CD_2H[N(SiMe_2CH_2\text{-}PPr^i_2)_2]$ **4.6**-d_4, and similarly the deuteride complexes $Zr(\eta^5\text{-}C_5H_5)CH_2CH_2D[N(SiMe_2CH_2\text{-}PPr^i_2)_2]$ **4.6**-d_1, and $Zr(\eta^5\text{-}C_5H_5)CD_2CD_3[N(SiMe_2CH_2PPr^i_2)_2]$ **4.6**-d_5 were synthesized by reacting **4.14**-d_1 with ethylene and ethylene-d_4, respectively. The comparison of the hyperfine coupling information obtained form the three deuterio ethyl derivatives and the non-deuterio ethyl derivative correlates well with the transfer of the hydride or the deuteride ligand to the β-position of the ethyl group. Solution monitoring by ESR spectroscopy of the deuteride

references on page 199

derivatives **4.6**-d_1 and **4.6**-d_4 shows that over a period of 72 hours there is no scrambling of the β-deuterium or the β-hydride into the α-position, consistent with no β-hydride elimination for these zirconium(III) alkyl derivatives. In this respect, these zirconium(III) alkyls mirror related zirconocene alkyl derivatives for which β-elimination is a slow process for unhindered alkyl derivatives.[35]

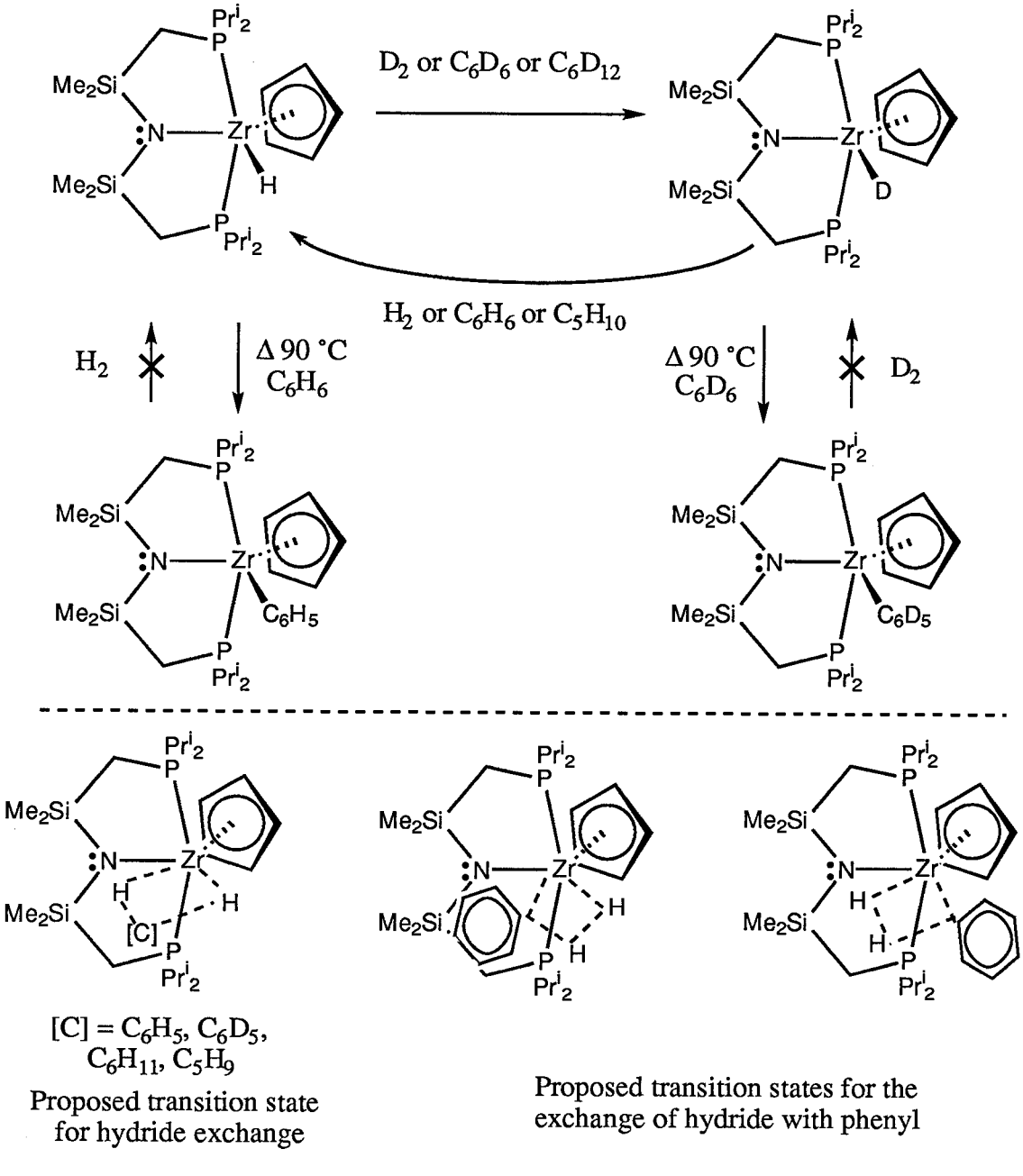

Scheme 4.9

references on page 199

The hydride ligand of complex **4.14** was found to undergo exchange reactions with deuterium from molecular deuterium gas or from the carbon-deuterium bonds of both aromatic and aliphatic compounds (Scheme **4.9**). Also, when the hydride complex **4.14** is heated in benzene at 90 °C the deep green color due to the hydride complex slowly changes to give a red solution. The ESR and UV-Vis. spectrum of this red solution indicates the formation of the phenyl derivative **4.4.**

It is presumed that these reaction involve a four centered transition state similar to the one proposed for σ-bond metathesis reactions in d^0 metal complexes.[36] According to the depictions shown in Scheme **2.8**, and considering only the steric factors, the exchange of hydrogen atoms between a metal-hydride bond and a carbon-hydrogen bond should be favored. The proposed mechanism is consistent with the experimental observation that the conversion of the zirconium(III) hydride to the phenyl derivative only takes place at elevated temperatures and with longer reaction times.

The reaction of the zirconium(III) hydride complex with a terminal acetylene did not show any evidence for the formation of the insertion product. For example, reacting Ph–C≡C–H with complex **4.14** and oxidizing the product with $PbCl_2$ gave a product which did not show any characteristic olefinic signals in the ^1H NMR spectrum. However, this crude sample contained mainly of one complex (>80 %) and the ^1H and $^{31}P\{^1H\}$ NMR features were consistent with the formula $Zr(\eta^5\text{-}C_5H_5)Cl(C{\equiv}CPh)[N(SiMe_2CH_2PPr^i_2)_2]$, **4.16**. This result suggests that the zirconium-hydride bond probably undergoes a rapid σ-bond metathesis with the terminal carbon–hydrogen bond of the acetylene to give the zirconium(III) acetylide derivative $Zr(\eta^5\text{-}C_5H_5)(C{\equiv}CPh)[N(SiMe_2CH_2PPr^i_2)_2]$.

4.5.4 Synthesis of Zirconium(III) Borohydride Complex

A variety of tetrahydroborate derivatives of early and late transition metals have been synthesized.[37] These complexes are potentially important as precursors to solid metal borides,[38] to metal hydrides,[39,40] to metal alkyls[41] and they may also function as olefin polymerization catalysts.[42] From a structural point of view, they are intriguing due to the versatility displayed

references on page 199

by the tetrahydroborate group in the mode of its coordination to the metal center, which may involve triple, double and single hydrogen bridges;[37] all of these ligation modes are known for group 4 transition metals.

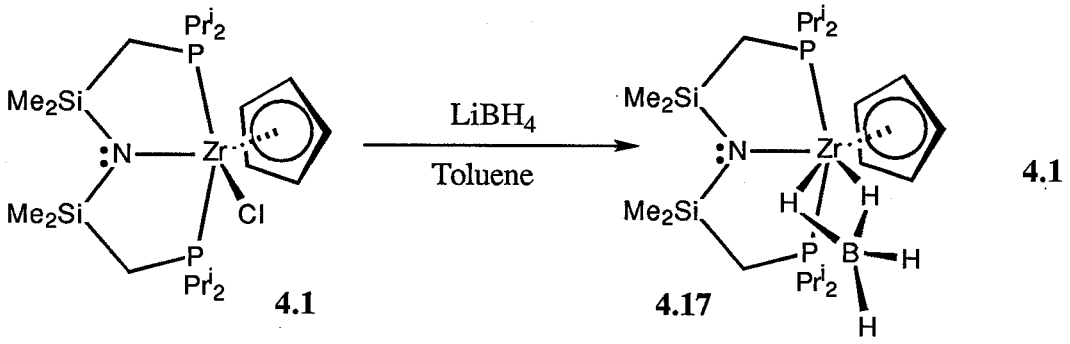

4.1

The reaction of the chloro derivative **4.1** with $LiBH_4$ in toluene slowly changed color from deep green to give a dark brown solution (Equation **4.1**). Recrystallization of the crude material from an Et_2O solution gave a pure crystalline material in greater than 80% yield with an elemental composition that was consistent with the formula $Zr(\eta^5\text{-}C_5H_5)(BH_4)[N(SiMe_2\text{-}CH_2PPr^i{}_2)_2]$, **4.17**. This zirconium(III) borohydride complex exhibits good thermal stability. For example, heating a toluene solution of the complex at 90 °C for 12 hours shows no decomposition by ESR spectroscopic analysis.

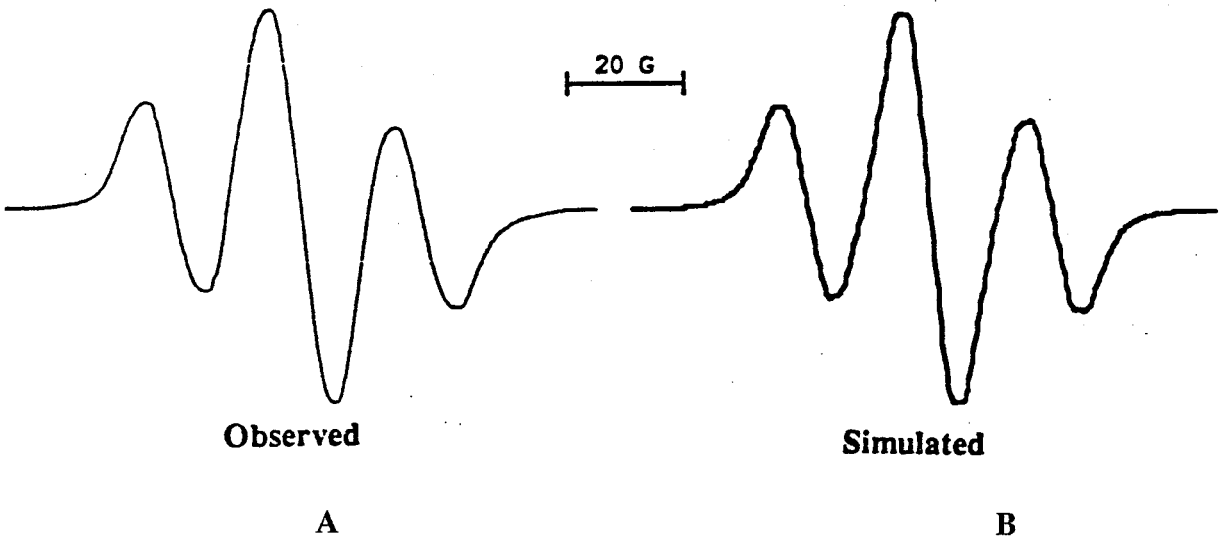

Figure 4.8 (**A**) Solution (toluene) ESR spectrum of **4.17** recorded at room temperature.
(**B**) The simulated spectrum of **4.17**.

references on page 199

The solution ESR spectrum of **4.17** consists of a broad binomial triplet due to coupling to two equivalent phosphorus nuclei; no satellites due to the magnetically dilute zirconium-91 nuclei were observed (Figure **4.8**). The ESR spectrum of **4.17** was simulated using the following parameters: g = 1.958; a (^{31}P) = 20.7 G, 2P; a(^{14}N) = 2.0 G, 1N and a(^{1}H) = 2.8 g, 4H; this last hyperfine coupling parameter suggests that all four hydrogens of the borohydride ligand have similar interactions with the metal center. The borohydride ligand may be undergoing some fluctional process that exchanges the positions of the terminal and bridging hydrides (Scheme **4.10**).[37]

The solid state infrared spectrum of the complex consists of bands at 2401 and 2374 cm^{-1} and strong absorptions at 2126 and 1460 cm^{-1}, consistent with a BH_4 ligand bound in a bidentate fashion. The bands at 2401 and 2392 cm^{-1} were assigned to the terminal B–H bond stretches and the absorption at 2124 cm^{-1} was assigned to the bridging B–H bond stretch. The solution (toluene) infrared spectrum of complex **4.17** was identical in the region associated with the B–H stretches, however the feature at 1460 cm^{-1} observed in the solid state was absent.

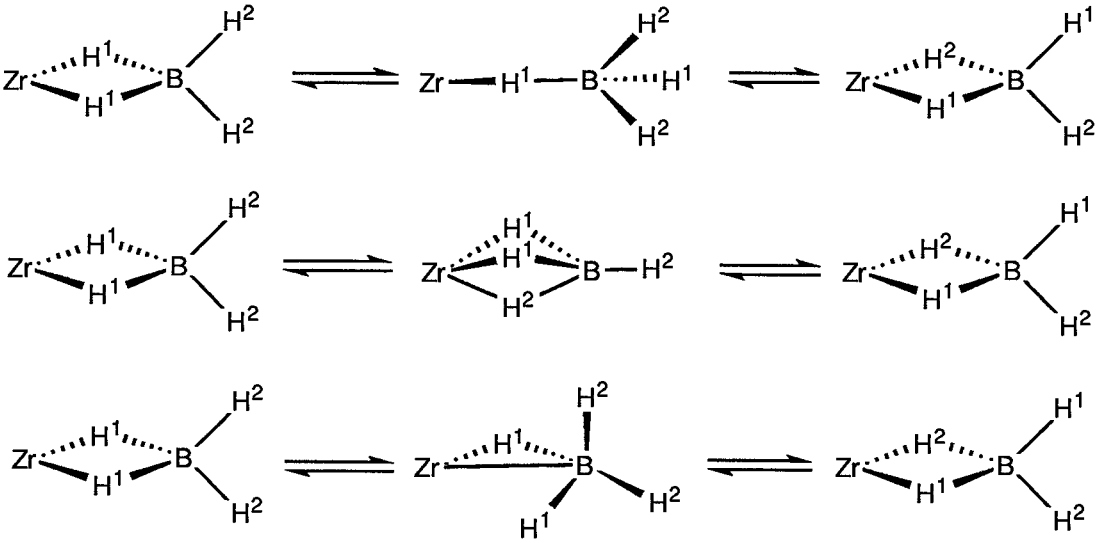

Scheme 4.10

A fluctional process that would exchange the terminal and bridging hydrogens could involve a monodentate or a tridentate or an agostic type intermediate (Scheme **4.9**). On the basis of the solution infrared spectra the tridentate intermediate seems unlikely since this would

references on page 199

significantly alter the B–H_t stretching region. In the literature it has been stated that the infrared spectra of monodentate and bidentate borohydride derivatives are likely to give similar features, particularly for the B–H stretches.[43] It is possible that the fluctional process could involve an agostic type intermediate. Such agostic type* bonding of the BH_4 ligand is known for the complex $(PMe_3)_2Ti(BH_4)_3$ where two of the BH_4 ligands are bound in an agostic fashion, involving the B–H bond.[44]

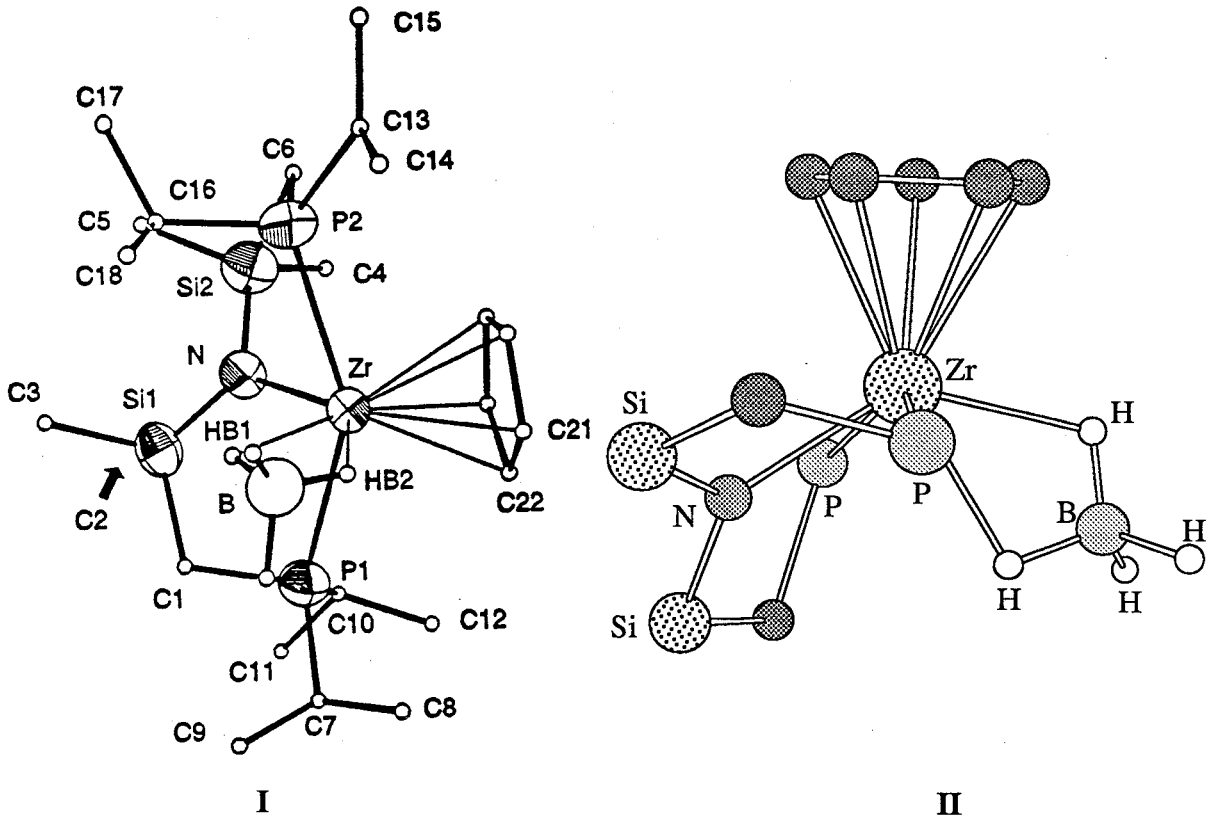

Figure 4.9 **I** ORTEP view showing the complete atom labeling scheme of complex $Zr(\eta^5\text{-}C_5H_5)(\eta^2\text{-}BH_4)[N(SiMe_2CH_2PPr^i_2)_2]$, **4.17**. **II** A Chem 3D® view showing the arrangement of the PNP and borohydride ligands around the zirconium center.

The X-ray structure of the borohydride derivative **4.17**, is depicted in Figure **4.9**. The structure clearly shows the complex to be mononuclear with the borohydride ligand bound in a bidentate fashion. All of the hydrogen atoms associated with borohydride ligand were located during the refinement of the X-ray structure. By comparison with the structures of the phenyl

* These interactions are also refered to as side-on bound borohydride ligand

references on page 199

4.4 and the CH_2SiMe_3 **4.8** derivatives the borohydride complex **4.17** is somewhat isostructural. Analysis of the bond angles around the zirconium center suggests a pseudo trigonal bipyramidal geometry with the phosphine donors occupying the axial positions. The centroid of the Cp ligand, the nitrogen and the two bridging hydrogens of the BH_4 ligand, all lie in the equatorial plane.

Table 4.6 Selected bond lengths of complex $Zr(\eta^5\text{-}C_5H_5)(\eta^2\text{-}BH_4)[N(SiMe_2CH_2PPr^i_2)_2]$, **4.17**

Atom	Atom	Distance (Å)	Atom	Atom	Distance (Å)
Zr	P(1)	2.7933 (15)	Zr	P(2)	2.7849 (15)
Zr	N	2.224 (4)	Zr	B	2.617 (7)
Zr	Cp	2.204 (3)	Zr	HB(1)	2.19 (5)
N	Si(1)	1.714 (4)	Zr	HB(2)	2.09 (4)
N	Si(2)	1.726 (4)	B	HB(1)	1.12 (5)

Table 4.7 Selected bond angles of complex $Zr(\eta^5\text{-}C_5H_5)(\eta^2\text{-}BH_4)[N(SiMe_2CH_2PPr^i_2)_2]$, **4.17**

Atom	Atom	Atom	Angle (°)	Atom	Atom	Atom	Angle (°)
P(1)	Zr	P(2)	147.66 (5)	P(1)	Zr	N	78.80 (10)
P(1)	Zr	Cp	105.55	P(2)	Zr	N	74.00 (10)
P(2)	Zr	Cp	104.74	P(1)	Zr	B	84.04
Cp	Zr	N	127.21	P(2)	Zr	B	90.29
Cp	Zr	B	120.48	N	Zr	B	112.32
HB(1)	Zr	HB(2)	47.0 (20)	Zr	HB(1)	B	99 (3)
Cp	Zr	HB(2)	98.2	Cp	Zr	HB(1)	145.1

Cp refers to the centroid of the Cp ligand. All structural parameters associated with the centroid of Cp and B for the complex **4.17** were taken from the Chem 3D® structure.

references on page 199

A comparison of the X-ray structures of the phenyl **4.4**, CH_2SiMe_3 **4.8**, and the borohydride **4.17**, show that the centroid of the Cp ligand the nitrogen of PNP and the ligating atoms of the third group, that is the phenyl or the CH_2SiMe_3 or the BH_4, lie in the pseudo equatorial plane. Also, the plane of the phenyl ring and the chelating ring of the BH_4 ligand lie on the equatorial plane. A Chem 3D® illustration of the equatorial planes of the three molecules are shown in Figure **4.10**.

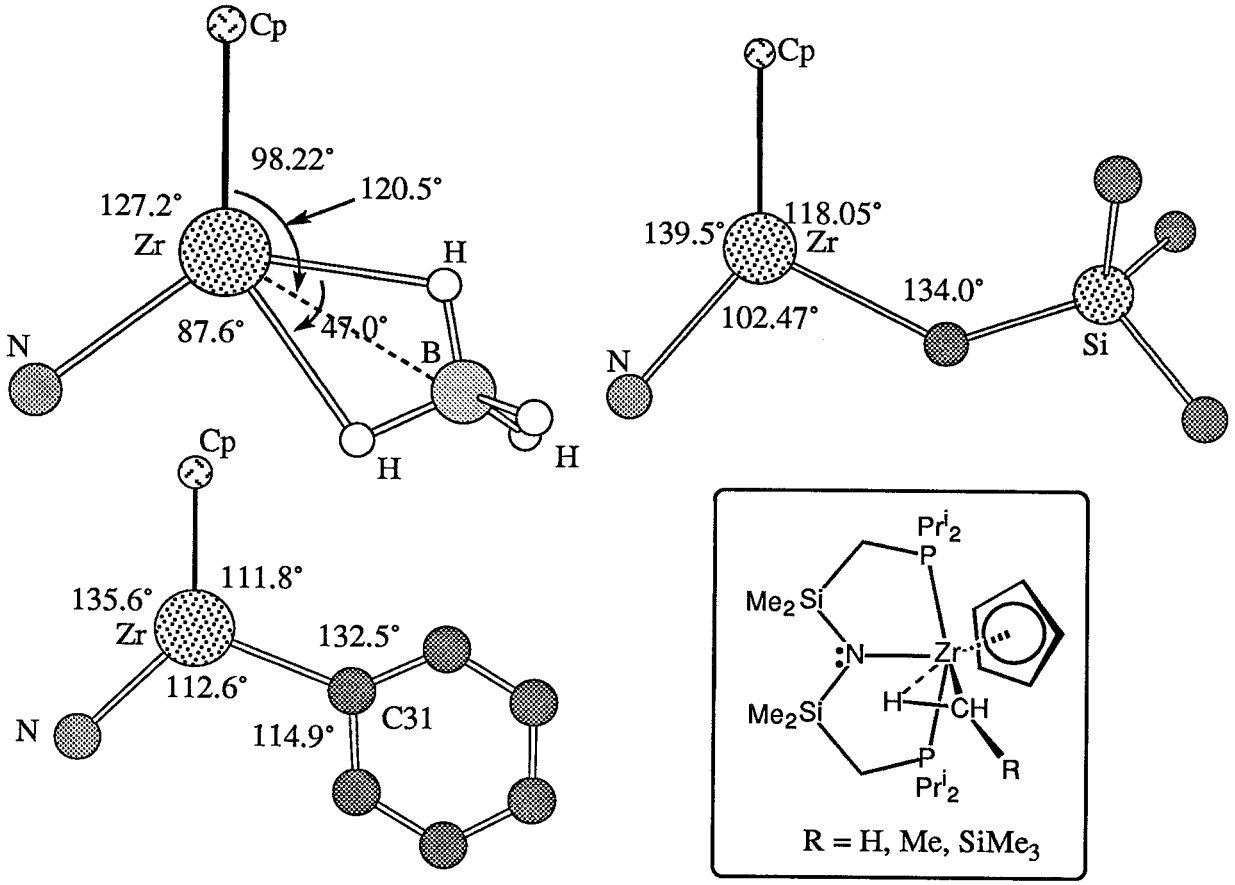

Figure 4.10 The Chem 3D® view of the equatorial planes of complexes **4.4**, **4.8** and **4.17**. All numerical values given correspond to the nearest bond angle. The Chem Draw® drawing inside the box is the proposed structure for the alkyl complexes in solution.

It seems that in the borohydride complex the site occupied by the hydrogen atom trans to the Cp ligand is probably the vacant site in the phenyl and the alkyl complexes. The unusual bond angles around the ipso-carbon of the phenyl group may be due to a weak interaction of the

references on page 199

ortho-hydrogen of the phenyl group with the metal centre. Also, for the alkyl derivatives the solution structure could be depicted as shown inside the box in Figure **4.10**, where one of the α-hydrogen is involved in a weak agostic type interaction in the equatorial plane.

The zirconium-Cp bond distance of 2.209 Å in the borohydride complex is comparable to the phenyl, **4.4** and the alkyl, **4.8** complexes and is shorter than the distances observed in complexes **2.7** and **2.9**. The zirconium-hydride distances, 2.19 (5) and 2.09 (4) Å are identical and the zirconium-boron distance was 2.617 (7) Å, all of which is consistent with the bidentate coordination of the BH_4 ligand. The calculated zirconium-boron distance for the tridentate and bidentate modes are 2.35 and 2.60 Å respectively.[45] The metal-BH_4 interactions in complex **4.17** are similar to those in $Zr_2H_3(BH_4)_5(PMe_3)_2$ and $Zr(BH_4)_4$.[37,39,46,47]

4.6 Disproportionation Reactions of Mononuclear Zirconium(III) Complexes

Treating a solution of the zirconium(III) chloro derivative **4.1** with an atmosphere of CO resulted in a rapid color change from deep green to dark brown. Monitoring the reaction by ^1H and $^{31}P\{^1H\}$ NMR spectroscopy showed the formation of diamagnetic species; the ESR spectrum of the same sample showed only a very weak signal.* However, upon removing CO from the aforementioned reaction, the color changed from dark brown to deep green and the ESR and NMR spectra of the resulting product were identical to the paramagnetic chloro derivative, **4.1**. This result clearly suggests a reversible reaction of complex **4.1** with CO. Upon monitoring the reaction by UV-Vis spectroscopy, a band at 450 nm was observed which disappears upon the removal of CO from the reaction mixture. The solution infrared spectrum of a CO saturated toluene solution of **4.1** shows a weak and a strong band at 1965 and 1871 cm^{-1}, respectively. A similar reaction involving the borohydride complex **4.17** with CO also gave diamagnetic species, for which some of the spectroscopic features (IR, UV-Vis and NMR) were identical to those observed for the diamagnetic species generated by the reaction of CO and **4.1**. As mentioned above, the reaction could be reversed by the removal of CO to give the paramagnetic borohydride derivative, **4.17**.

* The signal could be observed only at very high gain.

references on page 199

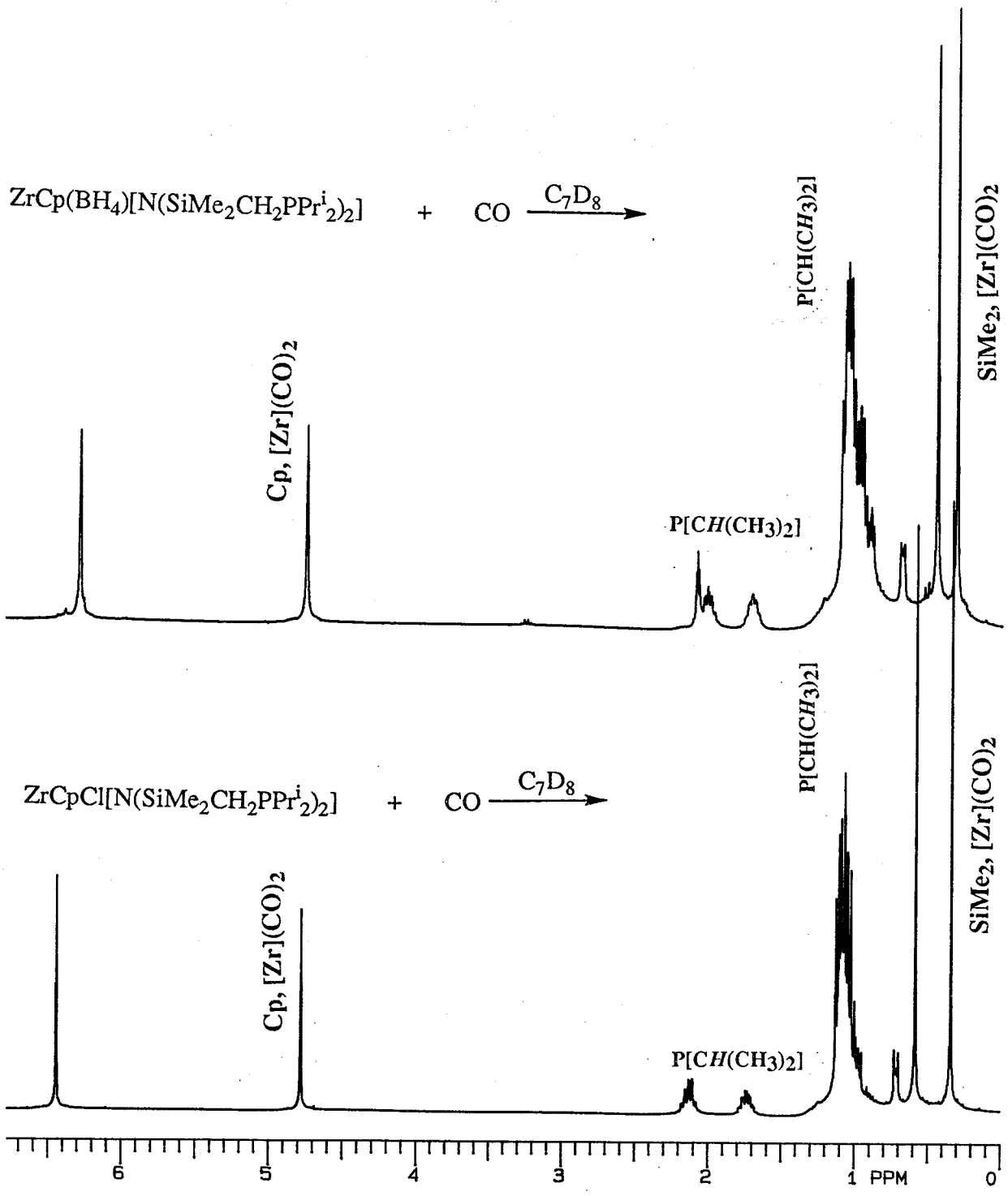

Figure 4.11 (top) ^{1}H (300 MHz, C_7D_8) spectrum of the diamagnetic species obtained from the reaction of **4.17** and CO. (bottom) ^{1}H NMR (300 MHz, C_7D_8) spectrum of the diamagnetic species obtained from the reaction of **4.1** and CO.

references on page 199

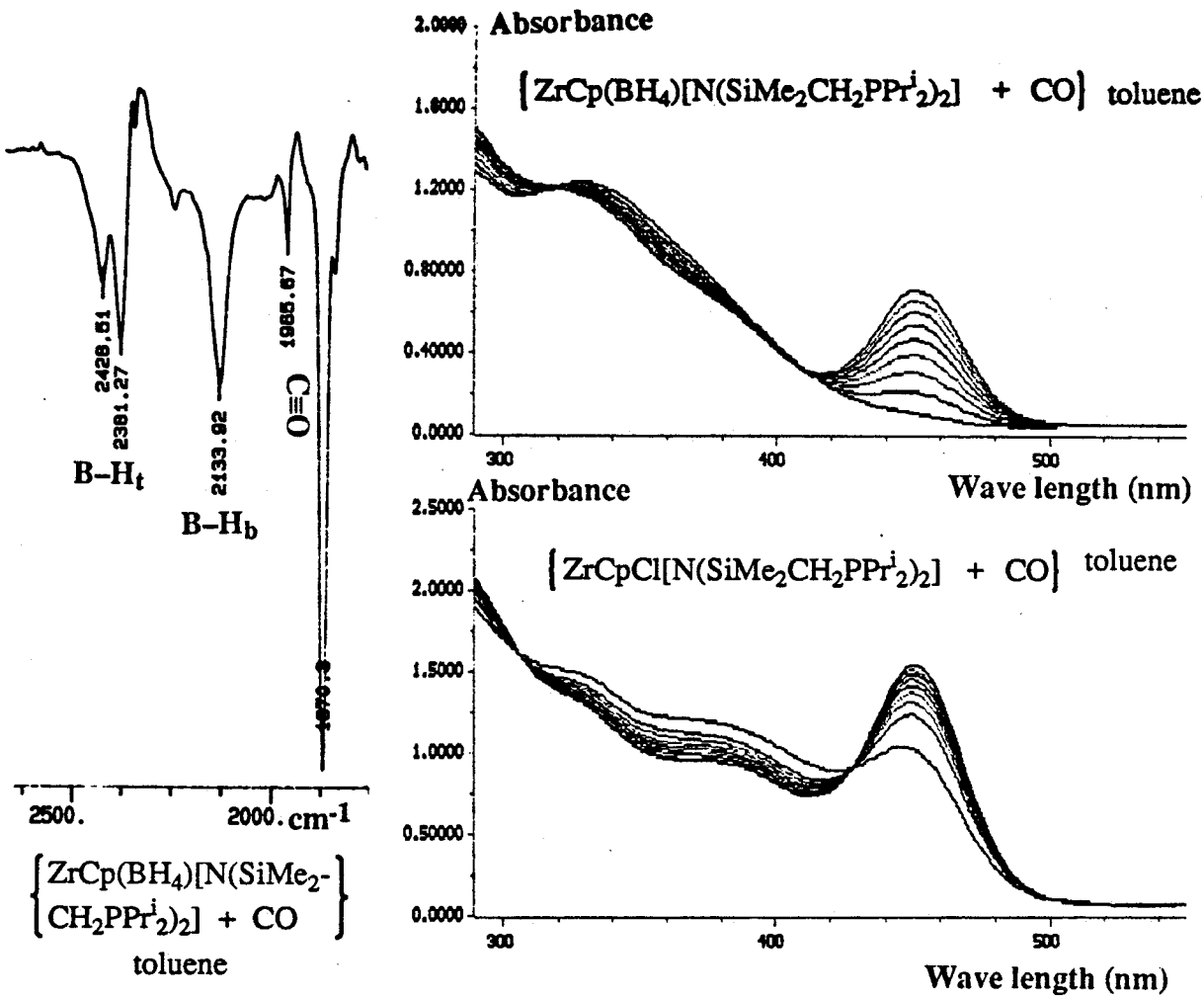

Figure 4.12 UV-Vis spectroscopic monitoring of the reaction of **4.17** (top right) and **4.1** (bottom right) with CO (1 atmosphere). (left) Infrared spectrum (solution in toluene) of the reaction of **4.17** with CO.

These results indicate that complexes **4.1** and **4.17** react with CO to give two complexes, with one of the products common for both reactions. On the basis of the spectroscopic features, the common species is formulated as the zirconium(II) dicarbonyl derivative, $Zr(\eta^5\text{-}C_5H_5)$-$(CO)_2[N(SiMe_2CH_2PPr^i_2)_2]$, **4.18**. The ^1H NMR spectrum of **4.18** has only a single resonance for the $SiMe_2$ groups and a triplet for the Cp ligand due to coupling to two equivalent phosphorus-31 nuclei. The singlet resonance at 37.91 ppm in the $^{31}P\{^1H\}$ NMR spectrum, which was common for both reactions, was assigned to the dicarbonyl complex **4.18**. The

references on page 199

complex could be envisaged as having a pseudooctahedral geometry with a meridionally bound PNP ligand and trans disposed CO ligands.

After assigning the NMR resonances associated with the dicarbonyl complex **4.18** the remaining spectroscopic features from the reaction of **4.1** with CO shows it to be the zirconium(IV) dichloro derivative $Zr(\eta^5\text{-}C_5H_5)Cl_2[N(SiMe_2CH_2PPr^i_2)_2]$, **2.6**. Therefore, it is presumed that the second diamagnetic species obtained from the reaction of the borohydride complex **4.17** is the zirconium(IV) bis(borohydride) derivative, $Zr(\eta^5\text{-}C_5H_5)(BH_4)_2[N(SiMe_2\text{-}CH_2PPr^i_2)_2]$, **4.19**.

The hafnium(III) chloro complex **4.3** also reacts with CO to give the hafnium(IV) dichloro complex $Hf(\eta^5\text{-}C_5H_5)Cl_2[N(SiMe_2CH_2PPr^i_2)_2]$ **4.2**, and the hafnium(II) dicarbonyl derivative $Hf(\eta^5\text{-}C_5H_5)(CO)_2[N(SiMe_2CH_2PPr^i_2)_2]$, **4.20**. Therefore, these disproportionation reactions could be given in a general form as shown in Scheme **4.11**.

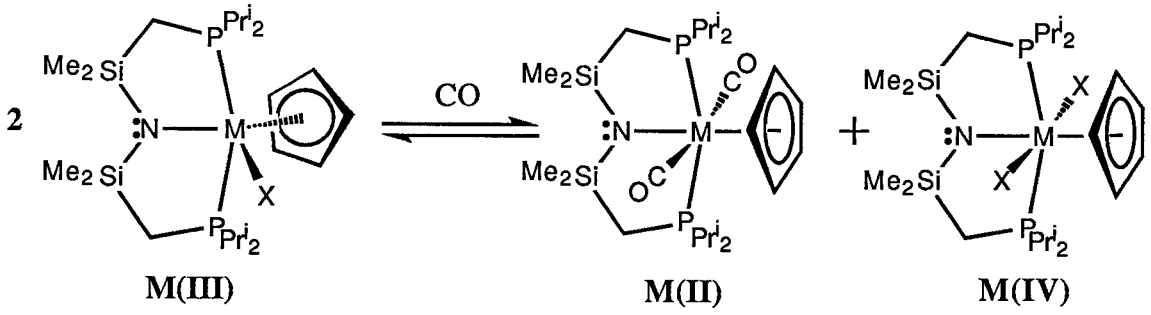

M = Zr; X = Cl, **4.1**; X = BH_4, **4.17**
M = Hf; X= Cl, **4.3**

M = Zr, **4.18**
M = Hf, **4.20**

M = Zr; X = Cl, **2.6**; BH_4, **4.19**
M = Hf; X = Cl, **4.2**

Scheme 4.11

The solution infrared spectrum of the bis(borohydride) complex **4.19** shows strong absorptions due to the terminal boron-hydrogen stretches at 2429 and 2381 cm^{-1} and a band at 2134 cm^{-1} corresponding to the bridging boron-hydrogen stretch. These boron-hydrogen stretching frequencies are comparable to that observed for the zirconium(III) borohydride complex, **4.17**. Therefore it is presumed that the BH_4 ligands in complex **4.17** are also bound in a bidentate fashion.

references on page 199

The NMR spectroscopic features of the bis(borohydride) derivative **4.19** suggest that it is isostructural with the dichloro derivative **2.6** with trans disposed BH_4 ligands. Also, the ^1H and $^{31}P\{^1H\}$ NMR spectra of **4.19** recorded at room temperature and at -85 °C were virtually identical; the resonances due to the BH_4 ligands were not located in the ^1H NMR spectrum.

Although the disproportionation of the zirconium(III) borohydride complex **4.17** proceeds quantitatively to give the bis(borohydride) complex **4.19**, attempts to synthesize it by other routes were unsuccessful. For example, reacting the dichloro complex **2.6** with $LiBH_4$ or attempts to oxidize complex **4.17** with $PbCl_2$ to make $Zr(\eta^5\text{-}C_5H_5)(BH_4)Cl[N(SiMe_2CH_2\text{-}PPr^i_2)_2]$ **4.17**, only produced intractable materials. Also, the reaction of the hafnium dichloro complex $Hf(\eta^5\text{-}C_5H_5)Cl_2[N(SiMe_2CH_2PPr^i_2)_2]$ **4.2**, with $LiBH_4$ gave only the monoborohydride complex $Hf(\eta^5\text{-}C_5H_5)(BH_4)Cl[N(SiMe_2CH_2PPr^i_2)_2]$, **4.21**.*

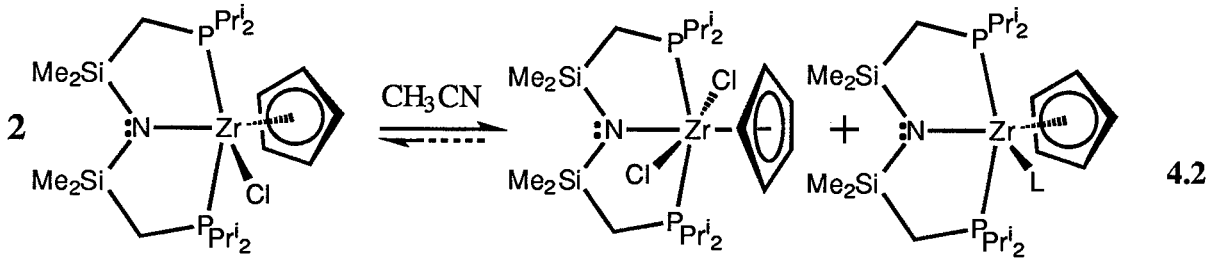

Zr(III) **4.1** | **Zr(IV)** **2.6** | **Zr(II)** **4.22** $L = CH_3CN$

The room temperature reaction of the zirconium(III) chloro derivative **4.1** with CH_3CN gave a deep red solution; the ^1H and $^{31}P\{^1H\}$ NMR spectral analysis showed the presence of zirconium(IV) dichloro complex **2.6** and some unidentified products, and no paramagnetic species were found by ESR spectroscopy. Monitoring the reaction by $^{31}P\{^1H\}$ NMR spectroscopy at low temperatures showed the formation of a second product, **4.22** which correlated to a resonance at 19.78 ppm. By comparison with the reaction of CO with **4.1**, the complex **4.22** could possibly be an acetonitrile adduct of a zirconium(II) species. Spectroscopic monitoring also showed that the zirconium(II) complex is only stable at lower temperatures and

* The solid state infrared spectrum of the complex **4.21** shows that the BH_4 ligand is bound in a bidentate fashion

references on page 199

rapidly decomposes at room temperature. Although the low temperature experiments show that the zirconium(III) chloro derivative **4.1** does undergo disproportionation reaction in the presence of acetonitrile, due to the instability of the zirconium(II) species it was difficult to establish whether the reaction is a reversible process.

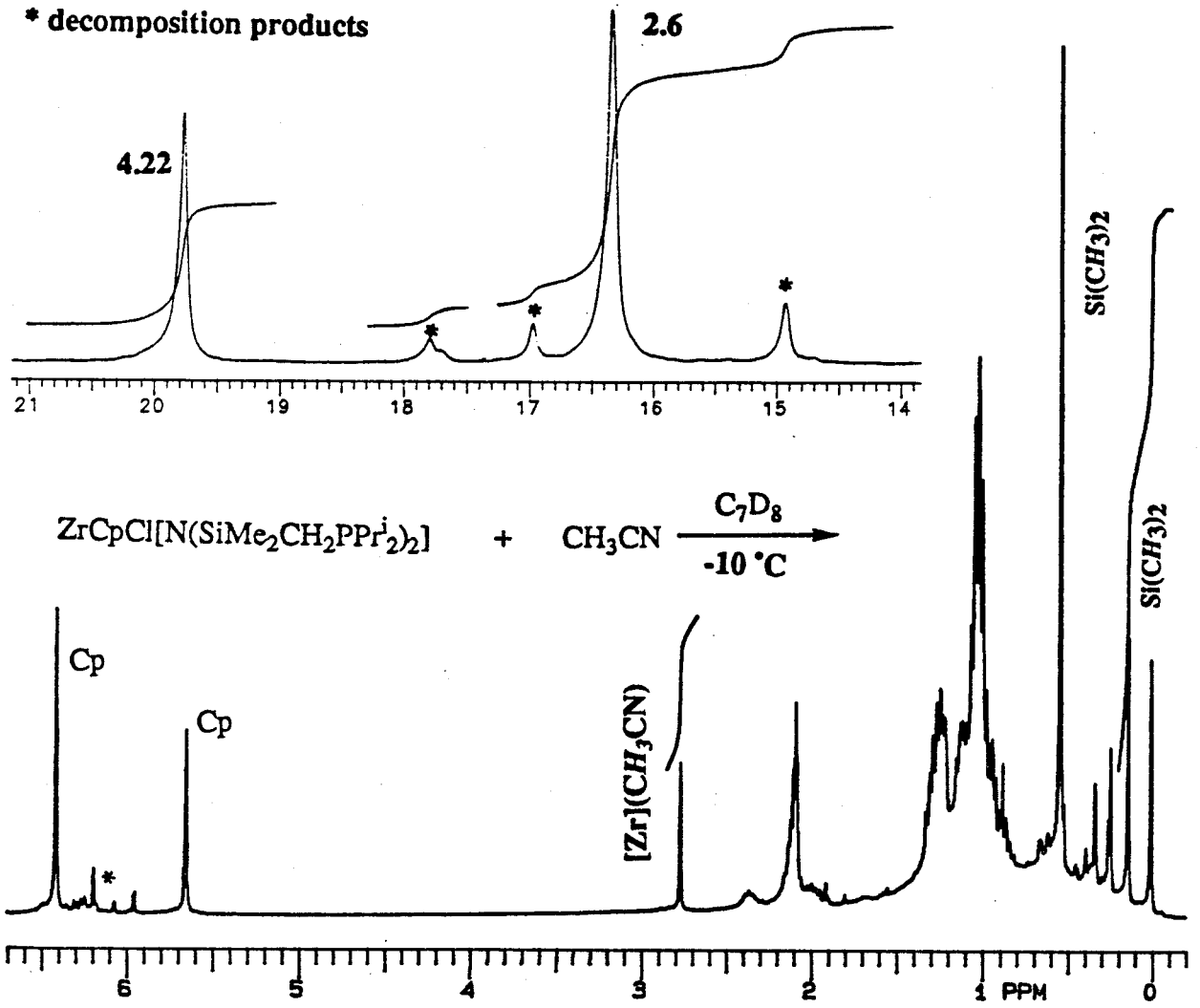

Figure 4.13 **A, B** Low temperature ^{1}H (300 MHz) and $^{31}P\{^{1}H\}$ (121 MHz) NMR spectra (C_7D_8) of the diamagnetic species obtained from the reaction of **4.1** and CH_3CN.

On the basis of the ^{1}H NMR spectrum of the zirconium(II) acetonitrile adduct **4.22**, the molecule appears to be less symmetric than the zirconium(II) dicarbonyl species, **4.18**. The ^{1}H NMR spectrum of **4.22** has two resonance in the $SiMe_2$ region and integration values suggest that the molecule has only one acetonitrile ligand. Considering that the complex gives only a

references on page 199

singlet in the $^{31}P\{^{1}H\}$ NMR spectrum, the geometry around the zirconium center in **4.22** could be described as a pseudo trigonal bipyramidal, with the phosphine donors occupying the apical positions (Equation **4.2**).

Some dinuclear zirconium(III) complexes (Chapter **3**) undergo thermally or photochemically induced disproportionation to give zirconium(IV) and zirconium(II) species where the zirconium(II) species can be trapped with ligands such as CO* and butadiene (top of Scheme **4.12**, also see Chapter **3**).[48] It was also shown that these dinuclear zirconium(III) complexes are stable in noncoordinating solvents like toluene and, in polar solvents like THF, they undergo decomposition. However, the mononuclear zirconium(III) complexes **4.1** or **4.17** do not shown any sign of such a disproportionation even at elevated temperatures or in the presence of ligands such as THF, ethylene or PMe_3.

The dicarbonyl titanium(II) complex $Cp_2Ti(CO)_2$, reacts with the titanium(IV) complex Cp_2TiX_2, where X = Cl or SPh, to give the dinuclear titanium(III) species $[Cp_2TiCl]_2(\mu\text{-}X)_2$.[49] A similar reaction has also been reported between $Cp_2Zr(CO)_2$ and Cp_2ZrX_2, where X = Cl or SPh.[50] These reactions are somewhat comparable to the reverse reactions shown in Scheme **4.11**.

The proposed mechanism for the reaction for the chloro complex **4.1** with CO is shown in Scheme **4.12**. It is believed that the initial step involves the formation of an adduct with CO, intermediate **A**, where, as shown in Scheme **4.11**, the CO could adopt a linear or a bent structure. Intermediates having bent CO ligands have been proposed for the hydrogen abstraction reactions by 19-electron metal carbonyl complexes, for example the reaction of $[Cr(CO)_6]^-$ with $HSnBu_3$ (bottom of Scheme **4.12**).[51] It could be argued that the formation of a bent CO ligand in 19-electron complexes enables the metal center to attain an 18-electron configuration. However, intermediate **A** is a 17-electron complex and therefore bending the CO ligand would give the metal center a 16-electron configuration. For electropositive metals like zirconium, a bent CO could also donate electrons from the oxygen. The intermediate **A** could disproportionate via a dimeric intermediate as shown in Scheme **4.12**.

---

* It is important to note that the disproportionation reactions in these dinuclear complexes are not initiated by CO.

references on page 199

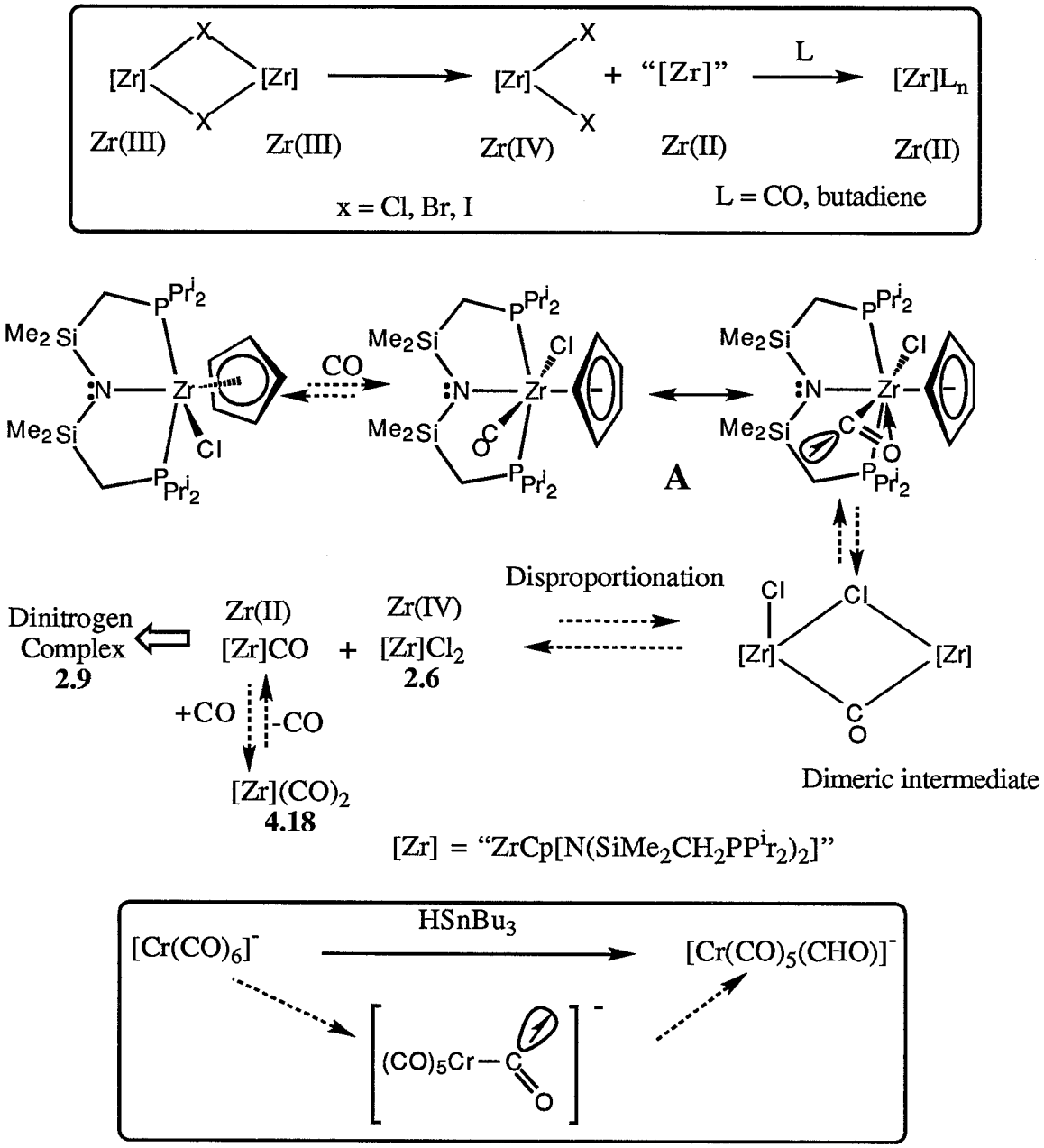

Scheme 4.12

It is noteworthy that a solution of the dicarbonyl complex under a dinitrogen atmosphere slowly converts to give the dinitrogen complex **2.9**. This suggests that the CO ligands of the dicarbonyl complex are labile, a process that is important for the reverse disproportionation reaction to occur. Removal of CO from the reaction could accelerate the dissociation of CO from **4.18** and lead to the formation of complex **4.1**. Acetonitrile and CO being similar ligands,

references on page 199

the disproportionation reactions involving acetonitrile may also proceed via an intermediate similar to **A**. Outer sphere electron transfer type process might also be important; however, it is difficult to rationalize the exchange of ligands that must occur to generate the product.

4.7 Further Reaction with CO: Formation of Zirconium Formyl Complex

The Fischer-Tropsch process involves the reaction of CO with dihydrogen over a heterogeneous metal catalyst to form a mixture of hydrocarbons and oxygenated products. Considerable efforts have been made to model different intermediates that are involved during the Fischer-Tropsch process. It is believed that the CO is reduced in a stepwise manner, where at the initial stages an intermediate containing a formyl type ligand has been invoked.[52,53]

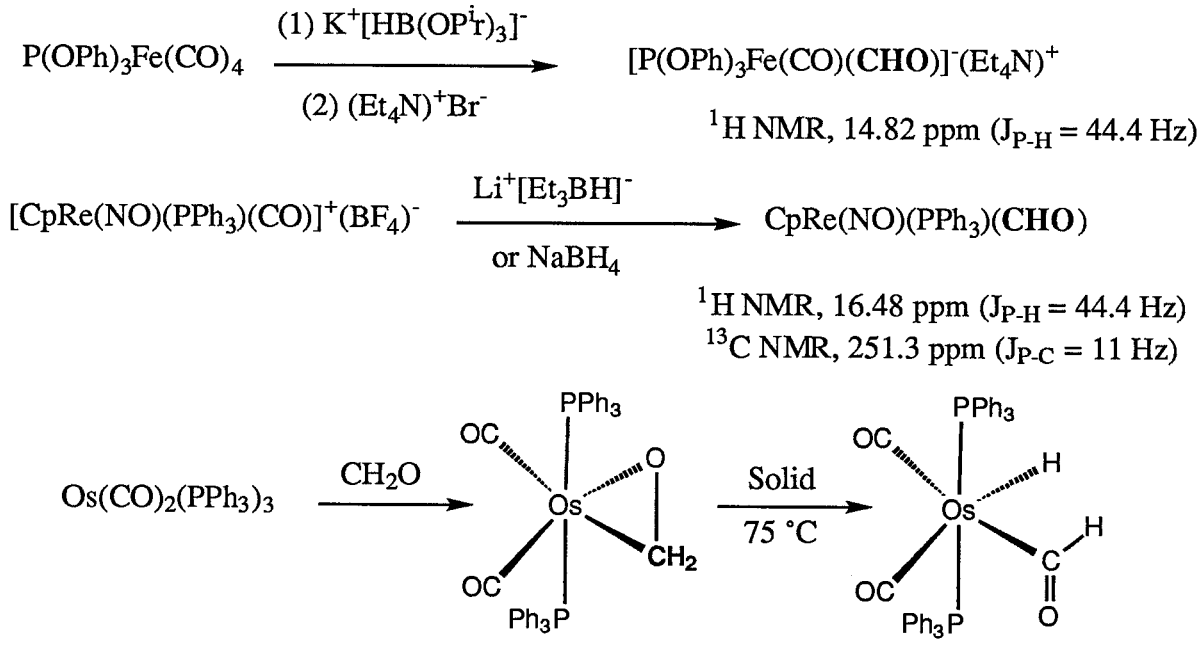

Scheme 4.13

Most of the known transition metal formyl complexes are synthesized by the addition of a hydride ligand to a coordinated carbonyl ligand (Scheme **4.13**).[54-58]. Only a few cases are known where the formyl ligand is formed by the reaction of a metal hydride complex with CO, where the reaction is presumed to take place by the insertion of CO into the metal-hydride bond (Scheme **4.14**).[59,60] However it is important to note that for d^0-metal complexes, the formyl

references on page 199

ligand is only observed at low temperatures or was found to be involved in some type of secondary interaction (Scheme **4.14**).[60,61]

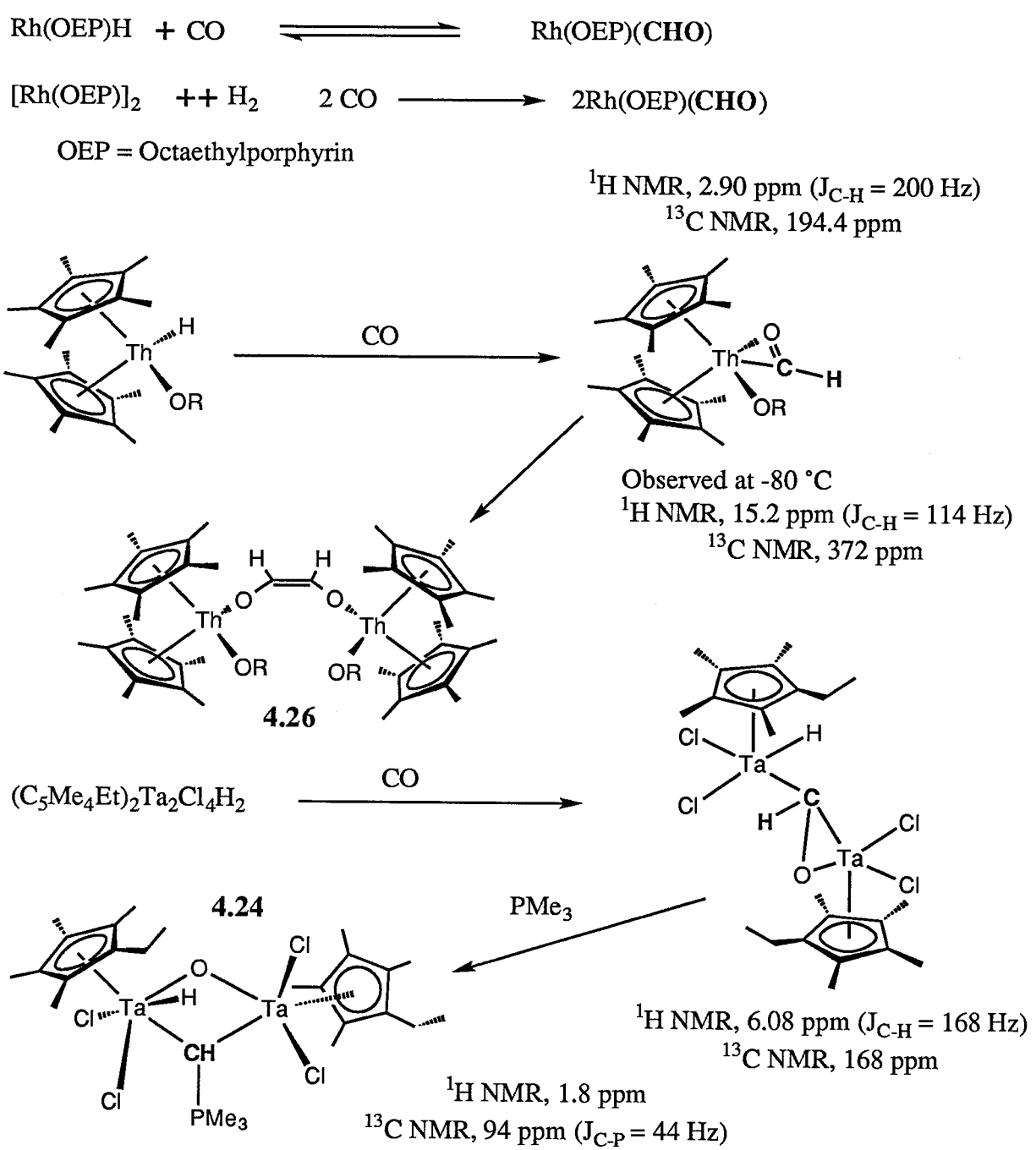

Scheme 4.14

The bis(borohydride) complex **4.19** formed from the disproportionation reaction reacts slowly with CO to give a complex which has an elemental composition that is consistent with

references on page 199

the formula $Zr(\eta^5\text{-}C_5H_5)(BH_4)_2(CO)[N(SiMe_2CH_2PPr^i_2)_2]$, **4.23**. The solid state infrared spectrum of this complex did not show any characteristic peak that would correspond to a terminal carbonyl stretch and also the boron-hydrogen stretching region clearly suggested that each BH_4 ligand is bound in a different fashion. The terminal B–H bond stretches at 2423 and 2378 cm^{-1} and the only bridging B–H band stretch at 2146 cm^{-1} suggests that one of the BH_4 ligands is bound in a bidentate fashion to zirconium.

The ^1H NMR spectrum (Figure **4.14**) of this complex shows four resonances for the $SiMe_2$ protons and the $^{31}P\{^1H\}$ NMR spectrum consists of a sharp peak at 39.72 ppm and a broad peak at 31.20 ppm, which are consistent with an unsymmetrical mononuclear complex. The multiplet underneath the $SiMe_2$ protons (around 0.25 ppm) and the broad resonance around 1.2 ppm could be attributed to the boron hydrides. The intriguing feature in the ^1H NMR spectrum is the doublet at 3.02 ppm which corresponds to one proton. Selective ^{31}P decoupled ^1H NMR experiments suggest that the resonance at 3.02 ppm is coupled to the ^{31}P resonance at 39.72 ppm with a coupling constant of $J_{P\text{-}H}$ = 27.4 Hz. The $^{11}B\{^1H\}$ NMR spectrum of this complex has a singlet at -101.3 ppm and a doublet at -127.2 ppm, the latter is probably due to the coupling with one phosphorus-31 nucleus ($J_{B\text{-}P}$ = 47.4 Hz).

The carbon-13 analogue of complex **4.23** was synthesized using ^{13}CO and shows that the resonance at 3.02 ppm in the ^1H NMR spectrum has an unusually large coupling constant to carbon, $J_{C\text{-}H}$ = 161.8 Hz; in addition, the $^{31}P\{^1H\}$ resonance at 39.72 ppm was now split into a doublet with $J_{P\text{-}C}$ = 55 Hz. In the $^{13}C\{^1H\}$ NMR spectrum the signal due to the enriched carbon was found to be a doublet at 60.73 ppm, $J_{P\text{-}C}$ = 55 Hz. One possibility, suggested by the spectroscopic data, is that the complex **4.23** has a formyl type ligand; a proposed structure is depicted in Scheme **4.15**. However, the main problem with this proposed structure is that the ^{13}C and ^1H NMR chemical shifts associated with the formyl ligand in complex **4.23** are significantly shifted to higher field than the usual shifts observed for a formyl ligand (Scheme **4.13** and **4.14**). Fortunately, we were able to grow single crystals of complex **4.23** and subject them to X-ray analysis.

references on page 199

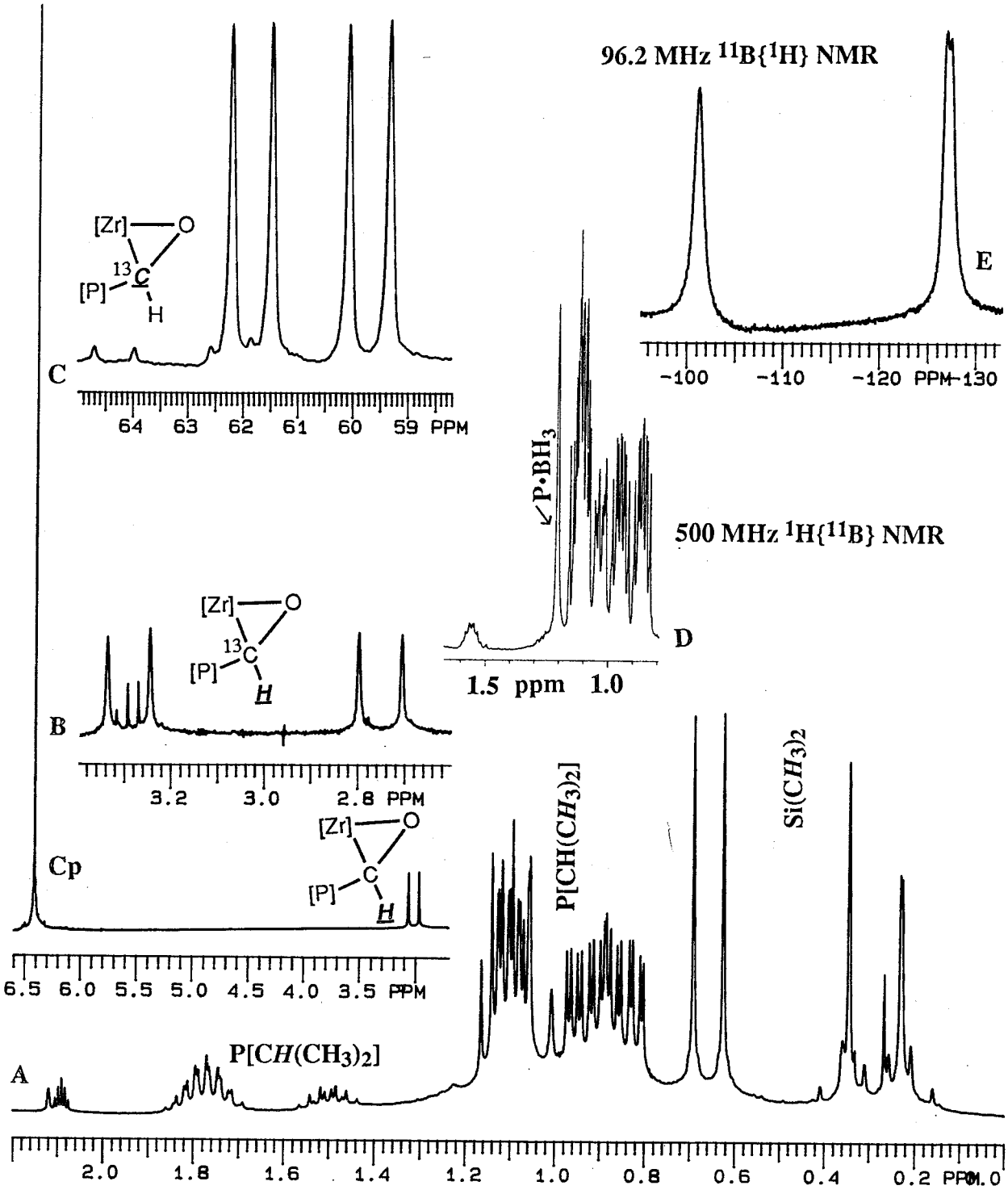

Figure 4.14 **A** ^1H NMR (300 MHz) spectrum of **4.23**. **B, C** ^1H (300 MHz) and gated decoupled ^{13}C (75.4 MHz) resonances associated with the formyl ligand of **4.23** labelled with ^{13}C. **D** $^1H\{^{11}B\}$ NMR (500 MHz) spectrum showing the BH_3 unit and **E** $^{11}B\{^1H\}$ NMR (96.2 MHz) spectrun of **4.23** (C_7D_8).

references on page 199

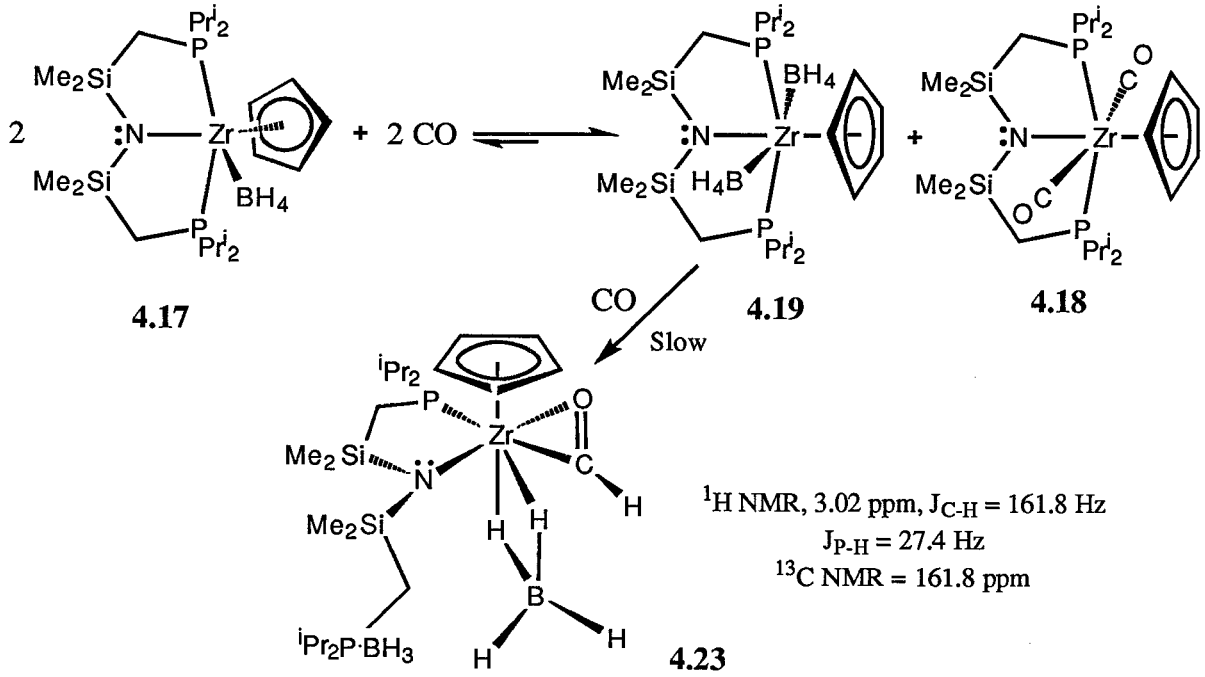

Scheme 4.15

The X-ray structure (Figure **4.15**) of the complex **4.23** agrees with most but not all of the features determined from the spectroscopic analysis. However, the original proposal has one of the phosphine donors of the PNP ligand coordinated to the zirconium whereas, in the X-ray structure, this phosphine ligand is bound to the carbon atom of the formyl ligand. Such a phosphine interaction would probably explain the relatively high field proton and carbon-13 NMR signals observed for the formyl ligand. In fact the coordination around the formyl carbon atom is somewhat comparable to the proposed structure of the tantalum formyl complex **4.24** (Scheme **4.14**) where a second tantalum atom is interacting in a similar fashion to the phosphine in **4.23**. Also, the NMR spectroscopic features associated with the formyl ligand of both complexes are comparable.[61] The structure also shows that the the second phosphine donor of the PNP ligand is coordinated to a BH_3 unit.

references on page 199

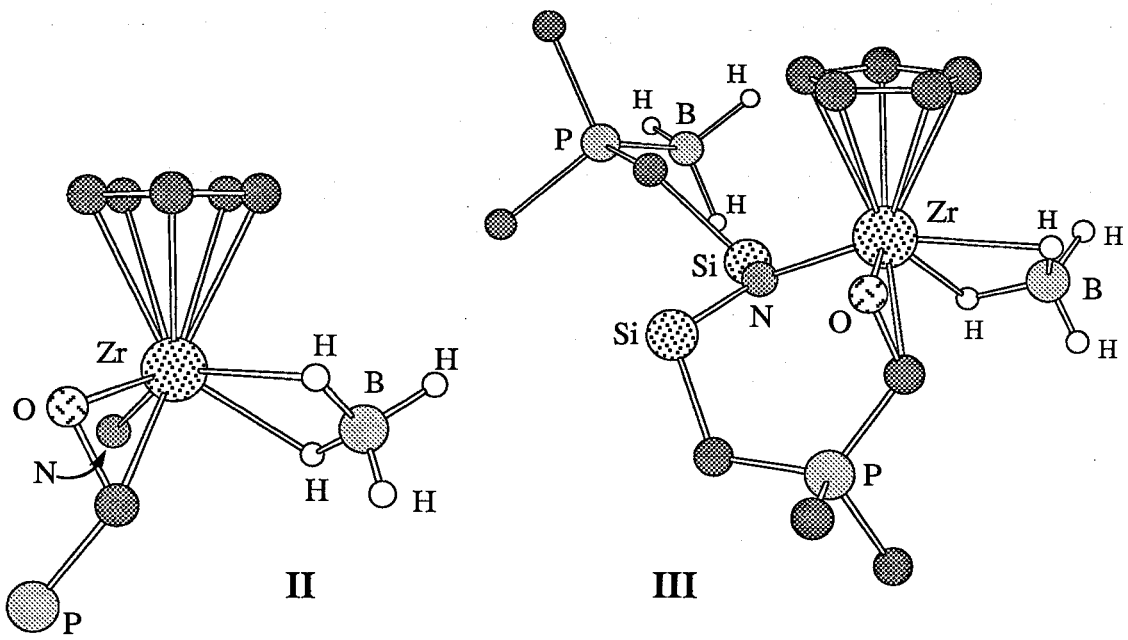

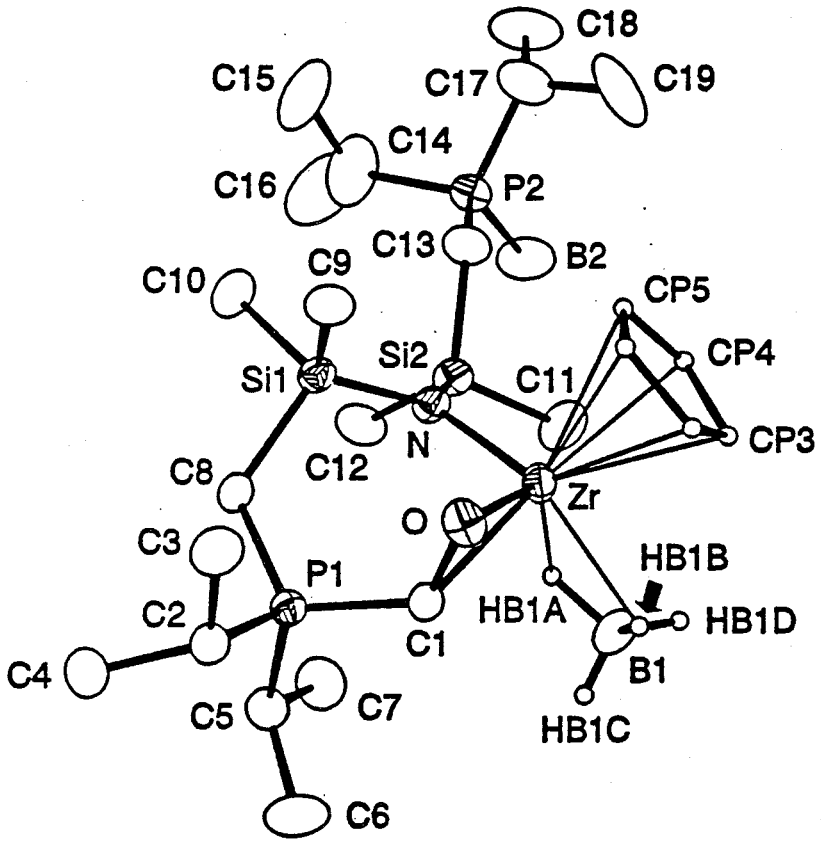

I

Figure 4.14 **I** ORTEP view showing the complete atom labeling scheme of complex $Zr(\eta^5\text{-}C_5H_5)(\eta^2\text{-}BH_4)(\eta^2\text{-}CHO)\{N(SiMe_2CH_2PPr^i_2)[SiMe_2CH_2(Pr^i_2P{\bullet}BH_3)]\}$, **4.23**. **II** and **III** are Chem 3D® views of complex **4.23**.

references on page 199

Table 4.8 Selected bond lengths of complex

$Zr(\eta^5\text{-}C_5H_5)(\eta^2\text{-}BH_4)(\eta^2\text{-}CHO)\{N(SiMe_2CH_2PPr^i_2)[SiMe_2CH_2(Pr^i_2P{\bullet}BH_3)]\}$, **4.23**

Atom	Atom	Distance (Å)	Atom	Atom	Distance (Å)
Zr	N	2.135 (3)	Zr	Cp	2.2855 (9)
Zr	O	1.987 (3)	Zr	C(1)	2.254 (4)
Zr	HB1A	2.09(4)	Zr	HB1B	2.31 (4)
P(1)	C(8)	1.795 (4)	Zr	B(1)	2.594 (6)
P(1)	C(1)	1.765 (4)	P(2)	B(2)	1.927 (7)
C(1)	O	1.429 (5)	Si(1)	N	1.731 (4)

Table 4.9 Selected bond angles of complex

$Zr(\eta^5\text{-}C_5H_5)(\eta^2\text{-}BH_4)(\eta^2\text{-}CHO)\{N(SiMe_2CH_2PPr^i_2)[SiMe_2CH_2(Pr^i_2P{\bullet}BH_3)]\}$, **4.23**

Atom	Atom	Atom	Angle (°)	Atom	Atom	Atom	Angle (°)
O	Zr	N	104.63 (13)	C(1)	Zr	N	95.70 (14)
O	Zr	Cp	105.68 (9)	C(1)	Zr	Cp	141.84 (12)
N	Zr	Cp	110.30 (9)	O	Zr	C(1)	38.73 (14)
Zr	O	C(1)	80.78 (21)	O	C(1)	Zr	60.49 (19)
P(1)	C(1)	O	116.1 (3)	P(1)	C(1)	Zr	129.48 (22)
C(1)	P(1)	C(8)	114.15 (20)	P(1)	C(8)	Si(1)	120.78 (23)
N	Si(1)	C(8)	110.55 (18)	Zr	N	Si(1)	115.11 (17)
Si(1)	N	Si(2)	122.11 (20)	Zr	N	Si(2)	122.76 (18)

In Scheme **4.16** the bonding parameters associated with the formyl ligand in complex **4.23** and a molybdenum complex containing an analogous phosphine stabilized acyl ligand **4.25** are shown.[62] The phosphorus-carbon bond distance of 1.831(5) Å in **4.25** is very similar to a single bond. By comparison, in the zirconium complex the distance was 1.765(4) Å and is significantly shorter. In fact it is comparable to a related tantalum formyl complex **4.24**,[61]

references on page 199

1.750(18) Å, and to the dinuclear iron complex, $Fe_2(CO)_6[C(CHO)P(Ph_2C_6H_4)]$, 1.748(6) Å.[63] In these complexes the bonding between the phosphorus and the carbon of the "R_3P–C" moiety is regarded as an ylid. The carbon-oxygen bond distance, 1.429(5) Å of the metallaoxirane ring of the zirconium complex, **4.23** is longer than the molybdenum complex, 1.367(6) Å; this is consistent with greater electron donation from oxygen to zirconium (Chapter **2**, Section **2.5.2**). The zirconium-carbon distance of 2.254(4) Å is within the range of 2.251(6) to 2.388(12) Å.

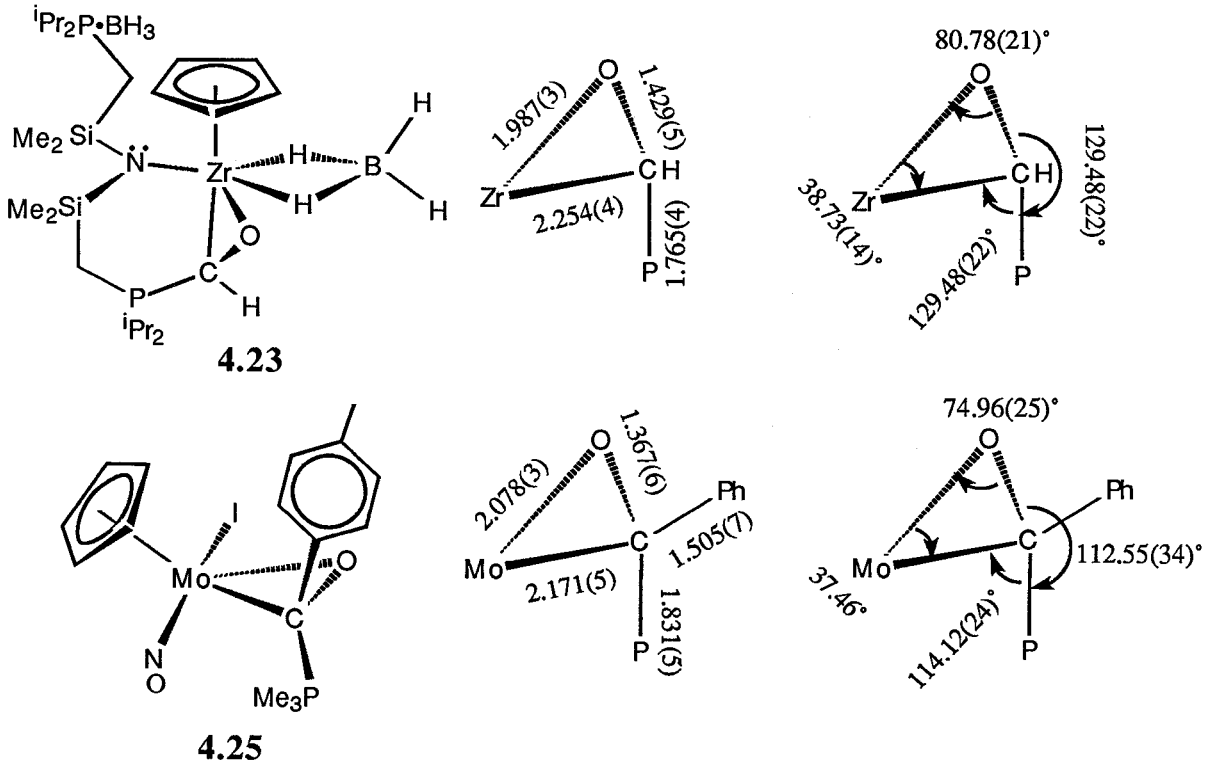

4.23 **4.25**

Scheme 4.16

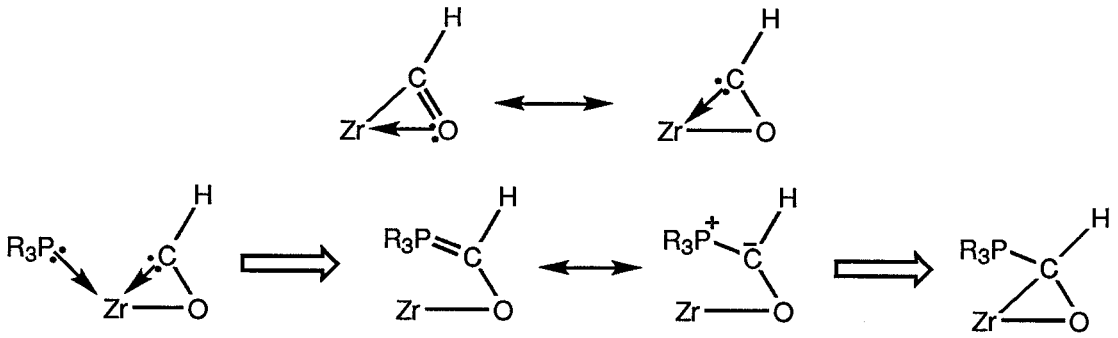

Scheme 4.17

references on page 199

The bonding of the formyl ligand can be described in terms of two limiting resonance forms as shown on the top of Scheme **4.17**, where one is an η^2-formyl and the other is an η^2 oxycarbene canonical structure.[61,64,65] In the case of d^0 transition metal complexes, the oxycarbene canonical form has a significant contribution towards the nature of the bonding of the formyl ligand. For example, the synthesis of complex **4.26** from the thorium formyl complex could be envisaged as a coupling of two thorium oxycarbene units (Scheme **4.14**). A similar rational could be extended to describe the derivation of the "formyl-ylid" ligand in complex **4.23** (Scheme **4.17**).

4.8 Conclusions

The reduction of the zirconium(IV) or the hafnium(IV) complex $M(\eta^5\text{-}C_5H_5)Cl_2\text{-}[N(SiMe_2CH_2PPr^i_2)_2]$, where M = Zr or Hf, has enabled the synthesis of the zirconium(III) and the hafnium(III) complexes. The zirconium(III) complex, $Zr(\eta^5\text{-}C_5H_5)Cl[N(SiMe_2CH_2\text{-}PPr^i_2)_2]$, **4.1** was obtained in excellent yields, and was used as a precursor to synthesize zirconium(III) alkyl, aryl and borohydride complexes via simple metathesis reactions. Most intriguingly, all of the zirconium(III) hydrocarbyl complexes, $Zr(\eta^5\text{-}C_5H_5)R[N(SiMe_2\text{-}CH_2PPr^i_2)_2]$, where R = Ph, Me, Et, Bz and CH_2SiMe_3, show very good thermal stability. The X-ray structure determination of the aryl (Ph), alkyl (CH_2SiMe_3) and the borohydride (BH_4) derivatives showed that all of the complexes are mononuclear and have closely related structures. These examples constitute the first well characterized zirconium(III) complexes containing hydrocarbyl and borohydride ligands.

The ESR spectroscopic studies indicate that the α-hydrogens of the alkyl ligands show different hyperfine coupling constants. Although this could be explained on the basis of restricted rotation about the zirconium-carbon bond, infrared studies and some structural features seem to suggest a weak agostic type interaction may be present between one of the α-hydrogens and the metal.

Hydrogenolysis of certain alkyl complexes shows a clean conversion to the mononuclear zirconium(III) hydride complex. This hydride complex undergoes an insertion reaction with

references on page 199

ethylene. By means of labeling studies with the ethyl zirconium(III) complex it was shown that no scrambling of the β-hydrogens occurred which mirrored the behavior of unhindered zirconium(IV) alkyls. The hydride complex also undergoes hydrogen exchange reactions with H–C(sp^2) and H–C(sp^3) bonds, presumably by way of σ-bond metathesis. Reactions with terminal acetylene predominantly gave the acetylide complex and no definitive evidence was found for the formation of the insertion product.

Complexes $Zr(\eta^5\text{-}C_5H_5)Cl[N(SiMe_2CH_2PPr^i_2)_2]$, **4.1** and $Zr(\eta^5\text{-}C_5H_5)(BH_4)[N(SiMe_2\text{-}CH_2PPr^i_2)_2]$, **4.17** undergo a reversible disproportionation reactions under a CO atmosphere to give zirconium(IV) and zirconium(II) derivatives. It was also shown that CH_3CN reacts in a similar fashion with **4.1**; however the reversibility of this reaction was not established. In the case of the borohydride complex the reaction with CO proceeds further to give a complex containing a "formyl-ylid" type ligand.

Finally it could be stated that the isopropyl version of the PNP ligand "$[N(SiMe_2CH_2PPr^i_2)_2]$" was very effective in stabilizing the zirconium(III) complexes. Also, these complexes have shown many different types of reactivity, which is in stark contrast to the bulky Cp ligand based zirconium(III) complexes where no reactivity has been reported.

4.9 Experimental Procedures

4.9a General

Unless otherwise stated all procedures were as described in section **2.9a**. Hydrogen gas, purchased from Matheson, was purified by passage through a column of activated 4Å molecular sieves and MnO supported on vermiculite. Deuterium (99.5 atom %D) gas and ethylene-d_4 (99.5 atom %D) were obtained from MSD Isotopes. Ethylene and CO were purchased from Matheson and were used as supplied. Phenyllithium,[66] ethyllithium,[67] benzylpotassium,[68] $LiCH_2SiMe_3$,[69] NaCp•DME[70] and dibenzyl-magnesium[71] were prepared according to literature procedures. Methylmagnesiumbromide (1.4 M solution in 75% toluene and 25% THF), benzylmagnesiumchloride (1 M solution in Et_2O), CH_3CN, $TiCl_3$, Ph_2S_2 and $PbCl_2$ were purchased from Aldrich and $LiBH_4$ was purchased from BDH. Diphenyldisulphide was

references on page 199

purified by sublimation, acetonitrile was dried over 4Å activated molecular sieves for 12 hours and then vacuum transferred and degassed by three freeze-pump-thaw cycles. Lead(II) dichloride and $LiBH_4$ were pumped under vacuum for 24 hours prior to use.

The ESR spectra were recorded on Varian E-3 spectrometer calibrated with a sample of $VO(acac)_2$, g = 1.965.[72] ESR simulations were done on a Macintosh IIx using ESR II from Calleo Scientific Software. The values of line broadening and coupling constants were obtained from the simulated spectra (see appendix **B1**). NMR, UV/Vis, IR and MS spectra were recorded on the instruments described in section **2.9a**.

The complex $Zr(\eta^5\text{-}C_5H_5)Cl_2[N(SiMe_2CH_2PPr^i_2)_2]$, **2.6** was prepared according to the procedure described in section **2.9b.2**. $HfCl_3[N(SiMe_2CH_2PPr^i_2)_2]$ was synthesized according to the published procedure.[73]

4.9b Synthesis of Complexes

4.9b.1 $Zr(\eta^5\text{-}C_5H_5)Cl[N(SiMe_2CH_2PPr^i_2)_2]$, 4.1. A solution of $Zr(\eta^5\text{-}C_5H_5)Cl_2[N(SiMe_2\text{-}CH_2PPr^i_2)_2]$ **2.6**, (1.50 g, 2.42 mmol) in toluene (80 mL) was transferred into a thick-walled reaction flask containing Na/Hg (100 g of 0.3% amalgam, 13.0 mmol). The flask was then evacuated under vacuum (3 minutes) and sealed. Upon stirring the reaction mixture turns deep green. After 48 hours the reaction mixture was decanted from the amalgam and filtered through a layer of Celite®. The amalgam was extracted with 20 mL portions of hexanes (total of 60 mL) until the washings showed no green color. Upon removal of the solvent from the combined filtrate and extracts a dark green solid was obtained (95%). ESR spectrum of this green solid shows only the presence of **4.1** and ^1H NMR shows <5% (estimated relative to the amount of C_6D_5H present in C_6D_6) diamagnetic impurities. Recrystallization from hexanes gave analytically pure material (1.25 g, 88%). ESR (toluene): g = 1.955; a(^{91}Zr) = 37.2 G, 1Zr; a(^{31}P) = 21.1 G, 2P; a(^{14}N) = 2.9 G, 1N; a(^1H) = 1.8 G, 5H; linewidth used for simulation, 2.3 G. $\mu_{eff.}$ (Evans method) = 1.57 B. M. UV-Vis (toluene, 1 cm quartz cell): λ_{max} = 324 nm, ε_{max} = 2600 $Lmol^{-1}cm^{-1}$; λ = 360 nm, ε = 2500 $Lmol^{-1}cm^{-1}$. Anal. Calcd for $C_{23}H_{49}ClNP_2Si_2Zr$: C, 47.27; H, 8.45; N, 2.40. Found: C, 46.99; H, 8.99; N, 2.20.

references on page 199

4.9b.2 Hf(η^5-C_5H_5)Cl_2[N($SiMe_2CH_2PPr^i_2$)$_2$], 4.2. To a solution of $HfCl_3$[N($SiMe_2CH_2PPr^i_2$)$_2$] (6.00 g, 8.89 mmol) in toluene (150 mL) was added solid NaCp•DME (1.736 g, 9.74 mmol) at room temperature. The NaCp•DME was added in three portions at 1 hour intervals and the resulting mixture was stirred for 12 hour. The salt (NaCl) was removed by filtering through Celite®, the filtrate concentrated to 15 mL, hexanes was added until the solution turned turbid and cooling at -30 °C gave a pale white crystalline material (5.52 g, 88%). ^{1}H NMR (δ, 300 MHz, C_6D_6): 0.60 (s, 12H, Si(CH_3)$_2$); 1.6 to 0.96 (m, 28H, P[CH(CH_3)$_2$]$_2$, SiCH_2P); 2.17 (sept, 4H, P[CH(CH_3)$_2$]$_2$, $^3J_{H\text{-}H}$ = 8.9 Hz); 6.46 (br s ~5H, C_5H_5). ^{31}P{^{1}H} NMR (δ, 121.421 MHz, C_6D_6): 20.04 (s). Anal. Calcd for $C_{23}H_{49}NCl_2P_2Si_2Hf$: C, 39.07; H, 6.98; N, 1.98. Found: C, 39.36; H, 7.16; N, 1.87.

4.9b.3 Hf(η^5-C_5H_5)Cl[N($SiMe_2CH_2PPr^i_2$)$_2$], 4.3. A solution of Hf(η^5-C_5H_5)Cl_2[N($SiMe_2CH_2PPr^i_2$)$_2$] (2.00 g, 2.83 mmol) in toluene (80 mL) was transferred into a thick-walled reaction flask containing Na/Hg (100 g of 0.33% amalgam, 14.1 mmol). The flask was then evacuated under vacuum (3 minutes) and sealed. Upon stirring the reaction mixture turns deep greenish brown. After 48 hours, the reaction mixture was decanted from the amalgam and filtered through a layer of Celite®. The amalgam was extracted with 20 mL portions of hexanes (total of 60 mL), until the extracts show no color. Upon stripping off solvent from the combined filtrate and extracts a dark brown solid was obtained. Pure material was obtained by recrystallization from a pentane solution (0.8 g, 47%). ESR spectrum of this brown solid shows the presence of **4.1** and **4.3**. ESR (toluene): g = 1.916. Anal. Calcd for $C_{23}H_{49}NClP_2Si_2Hf$: C, 41.13; H, 7.35; N, 2.09. Found: C, 41.49; H, 7.49; N, 1.96.

4.9b.4 Zr(η^5-C_5H_5)C_6H_5[N($SiMe_2CH_2PPr^i_2$)$_2$], 4.4. To a solution of **4.1** (240 mg, 0.41 mmol) in toluene (5 mL) was added PhLi (1.6 mL of 0.25 M solution in Et_2O, 0.40 mmol) at -78 °C and stirred for 5 minutes. After stirring the reaction at room temperature for 3 hours the solvent was removed under vacuum. The deep brown residue was extracted with pentane (20 mL) and the extract was filtered through Celite®. The filtrate was concentrated (2 mL) and then cooled at -40 °C to give hexagonally shaped crystals (190 mg, 74%). ESR (toluene): g = 1.981; a(^{91}Zr) = 20.7 G, 1Zr a(^{31}P) = 20.3 G, 2P; a(^{14}N) = 1.8 G, 1N; a(^{1}H) = 1.1 G, 5H; linewidth

references on page 199

used for simulation, 2.8 G. UV-Vis (toluene, 1 cm quartz cell): λ_{max} = 342 nm; λ_{max} = 478 nm. Anal. Calcd for $C_{29}H_{54}NSi_2P_2Zr$: C, 55.63; H, 8.69; N, 2.24. Found: C, 55.51; H, 8.68; N; 2.35.

4.9b.5 $Zr(\eta^5\text{-}C_5H_5)Me[N(SiMe_2CH_2PPr^i_2)_2]$, 4.5. To a solution of **4.1** (825 mg, 1.46 mmol) in toluene (25 mL) was added a solution of MeMgX (X = Br, 1.1 mL of 1.4 M solution, 1.54 mmol; X = Cl, 0.55 mL of 3.0M solution in THF, 1.6 mmol) at room temperature. The reaction mixture was stirred for 4 hours and then the solvent was stripped off under vacuum. The resulting solid was extracted with pentane (10 mL) and the extract was filtered through a layer of Celite®. The filtrate was concentrated (~ 3 mL) and then cooled at -40 °C to give a deep green crystalline product (480 mg, 58%). ESR (toluene): g = 1.963; a(^{91}Zr) = 28.0 G, 1Zr; a(^{31}P) = 21.1 G, 2P; a(^{1}H) = 6.6 G, 3H; a(^{14}N) = 2.1 G, 1N; linewidth used for simulation, 3.0 G. Anal. Calcd for $C_{24}H_{52}NP_2Si_2Zr(MgCl_2)_{0.22}$: C, 49.28; H, 8.96; N, 2.39; Cl 2.67. Found: C, 48.90; H, 9.08; N, 2.39; Cl, 2.52.

4.9b.6 $Zr(\eta^5\text{-}C_5H_5)CH_2CH_3[N(SiMe_2CH_2PPr^i_2)_2]$, 4.6. Method 1: To a solution of **4.1** (1.00 g, 1.71 mmol) in toluene (25 mL) was added a solution of CH_3CH_2Li (70 mg, 1.94 mmol) in toluene (10 mL) at -78 °C. The reaction mixture was allowed to warm to room temperature and stirred for 8 h. The solvent was stripped off under vacuum, the residue was extracted with pentane (10 mL) and the extract was filtered through a layer of Celite®. The filtrate was concentrated (3 mL) and then cooled to -40 °C to give a deep green crystalline product (560 mg, 56%). ESR (toluene): g = 1.962; a(^{31}P) = 20.9 G, 2P; a($^{1}H_\alpha$) = 9.3 G, 1H; a($^{1}H_\alpha$) = 3.2 G, 1H; a($^{1}H_\beta$) = 1.8 G, 3H; a(^{14}N) = 2.6 G, 1N; linewidth used for simulation, 2.2 G. Anal. Calcd for $C_{25}H_{54}NP_2Si_2Zr$: C, 51.95; H, 9.42; N, 2.42. Found: (a) C, 49.76; H, 9.02; N, 2.32; (b) C, 51.20; H 9.28; N 2.39. Case (a) was obtained from the first recrystallization and case (b) was obtained from the second recrystallization and the data seems to fit for 0.6 equivalents and 0.2 equivalents of LiCl respectively.

Method 2: To a solution **4.1** (300 mg, 0.51 mmol) was added a solution of MeMgBr (0.4 mL of 1.4 M solution) and this was stirred at room temperature for 4 hours. The solvent was then stripped off under vacuum and the resulting solid was extracted with pentane. Stripping off the

references on page 199

pentane gave a green solid containing **4.5**. The solid was dissolved in toluene (15 mL) and transferred into a thick walled reaction flask (150 mL). The solution was freeze-pump-thawed twice and stirred under 1 atmosphere of H_2 for 12 hours at room temperature to give **4.14**. The H_2 was removed under vacuum and ethylene was introduced into the reaction flask and stirred for 0.5 hours. After removing the ethylene under vacuum, dioxane (1.0 mL) was added and stirred for 1h. The solvent was stripped under vacuum and the resulting solid was extracted with pentane. ESR spectrum of the pentane shows only the presence of **4.6**.

4.9b.7 Zr(η^5-C_5H_5)CH_2CH_2D[N($SiMe_2CH_2PPr^i_2$)$_2$], 4.6-d_1. A solution of **4.14**-d_1 (~ 0.5 mmol) was prepared as described in the synthesis of **4.14** using D_2 gas. After removing the deuterium gas and stirring the solution under ethylene for 0.5 hours gave **4.6**-d_1. ESR (toluene): g = 1.962; a(^{31}P) = 20.9 G, 2P; a($^1H_\alpha$) = 9.3 G, 1H; a($^1H_\alpha$) = 3.2 G, 1H; a($^1H_\beta$) = 1.8 G, 2H; a($^2H_\beta$) = 0.3 G, 1D; a(^{14}N) = 2.6 G, 1N; linewidth used for simulation, 1.7 G. IR (cm^{-1}, toluene): 2169 (w, βC-D of Et ligand); 2143 (m, βC-D of Et ligand); 2109 (s, βC-D of Et ligand).

4.9b.8 Zr(η^5-C_5H_5)CD_2CD_2H[N($SiMe_2CH_2PPr^i_2$)$_2$], 4.6-d_4. A solution of **4.14** (~0.5mmol) was prepared as described in the synthesis of **4.14**. After removing the hydrogen gas and stirring the solution under ethylene-d_4 for 0.5 hours gave **4.6**-d_4. ESR (toluene): g = 1.962; a(^{31}P) = 20.9 G, 2P; a($^2H_\alpha$) = 1.5 G, 1D; a($^2H_\alpha$) = 0.5 G, 1D; a($^2H_\beta$) = 0.3 G, 2D; a($^1H_\beta$) = 1.8 G, 1H; a(^{14}N) = 2.6 G, 1N; linewidth used for simulation, 2.2 G.

4.9b.9 Zr(η^5-C_5H_5)CD_2CD_3[N($SiMe_2CH_2PPr^i_2$)$_2$], 4.6-d_5. A solution of **4.14**-d_1 (~0.5 mmol) was prepared as described in the synthesis of **4.14** using D_2 gas. After removing the deuterium gas and stirring the solution under ethylene-d_4 for 0.5 hours gave **4.6**-d_5. ESR (toluene): g = 1.962; a(^{91}Zr) = 28.4 G 1Zr; a(^{31}P) = 20.9 G, 2P; a($^2H_\alpha$) = 1.5 G, 1D; a($^2H_\alpha$) = 0.5 G, 1D; a($^2H_\beta$) = 0.3 G, 3D; a(^{14}N) = 2.6 G, 1N; linewidth used for simulation, 2.2 G. IR (cm^{-1}, toluene): 2192 (m, βC-D and possibly an αC-D of Et ligand); 2164 (m, βC-D of Et ligand); 2128 (m, βC-D of Et ligand); 2043 (s, αC-D of Et ligand).

4.9b.10 Zr(η^5-C_5H_5)CH_2Ph[N($SiMe_2CH_2PPr^i_2$)$_2$], 4.7. To a solution of **4.1** (315 mg, 0.57 mmol) in THF (20 mL) was added a solution of $PhCH_2K$ (70 mg, 0.54 mmol) in THF (5 mL) at

references on page 199

-40 °C. The reaction was warmed to room temperature and stirred for 5 hours. The solvent was stripped off under vacuum, and the resulting solid was extracted with hexanes (10 mL). The extract was filtered through a layer of Celite®, concentrated (~ 3 mL) and cooled at -40 °C to give a dark green crystalline product (275 mg, 75%). ESR (toluene): g = 1.956; a(^{31}P) = 18.6 G, 2P; a($^{1}H_{\alpha}$) = 3.2 G, 2H; a(^{14}N) = 3.4 G, 1N; a(^{1}H) = 1.2 G, 5H linewidth used for simulation, 1.6 G. Anal. Calcd for $C_{30}H_{56}NP_2Si_2Zr$: C, 56.29; H, 8.82; N, 2.19. Found: C, 56.58; H, 8.86; N, 2.25.

4.9b.11 $ZrCl(CH_2Ph)_2[N(SiMe_2CH_2PPr^i_2)_2]$, 4.9. To a solution of **4.1** (350 mg, 0.6 mmol) in toluene (30 mL) was added a solution of $PhCH_2MgCl$ (0.6 mL of 1 M solution in Et_2O, 0.6 mmol) at room temperature and stirred for 6 hours. The solvent was stripped off under vacuum, the resulting solid was extracted with toluene (10 mL) and filtered through a layer of Celite®. The filtrate was concentrated (1 mL), and added hexanes (10 mL) and cooling at -40 °C gave a pale yellow material (63 mg, 15%). Upon further recrystallization the zirconium-(III) benzyl derivative **4.7** was isolated. ^{1}H NMR (δ, 300 MHz, C_6D_6): 0.18 (s, 6H, $Si(CH_3)_2$); 0.45 (s, 6H, $Si(CH_3)_2$); 0.6 (m, 4H, $SiCH_2P$); 0.8 to 1.0 (m, 24H, $P[CH(CH_3)_2]_2$); 1.60 (sept, 2H, $P[CH(CH_3)_2]_2$, $^{3}J_{H\text{-}H}$ = 6.3 Hz); 1.70 (sept, 2H, $P[CH(CH_3)_2]_2$, $^{3}J_{H\text{-}H}$ = 7.5 Hz); 1.98 (s, 2H, CH_2Ph); 2.02 (s, 2H, CH_2Ph); 6.87 (t, 2H, *p*-Ph, $^{3}J_{H\text{-}H}$ = 6.6 Hz); 7.23 (m, 4H, *m*-Ph); 7.37 (d, 4H, *o*-Ph, $^{3}J_{H\text{-}H}$ = 6.6 Hz). $^{31}P\{^{1}H\}$ NMR (δ, 121.421 MHz, C_6D_6): -11.87 (s). Anal. Calcd for $C_{32}H_{58}ClNSi_2P_2Zr$: C, 54.78; H, 8.33; N, 2.00. Found: C, 55.08; H, 8.56; N; 1.89.

4.9b.12 $Zr(\eta^5\text{-}C_5H_5)CH_2SiMe_3[N(SiMe_2CH_2PPr^i_2)_2]$, 4.8. To a solution of **4.1** (250 mg, 0.43 mmol) in toluene (10 mL) was added a solution of Me_3SiCH_2Li (42 mg, 0.45 mmol) in toluene (3 mL) at room temperature. After stirring for 12 hours the solvent was stripped off under vacuum, and the resulting solid was extracted with pentane (10 mL). The filtrate was filtered through a layer of Celite® and concentrated (~ 3 mL) and then cooling this solution at -40 °C gave a dark green crystalline product (165 mg, 60%). ESR (toluene): g = 1.973; a(^{91}Zr) = 30.5 G, 1Zr; a(^{31}P) = 21.4 G, 2P; a($^{1}H_{\alpha}$) = 9.3 G, 1H; a($^{1}H_{\alpha}$) = 6.2 G, 1H; a(^{14}N) = 2.0 G, 1N; linewidth used for simulation, 2.6 G. $\mu_{eff.}$ (Evans method) = 1.71 B. M. UV-Vis (toluene, 1 cm quartz cell): λ_{max} = 334 nm, ε_{max} = 2700 $Lmol^{-1}cm^{-1}$; λ = 430 nm, ε = 1700 $Lmol^{-1}cm^{-1}$.

references on page 199

Anal. Calcd for $C_{27}H_{60}NP_2Si_3Zr$: C, 50.97; H, 9.51; N, 2.20. Found: C, 50.68; H, 9.46; N, 2.21.

4.9b.13 Zr(η^5-C_5H_5)OPh[N($SiMe_2CH_2PPr^i_2$)$_2$], 4.10. To a solution of **4.1** (200 mg, 0.34 mmol) in THF (10 mL) was added a solution of PhONa (40 mg, 0.34 mmol) in THF (5 mL) at -10 °C and stirred for 10 minutes. The reaction was then warmed to room temperature and stirred for 12 hours to give a deep green solution. The solvent was stripped off under vacuum, and the resulting solid was extracted with hexanes (10 mL). The extract was filtered through a layer of Celite®, concentrated (~ 3 mL) and cooled at -40 °C to give a dark green crystalline product (130 mg, 60%). ESR (toluene): g = 1.955; a(^{31}P) = 18.7 G, 2P. Anal. Calcd for $C_{29}H_{54}NOP_2Si_2Zr$: C, 54.25; H, 8.48; N, 2.18. Found: C, 54.04; H, 8.50; N, 2.13.

4.9b.14 Zr(η^5-C_5H_5)NPh$_2$[N($SiMe_2CH_2PPr^i_2$)$_2$], 4.11. To a solution of **4.1** (200 mg, 0.34 mmol) in THF (10 mL) was added a solution of $NaNPh_2$ (66 mg, 0.34 mmol) in THF (5 mL) at -10 °C and stirred for 10 minutes. The reaction was then warmed to room temperature and stirred for 12 hours to give a deep brown solution. The solvent was stripped off under vacuum, and the resulting solid was extracted with hexanes (10 mL). The extract was filtered through a layer of Celite® and stripping off the solvent gave an oil. ESR (toluene): g = 1.953; a(^{31}P) = 11.2 G, 2P.

4.9.15 Zr(η^5-C_5H_5)PPh$_2$[N($SiMe_2CH_2PPr^i_2$)$_2$], 4.12. To a solution of **4.1** (200 mg, 0.34 mmol) in THF (10 mL) was added a solution of $LiPPh_2$ (66 mg, 0.34 mmol) in THF (5 mL) at -10 °C and stirred for 10 minutes. The reaction was then warmed to room temperature and stirred for 12 hours to give a deep brown solution. The solvent was stripped off under vacuum, and the resulting solid was extracted with hexanes (10 mL). The extract was filtered through a layer of Celite® and stripping off the solvent gave an oil. ESR (toluene): g = 1.965; a(^{31}P) = 18.6 G, 2P; a(^{31}P) = 29.8 G.

4.9b.16 Zr(η^5-C_5H_5)H[N($SiMe_2CH_2PPr^i_2$)$_2$], 4.14. A solution of **4.5** or **4.8** (~ 0.1 mmol) in toluene (5 mL) was degassed by freeze-pump-thaw cycles and then stirred under 1 atm of H_2 for 10 to 12 hours at room temperature. Spectroscopic (ESR, NMR) analysis of the resulting solution shows clean formation of the hydride complex. A solution of **3** (0.05 mmol, 0.6 mL of

references on page 199

C_7D_8) in a sealable NMR tube was treated with H_2 as described above, and its ^1H NMR spectrum shows only the formation of Me_4Si and the ESR spectrum of the same sample shows only **7**. Treatment of **4.5** in a similar fashion with D_2 shows the formation of CH_3D (0.17 ppm, 1:1:1 triplet, $^2J_{H\text{-}D}$ = 1.9 Hz) and the formation of the deuteride **4.14**. ESR (toluene): g = 1.988; a(^{91}Zr) = 25.1 G, 1Zr; a(^{31}P) = 21.7 G, 2P; a(^{1}H) = 8.7 G, 1H or a(^{2}H) = 1.4 G, 1D; a(^{14}N) = 1.4 G, 1N; linewidth used for simulation, 1.6 G.

4.9b.17 [ZrHCp[N(SiMe$_2$CH$_2$PPr$^i_2$)]{CpZr[N(MeSiCH$_2$CH$_2$PPr$^i_2$)(SiMe$_2$CH$_2$PPr$^i_2$)]} -(μ-H)$_2$, 4.15.

Method 1: A solution of Zr(η^5-C_5H_5)Cl$_2$[N(SiMe$_2$CH$_2$PPr$^i_2$)$_2$] **2.6**, (300 mg, 0.48 mmol) in toluene (40 mL) was transferred into a thick-walled reaction flask (300 mL) containing Na/Hg (56 mg of 0.1% amalgam, 2.4 mmol of Na). The dinitrogen in the flask was removed under vacuum (approximately 5 mL of solvent was removed) and then the reaction mixture was degassed once by a freeze-pump-thaw cycle. The flask was then cooled to –196 °C, filled with 1 atmosphere of dihydrogen, sealed, and allowed to warm slowly to room temperature with stirring. Upon warming up to room temperature the reaction mixture quickly turned green (1 hour) and slowly the intensity of the green color decreased. After the disappearance of the green colour (7 days) the solution was decanted from the amalgam and filtered through a layer of Celite®. The amalgam was extracted with 15 mL portions of toluene (total of 60 mL), until the extracts showed no yellow colour. The filtrate and the extracts were combined and stripping off the solvent gave a yellow powder (0.20 g, 76%). The product was crystallized from a 1:1 mixture of toluene and Et_2O.

Method 2: Approximately 30 mg of the zirconium(III) alkyl derivative Zr(η^5-C_5H_5)R[N(SiMe$_2$CH$_2$PPr$^i_2$)$_2$], where R = Me, CH_2SiMe_3 or $C_6H_5CH_2$ was dissolved in 0.5 mL of C_6D_6 inside a NMR tube and the resulting solution was degassed by three freeze-pump-thaw cycles. Then the NMR tube was cooled to -196 °C, filled with 1 atmosphere of dihydrogen and sealed. Monitoring the reaction by NMR spectroscopy shows only the formation of the diamagnetic hydride complex.

references on page 199

Major isomer: $^{1}H\{^{31}P\}$ NMR (δ, 500 MHz, C_7D_8): 0.17, 0.25, 0.29, 0.39, 0.46, 0.50 and 0.68 (s, each 3H, $Si(CH_3)_2$); 0.84 to 0.92 (m, $SiCH_2P$); 1.0 to 1.30 (m, $(P[CH(CH_3)_2]_2$); 1.48 (d, 1H, $SiCH_2Zr$, $^{2}J_{H-H}$ = 11.2 Hz); 1.6 to 1.9 (overlapping sept, 7H, $P[CH(CH_3)_2]_2$, $^{3}J_{H-H}$ = 7.0 Hz); 2.16 (d, 1H, $SiCH_2Zr$, $^{2}J_{H-H}$ = 11.2 Hz); 2.45 (sept, 1H, $P[CH(CH_3)_2]_2$, $^{3}J_{H-H}$ = 7.0 Hz); 6.15 (t, ~5H, C_5H_5, $^{3}J_{P-H}$ = 1.4 Hz); 6.56 (s, ~5H, C_5H_5). $^{31}P\{^{1}H\}$ NMR (δ, 121.4 MHz, C_7D_8): Spectrum consisted of an ABMX spin system; 22.31 (d, 1P, $^{2}J_{P-P}$ = 64.7 Hz); 17.45 (d, 1P, $^{2}J_{P-P}$ = 64.7 Hz); 0.48 (s, 1P); -1.90 (s, 1P). $^{13}C\{^{1}H\}$ NMR (δ, 50.324 MHz, C_7D_8): 111.67 (s, Cp); 104.94 (s, Cp). Minor isomer: $^{1}H\{^{31}P\}$ NMR (δ, 500 MHz, C_7D_8): 6.12 (t, ~5H, C_5H_5, $^{3}J_{P-H}$ = 1.3 Hz); 6.39 (s, ~5H, C_5H_5). $^{31}P\{^{1}H\}$ NMR (δ, 121.4 MHz, C_7D_8): Spectrum consisted of an ABMX spin system; 22.00 (d, 1P, $^{2}J_{P-P}$ = 65.1 Hz); 18.38 (d, 1P, $^{2}J_{P-P}$ = 65.1 Hz); 0.90 (s, 1P); -1.34 (s, 1P). IR (cm^{-1}, KBr): 1435 (br s, Zr–H_t), 1159 (Zr–D_t). Anal. Calcd for $C_{23}H_{51}NP_2Si_2Zr$: C, 50.13; H, 9.33; N, 2.54. Found: C, 50.35; H, 9.15; N; 2.33.

4.9b.18 $Zr(\eta^5\text{-}C_5H_5)BH_4[N(SiMe_2CH_2PPr^i_2)_2]$, 4.17. To a solution of **4.1** (800 mg, 1.37 mmol) in toluene (40 mL) was added solid $LiBH_4$ (150 mg, 6.84 mmol) and was stirred at room temperature. After stirring for 12 hours the reaction mixture was filtered through a layer of Celite® and the filtrate was concentrated to give a black oil. The oil was dissolved in Et_2O (5 mL) and cooled at -40 °C to give black rectangular crystals (650 mg, 84%). ESR (toluene): g = 1.958; $a(^{31}P)$ = 20.7 G, 2P; $a(^{14}N)$ = 2.0 G, 1N; $a(^{1}H)$ = 2.8 G, 4H; linewidth used for simulation, 2.8 G. UV-Vis (toluene, 1 cm quartz cell): λ_{max} = 332 nm; ε_{max} = 2800 $Lmol^{-1}cm^{-1}$. IR (cm^{-1}, KBr): 2953, 2871, 2401 (s, B-H_t), 2379 (s, B-H_t), 2126 (s, B-H_b), 1457 (m, Zr-H), 1373, 1244, 1124. Anal. Calcd for $C_{23}H_{53}NBSi_2P_2Zr$: C, 49.00; H, 9.47; N, 2.48. Found: C, 48.82; H, 9.46; N; 2.48.

4.9b.19 $Zr(\eta^5\text{-}C_5H_5)(C{\equiv}CPh)[N(SiMe_2CH_2PPr^i_2)_2]$. A solution of **4.14** (~0.5 mmol) was prepared as described in the synthesis of **4.14**. The hydrogen gas was removed under vacuum, the solution cooled to -78 °C and then a solution (toluene) of PhC≡CH (1 equivalent) was added. Instantly the color changed from deep green to purple. The simulated spectrum was approximatly close to the observed spectrum: ESR (hexanes): g = 9.8; $a(^{31}P)$ = 15 G, 2P; $a(^{14}N)$ = 3.5 G, 1N; $a(^{1}H)$ = 1G , 5H.

references on page 199

4.9b.20 Zr(η^5-C_5H_5)(C≡CPh)Cl[N($SiMe_2CH_2PPr^i_2$)$_2$], 4.16. Complex Zr(η^5-C_5H_5)-(C≡CPh)[N($SiMe_2CH_2PPr^i_2$)$_2$] was oxidized with $PbCl_2$. ^1H NMR (δ, 300 MHz, C_7D_8): 0.55 (br s, 6H, Si(CH_3)$_2$); 0.60 (br s, 6H, Si(CH_3)$_2$); 0.86 (br s, 4H, SiCH_2P); 0.98 to 1.1 (m, 24H, P[CH(CH_3)$_2$]$_2$); 2.13 (br m, 4H, P[CH(CH_3)$_2$]$_2$); 6.53 (s, Cp, 5H); 6.95 (br, 1H, *p*-Ph); 7.08 (m, 2H, *m*-Ph); 7.35 (br, 2H, *o*-Ph). $^{31}P\{^1H\}$ NMR (δ, 121.421 MHz, C_6D_6): 16.32 (s).

4.9b.21 Hf(η^5-C_5H_5)Cl(BH_4)[N($SiMe_2CH_2PPr^i_2$)$_2$], 4.21. To a solution of **4.2** (250 mg, 0.35 mmol) in toluene (25 mL) was added solid $LiBH_4$ (60 mg, 2.74 mmol) and was stirred at room temperature. After stirring for 3 days the reaction mixture was filtered through a layer of Celite® and the filtrate was concentrated to give an oil. The oil was dissolved in hexanes and cooled at -40 °C to give a white crystalline material (170 mg, 71%). ^1H NMR (δ, 300 MHz, C_6D_6): 0.56 (s, 6H, Si(CH_3)$_2$); 0.59 (s, 6H, Si(CH_3)$_2$); 0.8 to 1.1 (m, 28H, P[CH(CH_3)$_2$]$_2$, SiCH_2P); 1.96 (sept, 2H, P[CH(CH_3)$_2$]$_2$, $^3J_{H-H}$ = 6.8 Hz); 2.24 (sept, 2H, P[CH(CH_3)$_2$]$_2$, $^3J_{H-H}$ = 6.8 Hz); 6.25 (br s ~5H, C_5H_5). $^{31}P\{^1H\}$ NMR (δ, 121.421 MHz, C_6D_6): 14.07 (s). $^{13}C\{^1H\}$ NMR (δ, 50.323 MHz, C_6D_6): 110.05 (s, C_5H_5). IR (cm^{-1}, KBr): 2488 (s, B-H_t), 2414 (s, B-H_t), 2143 (s, B-H_b), 1456 (m, Zr-H). Anal. Calcd for $C_{23}H_{57}NBClSi_2P_2Hf$: C, 40.24; H, 7.78; N, 2.04. Found: C, 40.02; H, 7.79; N; 1.98.

4.9c Disproportionation Reactions

A solution of ZrCp(BH_4)[N($SiMe_2CH_2PPr^i_2$)$_2$] **4.17**, (30 mg, 0.05 mmol) in C_7D_8 (0.5 mL) was transferred into an NMR tube and degassed three times by freeze-pump-thaw cycles. The NMR tube was then filled with 1 atmosphere of CO and sealed. The NMR spectroscopic analysis (within 15 minutes) shows the formation of two diamagnetic complexes, ZrCp(BH_4)$_2$[N($SiMe_2CH_2PPr^i_2$)$_2$] **4.19**, and ZrCp(CO)$_2$[N($SiMe_2CH_2PPr^i_2$)$_2$] **4.18** in 1:1 ratio. Upon standing (3 days) the peak associated with **4.19** decreases in intensity and two new peaks appear which correspond to the formyl complex, **4.23**.

The reactions with CO and the zirconium(III) chloro derivative **4.1**, or with the hafnium(III) chloro derivative **4.3**, were carried out as described for the borohydride complex **4.17**.

The reaction of the zirconium-(III) chloro derivative, **4.1** with CH_3CN was carried out at low temperature. A solution of **4.1** (30 mg in 0.5 mL of C_7D_8) was transferred into a NMR

references on page 199

tube, degassed three times by freeze-pump-thaw cycles, and using a constant volume gas apparatus 2 equivalents of CH_3CN vapor was condensed at -196 °C, and sealed. The sample was transferred into a -60 °C bath and allowing to stand for 1 hour gave a deep red solution. The NMR spectroscopic analysis shows the presence of two complexes, $ZrCpCl_2[N(SiMe_2CH_2PPr^i_2)_2]$ **2.6**, and $ZrCp(CH_3CN)[N(SiMe_2CH_2PPr^i_2)_2]$, **4.22**. Warming the sample to room temperature shows a rapid decrease in the intensity of the resonances associated with complex **4.22**.

4.9c.1 $ZrCp(CO)_2[N(SiMe_2CH_2PPr^i_2)_2]$, 4.18. ^1H NMR (δ, 300 MHz, C_6D_6): 0.31 (s, 12H, $Si(CH_3)_2$); 0.68 (m, 4H, $SiCH_2P$); 0.85 to 1.0 (m, 24H, $P[CH(CH_3)_2]_2$); 1.70 (br sept, 4H, $P[CH(CH_3)_2]_2$, $^3J_{H-H}$ = 7.4 Hz); 4.75 (t ~5H, C_5H_5, $^3J_{P-H}$ = 1.5 Hz). Gated decouplled ^{13}C NMR (δ, 75.4 MHz, C_7D_8): 92.12 (s, Cp, $^1J_{C-H}$ = 171.5 Hz); 249.0 (s, *C*O). $^{31}P\{^1H\}$ NMR (δ, 121.421 MHz, C_6D_6): 37.91 (s). IR (cm^{-1}, toluene): 1965 (w, CO); 1871 (s, CO); 1845 (shoulder, CO). Anal. Calcd for $C_{25}H_{49}NCl_2O_2P_2Si_2Zr$: C, 49.63; H, 8.16; N, 2.32. Found: C, 49.72; H, 8.35; N, 2.27.

4.9c.2 $ZrCp(BH_4)_2[N(SiMe_2CH_2PPr^i_2)_2]$, 4.19. ^1H NMR (δ, 300 MHz, C_6D_6): 0.44 (s, 12H, $Si(CH_3)_2$); 0.89 (br m, 4H, $SiCH_2P$); 1.0 to 1.1 (m, 24H, $P[CH(CH_3)_2]_2$); 2.00 (br sept, 4H, $P[CH(CH_3)_2]_2$, $^3J_{H-H}$ = 7.4 Hz); 6.28 (t ~5H, C_5H_5, $^3J_{P-H}$ = 1.5 Hz). ^{13}C NMR (δ, 75.4 MHz, C_6D_6): 109.53 (s, Cp). $^{31}P\{^1H\}$ NMR (δ, 121.421 MHz, C_6D_6): 5.80 (s). $^{11}B\{^1H\}$ NMR(δ, 96.2 MHz, C_7D_8): -92.00 (s, BH_4). IR (cm^{-1}, solution): 2427 (s, $B\text{-}H_t$), 2381 (s, $B\text{-}H_t$), 2130 (s, $B\text{-}H_b$).

4.9c.3 $HfCp(CO)_2[N(SiMe_2CH_2PPr^i_2)_2]$, 4.20. ^1H NMR (δ, 300 MHz, C_6D_6): 0.30 (s, 12H, $Si(CH_3)_2$); 0.75 (m, 4H, $SiCH_2P$); 0.55 to 1.1 (m, 24H, $P[CH(CH_3)_2]_2$); 1.70 (br sept, 4H, $P[CH(CH_3)_2]_2$, $^3J_{H-H}$ = 8.0 Hz); 4.68 (t, 5H, C_5H_5, $^3J_{P-H}$ = 1.5 Hz). $^{31}P\{^1H\}$ NMR (δ, 121.421 MHz, C_6D_6): 32.92 (s).

4.9c.4 $ZrCp(CH_3CN)[N(SiMe_2CH_2PPr^i_2)_2]$, 4.22. ^1H NMR (δ, 300 MHz, C_6D_6): at 10 °C, 0.02 (s, 6H, $Si(CH_3)_2$); 0.15 (s, 6H, $Si(CH_3)_2$); 1.12 to 1.26 (m, 24H, $P[CH(CH_3)_2]_2$); 2.00 (br sept, 2H, $P[CH(CH_3)_2]_2$, $^3J_{H-H}$ = 6.5 Hz); 2.36 (br sept, 2H, $P[CH(CH_3)_2]_2$, $^3J_{H-H}$ = 6.5 Hz);

references on page 199

2.78 (s, 3H, CH_3CN); 5.66 (s, 5H, C_5H_5). $^{31}P\{^1H\}$ NMR (δ, 121.421 MHz, C_6D_6): at -18 °C, 32.92 (s).

4.9c.5 $Cp(BH_4)Zr(^{13}\overline{CHO})[N(SiMe_2CH_2PPr^i_2)(SiMe_2CH_2Pr^i_2P{\bullet}BH_3)]$, 4.23.

^1H NMR (δ, 500 MHz, C_7D_8): 0.23, 0.35, 0.61, 0.69 (s, each 3H, $Si(CH_3)_2$); 0.60 (overlapping d of d, 6H, $(P[CH(CH_3)_2]_2)$, $^3J_{H-H}$ = 7.6 Hz, $^3J_{P-H}$ = 15.3 Hz); 0.94 (overlapping d of d, 6H, $(P[CH(CH_3)_2]_2)$, $^3J_{H-H}$ = 7.1 Hz, $^3J_{P-H}$ = 15.3 Hz); 1.03 (two overlapping d, 2H, $SiCH_2P$); 0.98 to 1.11 (m, 14H, $(P[CH(CH_3)_2]_2)$ and $SiCH_2P$); 1.54 (sept, 1H, $P[CH(CH_3)_2]_2$, $^3J_{H-H}$ = 7.1 Hz); 1.77 (sept, 1H, $P[CH(CH_3)_2]_2$, $^3J_{H-H}$ = 7.1 Hz); 1.80 (sept, 2H, $P[CH(CH_3)_2]_2$, $^3J_{H-H}$ = 7.6 Hz); 3.10 (d of d, 1H, CHO, $^2J_{P-H}$ = 27.4 Hz, $^1J_{C-H}$ = 161.9 Hz); 6.41 (s, 5H, C_5H_5). $^{31}P\{^1H\}$ NMR (δ, 121.4 MHz, C_7D_8): 31.20 (br, 1P); 39.72 (d, 1P, $^2J_{P-C}$ = 55.1 Hz). Gated decoupled ^{13}C NMR (δ, 75.4 MHz, C_7D_8): 60.73 (d of d, CHO, $^2J_{P-C}$ = 55.7 Hz, $^1J_{C-H}$ = 162.2); 113.5 (d, C_5H_5, $^1J_{C-H}$ = 170.8 Hz). $^{11}B\{^1H\}$ NMR (δ, 96.2 MHz, C_7D_8): -101.33 (br s, BH_4); -127.23 (br d, $(BH_3){\bullet}P[CH(CH_3)_2]_2$, $^1J_{P-B}$ = 47.4 Hz). $^1H\{^{11}B\}$ NMR (δ, 500 MHz, C_7D_8): 1.22 (s, 3H, probably $(BH_3){\bullet}P[CH(CH_3)_2]_2$); also showed some changes in the minor resonances located around 0.2 to 0.4 ppm (probably, BH_4). IR (cm^{-1}, KBr): 2423 (s, B-H_t), 2378 (s, B-H_t), 2355 (s, B-H_t); 2345 (s, B-H_t); 2146 (s, B-H_b), 1460 (m, Zr-H). Anal. Calcd for $C_{24}H_{57}B_2NOP_2Si_2Zr$: C, 47.52; H, 9.47; N, 2.31. Found: C, 47.93; H, 9.45; N, 2.64.

4.9e Oxidation Reactions

Oxidation reactions with $TiCl_3$ or $PbCl_2$ was carried out by adding an excess of solid oxidant (approximately 10 equivalents) to a cooled (approximately -10 °C) toluene solution of the zirconium(III) complex. The resulting yellow or orange solution was then decanted, toluene was striped off, and the residue was extracted with pentane and filtered through a layer of Celite®.

Oxidation with Ph_2S_2 was carried out by adding a toluene solution of the oxidant (0.5 equivalents) to a solution of the zirconium(III) complex at -78 °C. Analytically pure chlorothiolate complex, **4.13** was obtained (75%) by recrystallization from Et_2O. The alkylthiolate complexes gave only an oily material.

references on page 199

4.9e.1 ZrCpCl(SPh)[N(SiMe$_2$CH$_2$PPr$^i_2$)$_2$], 4.13. ^{1}H NMR (δ, 300 MHz, C_6D_6): 0.71 (s, 6H, Si(C*H*$_3$)$_2$); 0.74 (s, 6H, Si(C*H*$_3$)$_2$); 0.93 to 1.15 (m, 24H, P[CH(C*H*$_3$)$_2$]$_2$); 1.15 to 1.26 (m, 4H, SiC*H*$_2$P); 2.28 (m, 4H, P[C*H*(CH$_3$)$_2$]$_2$); 6.33 (s, 5H, Cp); 7.05 (t, 1H, *p*-Ph, $^3J_{H-H}$ = 7.4 Hz); 7.24 (m, 2H, *m*-Ph); 7.47 (d, 2H, *o*-Ph, $^3J_{H-H}$ = 7.4 Hz). ^{31}P{^{1}H} NMR (δ, 121.421 MHz, C_6D_6): 13.74 (s). ^{13}C{^{1}H} NMR (δ, 50.324 MHz, C_6D_6): 113.34 (s, Cp). Anal. Calcd for $C_{29}H_{54}NClSi_2P_2SZr$: C, 50.22; H, 7.85; N, 2.02. Found: C, 50.14; H, 7.87; N; 1.93.

4.9e.2 ZrCpClEt[N(SiMe$_2$CH$_2$PPr$^i_2$)$_2$]. Complex **4.6** was oxidized with $PbCl_2$. ^{1}H NMR (δ, 300 MHz, C_6D_6): 0.40 (br s, 6H, Si(C*H*$_3$)$_2$, $\Delta\nu_{1/2}$ = 40 Hz); 0.55 (s, 6H, Si(C*H*$_3$)$_2$, $\Delta\nu_{1/2}$ = 40 Hz); 0.75 to 0.90 (br, 6H, SiC*H*$_2$P and C*H*$_2$CH$_3$); 0.95 to 1.10 (m, 24H, P[CH(C*H*$_3$)$_2$]$_2$); 1.78 (br m, 4H, P[C*H*(CH$_3$)$_2$]$_2$); 1.78 (t, 3H, CH$_2$C*H*$_3$, $^3J_{H-H}$ = 7.6 Hz); 6.33 (s, Cp, 5H). ^{31}P{^{1}H} NMR (δ, 121.421 MHz, C_6D_6): -0.5 (br s, $\Delta\nu_{1/2}$ = 370 Hz); 8.0 (br s, $\Delta\nu_{1/2}$ = 370 Hz). Anal. Calcd for $C_{25}H_{54}ClNSi_2P_2SZr$: C, 48.94; H, 8.87; N, 2.28. Found: C, 48.30; H, 8.64; N; 2.20.

4.9e.3 ZrCpCl(CH$_2$Ph)[N(SiMe$_2$CH$_2$PPr$^i_2$)$_2$]. Complex **4.7** was oxidized with $TiCl_3$. ^{1}H NMR (δ, 300 MHz, C_6D_6): 0.40 (br s, 6H, Si(C*H*$_3$)$_2$); 0.50 (s, 6H, Si(C*H*$_3$)$_2$); 0.70 (br, 4H, SiC*H*$_2$P); 0.90 to 1.0 (m, 24H, P[CH(C*H*$_3$)$_2$]$_2$); 1.70 (br m, 4H, P[C*H*(CH$_3$)$_2$]$_2$); 2.68 (d, 1H, C*H*$_2$Ph, $^2J_{H-H}$ = 11 Hz); 2.98 (d, 1H, C*H*$_2$Ph, $^2J_{H-H}$ = 11 Hz); 6.20 (s, Cp, 5H). ^{31}P{^{1}H} NMR (δ, 121.421 MHz, C_6D_6): -0.5 (br s, $\Delta\nu_{1/2}$ = 370 Hz); 8.0 (br s, $\Delta\nu_{1/2}$ = 370 Hz).

4.9e.4 ZrCp(CH$_2$SiMe$_3$)(SPh)[N(SiMe$_2$CH$_2$PPr$^i_2$)$_2$]. Spectra were recorded within 2 hours after the reaction. ^{1}H NMR (δ, 300 MHz, C_6D_6): 0.32 (s, 9H, CH$_2$Si(C*H*$_3$)$_3$); 0.42 (s, 6H, Si(C*H*$_3$)$_2$); 0.52 (s, 6H, Si(C*H*$_3$)$_2$); 0.87 (m, 4H, SiC*H*$_2$P); 0.98 to 1.12 (m, 26H, P[CH(C*H*$_3$)$_2$]$_2$ and C*H*$_2$Si(CH$_3$)$_3$); 1.80 (m, 4H, P[C*H*(CH$_3$)$_2$]$_2$); 6.40 (s, 5H, Cp); 6.98 (t, 1H, *p*-Ph, $^3J_{H-H}$ = 7.3 Hz); 7.18 (m, 2H, *m*-Ph); 7.83 (d, 2H, *o*-Ph, $^3J_{H-H}$ = 7.4 Hz). ^{31}P{^{1}H} NMR (δ, 121.421 MHz, C_6D_6): 2.50 (br s).

Complicated spectra were obtained after 7 days. ^{1}H NMR (δ, 300 MHz, C_6D_6): 6.08 (s, 5H, Cp); 6.28 (s, 5H, Cp). ^{31}P{^{1}H} NMR (δ, 121.421 MHz, C_6D_6): -1.9 (s), -2.2 (s), 18.6 (s), 18.8 (s).

4.9e.5 ZrCp(CH$_2$CH$_3$)(SPh)[N(SiMe$_2$CH$_2$PPr$^i_2$)$_2$]. Spectra were recorded within 2 hours after the reaction. ^{1}H NMR (δ, 300 MHz, C_6D_6): 0.45 (br s, 6H, Si(C*H*$_3$)$_2$, $\Delta\nu_{1/2}$ = 35 Hz); 0.68

references on page 199

(br s, 6H, Si(CH_3)$_2$, $\Delta\nu_{1/2}$ = 35 Hz); 0.85 to 0.90 (br m, 6H, SiCH_2P and CH_2CH_3); 0.95 to 1.15 (m, 24H, P[CH(CH_3)$_2$]$_2$); 1.75 (m, 4H, P[CH(CH$_3$)$_2$]$_2$); 1.81 (t, 3H, CH_2CH_3, $^3J_{H-H}$ = 6.7 Hz); 6.13 (s, 5H, Cp); 7.00 (t, 1H, *p*-Ph, $^3J_{H-H}$ = 7.0 Hz); 7.18 (m, 2H, *m*-Ph); 7.70 (d, 2H, *o*-Ph, $^3J_{H-H}$ = 7.0 Hz). $^{31}P\{^1H\}$ NMR (δ, 121.421 MHz, C_6D_6): -1.0 (br s, $\Delta\nu_{1/2}$ = 250 Hz); 11.0 (br s, $\Delta\nu_{1/2}$ = 250 Hz).

Complex spectra were obtained after 7 days. ^1H NMR (δ, 300 MHz, C_6D_6): 6.05 (s, 5H, Cp); 6.24 (s, 5H, Cp). $^{31}P\{^1H\}$ NMR (δ, 121.421 MHz, C_6D_6): -1.8 (s), -2.1 (s), 18.6 (s), 18.8 (s).

4.10 Refferences

(1) Ashworth, T. V.; Agreda, T. C.; Herdtweck, E.; Herrmann, W. A. *Angew. Chem.,Int. Ed. Engl.* **1986**, *25*, 289

(2) Lappert, M. F.; Pickett, C. J.; Riley, P. I.; Yarrow, P. I. W. *J. Chem. Soc., Dalton Trans.* **1981**, 805.

(3) Blenkers, J.; Bruin, P.; Teuben, J. H. *J. Organomet. Chem.* **1985**, *297*, 61.

(4) Morse, P. M.; Wilson, S. R.; Girolami, G. S. *Inorg. Chem.* **1990**, *29*, 3200.

(5) Lubben, T. V.; Wolczanski, P. T.; vanDuyne, G. D. *Organometallics* **1984**, *3*, 977.

(6) Baker, R. T.; Whitney, J. F.; Wreford, S. S. *Organometallics* **1983**, *2*, 1049.

(7) Fryzuk, M. D.; Haddad, T. S.; Berg, D. J. *Coord. Chem. Rev.* **1990**, *99*, 137.

(8) Fryzuk, M. D.; Montgomery, C. D. *Coord. Chem. Rev.* **1989**, *95*, 1.

(9) Fryzuk, M. D. *Can. J. Chem.* **1992**, *70*, 2849.

(10) Jeffery, J.; Lappert, M. F.; Luong-Thi, N. T.; Atwood, J. L.; Hunter, W. E. *J. Chem. Soc., Chem. Commun.* **1978**, 1081.

(11) Lappert, M. F.; Riley, P. I.; Yarrow, P. I. W.; Atwood, J. L.; Hunter, W. E.; Zaworotko, M. J. *J. Chem. Soc., Dalton Trans.* **1981**, 814.

(12) Atwood, J. L.; Barker, G. K.; Holton, J.; Hunter, W. E.; Lappert, M. F.; Pearce, R. *J. Am. Chem. Soc.* **1977**, *99*, 6645.

(13) Fryzuk, M. D.; Haddad, T. S.; Rettig, S. J. *Organometallics* **1989**, *8*, 1723.

(14) Fitzgerald, R. J.; Drago, R. S. *J. Am. Chem. Soc.* **1968**, *90*, 2523.

(15) Fessenden, R. W.; Schuler, R. H. *J. Chem. Phys.* **1963**, *39*, 2147.

(16) Brookhart, M.; Green, M. L. H.; Wong, L. *Prog. Inorg. Chem.* **1988**, *36*, 1.

(17) Brookhart, M.; Green, M. L. H. *J. Organomet. Chem.* **1983**, *250*, 395.

(18) Crabtree, R. H.; Hamilton, D. G. *Adv. Organomet. Chem.* **1988**, *28*, 299.

(19) Crabtree, R. H.; Holt, E. M.; Lavin, M.; Morehouse, S. M. *Inorg. Chem.* **1985**, *24*, 1986.

(20) Wielstra, Y.; Gambarotta, S.; Spek, A. L.; Smeets, W. J. J. *Organometallics* **1990**, *9*, 2142.

(21) Cardin, D. J.; Lappert, M. F.; Raston, C. L. *Chemistry of Organo-Zirconium and Hafnium Compounds;* 1 ed.; Ellis Horwood Limited: Toronto, 1986.
(22) Bajgur, C. S.; Jones, C. B.; Petersen, J. F. *Organometallics* **1985**, *4*, 1929.
(23) Choukroun, R.; Gervais, D. *J. Chem. Soc., Chem. Commun.* **1985**, 224.
(24) Choukroun, R.; Basso-Bert, M.; Gervais, D. *J. Chem. Soc., Chem. Commun.* **1986**, 1317.
(25) Choukroun, R.; Dahan, F.; Larsonneur, A. M.; Samuel, E.; Peterson, J.; Meunier, P.; Sornay, C. *Organometallics* **1991**, *10*, 374.
(26) Jones, C. B.; Petersen, J. F. *J. Am. Chem. Soc.* **1983**, *105*, 5503.
(27) Raoult, Y.; Choukroun, R.; blandy, C. *Organometallics* **1992**, *11*, 2443.
(28) Samuel, E. *Inorg. Chem.* **1983**, *22*, 2967.
(29) Elson, I. H.; Kochi, J. K.; Klabunde, U.; Manzer, L. E.; Parshall, G. W.; Tebbe, F. N. *J. Am. Chem. Soc.* **1974**, *96*, 7374.
(30) Bercaw, J.; Brintzinger, H. *J. Am. Chem. Soc.* **1969**, *91*, 7301.
(31) Brintzinger, H. *J. Am. Chem. Soc.* **1967**, *89*, 6871.
(32) Kenworthy, J. G.; Myatt, J.; Todd, P. F. *J. Chem. Soc. (B)* **1970**, 791.
(33) Luetkens, M. L.; Huffman, J. C.; Sattelberger, A. P. *J. Am. Chem. Soc.* **1983**, *105*, 4474.
(34) Jones, C. B.; Petersen, J. F. *Inorg. Chem.* **1981**, *20*, 2889.
(35) Schwartz, J.; Libinger, J. A. *Angew. Chem., Int. Ed. Engl.* **1976**, *15*, 333.
(36) Collman, J. P.; Hegedus, L. S.; Norton, J. R.; Finke, R. G. *Principles and Applications of Organotranstion Metal Chemistry;* second edition ed.; University Science Books: Mill Valley, CA., 1987.
(37) Marks, T. J.; Kolb, J. R. *Chem. Rev.* **1977**, *77*, 263.
(38) Jensen, J. A.; Gozum, J. E.; Pollina, D. M.; Girolami, G. S. *J. Am. Chem. Soc.* **1988**, *110*, 1643.
(39) Fryzuk, M. D.; Rettig, S. J.; Westerhaus, A.; Williams, H. G. *Inorg. Chem.* **1985**, *24*, 4316.
(40) Luetkens, M. L.; Huffman, J. C.; Sattelberger, A. P. *J. Am. Chem. Soc.* **1985**, *107*, 3361.
(41) Jensen, J. A.; Wilson, S. R.; Schultz, A. J.; Girolami, G. S. *J. Am. Chem. Soc.* **1987**, *109*, 8094.
(42) Raum, A. L. J.; Frazer, D. A. *British Patent.* **1958**, 801401.
(43) Marks, T. J.; Kennelly, W. J.; Kolb, J. R.; Shimp, L. A. *Inorg. Chem.* **1972**, *11*, 2540.
(44) Jensen, J. A.; Girolami, G. S. *J. Chem. Soc., Chem. Commun.* **1986**, 1160.
(45) Edelstein, N. *Inorg. Chem.* **1981**, *20*, 297.
(46) Gozum, J. E.; Girolami, G. S. *J. Am. Chem. Soc.* **1991**, *113*, 3829.
(47) Plato, V.; Hedberg, K. *Inorg. Chem.* **1971**, *10*, 590.
(48) Wielstra, Y.; Gambarotta, S.; Meetsma, A. *Organometallics* **1989**, *8*, 2948.
(49) Floriani, C.; Fachinetti, G. *J. Chem. Soc., Dalton Trans.* **1973**, 1954.

(50) Fochi, G.; Guidi, G.; Floriani, C. *J. Chem. Soc., Dalton Trans.* **1984**, 1253.
(51) Tyler, D. R. *Prog. Inorg. Chem.* **1988**, *36*, 125.
(52) Masters, C. *Adv. Organomet. Chem.* **1979**, *17*, 61.
(53) Herrmann, W. A. *Angew. Chem., Int. Ed. Engl.* **1982**, *21*, 117.
(54) Dumond, D. S.; Richmond, M. G. *J. Am. Chem. Soc.* **1988**, *110*, 7547.
(55) Gladysz, J. A.; Tam, W. *J. Am. Chem. Soc.* **1978**, *100*, 2545.
(56) Casey, C. P.; Neumann, S. M. *J. Am. Chem. Soc.* **1978**, *100*, 2544.
(57) Casey, C. P.; Andrews, M. A.; McAlister, D. R.; Rinz, J. E. *J. Am. Chem. Soc.* **1980**, *102*, 1925.
(58) Tam, W.; Lin, G. Y.; Wong, W. K.; Kiel, W. A.; Wong, V. K.; Gladysz, J. A. *J. Am. Chem. Soc.* **1982**, *104*, 141.
(59) Wayland, B. B.; Woods, B. A.; Pierce, R. *J. Am. Chem. Soc.* **1982**, *104*, 302.
(60) Fagan, P. J.; Moloy, K. G.; Marks, T. J. *J. Am. Chem. Soc.* **1981**, *103*, 6959.
(61) Belmonte, P.; Schrock, R. R.; Churchill, M. R.; Youngs, W. J. *J. Am. Chem. Soc.* **1980**, *102*, 2858.
(62) Bonnesen, P. V.; Yau, P. K. L.; Hersh, W. H. *Organometallics* **1987**, *6*, 1587.
(63) Churchill, M. R.; Rotella, F. J. *Inorg. Chem.* **1978**, *17*, 2614.
(64) Wolczanski, P. T.; Bercaw, J. E. *Acc. Chem. Res.* **1980**, *13*, 121.
(65) Wolczanski, P. T.; Threlkel, R. S.; Bercaw, J. E. *J. Am. Chem. Soc.* **1979**, *101*, 218.
(66) Schlosser, M.; Ladenberger, V. *J. Organomet. Chem.* **1967**, *8*, 193.
(67) Bryce-Smith, D.; Turnrt, E. E. *J. Chem. Soc.* **1953**, 861.
(68) Schlosser, M.; Hartmann, J. *Angew. Chem., Int. Ed. Engl.* **1973**, *12*, 508.
(69) Schrock, R. R.; Fellmann, J. D. *J. Am. Chem. Soc.* **1978**, *100*, 3359.
(70) Smart, J. C.; Curtis, C. J. *Inorg. Chem.* **1977**, *16*, 1788.
(71) Schrock, R. R. *J. Organomet. Chem.* **1976**, *122*, 209.
(72) Stewart, C. P.; Porte, L. A. *J. Chem. Soc., Dalton Trans.* **1972**, *15*, 1661.
(73) Fryzuk, M. D.; Carter, A.; Westerhaus, A. *Inorg. Chem.* **1985**, *24*, 642.
(74) Figgis, B. N.; Lewis, J.; *Prog. Inorg. Chem.* **1964**, *6*, 37.

Chapter 5

On-Going and Future Prospects

Dinitrogen Chemistry

Synthesis

The synthesis of side-on dinitrogen complexes having favorable solubility properties in hydrocarbon solvents is very important in order to investigate their stoichiometric reactions. The following possibilities could be considered: (a) to investigate the synthesis of side-on dinitrogen complexes analogous to **2.12** by incorporating aryloxy ligands having substituents on the para positions; (b) to reduce ditriflate precursors of the type $ZrR(OSO_2CF_3)_2[N(SiMe_2CH_2PPr^i_2)_2]$, where R = alkyl or aryl ligands (Scheme **5.1**). In comparison with the reduction of the dichloro precursors, for example reduction of $ZrCl_2(OAr^*)[N(SiMe_2CH_2PP^ir_2)_2]$ **4.11**, the second possibility may give better yields of the dinitrogen complex.

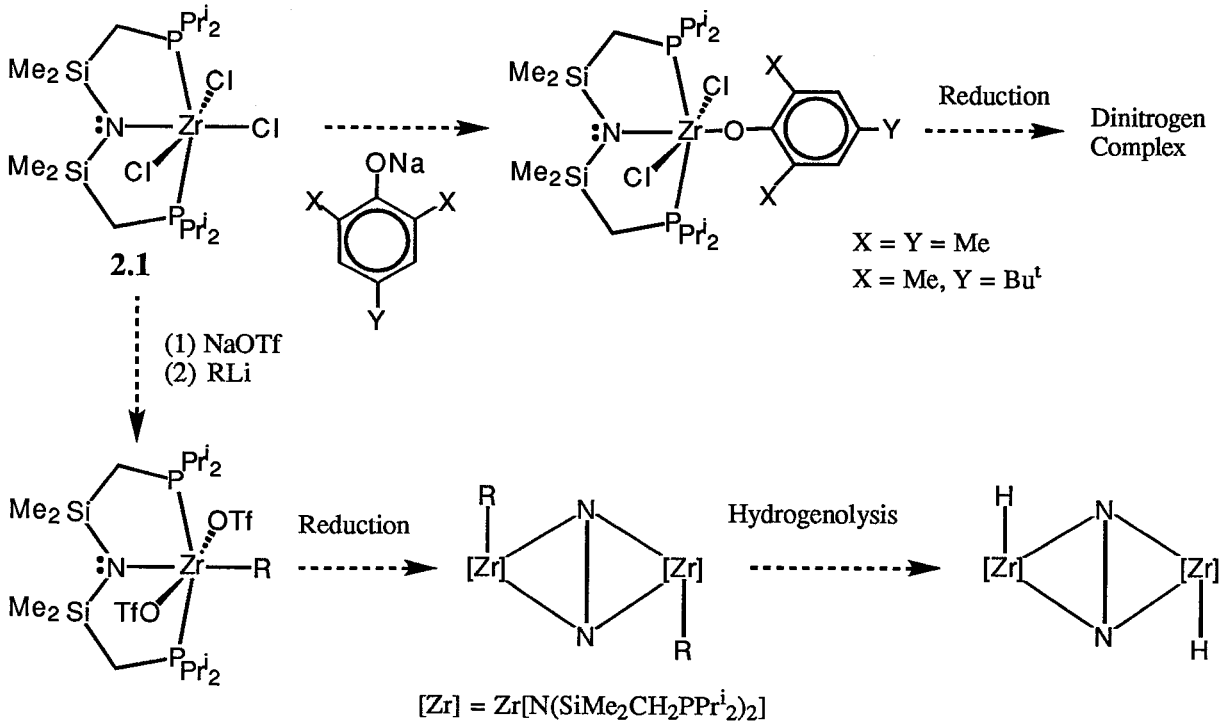

Scheme 5.1

Electrochemical studies with concomitant ESR measurements on the side-on dinitrogen complexes could provide valuable information. ESR spectra of the oxidized species could yield

some information about the δ-MO (HOMO) which in turn can be compared with the results of the MO analysis.

Reactivity Studies

Reactions that would lead to the formation of Lewis-acid Lewis-base type "adducts" will provide useful information regarding the nature of the dinitrogen ligand, particularly in the side-on dinitrogen complexes. The usefulness of such investigation will depend on the X-ray structure determination of the final product. The reactions shown in Scheme **5.2** are similar to the reaction of $LiBEt_4$ with the side-on dinitrogen complexes discussed in chapter **2**.

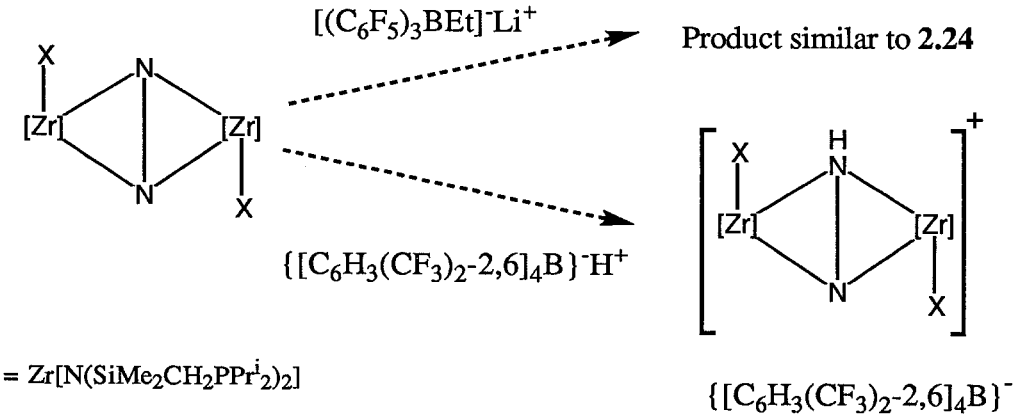

Scheme 5.2

Some reactions with alkyl halides that could be investigated are shown in Scheme **5.3**. The motive for such reactions would be to incorporate the activated dinitrogen ligand into organic molecules. Such reactions could also be useful for incorporating nitrogen-15 into organic molecules. It is important to note that the end-on complex **2.6** is synthesized in greater than 90% yields and therefore is an ideal candidate to explore its reactivity with alkyl halides. The suggestions given in Scheme **5.3** take into consideration what has been discussed under the section on reactivity of dinitrogen complexes in Chapter **2**. Preliminary reactivity studies with $Br(CH_2)_3Br$ and $Cl(CH_2)_4Cl$ and dinitrogen complexes show a clean reaction, but the organic products are not yet identified.

Controlled reaction of the end-on dinitrogen complex with two equivalents of ketone could provide a route to synthesize a zirconium oxo complex (Scheme **5.3**).

In the case of the side-on dinitrogen complexes the dinitrogen ligand forms a three membered ring with each zirconium. The possibility of expanding these three membered metallacycles by the insertion of other unsaturated functionalities may be investigated (Scheme **5.3**).

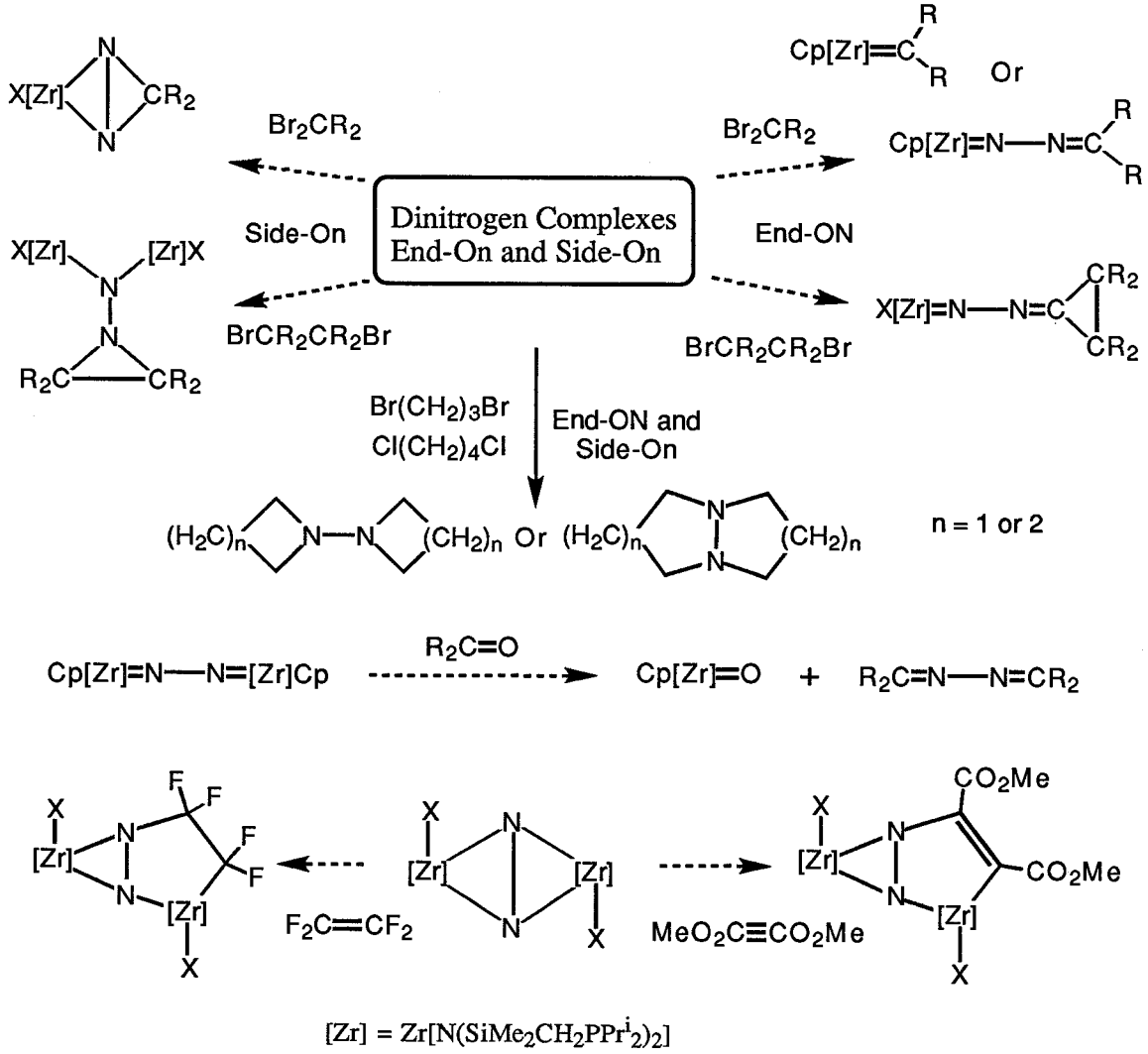

Scheme 5.3

The mechanism for the formation of the end-on dinitrogen complex could be envisaged as follows: during the reduction of the zirconium(IV) complex $ZrCpCl_2[N(SiMe_2CH_2PPr^i_2)_2]$, a

zirconium(II) species of the type "$ZrCp[N(SiMe_2CH_2PPr^i_2)_2]$" is probably formed which reacts further with dinitrogen to yield the end-on dinitrogen complex **2.9**. This suggested mechanism could be corroborated by the fact that stable zirconium(II) complexes, for example $ZrCp(CO)_2[N(SiMe_2CH_2PPr^i_2)_2]$, have been isolated. However, the reduction of $ZrCl_3[N(SiMe_2CH_2PPr^i_2)_2]$ **2.1**, may involve a different pathway. Attempts to isolate any zirconium(II) species formed during the reduction of **2.1**, for example reductions carried out in the presence of PMe_3, gave a brown material which contained mainly one product. Although it was important to reduce **2.1** in the presence of PMe_3 the ^1H and $^{31}P\{^1H\}$ NMR spectra of this brown product did not show any resonances that could be attributed to a PMe_3 ligand. This product is formulated as a dimeric species $\{ZrCl[N(SiMe_2CH_2PPr^i_2)_2]\}_2$, which did not show any reactivity with dinitrogen at room temperature.

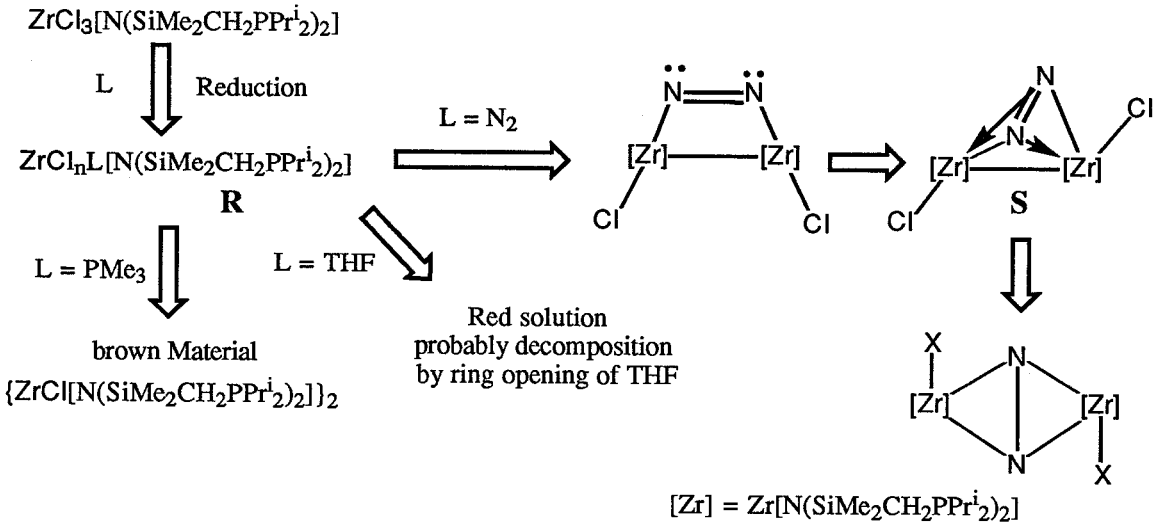

Scheme 5.4

It is noteworthy that the reduction of $ZrCl_3[N(SiMe_2CH_2PPr^i_2)_2]$ **2.1** in toluene under vacuum gave uncoordinated PNP ligand whereas, repeating the same reduction in THF (Haddad, T. S.; UBC, unpublished work) gave a deep red solution. These results suggest that during the reduction of **2.1** an intermediate of the type "$ZrCl_nL[N(SiMe_2CH_2PPr^i_2)_2]$", **R**, where $n<3$ and L = dinitrogen, PMe_3 or THF is produced. A speculative but intriguing mechanism for the formation of the side-on complex is shown in Scheme **5.4**. In the case of the

intermediate **S** if the metal-metal bond has π symmetry then the insertion of the π*-orbital (that is contained in a plane parallel to the π-orbital associated with the metal-metal bond) of the "N_2" unit should be symmetry allowed. It is important to point out that when model **F** (Section **2.7.4**) was modified by removing the dinitrogen ligand and then subjecting to INDO1/MO analysis showed the presence of one σ and one π bond between the two zirconium centers. Investigating the reduction of $ZrCl_3[N(SiMe_2CH_2\text{-}PPr^i_2)_2]$ with different substrates (e.g., butadiene or R–C≡C–R) may provide some useful information about the reduced zirconium species formed during the reduction of **2.1.**

Zirconium(III) Chemistry

Synthesis and Characterization

Since complexes of the type "$ZrCp[N(SiMe_2CH_2PPr^i_2)_2]$" gave stable zirconium(III) complexes electrochemical measurements on these systems would be valuable information. The choice of the supporting electrolyte during electrochemical measurements is critical; for example, attempts to use $[NBu_4]^+[PF_6]^-$ resulted in rapid decomposition of the zirconium complex, presumably due to the attack by fluoride ions on the PNP ligand. The zirconium complexes may be stable in the presence of electrolytes like $[NBu_4]^+[BPh_4]^-$.

Low temperature solution and frozen glass ESR spectra with better resolution may be obtained for the alkyl and the borohydride derivatives.

Disproportionation reactions could be extended to other ligands comparable to CO, for example benzonitrile and tert-butylisocyanide. Monitoring the disproportionation reactions of the zirconium(III) chloro and the borohydride derivatives by UV-Vis spectroscopy shows the presence of two isobestic points. By monitoring the band associated with the dicarbonyl complex useful kinetic data could be obtained. The hydrogenolysis of the zirconium(III) alkyls also warrants kinetic measurements. Importantly, measurement of the kinetic isotope effect for the hydrogenolysis would show whether the reaction proceeds by σ-bond metathesis. Attempts to investigate such studies using NMR techniques did show that the hydrogenolysis obeys

overall second order kinetics. However, more accurate (and reliable) measurements could be obtained by performing the experiments in a gas uptake apparatus.

Excessive solubility of the zirconium(III) hydride complex has hindered the isolation of this complex as a solid material. Incorporating the phenyl version of PNP may lower the solubility of the hydride complex and thereby enable the isolation of the complex as a pure solid material. It important to note that previous attempts in our laboratory has shown that reacting $Li[N(SiMe_2CH_2Ph_2)_2]$ with $ZrCl_4$ results in the formation of the bis ligand complex $ZrCl_2[N(SiMe_2CH_2PPh_2)_2]_2$. However, using a different zirconium precursor may lead to the desired product; for example, reaction involving $Li[N(SiMe_2CH_2Ph_2)_2]$ and $CpZrCl_3$•(DME) could yield complex $ZrCpCl_2[N(SiMe_2CH_2Ph_2)_2]$ (Scheme **5.5**). It is known that the reaction of $CpZrCl_3$•(DME) with the less bulky PN ligand $Li[N(PhCH_2)(SiMe_2CH_2PPh_2)]$ forms the mono PN derivative of zirconium, $ZrCpCl_2[N(PhCH_2)(SiMe_2CH_2PPh_2)]$.

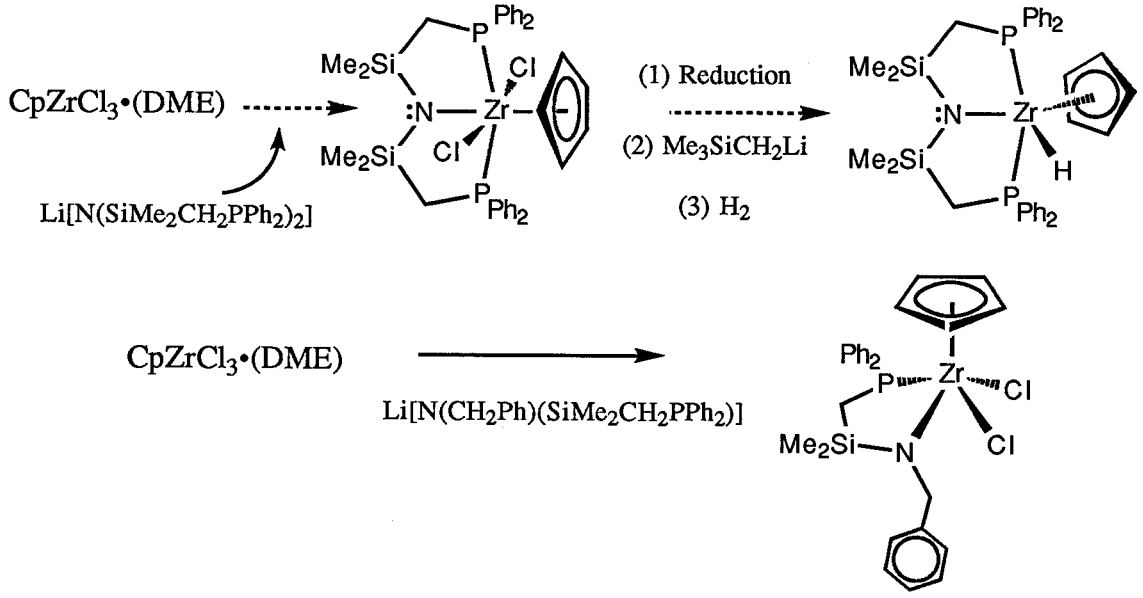

Scheme 5.5

Reactivity

Reactions involving some zirconium(III) complexes (e.g., **4.1**) and $B(C_6F_5)_3$ gave a deep blue solution which is stable for approximately 10 minutes at room temperature. The formation of the blue color seems to suggest the formation of the radical anion, $[B(C_6F_5)_3]^{\bullet-}$.

For comparison the radical anion $\{B[C_6H_3(CF_3)_2\text{-}2,6]_3\}^{\bullet-}$ is stable at room temperature and has an intense blue color in solution. Therefore reactions with $B[C_6H_3(CF_3)_2\text{-}2,6]_3$ and zirconium(III) complexes could be investigated.

Cationic Complexes

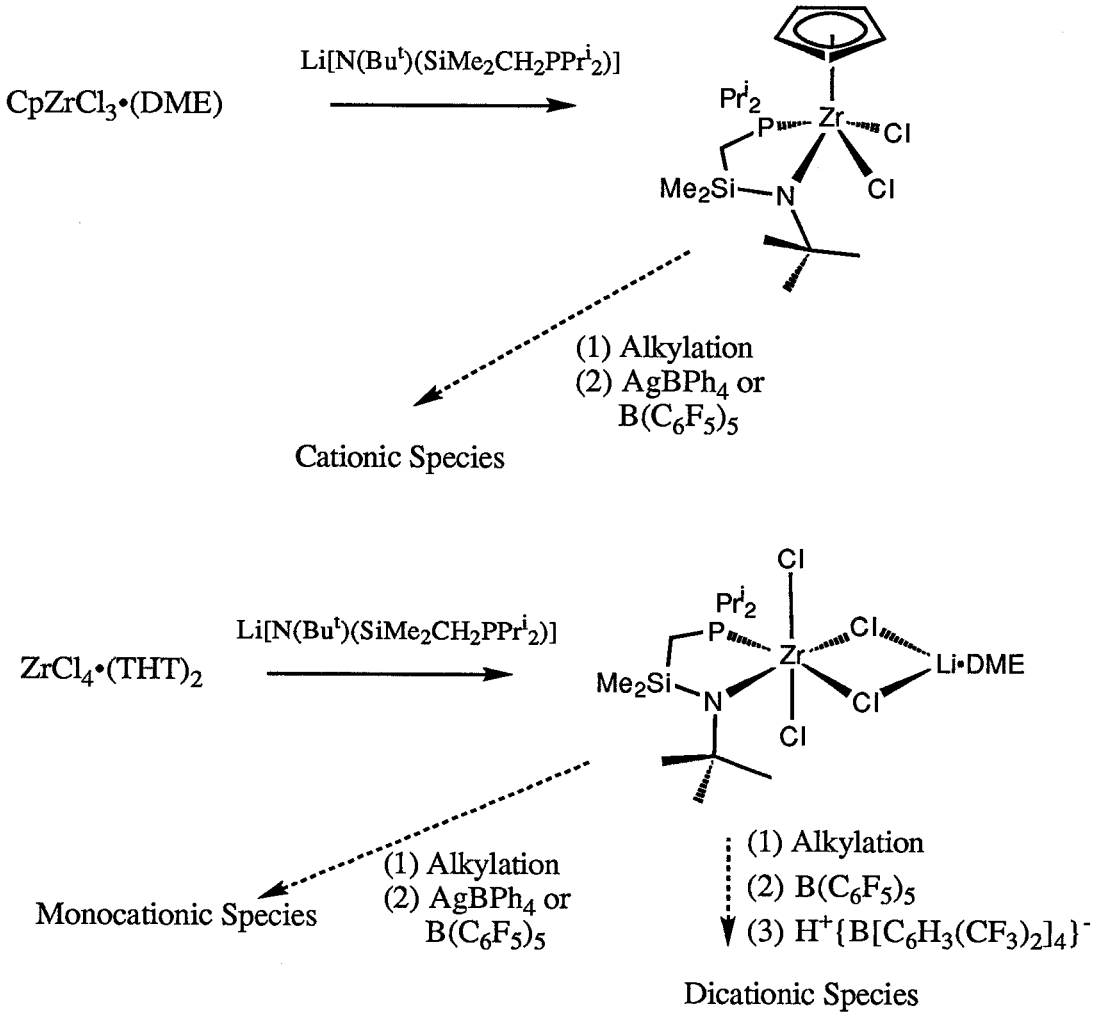

Scheme 5.6

Species generated by treating $ZrCpCl_2[N(SiMe_2CH_2PPr^i_2)_2]$ and alumoxanes have been shown to be catalytically active towards ethylene polymerization (see Section **2.2.1**, page 28). Many of the precursors that have been synthesized during the investigation of the dinitrogen chemistry are potential candidates for generating cationic complexes. Spectroscopic evidence

(^1H and $^{31}P\{^1H\}$ NMR) suggests that the methyl derivative $ZrCpMe_2[N(SiMe_2CH_2PPr^i_2)_2]$ reacts with $AgBPh_4$ in THF to yield two isomeric cationic species. Also, the dibenzyl derivative $Zr(OAr^*)(PhCH_2)_2[N(SiMe_2CH_2PPr^i_2)_2]$ reacts with $B(C_6F_5)_3$ to generate species which could be formulated as $Zr(OAr^*)(PhCH_2)[PhCH_2{\bullet}(B(C_6F_5)_3)][N(SiMe_2CH_2PPr^i_2)_2]$.

Oue efforts in ligand design have so far concentrated on the tridentate PNP systems. Very recently, we have developed an isopropyl version of the PN ligand, $Li[N(SiMe_2CH_2PPr^i_2)(Bu^t)]$ that has been incorporated on to zirconium (Scheme **5.6**). Some suggested reactions that could lead to the synthesis of mono and dicationic species are shown in Scheme **5.6**.

Appendix

A.1 UV-Vis Spectra of Complexes 2.2 and 2.9

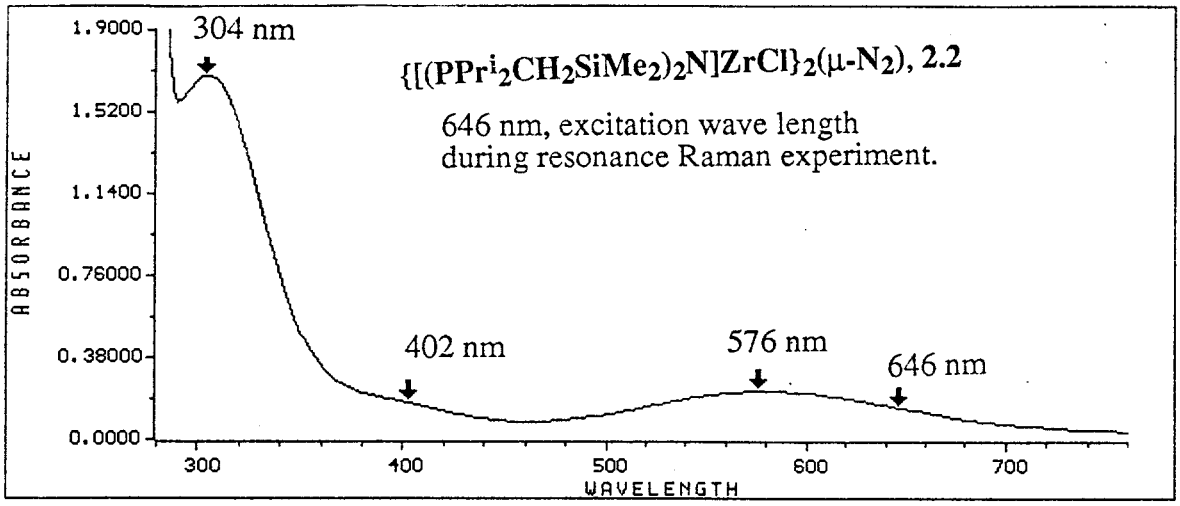

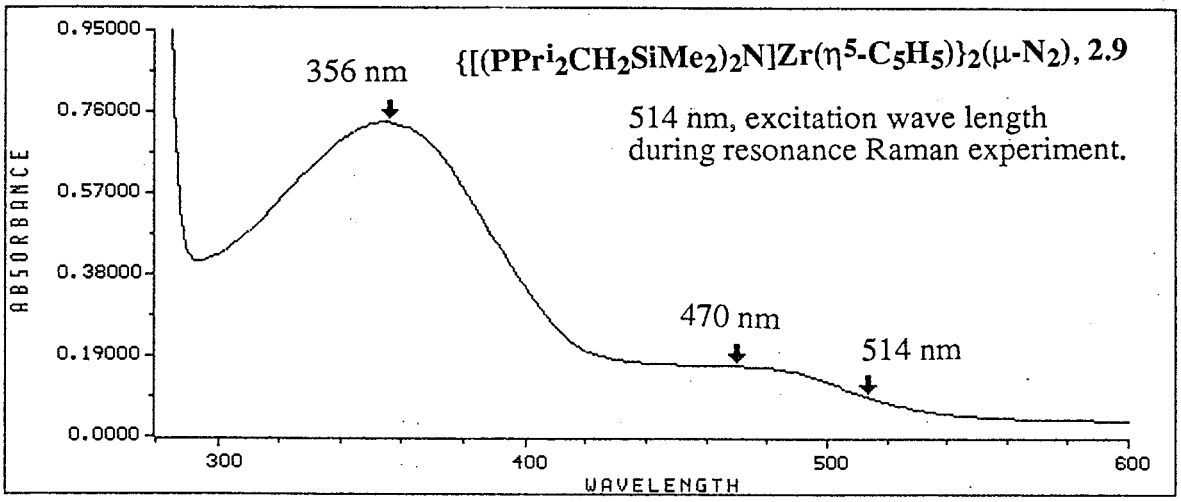

B.1 ESR Simulations

The solution ESR spectra of the zirconium(III) complexes, i.e., complexes incorporating PNP ligand, consist mainly of a triplet due to the coupling of two equivalent phosphorus nuclei of the PNP ligand. Therefore the a(^{31}P) values used for the simulations were measured directly from the actual solution spectra. The coupling constants due to other nuclei were obtained by iteration and the values reported gave the best possible fit between the observed and simulated spectra. Simulations were carried out in such a manner that a lowest possible value is obtained for line broadening. When the coupling constants were lower than the value obtained for line broadening it could be considered as the upper or the lower limit for the given nucleus where the limits are within 0.5 G. For example, in **4.17** the a(^{14}N) value is the upper limit of the estimated coupling constant due to nitrogen of the PNP. It is important to note that in the case of the ethyl derivative the values obtained from simulation correlate well with the deuterio derivatives, i.e., a(^{2}H) ≅ 1/6 a(^{1}H).

(I) line broadening = 2.8 G; a(^{1}H) = 8.0 MHz, 4H; a(^{14}N) = 5.5 MHz, 1N; a(^{31}P) = 58.0 MHz, 2P. rest of the parameters were identical for simulations **I, II** and **III**.

(II) different from **I** is a(^{14}N) = 4.5 MHz,1N.

(III) different from **I** is line broadening = 2.5 G.

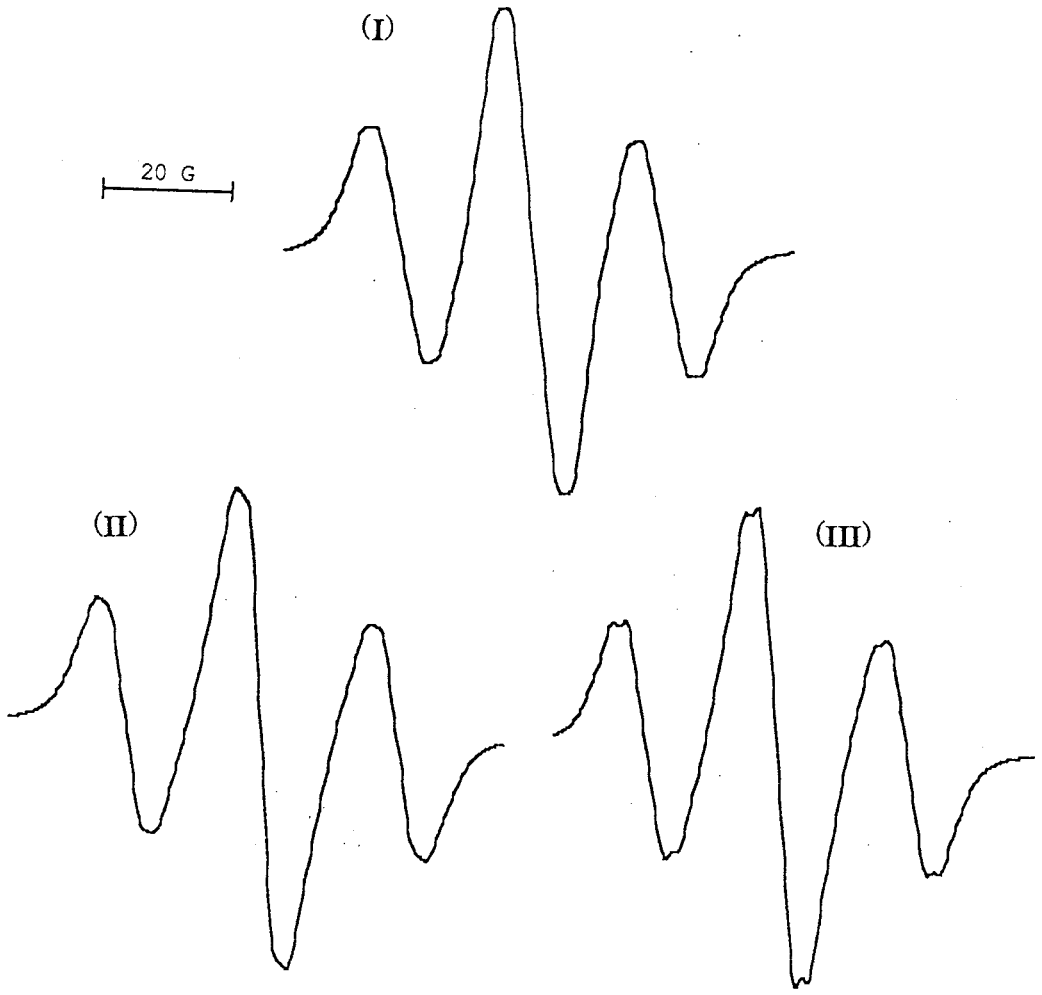

Appendix

C.1 The Cartesian Coordinates for the Model Complexes Used in INDO/1-MO Analysis

C.1.1 The Atom Numbering Scheme and the Cartesian Coordinates for the Model Complex A

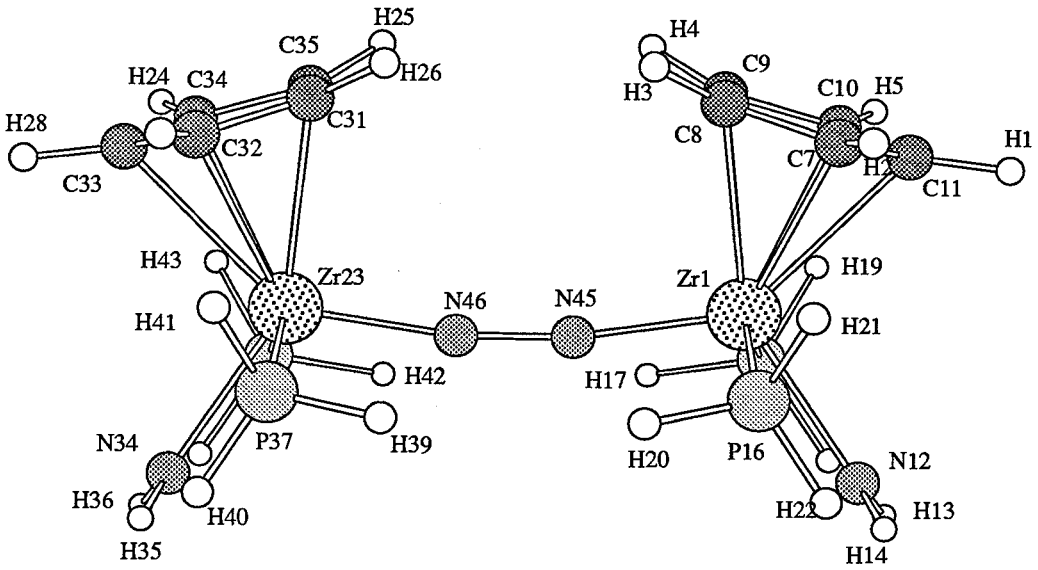

Atom	X	Y	Z	Atom	X	Y	Z
Zr(1)	2.832	-0.227	0.138	P(38)	-2.440	-0.722	-2.597
C(7)	3.879	1.743	1.435	H(39)	-1.204	-1.426	3.251
C(8)	2.612	2.182	1.035	H(40)	-3.233	-2.285	2.778
C(9)	2.614	2.295	-0.360	H(41)	-3.056	-0.180	3.562
C(10)	3.881	1.924	-0.822	H(42)	-1.175	-0.931	-3.110
C(11)	4.664	1.583	0.287	H(43)	-3.025	0.350	-3.240
N(12)	4.096	-2.141	-0.021	H(44)	-3.208	-1.851	-2.793
P(15)	3.024	-0.746	-2.606	N(45)	0.934	-0.498	0.116
P(16)	3.000	-1.214	2.753	N(46)	-0.366	-0.486	0.118
H(17)	1.760	-0.926	-3.130	H(2)	4.261	1.739	2.487
H(18)	3.772	-1.888	-2.807	H(3)	1.826	2.595	1.716

H(19)	3.634	0.320	-3.235	H(4)	1.800	2.811	-0.929
H(20)	1.731	-1.481	3.226	H(5)	4.269	2.098	-1.857
H(21)	3.603	-0.273	3.562	H(6)	5.772	1.432	0.274
H(22)	3.747	-2.374	2.760	H(13)	4.390	-2.510	-0.981
Zr(23)	-2.258	-0.180	0.144	H(14)	4.391	-2.663	0.866
C(29)	-3.267	1.994	-0.810	H(24)	-3.648	2.170	-1.848
C(30)	-1.993	2.338	-0.346	H(25)	-1.198	2.843	-0.951
C(31)	-1.995	2.221	1.049	H(26)	-1.173	2.622	1.694
C(32)	-3.270	1.802	1.446	H(27)	-3.655	1.811	2.496
C(33)	-4.056	1.662	0.297	H(28)	-5.168	1.531	0.287
N(34)	-3.557	-2.072	-0.012	H(35)	-3.859	-2.588	0.875
P(37)	-2.464	-1.140	2.766	H(36)	-3.860	-2.436	-0.972

C.1..2 The Atom Numbering Scheme and the Cartesian Coordinates for the Model Complex B

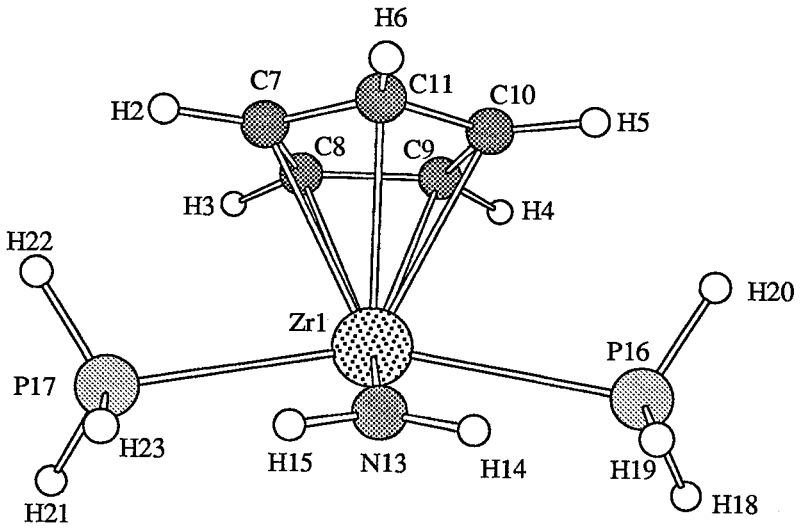

Atom	X	Y	Z	Atom	X	Y	Z
Zr(1)	-0.031	-0.734	-0.065	H(20)	3.408	-0.100	0.236
C(7)	-1.127	1.553	-0.536	H(21)	-3.252	-2.126	-0.138
C(8)	-0.757	1.044	-1.786	H(22)	-3.408	0.023	0.521
C(9)	0.641	1.010	-1.842	H(23)	-2.757	-1.561	1.986
C(10)	1.135	1.496	-0.627	H(2)	-2.147	1.706	-0.182
C(11)	0.042	1.832	0.181	H(3)	-1.438	0.730	-2.577
N(13)	0.047	-1.404	2.134	H(4)	1.240	0.665	-2.685
P(16)	2.674	-1.249	0.444	H(5)	2.186	1.595	-0.356
P(17)	-2.700	-1.153	0.669	H(6)	0.093	2.240	1.191
H(18)	3.121	-2.240	-0.406	H(14)	0.990	-1.582	2.606
H(19)	2.826	-1.661	1.752	H(15)	-0.861	-1.537	2.685

C.1.3 The Atom Numbering Scheme and the Cartesian Coordinates for the Model Complex H

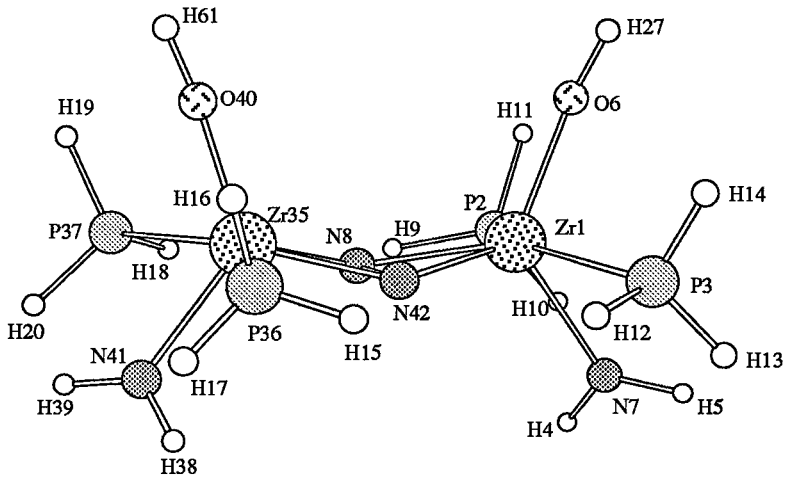

Atom	X	Y	Z	Atom	X	Y	Z
Zr(1)	1.900	0.018	-0.632	P(37)	-3.290	0.107	-1.556
P(2)	1.634	0.176	-3.468	O(40)	-2.190	1.834	1.168
P(3)	3.664	-0.492	1.507	N(41)	-2.884	-1.820	0.921
O(6)	2.605	1.911	-0.666	N(42)	0.414	-0.495	0.700
N(7)	3.063	-1.725	-1.344	H(61)	-2.607	2.792	1.068
N(8)	-0.132	-0.307	-0.737	H(4)	2.584	-2.348	-2.070
H(9)	0.324	-0.074	-3.821	H(5)	4.059	-1.952	-1.027
H(10)	2.457	-0.760	-4.061	H(15)	-0.167	-1.009	3.803
H(11)	1.992	1.439	-3.894	H(16)	-1.741	0.555	4.198
H(12)	2.948	-0.945	2.596	H(17)	-2.347	-1.580	3.809
H(13)	4.582	-1.451	1.129	H(18)	-2.553	-0.108	-2.703
H(14)	4.327	0.671	1.844	H(19)	-3.874	1.356	-1.613
H(27)	3.075	2.794	-0.349	H(20)	-4.273	-0.856	-1.454
Zr(35)	-1.595	-0.037	0.692	H(38)	-2.473	-2.631	1.485
P(36)	-1.443	-0.589	3.486	H(39)	-3.877	-1.896	0.530

C.1.4 The Atom Numbering Scheme and the Cartesian Coordinates for the Model Complex M

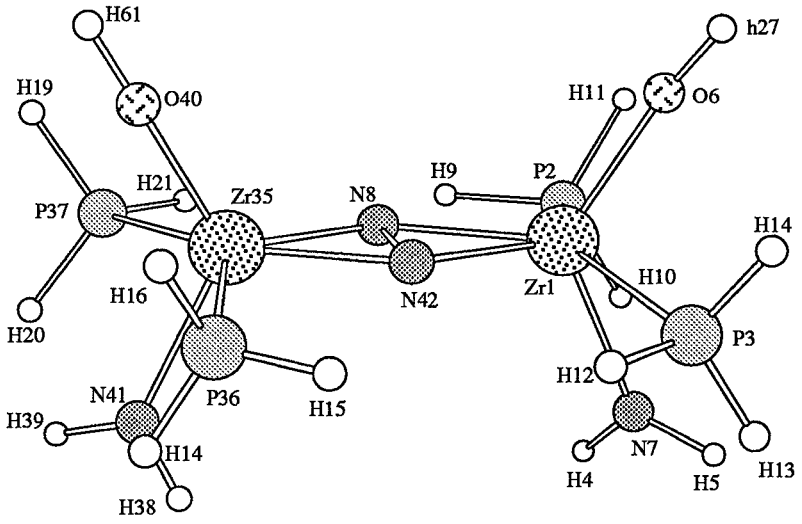

Atom	X	Y	Z	Atom	X	Y	Z
Zr(1)	1.815	-0.023	-0.502	P(37)	-3.263	0.262	-2.011
P(2)	1.820	0.400	-3.323	O(40)	-2.869	1.494	1.142
P(3)	3.238	-1.084	1.688	N(41)	-2.862	-2.079	0.081
O(6)	2.930	1.651	-0.322	N(42)	0.148	-0.272	0.685
N(7)	2.605	-1.932	-1.294	H(61)	-3.432	2.380	1.159
N(8)	-0.224	0.143	-0.761	H(4)	2.057	-2.371	-2.102
H(9)	0.520	0.489	-3.777	H(5)	3.495	-2.406	-0.938
H(10)	2.455	-0.655	-3.946	H(15)	-0.752	-1.530	3.486
H(11)	2.488	1.573	-3.611	H(16)	-2.617	-0.335	3.900
H(12)	2.352	-1.437	2.685	H(17)	-2.776	-2.398	3.010
H(13)	3.942	-2.200	1.282	H(18)	-2.350	0.411	-3.034
H(14)	4.117	-0.135	2.168	H(19)	-4.046	1.395	-1.924
H(27)	3.560	2.376	0.102	H(20)	-4.064	-0.833	-2.264
Zr(35)	-1.892	-0.121	0.423	H(38)	-2.395	-2.925	0.541
P(36)	-2.027	-1.240	3.043	H(39)	-3.763	-2.212	-0.480

D.1 X-ray Crystallographic Analysis Data

D.1.1 X-ray Crystallographic Analysis of $Zr(\eta^5\text{-}C_5H_5)Br_2[N(SiMe_2CH_2PPr^i_2)_2]$, 2.7

A. Crystal Data

Empirical Formula	$C_{23}H_{49}Br_2NP_2Si_2Zr$
Formula Weight	708.79
Crystal Color, Habit	yellow, hexagonal
Crystal Dimensions (mm)	0.080 X 0.300 X 0.300
Crystal System	monoclinic
No. Reflections Used for Unit Cell Determination (2θ range)	25 (28.5 - 37.6°)
Omega Scan Peak Width at Half-height	0.41
Lattice Parameters:	a = 16.310 (2)Å b = 10.678 (2)Å c = 18.306 (3)Å β = 100.59 (1)° V = 3133.9 (9)Å^3
Space Group	$P2_1/a$ (#14)
Z value	4
D_{calc}	1.502 g/cm^3
F_{000}	1448
$\mu_{(MoK\alpha)}$	30.59 cm^{-1}

B. Intensity Measurements

Diffractometer	Rigaku AFC6S
Radiation	MoKα (λ = 0.71069 Å)
Temperature	21°C
Take-off Angle	6.0°
Detector Aperture	6.0 mm horizontal 6.0 mm vertical
Crystal to Detector Distance	285 mm
Scan Type	ω-2θ
Scan Rate	16.0°/min (in omega) (8 rescans)
Scan Width	(1.05 + 0.35 tanθ)°
$2\theta_{max}$	55.0°
No. of Reflections Measured	Total: 7845 Unique: 7582 (R_{int} = .045)
Corrections	Lorentz-polarization Absorption (trans. factors: 0.54 - 1.00) Decay (-3.10% decline) Secondary Extinction (coefficient: 0.30238E-06)

C. Structure Solution and Refinement

Structure Solution	Patterson Method
Refinement	Full-matrix least-squares
Function Minimized	Σ w (|Fo| - |Fc|)^2
Least-squares Weights	$4Fo^2/\sigma^2(Fo^2)$
p-factor	0.02
Anomalous Dispersion	All non-hydrogen atoms
No. Observations (I>3.00σ(I)) No. Variables Reflection/Parameter Ratio	3645 281 12.97
Residuals: R; R_w	0.031; 0.030
Goodness of Fit Indicator	1.27
Max Shift/Error in Final Cycle	0.01
Maximum Peak in Final Diff. Map Minimum Peak in Final Diff. Map	0.37 e$^-$/Å^3 -0.41 e$^-$/Å^3

D.1.1 X-ray Crystallographic Analysis of $Zr(\eta^5\text{-}C_5H_5)Br_2[N(SiMe_2CH_2PPr^i_2)_2]$, 2.7 continued

Final atomic coordinates (fractional) and B_{eq} ($Å^2$)*

atom	x	y	z	B_{eq}
Zr(1)	0.29705(2)	0.37118(4)	0.25013(2)	2.25(2)
Br(1)	0.44783(3)	0.30222(5)	0.32472(3)	3.71(2)
Br(2)	0.17026(3)	0.50463(5)	0.17361(3)	3.86(2)
P(1)	0.26513(7)	0.4991(1)	0.37654(7)	2.84(5)
P(2)	0.36988(7)	0.3501(1)	0.12231(6)	2.79(5)
Si(1)	0.32572(8)	0.6925(1)	0.27709(7)	3.00(5)
Si(2)	0.45539(8)	0.5683(1)	0.21340(7)	3.05(5)
N(1)	0.3629(2)	0.5532(3)	0.2469(2)	2.3(1)
C(1)	0.2503(3)	0.6570(4)	0.3415(2)	3.2(2)
C(2)	0.4684(3)	0.4274(4)	0.1531(2)	3.2(2)
C(3)	0.3600(3)	0.5045(5)	0.4501(3)	3.9(2)
C(4)	0.1738(3)	0.4598(5)	0.4203(3)	4.4(2)
C(5)	0.3721(4)	0.3798(6)	0.4930(3)	5.5(3)
C(6)	0.3693(3)	0.6174(6)	0.5029(3)	5.7(3)
C(7)	0.1737(4)	0.5150(6)	0.4964(4)	6.7(3)
C(8)	0.0931(3)	0.4956(6)	0.3687(4)	6.1(3)
C(9)	0.3118(3)	0.4465(5)	0.0453(3)	3.8(2)
C(10)	0.3940(3)	0.1985(4)	0.0811(3)	3.8(2)
C(11)	0.2345(3)	0.3758(6)	0.0068(3)	5.2(3)
C(12)	0.3606(4)	0.5018(6)	-0.0106(3)	5.7(3)
C(13)	0.4445(3)	0.1140(5)	0.1406(3)	5.2(3)
C(14)	0.4367(4)	0.2063(6)	0.0143(3)	6.8(3)
C(15)	0.2702(3)	0.7997(4)	0.2028(3)	4.6(2)
C(16)	0.4098(3)	0.7913(5)	0.3330(3)	4.8(3)

Table . Final atomic coordinates (fractional) and B_{eq} ($Å^2$)* (cont.)

atom	x	y	z	B_{eq}
C(17)	0.5541(3)	0.5806(5)	0.2841(3)	4.6(2)
C(18)	0.4565(3)	0.7092(5)	0.1517(3)	4.9(3)
C(19)	0.2555(3)	0.1477(4)	0.2039(3)	4.2(2)
C(20)	0.2910(3)	0.1344(5)	0.2774(4)	5.1(3)
C(21)	0.2398(4)	0.1941(5)	0.3197(3)	5.1(3)
C(22)	0.1720(3)	0.2407(5)	0.2708(4)	4.8(3)
C(23)	0.1812(3)	0.2127(5)	0.1998(3)	4.3(2)

$$*B_{eq} = (8/3)\pi^2 \Sigma\Sigma U_{ij} a_i * a_j * (a_i \cdot a_j)$$

D.1.1 X-ray Crystallographic Analysis of $Zr(\eta^5\text{-}C_5H_5)Br_2[N(SiMe_2CH_2PPr^i_2)_2]$, 2.7 continued

Table . Bond angles (deg) with estimated standard deviations.

atom	atom	atom	angle	atom	atom	atom	angle
Br(1)	Zr(1)	Br(2)	162.95(2)	C(9)	P(2)	C(10)	106.9(2)
Br(1)	Zr(1)	P(1)	90.31(3)	N(1)	Si(1)	C(1)	109.4(2)
Br(1)	Zr(1)	P(2)	85.08(3)	N(1)	Si(1)	C(15)	116.2(2)
Br(1)	Zr(1)	N(1)	81.50(8)	N(1)	Si(1)	C(16)	113.1(2)
Br(1)	Zr(1)	Cp(1)	99.02(7)	C(1)	Si(1)	C(15)	106.9(2)
Br(2)	Zr(1)	P(1)	86.00(3)	C(1)	Si(1)	C(16)	105.5(2)
Br(2)	Zr(1)	P(2)	90.62(3)	C(15)	Si(1)	C(16)	105.0(2)
Br(2)	Zr(1)	N(1)	81.46(8)	N(1)	Si(2)	C(2)	109.2(2)
Br(2)	Zr(1)	Cp(1)	98.03(6)	N(1)	Si(2)	C(17)	117.0(2)
P(1)	Zr(1)	P(2)	152.82(4)	N(1)	Si(2)	C(18)	113.0(2)
P(1)	Zr(1)	N(1)	76.18(9)	C(2)	Si(2)	C(17)	106.4(2)
P(1)	Zr(1)	Cp(1)	103.02(7)	C(2)	Si(2)	C(18)	105.6(2)
P(2)	Zr(1)	N(1)	76.65(9)	C(17)	Si(2)	C(18)	104.9(2)
P(2)	Zr(1)	Cp(1)	104.16(7)	Zr(1)	N(1)	Si(1)	122.8(2)
N(1)	Zr(1)	Cp(1)	179.2(1)	Zr(1)	N(1)	Si(2)	123.0(2)
Zr(1)	P(1)	C(1)	101.2(1)	Si(1)	N(1)	Si(2)	114.2(2)
Zr(1)	P(1)	C(3)	110.8(2)	P(1)	C(1)	Si(1)	110.4(2)
Zr(1)	P(1)	C(4)	121.8(2)	P(2)	C(2)	Si(2)	110.9(2)
C(1)	P(1)	C(3)	105.6(2)	P(1)	C(3)	C(5)	110.8(4)
C(1)	P(1)	C(4)	107.3(2)	P(1)	C(3)	C(6)	117.0(4)
C(3)	P(1)	C(4)	108.7(2)	C(5)	C(3)	C(6)	111.6(4)
Zr(1)	P(2)	C(2)	101.0(1)	P(1)	C(4)	C(7)	116.4(4)
Zr(1)	P(2)	C(9)	110.6(2)	P(1)	C(4)	C(8)	110.3(4)
Zr(1)	P(2)	C(10)	124.0(2)	C(7)	C(4)	C(8)	109.0(4)
C(2)	P(2)	C(9)	106.5(2)	P(2)	C(9)	C(11)	109.8(4)
C(2)	P(2)	C(10)	106.4(2)	P(2)	C(9)	C(12)	117.9(4)

Table . Bond lengths (Å) with estimated standard deviations.*

atom	atom	distance	atom	atom	distance
Zr(1)	Br(1)	2.6871(7)	Si(1)	C(15)	1.879(5)
Zr(1)	Br(2)	2.6842(7)	Si(1)	C(16)	1.877(5)
Zr(1)	P(1)	2.817(1)	Si(2)	N(1)	1.738(3)
Zr(1)	P(2)	2.821(1)	Si(2)	C(2)	1.900(5)
Zr(1)	N(1)	2.227(3)	Si(2)	C(17)	1.876(5)
Zr(1)	C(19)	2.581(5)	Si(2)	C(18)	1.884(5)
Zr(1)	C(20)	2.583(5)	C(3)	C(5)	1.541(7)
Zr(1)	C(21)	2.551(5)	C(3)	C(6)	1.535(7)
Zr(1)	C(22)	2.555(5)	C(4)	C(7)	1.514(8)
Zr(1)	C(23)	2.578(5)	C(4)	C(8)	1.522(8)
Zr(1)	Cp(1)	2.286(2)	C(9)	C(11)	1.527(7)
P(1)	C(1)	1.804(4)	C(9)	C(12)	1.526(7)
P(1)	C(3)	1.856(5)	C(10)	C(13)	1.532(7)
P(1)	C(4)	1.863(5)	C(10)	C(14)	1.517(7)
P(2)	C(2)	1.802(4)	C(19)	C(20)	1.371(7)
P(2)	C(9)	1.858(5)	C(19)	C(23)	1.386(7)
P(2)	C(10)	1.859(5)	C(20)	C(21)	1.393(8)
Si(1)	N(1)	1.734(3)	C(21)	C(22)	1.382(8)
Si(1)	C(1)	1.893(5)	C(22)	C(23)	1.369(7)

* Here and elsewhere, Cp(1) refers to the unweighted centroid of the C(19-23) cyclopentadienyl ring.

D.1.2 X-ray Crystallographic Analysis of {[(PPr$^i_2$CH$_2$SiMe$_2$)$_2$N]Zr(η^5-C$_5$H$_5$)}$_2$(μ-N$_2$), 2.9

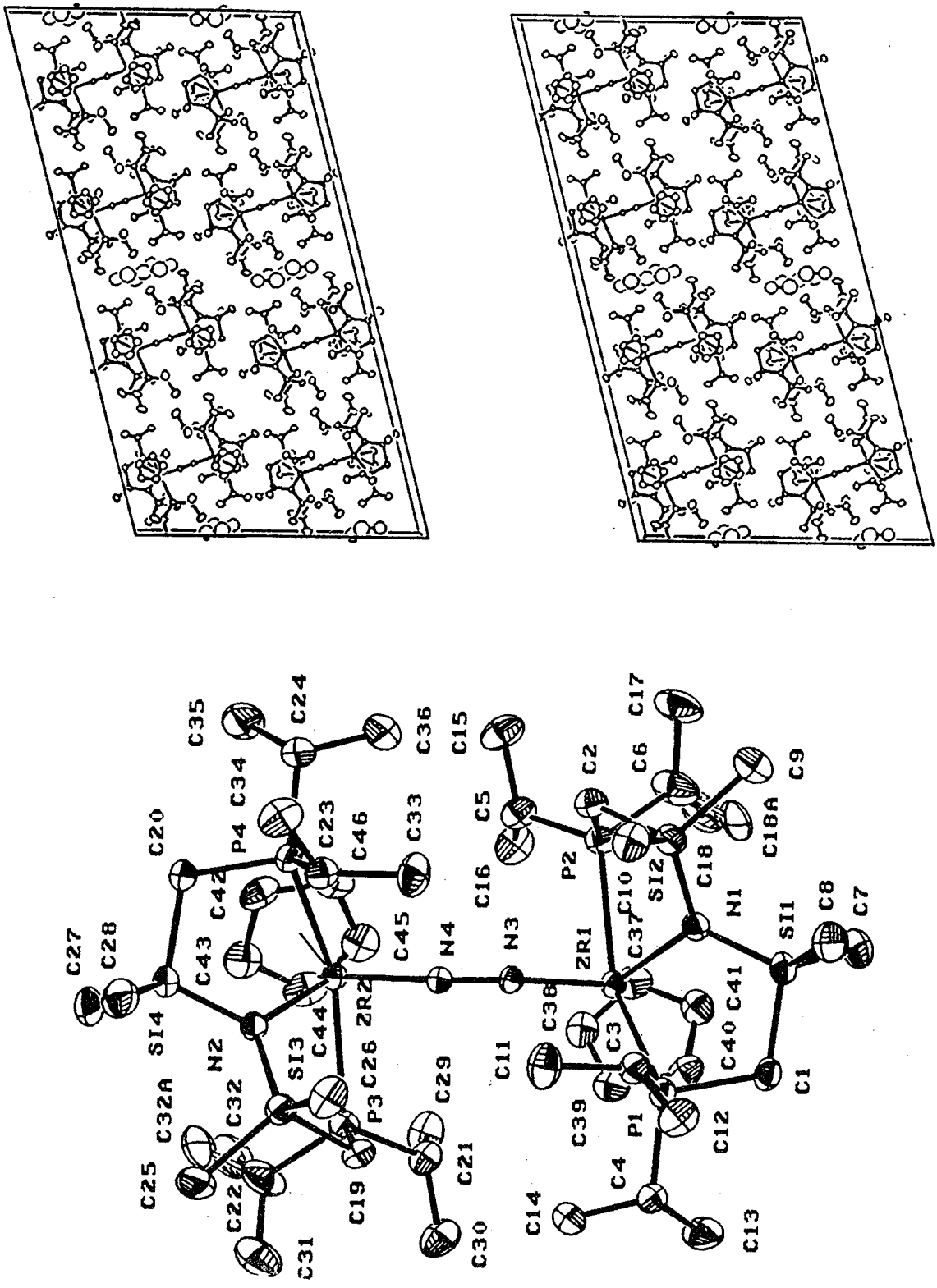

D.1.2 X-ray Crystallographic Analysis of {{[(PPr$^i_2$CH$_2$SiMe$_2$)$_2$N]Zr(η^5-C$_5$H$_5$)}$_2$(μ-N$_2$), 2.9 continued

EXPERIMENTAL DETAILS

A. Crystal Data

Empirical Formula	$C_{49}H_{103}N_4P_4Si_4Zr_2$
Formula Weight	1167.06
Crystal Color, Habit	red-brown, prism
Crystal Dimensions (mm)	0.120 X 0.250 X 0.450
Crystal System	monoclinic
No. Reflections Used for Unit Cell Determination (2θ range)	25 (29.2 - 33.8°)
Omega Scan Peak Width at Half-height	0.36
Lattice Parameters:	a = 48.755 (4)Å b = 10.226 (7)Å c = 25.987 (4)Å β = 104.582 (9)° V = 12539 (9)Å^3
Space Group	C2/c (#15)
Z value	8
D_{calc}	1.236 g/cm^3
F_{000}	4968
$\mu_{(MoK\alpha)}$	5.34 cm^{-1}

B. Intensity Measurements

Diffractometer	Rigaku AFC6S
Radiation	MoKα (λ = 0.71069 Å)
Temperature	21°C
Take-off Angle	6.0°
Detector Aperture	6.0 mm horizontal 6.0 mm vertical
Crystal to Detector Distance	285 mm
Scan Type	ω
Scan Rate	32.0°/min (in omega) (8 rescans)
Scan Width	(0.91 + 0.35 tanθ)°
$2\theta_{max}$	55.0°
No. of Reflections Measured	Total: 15389 Unique: 15197 (R_{int} = .025)
Corrections	Lorentz-polarization Absorption (trans. factors: 0.97 - 1.00)

C. Structure Solution and Refinement

Structure Solution	Patterson Method
Refinement	Full-matrix least-squares
Function Minimized	Σ w (|Fo| - |Fc|)^2
Least-squares Weights	$4Fo^2/\sigma^2(Fo^2)$
p-factor	0.02
Anomalous Dispersion	All non-hydrogen atoms
No. Observations (I>3.00σ(I)) No. Variables Reflection/Parameter Ratio	7287 573 12.72
Residuals: R; R_w	0.034; 0.035
Goodness of Fit Indicator	1.40
Max Shift/Error in Final Cycle	0.21
Maximum Peak in Final Diff. Map Minimum Peak in Final Diff. Map	0.37 e$^-$/Å^3 -0.27 e$^-$/Å^3

D.1.2 X-ray Crystallographic Analysis of {{[(PPr$^i_2$CH$_2$SiMe$_2$)$_2$N]Zr(η^5-C$_5$H$_5$)}$_2$(μ-N$_2$), 2.9 continued

Table . Final atomic coordinates (fractional) and B_{eq} (Å^2)* (cont.)

atom	x	y	z	B_{eq}	occ.
C(11)	0.1526(1)	0.4564(4)	0.1775(2)	5.5(2)	
C(12)	0.1522(1)	0.5547(4)	0.0885(2)	4.6(2)	
C(13)	0.1909(1)	0.1769(5)	0.0516(2)	5.7(2)	
C(14)	0.20304(9)	0.2428(5)	0.1470(2)	5.7(2)	
C(15)	0.0346(1)	-0.0340(5)	0.2368(2)	6.7(3)	
C(16)	0.0723(1)	-0.1851(5)	0.2188(2)	6.5(3)	
C(17)	0.0011(1)	0.0208(6)	0.1086(2)	7.9(3)	
C(18)	0.0324(2)	-0.144(1)	0.0781(5)	7.9(6)	0.565
C(18A)	0.0331(3)	-0.051(2)	0.0548(5)	7.9(8)	0.435
C(19)	0.20888(8)	0.2406(4)	0.2986(1)	3.7(2)	
C(20)	0.13492(8)	0.3229(4)	0.4371(1)	3.8(2)	
C(21)	0.2051(1)	-0.0219(4)	0.2564(2)	4.6(2)	
C(22)	0.2346(1)	0.0304(6)	0.3700(2)	7.3(3)	
C(23)	0.11695(8)	0.4624(4)	0.3389(1)	3.6(2)	
C(24)	0.07689(8)	0.2869(4)	0.3714(2)	4.2(2)	
C(25)	0.23721(9)	0.4001(5)	0.3984(2)	5.6(2)	
C(26)	0.1900(1)	0.5132(4)	0.3149(2)	4.9(2)	
C(27)	0.1937(1)	0.2362(5)	0.4961(2)	6.0(2)	
C(28)	0.1837(1)	0.5119(5)	0.4555(2)	5.6(2)	
C(29)	0.1977(1)	-0.1658(5)	0.2604(2)	6.8(3)	
C(30)	0.2326(1)	-0.0088(5)	0.2381(2)	6.5(3)	
C(31)	0.2630(1)	0.0808(5)	0.3648(2)	7.8(3)	
C(32)	0.2326(3)	0.013(2)	0.4203(4)	8.1(7)	0.510
C(32A)	0.2336(3)	-0.092(1)	0.4002(6)	8.1(7)	0.490
C(33)	0.1058(1)	0.4622(4)	0.2789(2)	5.4(2)	

Table . Final atomic coordinates (fractional) and B_{eq} (Å^2)*

atom	x	y	z	B_{eq}	occ.
Zr(1)	0.113703(7)	0.09216(3)	0.13299(1)	2.83(1)	
Zr(2)	0.150099(7)	0.11657(3)	0.33438(1)	2.77(1)	
P(1)	0.14629(2)	0.2757(1)	0.09337(4)	3.12(4)	
P(2)	0.06178(2)	0.0400(1)	0.15426(4)	3.71(5)	
P(3)	0.20307(2)	0.0731(1)	0.31595(4)	3.52(4)	
P(4)	0.11478(2)	0.2988(1)	0.36856(4)	3.12(4)	
Si(1)	0.08718(2)	0.2905(1)	0.02207(4)	3.79(5)	
Si(2)	0.05801(2)	0.3162(1)	0.10898(4)	3.71(5)	
Si(3)	0.20215(2)	0.3570(1)	0.35039(4)	3.49(5)	
Si(4)	0.17371(2)	0.3367(1)	0.43869(4)	3.75(5)	
N(1)	0.08336(6)	0.2446(3)	0.0834(1)	3.2(1)	
N(2)	0.17794(6)	0.2841(3)	0.3784(1)	3.0(1)	
N(3)	0.12671(6)	0.1315(3)	0.2074(1)	2.7(1)	
N(4)	0.13675(6)	0.1382(3)	0.2587(1)	2.6(1)	
C(1)	0.12611(8)	0.2856(4)	0.0241(1)	3.7(2)	
C(2)	0.05336(8)	0.2081(4)	0.1654(2)	3.9(2)	
C(3)	0.14174(8)	0.4433(4)	0.1175(1)	3.4(2)	
C(4)	0.18427(8)	0.2707(4)	0.0920(1)	3.7(2)	
C(5)	0.0621(1)	-0.0427(4)	0.2175(2)	4.8(2)	
C(6)	0.0305(1)	-0.0207(6)	0.1030(2)	7.5(3)	
C(7)	0.0685(1)	0.1792(5)	-0.0327(2)	5.8(2)	
C(8)	0.0750(1)	0.4617(5)	0.0007(2)	5.6(2)	
C(9)	0.0223(1)	0.3373(5)	0.0602(2)	6.0(2)	
C(10)	0.0674(1)	0.4827(4)	0.1380(2)	4.8(2)	

D.1.2 X-ray Crystallographic Analysis of $\{[(PPr^i_2CH_2SiMe_2)_2N]Zr(\eta^5\text{-}C_5H_5)\}_2(\mu\text{-}N_2)$, 2.9 continued

Table . Final atomic coordinates (fractional) and B_{eq} ($Å^2$)* (cont.)

atom	x	y	z	B_{eq}	occ.
C(34)	0.1049(1)	0.5753(4)	0.3644(2)	5.0(2)	
C(35)	0.0718(1)	0.2046(5)	0.4160(2)	6.8(3)	
C(36)	0.0579(1)	0.2439(6)	0.3183(2)	7.0(3)	
C(37)	0.1081(1)	-0.1573(4)	0.1142(2)	4.9(2)	
C(38)	0.1343(1)	-0.1375(4)	0.1494(2)	4.9(2)	
C(39)	0.1514(1)	-0.0698(4)	0.1232(2)	4.8(2)	
C(40)	0.1357(1)	-0.0498(4)	0.0706(2)	5.0(2)	
C(41)	0.1089(1)	-0.1025(4)	0.0656(2)	5.0(2)	
C(42)	0.1297(1)	-0.0177(4)	0.4008(2)	5.3(2)	
C(43)	0.1572(1)	-0.0620(5)	0.4090(2)	5.7(2)	
C(44)	0.1596(1)	-0.1245(4)	0.3630(2)	5.7(2)	
C(45)	0.1336(1)	-0.1200(4)	0.3262(2)	5.4(2)	
C(46)	0.1148(1)	-0.0518(4)	0.3491(2)	5.1(2)	
C(47)	0.4857(2)	0.107(1)	0.1510(4)	15.4(3)	
C(48)	1/2	0.055(3)	1/4	21.3(8)	0.500
C(49)	0.4873(7)	0.115(3)	0.216(2)	23(1)	0.500
C(50)	0.4944(3)	0.035(2)	0.1934(7)	22.7(6)	

$*B_{eq} = (8/3)\pi^2 \Sigma\Sigma U_{ij} a_i * a_j * (a_i \cdot a_j)$

Intramolecular Bond Angles

atom	atom	atom	angle	atom	atom	atom	angle
P(1)	Zr(1)	P(2)	145.87(4)	Zr(1)	P(2)	C(2)	96.0(1)
P(1)	Zr(1)	N(1)	71.74(8)	Zr(1)	P(2)	C(5)	117.5(1)
P(1)	Zr(1)	N(3)	98.92(8)	Zr(1)	P(2)	C(6)	123.1(2)
P(1)	Zr(1)	Cp(1)	102.89(6)	C(2)	P(2)	C(5)	104.1(2)
P(2)	Zr(1)	N(1)	75.66(8)	C(2)	P(2)	C(6)	104.7(2)
P(2)	Zr(1)	N(3)	85.76(8)	C(5)	P(2)	C(6)	107.9(3)
P(2)	Zr(1)	Cp(1)	104.84(6)	Zr(2)	P(3)	C(19)	95.9(1)
N(1)	Zr(1)	N(3)	115.1(1)	Zr(2)	P(3)	C(21)	118.4(1)
N(1)	Zr(1)	Cp(1)	127.61(9)	Zr(2)	P(3)	C(22)	122.4(2)
N(3)	Zr(1)	Cp(1)	117.2(1)	C(19)	P(3)	C(21)	104.1(2)
P(3)	Zr(2)	P(4)	145.65(3)	C(19)	P(3)	C(22)	105.0(2)
P(3)	Zr(2)	N(2)	75.37(7)	C(21)	P(3)	C(22)	107.5(2)
P(3)	Zr(2)	N(4)	86.10(8)	Zr(2)	P(4)	C(20)	100.1(1)
P(3)	Zr(2)	Cp(2)	104.84(6)	Zr(2)	P(4)	C(23)	111.1(1)
P(4)	Zr(2)	N(2)	71.53(8)	Zr(2)	P(4)	C(24)	130.9(1)
P(4)	Zr(2)	N(4)	99.76(8)	C(20)	P(4)	C(23)	102.2(2)
P(4)	Zr(2)	Cp(2)	102.41(6)	C(20)	P(4)	C(24)	105.4(2)
N(2)	Zr(2)	N(4)	115.3(1)	C(23)	P(4)	C(24)	103.6(2)
N(2)	Zr(2)	Cp(2)	127.49(9)	N(1)	Si(1)	C(1)	108.1(2)
N(4)	Zr(2)	Cp(2)	117.1(1)	N(1)	Si(1)	C(7)	113.2(2)
Zr(1)	P(1)	C(1)	100.6(1)	N(1)	Si(1)	C(8)	115.3(2)
Zr(1)	P(1)	C(3)	111.4(1)	C(1)	Si(1)	C(7)	107.4(2)
Zr(1)	P(1)	C(4)	130.1(1)	C(1)	Si(1)	C(8)	105.8(2)
C(1)	P(1)	C(3)	101.7(2)	C(7)	Si(1)	C(8)	106.5(2)
C(1)	P(1)	C(4)	105.9(2)	N(1)	Si(2)	C(2)	106.9(2)
C(3)	P(1)	C(4)	103.7(2)	N(1)	Si(2)	C(9)	115.0(2)

Angles are in degrees. Estimated standard deviations in the least significant figure are given in parentheses.

D.1.2 X-ray Crystallographic Analysis of $\{[(PPr^{i}_{2}CH_2SiMe_2)_2N]Zr(\eta^5\text{-}C_5H_5)\}_2(\mu\text{-}N_2)$, 2.9 continued

Intramolecular Bond Angles (cont.)

atom	atom	atom	angle	atom	atom	atom	angle
N(1)	Si(2)	C(10)	114.8(2)	P(1)	C(3)	C(11)	112.8(3)
C(2)	Si(2)	C(9)	108.4(2)	P(1)	C(3)	C(12)	116.1(3)
C(2)	Si(2)	C(10)	106.5(2)	C(11)	C(3)	C(12)	111.5(3)
C(9)	Si(2)	C(10)	104.9(2)	P(1)	C(4)	C(13)	114.7(3)
N(2)	Si(3)	C(19)	107.0(2)	P(1)	C(4)	C(14)	110.7(3)
N(2)	Si(3)	C(25)	115.3(2)	C(13)	C(4)	C(14)	110.5(4)
N(2)	Si(3)	C(26)	114.7(2)	P(2)	C(5)	C(15)	116.6(3)
C(19)	Si(3)	C(25)	109.0(2)	P(2)	C(5)	C(16)	112.6(3)
C(19)	Si(3)	C(26)	106.1(2)	C(15)	C(5)	C(16)	110.4(4)
C(25)	Si(3)	C(26)	104.3(2)	P(2)	C(6)	C(17)	117.1(4)
N(2)	Si(4)	C(20)	107.8(2)	P(2)	C(6)	C(18)	118.9(6)
N(2)	Si(4)	C(27)	113.4(2)	P(2)	C(6)	C(18A)	119.9(7)
N(2)	Si(4)	C(28)	115.3(2)	C(17)	C(6)	C(18)	117.0(6)
C(20)	Si(4)	C(27)	107.2(2)	C(17)	C(6)	C(18A)	117.7(8)
C(20)	Si(4)	C(28)	106.0(2)	P(3)	C(19)	Si(3)	110.6(2)
C(27)	Si(4)	C(28)	106.6(2)	P(4)	C(20)	Si(4)	108.8(2)
Zr(1)	N(1)	Si(1)	120.0(1)	P(3)	C(21)	C(29)	112.7(3)
Zr(1)	N(1)	Si(2)	119.8(1)	P(3)	C(21)	C(30)	116.5(3)
Si(1)	N(1)	Si(2)	120.2(2)	C(29)	C(21)	C(30)	110.1(4)
Zr(2)	N(2)	Si(3)	119.9(1)	P(3)	C(22)	C(31)	117.0(4)
Zr(2)	N(2)	Si(4)	119.7(1)	P(3)	C(22)	C(32)	121.3(6)
Si(3)	N(2)	Si(4)	120.5(2)	P(3)	C(22)	C(32A)	117.8(6)
Zr(1)	N(3)	N(4)	170.6(2)	C(31)	C(22)	C(32)	115.0(7)
Zr(2)	N(4)	N(3)	170.1(2)	C(31)	C(22)	C(32A)	119.1(6)
P(1)	C(1)	Si(1)	108.5(2)	P(4)	C(23)	C(33)	112.5(3)
P(2)	C(2)	Si(2)	110.8(2)	P(4)	C(23)	C(34)	115.7(3)

Angles are in degrees. Estimated standard deviations in the least significant figure are given in parentheses.

Intramolecular Distances

atom	atom	distance	atom	atom	distance
Zr(1)	P(1)	2.816(1)	P(3)	C(19)	1.812(4)
Zr(1)	P(2)	2.776(1)	P(3)	C(21)	1.852(4)
Zr(1)	N(1)	2.306(3)	P(3)	C(22)	1.854(5)
Zr(1)	N(3)	1.920(3)	P(4)	C(20)	1.821(4)
Zr(1)	C(37)	2.599(4)	P(4)	C(23)	1.857(4)
Zr(1)	C(38)	2.547(4)	P(4)	C(24)	1.871(4)
Zr(1)	C(39)	2.536(4)	Si(1)	N(1)	1.716(3)
Zr(1)	C(40)	2.600(4)	Si(1)	C(1)	1.887(4)
Zr(1)	C(41)	2.624(4)	Si(1)	C(7)	1.870(4)
Zr(1)	Cp(1)	2.294(2)	Si(1)	C(8)	1.887(5)
Zr(2)	P(3)	2.778(1)	Si(2)	N(1)	1.709(3)
Zr(2)	P(4)	2.828(1)	Si(2)	C(2)	1.895(4)
Zr(2)	N(2)	2.303(3)	Si(2)	C(9)	1.890(4)
Zr(2)	N(4)	1.923(3)	Si(2)	C(10)	1.872(4)
Zr(2)	C(42)	2.591(4)	Si(3)	N(2)	1.706(3)
Zr(2)	C(43)	2.622(4)	Si(3)	C(19)	1.887(4)
Zr(2)	C(44)	2.583(4)	Si(3)	C(25)	1.897(4)
Zr(2)	C(45)	2.541(4)	Si(3)	C(26)	1.865(4)
Zr(2)	C(46)	2.529(4)	Si(4)	N(2)	1.718(3)
Zr(2)	Cp(2)	2.286(2)	Si(4)	C(20)	1.886(4)
P(1)	C(1)	1.825(4)	Si(4)	C(27)	1.870(4)
P(1)	C(3)	1.857(4)	Si(4)	C(28)	1.879(5)
P(1)	C(4)	1.862(4)	N(3)	N(4)	1.301(3)
P(2)	C(2)	1.808(4)	C(3)	C(11)	1.520(5)
P(2)	C(5)	1.845(4)	C(3)	C(12)	1.523(5)
P(2)	C(6)	1.860(5)	C(4)	C(13)	1.515(5)

Distances are in angstroms. Estimated standard deviations in the least significant figure are given in parentheses.

D.1.3 X-ray Crystallographic Analysis of $\{[(PPr^i_2CH_2SiMe_2)_2N]Zr(OAr^*)\}_2(\mu\text{-}N_2)$, 2.12a

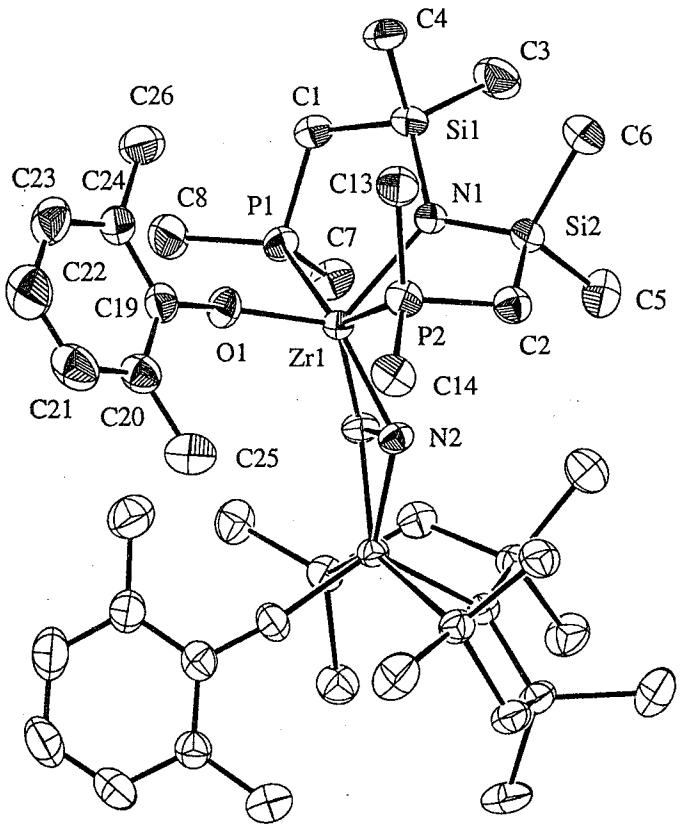

EXPERIMENTAL DETAILS

A. Crystal Data

Empirical Formula	$C_{52}H_{106}N_4P_4Si_4O_2Zr_2$
Formula Weight	1238.11
Crystal Color, Habit	dark, prism
Crystal Dimensions	0.15 X 0.25 X 0.25 mm
Crystal System	orthorhombic
Lattice Type	Primitive
No. of Reflections Used for Unit Cell Determination (2θ range)	25 (46.4 - 72.7°)
Omega Scan Peak Width at Half-height	0.38°
Lattice Parameters	a = 14.384(1) Å b = 17.754(1) Å c = 25.997(1) Å
	V = 6638.8(7) Å^3
Space Group	Pbcn (#60)
Z value	4
D_{calc}	1.239 g/cm^3
F_{000}	2632
μ(CuKα)	45.53 cm^{-1}

B. Intensity Measurements

Diffractometer	Rigaku AFC6S
Radiation	CuKα (λ = 1.54178 Å) graphite monochromated
Take-off Angle	6.0°

D.1.3 X-ray Crystallographic Analysis of $\{[(PPr^i_2CH_2SiMe_2)_2N]Zr(OAr^*\}_2(\mu\text{-}N_2)$, 2.12a continued

Table II. Atomic coordinates and B_{eq}

atom	x	y	z	B_{eq}
Zr(1)	0.02851(3)	0.25905(2)	0.17979(1)	2.990(7)
P(1)	0.22304(9)	0.27162(8)	0.17013(5)	3.85(3)
P(2)	-0.14513(9)	0.26760(8)	0.12761(5)	4.01(3)
Si(1)	0.1306(1)	0.37463(9)	0.08792(6)	4.34(4)
Si(2)	-0.0524(1)	0.42082(8)	0.13069(5)	3.92(3)
O(1)	0.0407(2)	0.1522(2)	0.1539(1)	4.37(9)
N(1)	0.0391(3)	0.3585(2)	0.1289(1)	3.36(9)
N(2)	-0.0514(2)	0.2812(2)	0.2426(1)	3.49(9)
C(1)	0.2335(4)	0.3145(3)	0.1066(2)	4.5(1)
C(2)	-0.1621(3)	0.3659(3)	0.1441(2)	4.3(1)
C(3)	0.1714(4)	0.4750(3)	0.0843(2)	6.7(2)
C(4)	0.1029(4)	0.3477(3)	0.0201(2)	6.0(2)
C(5)	-0.0394(4)	0.4923(3)	0.1825(2)	6.0(2)
C(6)	-0.0739(4)	0.4746(3)	0.0695(2)	5.9(2)
C(7)	0.2788(4)	0.3375(3)	0.2157(2)	5.2(2)
C(8)	0.2961(4)	0.1859(4)	0.1671(3)	6.4(2)
C(9)	0.2276(4)	0.4113(3)	0.2172(2)	6.1(2)
C(10)	0.3822(5)	0.3496(5)	0.2096(3)	10.3(3)
C(11)	0.2974(6)	0.1423(4)	0.2137(3)	10.4(3)
C(12)	0.3853(4)	0.1886(4)	0.1366(3)	6.9(2)
C(13)	-0.1389(4)	0.2706(3)	0.0568(2)	5.1(1)
C(14)	-0.2518(4)	0.2174(3)	0.1481(2)	5.4(2)
C(15)	-0.1117(5)	0.1954(4)	0.0323(2)	6.9(2)
C(16)	-0.2208(5)	0.3072(4)	0.0282(2)	7.0(2)

Detector Aperture	6.0 mm horizontal 6.0 mm vertical
Crystal to Detector Distance	285 mm
Temperature	21.0°C
Scan Type	ω-2θ
Scan Rate	16.0°/min (in ω) (up to 9 scans)
Scan Width	$(0.84 + 0.20 \tan\theta)°$
$2\theta_{max}$	155.5°
No. of Reflections Measured	Total: 6948
Corrections	Lorentz-polarization Absorption (trans. factors: 0.78 - 1.00) Decay (2.01% decline) Secondary Extinction (coefficient: 9.2(5) x $^{-8}$)

C. Structure Solution and Refinement

Structure Solution	Patterson Methods (DIRDIF92 PATTY)
Refinement	Full-matrix least-squares
Function Minimized	$\Sigma\omega(\|Fo\| - \|Fc\|)^2$
Least Squares Weights	$\frac{1}{\sigma^2(Fo)} = \frac{4Fo^2}{\sigma^2(Fo^2)}$
p-factor	0.000
Anomalous Dispersion	All non-hydrogen atoms
No. Observations (I>3.00σ(I))	3444
No. Variables	308
Reflection/Parameter Ratio	11.18
Residuals: R; Rw	0.037 ; 0.034
Goodness of Fit Indicator	1.64
Max Shift/Error in Final Cycle	0.0003

D.1.3 X-ray Crystallographic Analysis of {[(PPr$^i_2$CH$_2$SiMe$_2$)$_2$N]Zr(OAr*}$_2$(μ-N$_2$), 2.12a continued

Table II. Atomic coordinates and B_{eq} (continued)

atom	x	y	z	B_{eq}
C(17)	-0.2603(5)	0.1400(4)	0.1246(3)	7.7(2)
C(18)	-0.3433(4)	0.2603(4)	0.1430(3)	8.4(2)
C(19)	0.0193(4)	0.0845(3)	0.1354(2)	4.2(1)
C(20)	-0.0447(4)	0.0387(3)	0.1614(2)	5.1(2)
C(21)	-0.0655(5)	-0.0316(4)	0.1412(3)	7.1(2)
C(22)	-0.0240(6)	-0.0571(4)	0.0964(3)	7.8(2)
C(23)	0.0371(5)	-0.0118(4)	0.0705(2)	6.2(2)
C(24)	0.0593(4)	0.0599(3)	0.0895(2)	4.4(1)
C(25)	-0.0951(5)	0.0653(4)	0.2091(2)	6.9(2)
C(26)	0.1240(4)	0.1096(3)	0.0594(2)	6.2(2)

$$B_{eq} = \frac{8}{3}\pi^2(U_{11}(aa^*)^2 + U_{22}(bb^*)^2 + U_{33}(cc^*)^2 + 2U_{12}aa^*bb^*\cos\gamma + 2U_{13}aa^*cc^*\cos\beta + 2U_{23}bb^*cc^*\cos\alpha)$$

Table III. Bond Lengths(Å)*

atom	atom	distance	atom	atom	distance
Zr(1)	P(1)	2.818(1)	Zr(1)	P(2)	2.846(1)
Zr(1)	O(1)	2.020(3)	Zr(1)	N(1)	2.211(3)
Zr(1)	N(2)	2.034(4)	Zr(1)	N(2)'	2.082(4)
P(1)	C(1)	1.824(5)	P(1)	C(7)	1.848(6)
P(1)	C(8)	1.851(6)	P(2)	C(2)	1.813(5)
P(2)	C(13)	1.844(5)	P(2)	C(14)	1.852(6)
Si(1)	N(1)	1.718(4)	Si(1)	C(1)	1.890(5)
Si(1)	C(3)	1.878(6)	Si(1)	C(4)	1.870(6)
Si(2)	N(1)	1.720(4)	Si(2)	C(2)	1.887(5)
Si(2)	C(5)	1.861(6)	Si(2)	C(6)	1.881(5)
O(1)	C(19)	1.331(6)	N(2)	N(2)'	1.528(7)

P(2)	C(14)	C(18)	116.7(4)	C(17)	C(14)	C(18)	110.5(5)
O(1)	C(19)	C(20)	120.1(5)	O(1)	C(19)	C(24)	119.8(5)

Table IV. Bond Angles(°)

atom	atom	atom	angle	atom	atom	atom	angle
P(1)	Zr(1)	P(2)	145.54(4)	P(1)	Zr(1)	O(1)	87.6(1)
P(1)	Zr(1)	N(1)	79.4(1)	P(1)	Zr(1)	N(2)	128.10(10)
P(1)	Zr(1)	N(2)'	85.10(10)	P(2)	Zr(1)	O(1)	88.1(1)
P(2)	Zr(1)	N(1)	74.5(1)	P(2)	Zr(1)	N(2)	82.89(10)
P(2)	Zr(1)	N(2)'	126.19(10)	O(1)	Zr(1)	N(1)	123.0(1)
O(1)	Zr(1)	N(2)	119.8(1)	O(1)	Zr(1)	N(2)'	119.1(1)
N(1)	Zr(1)	N(2)	111.4(1)	N(1)	Zr(1)	N(2)'	114.7(1)
N(2)	Zr(1)	N(2)'	43.6(2)	Zr(1)	P(1)	C(1)	101.3(2)
Zr(1)	P(1)	C(7)	115.1(2)	Zr(1)	P(1)	C(8)	120.1(2)
C(1)	P(1)	C(7)	106.3(3)	C(1)	P(1)	C(8)	104.9(3)
C(7)	P(1)	C(8)	107.6(3)	Zr(1)	P(2)	C(2)	93.3(2)
Zr(1)	P(2)	C(13)	115.8(2)	Zr(1)	P(2)	C(14)	124.4(2)
C(2)	P(2)	C(13)	102.3(2)	C(2)	P(2)	C(14)	106.5(3)
C(13)	P(2)	C(14)	109.9(3)	N(1)	Si(1)	C(1)	110.3(2)
N(1)	Si(1)	C(3)	115.4(2)	N(1)	Si(1)	C(4)	112.3(2)
C(1)	Si(1)	C(3)	107.7(3)	C(1)	Si(1)	C(4)	105.4(2)
C(3)	Si(1)	C(4)	105.1(3)	N(1)	Si(2)	C(2)	108.2(2)
N(1)	Si(2)	C(5)	112.4(2)	N(1)	Si(2)	C(6)	115.4(2)
C(2)	Si(2)	C(5)	107.7(2)	C(2)	Si(2)	C(6)	106.3(2)
C(5)	Si(2)	C(6)	106.4(3)	Zr(1)	O(1)	C(19)	161.5(4)
Zr(1)	N(1)	Si(1)	123.9(2)	Zr(1)	N(1)	Si(2)	116.4(2)
Si(1)	N(1)	Si(2)	119.7(2)	Zr(1)	N(2)	Zr(1)'	130.7(2)
Zr(1)	N(2)	N(2)'	69.9(2)	Zr(1)'	N(2)	N(2)'	66.5(2)

D.1.4 X-ray Crystallographic Analysis of $Zr(\eta^5\text{-}C_5H_5)Ph[N(SiMe_2CH_2PPr^i_2)_2]$, 4.4

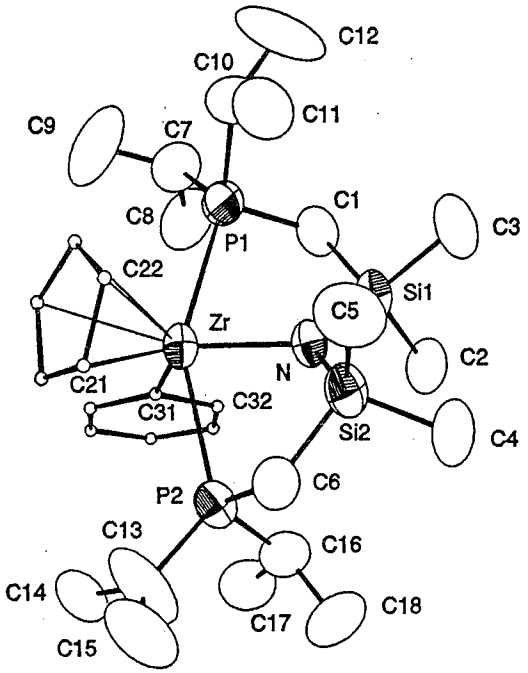

Space Group and Cell Dimensions Triclinic, P -1
a 9.0970(10) b 10.512(3) c 19.079(5)
alpha 90.90(3) beta 95.890(10) gamma 107.390(20)
Volume 1729.8(7)Å^3

Empirical formula : $ZrSi_2P_2NC_{29}H_{54}$

Cell dimensions were obtained from 24 reflections with 2Theta angle in the range 28.00 - 36.00 degrees.

Crystal dimensions : 0.30 X 0.40 X 0.50 mm

FW = 626.08 Z = 2 F(000) = 660

Dcalc 1.202Mg.m-3, mu 0.49mm-1, lambda 0.70930Å, 2Theta(max) 44.9

The intensity data were collected on a Nonius diffractometer, using the omega scan mode.
The h,k,l ranges are :-- -9 9, 0 11, -20 20
No. of reflections measured 7929
No. of unique reflections 4512
No. of reflections with Inet > 3.0sigma(Inet) 3361
Absorption corrections were made.
The minimum and maximum transmission factors are 0.831 and 1.00.

The last least squares cycle was calculated with
89 atoms, 316 parameters and 3361 out of 4512 reflections.
Weights based on counting-statistics were used.
The weight modifier K in KFo^2 is 0.000050

The residuals are as follows :--
For significant reflections, RF 0.036, Rw 0.038 GoF 2.67
For all reflections, RF 0.036, Rw 0.038.
where RF = Sum(Fo-Fc)/Sum(Fo),
Rw = Sqrt[Sum(w(Fo-Fc)^2)/Sum(wFo^2)] and
GoF = Sqrt[Sum(w(Fo-Fc)^2)/(No. of reflns - No. of params.)]
The maximum shift/sigma ratio was 0.008.

In the last D-map, the deepest hole was -0.280e/Å^3,
and the highest peak 0.240e/Å^3.

D.1.4 X-ray Crystallographic Analysis of $Zr(\eta^5\text{-}C_5H_5)Ph[N(SiMe_2CH_2PPr^i_2)_2]$, 4.4 continued

Atomic Parameters x,y,z and B_{iso}

	x	y	z	B_{iso}
Zr	0.92623(5)	0.33970(4)	0.26186(3)	3.716(20)
P1	1.15726(14)	0.35823(12)	0.37245(7)	4.38 (6)
P2	0.78042(13)	0.23576(11)	0.12882(7)	4.45 (6)
Si1	1.12160(14)	0.10076(11)	0.28202(8)	4.29 (7)
Si2	0.79039(15)	0.00660(12)	0.22164(8)	4.78 (7)
N	0.9521 (3)	0.1357 (3)	0.25364(18)	3.75 (18)
C1	1.2555 (5)	0.2491 (4)	0.3364 (3)	4.8 (3)
C2	1.2305 (5)	0.0727 (4)	0.2077 (3)	5.6 (3)
C3	1.0972 (6)	-0.0516 (5)	0.3352 (3)	6.8 (3)
C4	0.8312 (6)	-0.1360 (4)	0.1759 (3)	7.2 (3)
C5	0.6687 (6)	-0.0675 (5)	0.2911 (3)	7.6 (3)
C6	0.6673 (5)	0.0731 (4)	0.1552 (3)	4.8 (3)
C7	1.3134 (6)	0.5149 (5)	0.4041 (3)	6.2 (3)
C8	1.4275 (6)	0.5681 (5)	0.3529 (3)	7.3 (3)
C9	1.2491 (7)	0.6189 (6)	0.4319 (4)	10.1 (4)
C10	1.0984 (6)	0.2909 (5)	0.4587 (3)	6.4 (3)
C11	0.9545 (7)	0.1719 (5)	0.4509 (3)	7.6 (3)
C12	1.2291 (8)	0.2657 (8)	0.5079 (4)	11.9 (5)
C13	0.6458 (7)	0.3020 (5)	0.0723 (4)	10.7 (4)
C14	0.7095 (6)	0.4480 (5)	0.0582 (3)	6.4 (3)
C15	0.4989 (7)	0.2321 (6)	0.0474 (4)	10.1 (4)
C16	0.9058 (6)	0.1930 (5)	0.0669 (3)	5.7 (3)
C17	0.9991 (6)	0.3133 (5)	0.0288 (3)	7.3 (3)
C18	0.8272 (7)	0.0788 (5)	0.0136 (3)	8.4 (4)
C21	0.8565 (6)	0.5348 (4)	0.3143 (3)	5.8 (3)
C22	0.8293 (6)	0.4390 (5)	0.3639 (3)	6.7 (3)
C23	0.7098 (6)	0.3301 (5)	0.3366 (3)	7.7 (4)
C24	0.6606 (5)	0.3568 (5)	0.2681 (3)	6.8 (3)
C25	0.7543 (5)	0.4861 (5)	0.2539 (3)	6.0 (3)
C31	1.1072 (4)	0.4931 (4)	0.20838(22)	3.63 (21)
C32	1.2228 (5)	0.4462 (4)	0.18375(25)	4.62 (25)
C33	1.3475 (5)	0.5248 (5)	0.1532 (3)	5.6 (3)
C34	1.3640 (5)	0.6560 (5)	0.1454 (3)	6.4 (3)
C35	1.2556 (6)	0.7081 (4)	0.1664 (3)	6.4 (3)
C36	1.1309 (5)	0.6299 (4)	0.1972 (3)	5.3 (3)

B_{iso} is the Mean of the Principal Axes of the Thermal Ellipsoid

Interatomic Distances and Angles

Distances (Å)

Zr-P(1)	2.7819(14)	Si(2)-C(5)	1.846(6)
Zr-P(2)	2.7843(16)	Si(2)-C(6)	1.885(5)
Zr-N	2.231(3)	C(7)-C(8)	1.490(8)
Zr-C(21)	2.540(4)	C(7)-C(9)	1.498(8)
Zr-C(22)	2.549(5)	C(10)-C(11)	1.508(7)
Zr-C(23)	2.526(5)	C(10)-C(12)	1.527(8)
Zr-C(24)	2.491(4)	C(13)-C(14)	1.509(7)
Zr-C(25)	2.497(4)	C(13)-C(15)	1.350(8)
Zr-C(31)	2.272(4)	C(16)-C(17)	1.537(7)
P(1)-C(1)	1.817(5)	C(16)-C(18)	1.512(7)
P(1)-C(7)	1.868(5)	C(21)-C(22)	1.378(7)
P(1)-C(10)	1.868(5)	C(21)-C(25)	1.390(7)
P(2)-C(6)	1.821(4)	C(22)-C(23)	1.373(8)
P(2)-C(13)	1.846(5)	C(23)-C(24)	1.397(9)
P(2)-C(16)	1.861(5)	C(24)-C(25)	1.420(7)
Si(1)-N	1.726(3)	C(31)-C(32)	1.405(6)
Si(1)-C(1)	1.883(5)	C(31)-C(36)	1.412(6)
Si(1)-C(2)	1.878(5)	C(32)-C(33)	1.378(6)
Si(1)-C(3)	1.878(5)	C(33)-C(34)	1.355(7)
Si(2)-N	1.725(3)	C(34)-C(35)	1.352(8)
Si(2)-C(4)	1.871(5)	C(35)-C(36)	1.380(7)

Angles (°)

P(1)-Zr-P(2)	150.09(4)	C(4)-Si(2)-C(6)	106.63(23)
P(1)-Zr-N	79.47(9)	C(5)-Si(2)-C(6)	107.32(23)
P(1)-Zr-C(31)	87.04(11)	Zr-N-Si(1)	123.21(16)
P(2)-Zr-N	75.01(10)	Zr-N-Si(2)	117.54(16)
P(2)-Zr-C(24)	78.50(13)	Si(1)-N-Si(2)	119.15(17)
P(2)-Zr-C(25)	85.80(12)	P(1)-C(1)-Si(1)	113.90(22)
P(2)-Zr-C(31)	88.57(11)	P(2)-C(6)-Si(2)	109.65(22)
N-Zr-C(24)	117.57(14)	P(1)-C(7)-C(8)	114.5(4)
N-Zr-C(25)	149.07(14)	P(1)-C(7)-C(9)	112.0(4)
N-Zr-C(31)	112.60(13)	C(8)-C(7)-C(9)	112.6(4)
Zr-P(1)-C(1)	99.87(16)	P(1)-C(10)-C(11)	113.1(4)
Zr-P(1)-C(7)	124.83(17)	P(1)-C(10)-C(12)	114.3(4)
Zr-P(1)-C(10)	118.31(17)	C(11)-C(10)-C(12)	112.0(4)
C(1)-P(1)-C(7)	105.65(22)	P(2)-C(13)-C(14)	114.4(4)
C(1)-P(1)-C(10)	106.44(22)	P(2)-C(13)-C(15)	125.0(4)
C(7)-P(1)-C(10)	100.10(23)	C(14)-C(13)-C(15)	120.5(5)
Zr-P(2)-C(6)	97.73(16)	P(2)-C(16)-C(17)	113.7(3)
Zr-P(2)-C(13)	125.97(24)	P(2)-C(16)-C(18)	116.1(4)
Zr-P(2)-C(16)	115.96(16)	C(17)-C(16)-C(18)	109.3(4)
C(6)-P(2)-C(13)	106.77(22)	C(22)-C(21)-C(25)	108.7(4)
C(6)-P(2)-C(16)	103.08(21)	C(21)-C(22)-C(23)	109.1(5)
C(13)-P(2)-C(16)	104.4(3)	C(22)-C(23)-C(24)	108.0(5)
N-Si(1)-C(1)	108.72(17)	C(23)-C(24)-C(25)	107.5(4)
N-Si(1)-C(2)	113.18(20)	C(21)-C(25)-C(24)	106.7(5)
N-Si(1)-C(3)	115.19(20)	Zr-C(31)-C(32)	114.9(3)
C(1)-Si(1)-C(2)	105.86(21)	Zr-C(31)-C(36)	132.5(3)
C(1)-Si(1)-C(3)	108.66(23)	C(32)-C(31)-C(36)	112.5(4)
C(2)-Si(1)-C(3)	104.75(23)	C(31)-C(32)-C(33)	124.1(4)
N-Si(2)-C(4)	115.13(20)	C(32)-C(33)-C(34)	120.0(4)
N-Si(2)-C(5)	112.86(22)	C(33)-C(34)-C(35)	119.5(4)
N-Si(2)-C(6)	108.72(17)	C(34)-C(35)-C(36)	120.7(4)
C(4)-Si(2)-C(5)	105.7(3)	C(31)-C(36)-C(35)	123.2(4)

D.1.5 X-ray Crystallographic Analysis of $Zr(\eta^5\text{-}C_5H_5)CH_2SiMe_3[N(SiMe_2CH_2PPr^i_2)_2]$, 4.8

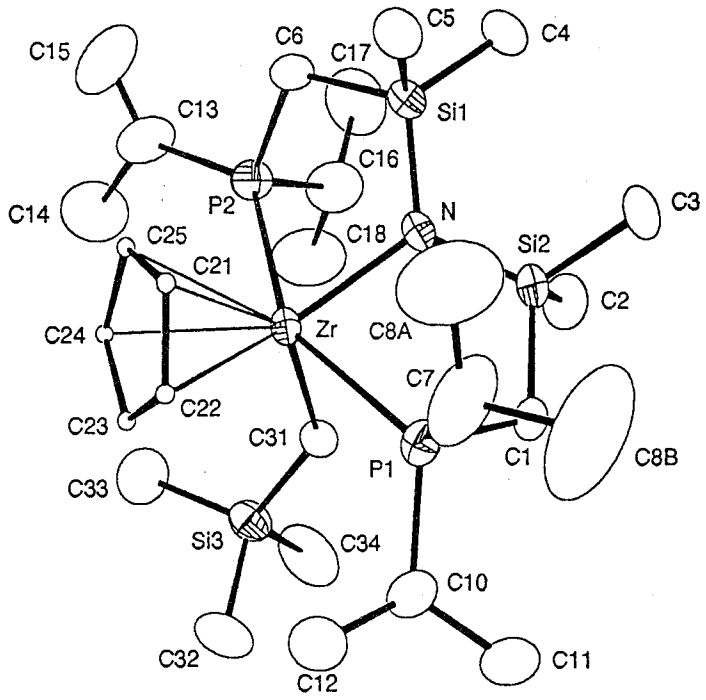

Space Group and Cell Dimensions Monoclinic, P $2_1/c$
a 10.0813(19) b 17.7883(18) c 20.414(4)
beta 100.243(22)
Volume 3602.5(10)Å^3

Empirical formula : Zr Si_3 P_2 N C_{27} H_{60}

Cell dimensions were obtained from 24 reflections with 2Theta angle in the range 37.00 - 44.00 degrees.
Crystal dimensions : 0.40 X 0.60 X 0.90 mm
FW = 636.21 Z = 4 F(000) = 1364
D_{calc} 1.17Mg.m-3, mu 0.50mm-1, λ 0.70930Å, 2Theta(max) 45.0
The intensity data were collected on a Nonius CAD-4 diffractometer, using the omega scan mode.
The h,k,l ranges used during structure solution and refinement are :--
Hmin,max -10 10; Kmin,max 0 19; Lmin,max 0 21
No. of reflections measured 4831
No. of unique reflections 4686
No. of reflections with I_{act} > 3.0sigma(I_{act}) 3647
Merging R-value on intensities 0.026
Absorption corrections were made.
The minimum and maximum transmission factors are 0.887 and 0.999.
The last least squares cycle was calculated with
88 atoms, 319 parameters and 3647 out of 4686 reflections.
Weights based on counting-statistics were used.
The weight modifier K in KFo^2 is 0.000006
The residuals are as follows :--
For significant reflections, RF 0.039, Rw 0.043 GoF 4.37
For all reflections, RF 0.039, Rw 0.043.
where RF = Sum(Fo-Fc)/Sum(Fo),
Rw = Sqrt[Sum(w(Fo-Fc)^2)/Sum(wFo^2)] and
GoF = Sqrt[Sum(w(Fo-Fc)^2)/(No. of reflns - No. of params.)]
The maximum shift/sigma ratio was 0.000.
In the last D-map, the deepest hole was -0.330e/Å^3,
and the highest peak 0.400e/Å^3.

D.1.5 X-ray Crystallographic Analysis of $Zr(\eta^5\text{-}C_5H_5)CH_2SiMe_3[N(SiMe_2CH_2PPr^i_2)_2]$, 4.8 continued

Atomic Parameters x,y,z and B_{iso}

	x	y	z	B_{iso}
Zr	0.10188(5)	0.78205(3)	0.16239(3)	2.987(22)
P1	-0.05298(14)	0.71414(9)	0.05109(7)	4.02 (7)
P2	0.30818(15)	0.77622(9)	0.27798(8)	4.48 (7)
Si1	0.14827(17)	0.62939(9)	0.26445(8)	4.27 (8)
Si2	0.15093(18)	0.59864(9)	0.12111(9)	4.45 (9)
Si3	0.31782(17)	0.89647(10)	0.06021(9)	4.87 (8)
N	0.1386 (4)	0.66093(21)	0.18376(20)	3.35 (21)
C1	0.0631 (5)	0.6390 (3)	0.0391 (3)	3.9 (3)
C2	0.3286 (7)	0.5826 (4)	0.1106 (3)	7.3 (4)
C3	0.0751 (8)	0.5041 (3)	0.1301 (3)	7.9 (5)
C4	0.2493 (6)	0.5413 (3)	0.2865 (3)	5.9 (3)
C5	-0.0214 (6)	0.6121 (3)	0.2851 (3)	5.8 (3)
C6	0.2265 (6)	0.7061 (3)	0.3227 (3)	4.8 (3)
C7	-0.2113 (9)	0.6666 (7)	0.0598 (6)	10.1 (6)
C8A	-0.2234 (23)	0.6417 (15)	0.1234 (9)	15.6 (15)
C8B	-0.2560 (10)	0.5977 (7)	0.0130 (5)	20.4 (10)
C8C	-0.3241 (23)	0.7018 (12)	0.0710 (20)	19.7 (24)
C10	-0.0813 (8)	0.7629 (4)	-0.0318 (3)	8.2 (4)
C11	-0.1079 (8)	0.7163 (4)	-0.0930 (3)	8.8 (5)
C12	-0.1504 (9)	0.8325 (5)	-0.0358 (4)	10.0 (5)
C13	0.3682 (9)	0.8488 (5)	0.3424 (4)	9.3 (5)
C14	0.4163 (11)	0.9197 (5)	0.3189 (5)	14.0 (7)
C15	0.3390 (13)	0.8486 (6)	0.4024 (5)	16.3 (9)
C16	0.4630 (6)	0.7252 (5)	0.2631 (4)	7.4 (4)
C17	0.5365 (8)	0.6820 (5)	0.3200 (5)	11.1 (6)
C18	0.5526 (7)	0.7767 (6)	0.2327 (4)	11.3 (6)
C21	-0.1028 (7)	0.8296 (4)	0.2031 (5)	6.8 (5)
C22	-0.1120 (7)	0.8626 (4)	0.1410 (4)	6.2 (4)
C23	-0.0059 (7)	0.9115 (3)	0.1426 (4)	5.4 (4)
C24	0.0705 (6)	0.9094 (3)	0.2061 (4)	5.4 (4)
C25	0.0108 (8)	0.8591 (4)	0.2444 (3)	5.8 (4)
C31	0.2534 (5)	0.8088 (3)	0.0912 (3)	3.9 (3)
C32	0.1950 (7)	0.9403 (4)	-0.0077 (4)	7.6 (4)
C33	0.3617 (8)	0.9709 (4)	0.1235 (4)	9.1 (5)
C34	0.4712 (7)	0.8801 (4)	0.0223 (4)	9.7 (5)

B_{iso} is the Mean of the Principal Axes of the Thermal Ellipsoid

Interatomic Distances (Å) and Angles (°)
$Pr^i_2PCH_2SiMe_2)_2N]Cp(CH_2SiMe_3)Zr$

Distances

Zr-P1	2.7923(16)	Si2-C2	1.864(7)
Zr-P2	2.8563(17)	Si2-C3	1.870(6)
Zr-N	2.216(4)	Si3-C31	1.843(5)
Zr-C21	2.505(6)	Si3-C32	1.858(7)
Zr-C22	2.561(6)	Si3-C33	1.848(7)
Zr-C23	2.549(5)	Si3-C34	1.871(7)
Zr-C24	2.475(5)	C7-C8A	1.396(22)
Zr-C25	2.463(6)	C7-C8B	1.571(13)
Zr-C31	2.337(5)	C7-C8C	1.353(23)
P1-C1	1.821(5)	C8A-C8C	1.71(5)
P1-C7	1.842(8)	C10-C11	1.483(10)
P1-C10	1.877(7)	C10-C12	1.416(10)
P2-C6	1.826(5)	C13-C14	1.463(11)
P2-C13	1.866(7)	C13-C15	1.308(13)
P2-C16	1.876(7)	C16-C17	1.477(11)
Si1-N	1.726(4)	C16-C18	1.497(11)
Si1-C4	1.879(6)	C21-C22	1.385(13)
Si1-C5	1.858(6)	C21-C25	1.398(12)
Si1-C6	1.889(6)	C22-C23	1.375(12)
Si2-N	1.713(4)	C23-C24	1.385(11)
Si2-C1	1.890(5)	C24-C25	1.393(11)

Zr-Cent 2.2162(5)

Angles

P1-Zr-P2	151.17(5)	C1-Si2-C3	107.0(3)
P1-Zr-N	77.83(11)	C2-Si2-C3	107.0(3)
P1-Zr-C21	92.39(22)	C31-Si3-C32	112.5(3)
P1-Zr-C24	126.89(17)	C31-Si3-C33	114.9(3)
P1-Zr-C25	124.85(19)	C31-Si3-C34	112.2(3)
P1-Zr-C31	85.13(13)	C32-Si3-C33	105.4(4)
P2-Zr-N	74.37(11)	C32-Si3-C34	104.3(3)
P2-Zr-C21	105.06(24)	C33-Si3-C34	106.7(4)
P2-Zr-C24	81.75(17)	Zr-N-Si1	118.88(21)
P2-Zr-C25	76.33(17)	Zr-N-Si2	120.90(21)
P2-Zr-C31	93.47(13)	Si1-N-Si2	120.18(23)
N-Zr-C21	112.41(20)	P1-C1-Si2	111.8(3)
N-Zr-C24	147.80(22)	P2-C6-Si1	110.7(3)
N-Zr-C25	118.45(20)	P1-C7-C8A	117.1(9)
N-Zr-C31	102.47(16)	P1-C7-C8B	117.3(6)
C21-Zr-C24	53.55(22)	P1-C7-C8C	124.9(11)
C21-Zr-C25	32.7(3)	C8A-C7-C8B	104.7(12)
C21-Zr-C31	143.69(23)	C8A-C7-C8C	77.0(23)
C24-Zr-C25	32.8(3)	C8B-C7-C8C	107.8(12)
C24-Zr-C31	100.21(21)	C7-C8A-C8C	50.4(14)
P1-Zr-Cent	103.95(4)	N-Zr-Cent	139.47(10)
P2-Zr-Cent	102.08(4)	C31-Zr-Cent	118.05(13)

D.1.6 X-ray Crystallographic Analysis of $Zr(\eta^5\text{-}C_5H_5)(\eta^2\text{-}BH_4)[N(SiMe_2CH_2PPr^i_2)_2]$, 4.17

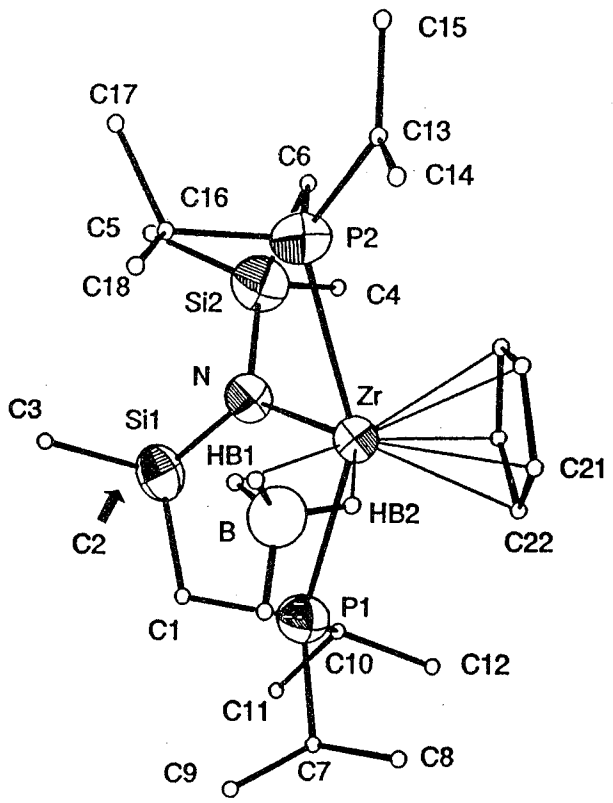

Space Group and Cell Dimensions Monoclinic, I 2/a
a 17.1426(19) b 10.8752(14) c 33.754(4)
beta 90.804(9)
Volume 6292.1(13)Å^3

Empirical formula : $ZrP_2Si_2NC_{23}H_{53}\beta$

Cell dimensions were obtained from 25 reflections with 2Theta angle in the range 30.00 - 40.00 degrees.

Crystal dimensions : 0.20 X 0.30 X 0.80 mm

FW = 553.02 Z = 8 F(000) = 2366

Dcalc 1.168Mg.m-3, mu 0.53mm-1, lambda 0.70930A, 2Theta(max) 47.9

The intensity data were collected on a Siemens P3/PC diffractometer, using the omega scan mode.
The h,k,l ranges are :-- -19 19, 0 12, 0 38
No. of reflections measured 5096
No. of unique reflections 4903
No. of reflections with Inet > 3.0sigma(Inet) 3370
An empirical absorption correction was made .

The last least squares cycle was calculated with
83 atoms, 287 parameters and 3370 out of 4903 reflections.
Weights based on counting-statistics were used.
The weight modifier K in KFo^2 is 0.000100

The residuals are as follows :--
For significant reflections, RF 0.041, Rw 0.045 GoF 2.00
For all reflections, RF 0.041, Rw 0.045.
where RF = Sum(Fo-Fc)/Sum(Fo),
Rw = Sqrt[Sum(w(Fo-Fc)^2)/Sum(wFo^2)] and
GoF = Sqrt[Sum(w(Fo-Fc)^2)/(No. of reflns - No. of params.)]
The maximum shift/sigma ratio was 0.001.

In the last D-map, the deepest hole was -0.460e/Å^3,
and the highest peak 0.470e/Å^3.

Hydrogen atoms were treated as follows:
Located and refined with isotropic thermal parameters: BH_4^-
Located and fixed with isotropic thermal parameters: CH_3 groups
Calculated (D_{C-H} = 1.08Å) and fixed with isotropic thermal parameters: CH_2, CH groups.

D.1.6 X-ray Crystallographic Analysis of $Zr(\eta^5\text{-}C_5H_5)(\eta^2\text{-}BH_4)[N(SiMe_2CH_2PPr^i_2)_2]$, 4.17

continued

Atomic Parameters x,y,z and B_{iso}

	x	y	z	B_{iso}
Zr	0.61108(3)	0.31118(4)	0.152689(14)	3.402(19)
P1	0.55982(9)	0.21150(14)	0.08063 (4)	4.70 (7)
P2	0.63355(8)	0.52057(14)	0.19895 (4)	4.24 (6)
Si1	0.58831(9)	0.48788(15)	0.06837 (4)	4.44 (7)
Si2	0.72058(8)	0.55335(15)	0.12248 (4)	4.61 (7)
N	0.64155(21)	0.4612 (4)	0.11086 (11)	3.61 (17)
C1	0.5213 (3)	0.3529 (5)	0.05972 (15)	4.8 (3)
C2	0.6489 (4)	0.5102 (7)	0.02310 (17)	7.5 (4)
C3	0.5216 (3)	0.6245 (6)	0.07138 (19)	6.4 (3)
C4	0.8147 (3)	0.4838 (7)	0.10542 (19)	6.9 (4)
C5	0.7164 (4)	0.7129 (6)	0.10101 (20)	7.6 (4)
C6	0.7254 (3)	0.5741 (5)	0.17823 (15)	4.64 (25)
C7	0.4839 (4)	0.0908 (7)	0.07280 (23)	8.3 (4)
C8	0.4825 (5)	-0.0037 (8)	0.10478 (25)	10.3 (5)
C9	0.4064 (4)	0.1322 (8)	0.0618 (3)	11.3 (6)
C10	0.6388 (4)	0.1675 (6)	0.04443 (17)	6.6 (3)
C11	0.6146 (5)	0.1785 (8)	0.00115 (22)	9.7 (5)
C12	0.6717 (5)	0.0368 (8)	0.05227 (21)	9.4 (5)
C13	0.6524 (5)	0.5156 (7)	0.25340 (18)	8.7 (4)
C14	0.5872 (4)	0.4572 (7)	0.27576 (18)	7.6 (4)
C15	0.6991 (4)	0.6005 (8)	0.27316 (18)	8.2 (4)
C16	0.5645 (3)	0.6473 (5)	0.18681 (18)	5.6 (3)
C17	0.5930 (4)	0.7775 (6)	0.19446 (23)	7.5 (4)
C18	0.4843 (4)	0.6311 (6)	0.2042 (3)	9.1 (5)
C21	0.7285 (4)	0.1789 (6)	0.14958 (19)	5.9 (3)
C22	0.6684 (4)	0.0957 (6)	0.15739 (19)	5.9 (3)
C23	0.6403 (4)	0.1179 (6)	0.19428 (20)	6.0 (3)
C24	0.6799 (4)	0.2159 (6)	0.21001 (17)	6.2 (3)
C25	0.7365 (3)	0.2544 (6)	0.18292 (23)	6.1 (3)
B	0.4627 (4)	0.3106 (8)	0.16984 (23)	5.0 (3)
HB1	0.491 (3)	0.382 (5)	0.1515 (14)	5.8 (13)
HB2	0.508 (3)	0.252 (4)	0.1788 (13)	4.8 (12)
HB3	0.434 (3)	0.354 (5)	0.1927 (15)	6.5 (15)
HB4	0.420 (3)	0.246 (6)	0.1494 (17)	8.2 (15)

B_{iso} is the Mean of the Principal Axes of the Thermal Ellipsoid

D.1.6 X-ray Crystallographic Analysis of $Zr(\eta^5\text{-}C_5H_5)(\eta^2\text{-}BH_4)[N(SiMe_2CH_2PPr^i_2)_2]$, 4.17 continued

Distances

Zr-P(1)	2.7933(15)	C(12)-H(12B)	1.117(9)	C(9)-H(9A)	1.126(8)
Zr-P(2)	2.7849(15)	C(12)-H(12C)	1.110(7)	C(9)-H(9B)	1.100(10)
Zr-N	2.224(4)	C(13)-C(14)	1.499(9)	C(9)-H(9C)	1.099(9)
Zr-C(21)	2.477(5)	C(13)-C(15)	1.386(10)	C(10)-C(11)	1.518(10)
Zr-C(22)	2.545(6)	C(13)-H(13)	1.042(9)	C(10)-C(12)	1.551(10)
Zr-C(23)	2.573(6)	C(14)-H(14A)	0.986(6)	C(10)-H(10)	1.011(7)
Zr-C(24)	2.479(5)	C(14)-H(14B)	0.974(7)	C(10)-H(12B)	1.782(7)
Zr-C(25)	2.446(5)	C(14)-H(14C)	1.147(8)	C(11)-H(11A)	0.999(8)
Zr-B	2.617(7)	C(15)-H(13)	1.848(8)	C(11)-H(11B)	1.158(8)
Zr-HB(1)	2.19(5)	C(15)-H(15A)	1.032(7)	C(11)-H(11C)	1.100(9)
Zr-HB(2)	2.09(4)	C(15)-H(15B)	1.040(6)	C(12)-H(12A)	0.936(7)
P(1)-C(1)	1.813(6)	C(15)-H(15C)	1.134(8)		
P(1)-C(7)	1.866(7)	C(16)-C(17)	1.519(8)	H(12A)-H(12C)	1.71165(19)
P(1)-C(10)	1.898(6)	C(16)-C(18)	1.513(9)	H(14A)-H(14B)	1.50581(15)
P(2)-C(6)	1.826(5)	C(16)-H(16)	1.019(6)	H(14A)-H(14C)	1.47993(13)
P(2)-C(13)	1.862(6)	C(17)-H(17A)	1.122(8)	H(14B)-H(14C)	1.46254(18)
P(2)-C(16)	1.859(6)	C(17)-H(17B)	0.970(7)	H(15A)-H(15C)	1.66048(17)
Si(1)-N	1.714(4)	C(17)-H(17C)	0.755(7)	H(15B)-H(15C)	1.66109(14)
Si(1)-C(1)	1.884(6)	C(18)-H(18A)	1.119(8)	H(17A)-H(17B)	1.70590(17)
Si(1)-C(2)	1.876(6)	C(18)-H(18B)	0.865(7)	H(17A)-H(17C)	1.58234(18)
Si(1)-C(3)	1.878(6)	C(18)-H(18C)	1.184(8)	H(17B)-H(17C)	1.37468(14)
Si(2)-N	1.726(4)	C(21)-C(22)	1.399(10)	H(18A)-H(18B)	1.70246(17)
Si(2)-C(4)	1.879(6)	C(21)-C(25)	1.399(10)	H(18B)-H(18C)	1.64798(15)
Si(2)-C(5)	1.882(7)	C(21)-H(21)	1.014(6)		
Si(2)-C(6)	1.896(5)	C(22)-C(23)	1.363(10)		
Si(2)-H(4C)	2.2679(15)	C(22)-H(22)	1.036(6)		
C(1)-H(1A)	1.009(5)	C(23)-C(24)	1.367(10)		
C(1)-H(1B)	1.021(5)	C(23)-H(23)	1.046(7)		
C(2)-H(2A)	0.940(7)	C(24)-C(25)	1.406(11)		
C(2)-H(2B)	1.017(7)	C(24)-H(24)	1.038(6)		
C(2)-H(2C)	1.066(6)	C(25)-H(25)	1.031(6)		
C(3)-H(3A)	1.010(6)	B-HB(1)	1.12(5)		
C(3)-H(3B)	1.136(7)	B-HB(2)	1.04(5)		
C(3)-H(3C)	0.986(6)	B-HB(3)	1.04(5)		
C(4)-H(4A)	0.969(7)	B-HB(4)	1.22(6)		
C(4)-H(4B)	1.076(6)	HB(1)-HB(2)	1.71(7)		
C(4)-H(4C)	0.969(6)	H(1A)-H(1B)	1.63295(18)		
C(5)-H(5A)	0.879(6)	H(2A)-H(2B)	1.36590(17)		
C(5)-H(5B)	1.028(7)	H(2A)-H(2C)	1.62532(15)		
C(5)-H(5C)	1.140(7)	H(2B)-H(2C)	1.66291(16)		
C(6)-H(6A)	1.007(5)	H(3A)-H(3B)	1.64914(19)		
C(6)-H(6B)	1.023(5)	H(3A)-H(3C)	1.59300(14)		
C(7)-C(8)	1.491(12)	H(4A)-H(4B)	1.55129(18)		
C(7)-C(9)	1.446(11)	H(4B)-H(4C)	1.56897(17)		
C(7)-H(7)	1.017(8)	H(5A)-H(5B)	1.47341(15)		
C(7)-H(9B)	1.853(8)	H(6A)-H(6B)	1.63295(18)		
C(8)-H(8A)	1.001(7)	H(8A)-H(8B)	1.46359(12)		
C(8)-H(8B)	1.059(8)	H(8A)-H(8C)	1.63738(16)		
C(8)-H(8C)	1.161(10)	H(8B)-H(8C)	1.68244(18)		

Angles

P(1)-Zr-P(2)	147.66(5)	H(9A)-C(9)-H(9C)	114.5(7)
P(1)-Zr-N	78.80(10)	H(9B)-C(9)-H(9C)	113.5(7)
P(1)-Zr-C(21)	89.06(17)	P(1)-C(10)-C(11)	114.3(5)
P(1)-Zr-C(24)	131.14(15)	P(1)-C(10)-C(12)	112.4(5)
P(1)-Zr-C(25)	121.96(18)	P(1)-C(10)-H(10)	106.0(4)
P(1)-Zr-HB(1)	80.7(12)	C(11)-C(10)-C(12)	109.3(5)
P(1)-Zr-HB(2)	89.5(13)	C(11)-C(10)-H(10)	106.9(6)
P(2)-Zr-N	74.00(10)	C(12)-C(10)-H(10)	107.5(6)
P(2)-Zr-C(21)	113.10(18)	C(10)-C(11)-H(11A)	105.2(6)
P(2)-Zr-C(24)	81.00(16)	C(10)-C(11)-H(11B)	98.0(6)
P(2)-Zr-C(25)	81.86(17)	C(10)-C(11)-H(11C)	109.2(7)
P(2)-Zr-HB(1)	81.0(13)	H(11A)-C(11)-H(11B)	112.7(8)
P(2)-Zr-HB(2)	97.2(13)	H(11A)-C(11)-H(11C)	115.8(8)
N-Zr-C(21)	101.58(18)	H(11B)-C(11)-H(11C)	113.9(6)
N-Zr-C(24)	133.50(22)	C(10)-C(12)-H(12A)	108.0(7)
N-Zr-C(25)	103.71(20)	C(10)-C(12)-H(12B)	82.1(5)
N-Zr-HB(1)	87.6(14)	C(10)-C(12)-H(12C)	105.5(6)
N-Zr-HB(2)	134.5(14)	H(12A)-C(12)-H(12B)	132.8(8)
C(21)-Zr-C(24)	54.00(21)	H(12A)-C(12)-H(12C)	113.3(8)
C(21)-Zr-C(25)	33.00(24)	H(12B)-C(12)-H(12C)	107.5(6)
C(21)-Zr-HB(1)	164.8(14)	P(2)-C(13)-C(14)	112.9(5)
C(21)-Zr-HB(2)	122.2(14)	P(2)-C(13)-C(15)	123.1(5)
C(24)-Zr-C(25)	33.2(3)	P(2)-C(13)-H(13)	99.0(4)
C(24)-Zr-HB(1)	126.6(13)	C(14)-C(13)-C(15)	118.0(5)
C(24)-Zr-HB(2)	86.5(14)	C(14)-C(13)-H(13)	97.3(6)
C(25)-Zr-HB(1)	156.0(12)	C(15)-C(13)-H(13)	98.1(7)
C(25)-Zr-HB(2)	119.4(14)	C(13)-C(14)-H(14A)	129.4(6)
HB(1)-Zr-HB(2)	47.0(20)	C(13)-C(14)-H(14B)	129.8(6)
Zr-P(1)-C(1)	96.79(17)	C(13)-C(14)-H(14C)	89.2(5)
Zr-P(1)-C(7)	127.37(25)	H(14A)-C(14)-H(14B)	100.4(5)
Zr-P(1)-C(10)	116.08(20)	H(14A)-C(14)-H(14C)	87.5(5)
C(1)-P(1)-C(7)	107.0(3)	H(14B)-C(14)-H(14C)	86.8(6)
C(1)-P(1)-C(10)	102.8(3)	C(13)-C(15)-H(15A)	114.8(6)
C(7)-P(1)-C(10)	103.6(3)	C(13)-C(15)-H(15B)	110.9(6)
Zr-P(2)-C(6)	99.15(17)	C(13)-C(15)-H(15C)	97.4(6)
Zr-P(2)-C(13)	123.4(3)	H(15A)-C(15)-H(15B)	126.9(6)
Zr-P(2)-C(16)	113.58(19)	H(15A)-C(15)-H(15C)	99.9(6)
C(6)-P(2)-C(13)	104.4(3)	H(15B)-C(15)-H(15C)	99.5(6)
C(6)-P(2)-C(16)	103.2(3)	P(2)-C(16)-C(17)	116.8(4)
C(13)-P(2)-C(16)	109.9(3)	P(2)-C(16)-C(18)	114.1(4)

D.1.7 X-ray Crystallographic Analysis of $Zr(\eta^5\text{-}C_5H_5)(\eta^2\text{-}BH_4)(\eta^2\text{-}CHO)\{[N(SiMe_2CH_2PPr^i_2)\text{-}[SiMe_2CH_2(Pr^i_2P{\bullet}BH_3)]\}$, 4.23

Space Group and Cell Dimensions Monoclinic, P 21/c
a 13.303(3) b 9.5813(7) c 27.518(7)
beta 103.42(5)
Volume 3411.8(12)Å^3

Empirical formula : Zr P_2 Si_2 O N C_{24} B_2 H_{57}

Cell dimensions were obtained from 24 reflections with 2θ angle in the range 36.00 - 40.00 degrees.

Crystal dimensions : 0.40 X 0.50 X 0.60 mm

FW = 606.67 Z = 4 F(000) = 1296

D_{calc} 1.18Mg.m-3, μ 0.41mm-1, λ 0.70930A, 2θ(max) 45.0°

The intensity data were collected on a Nonius CAD-4 diffractometer, using the omega scan mode.
The h,k,l ranges used during structure solution and refinement are :--
Hmin,max -14 13; Kmin,max 0 10; Lmin,max 0 29
No. of reflections measured 4680
No. of unique reflections 4447
No. of reflections with $I_{net} > 3.0\text{sigma}(I_{net})$ 3626
Merging R-value on intensities 0.018
Absorption corrections were made.
The minimum and maximum transmission factors are 0.843 and 0.992.

The last least squares cycle was calculated with
90 atoms, 314 parameters and 3626 out of 4447 reflections.
Weights based on counting-statistics were used.
The weight modifier K in KFo^2 is 0.000004

The residuals are as follows :--
For significant reflections, RF 0.038, Rw 0.042 GoF 4.53
For all reflections, RF 0.038, Rw 0.042.
where RF = Sum(Fo-Fc)/Sum(Fo),
Rw = Sqrt[Sum(w(Fo-Fc)^2)/Sum(wFo^2)] and
GoF = Sqrt[Sum(w(Fo-Fc)^2)/(No. of reflns - No. of params.)]
The maximum shift/sigma ratio was 0.005.

In the last D-map, the deepest hole was -0.430e/Å^3,
and the highest peak 0.420e/Å^3.

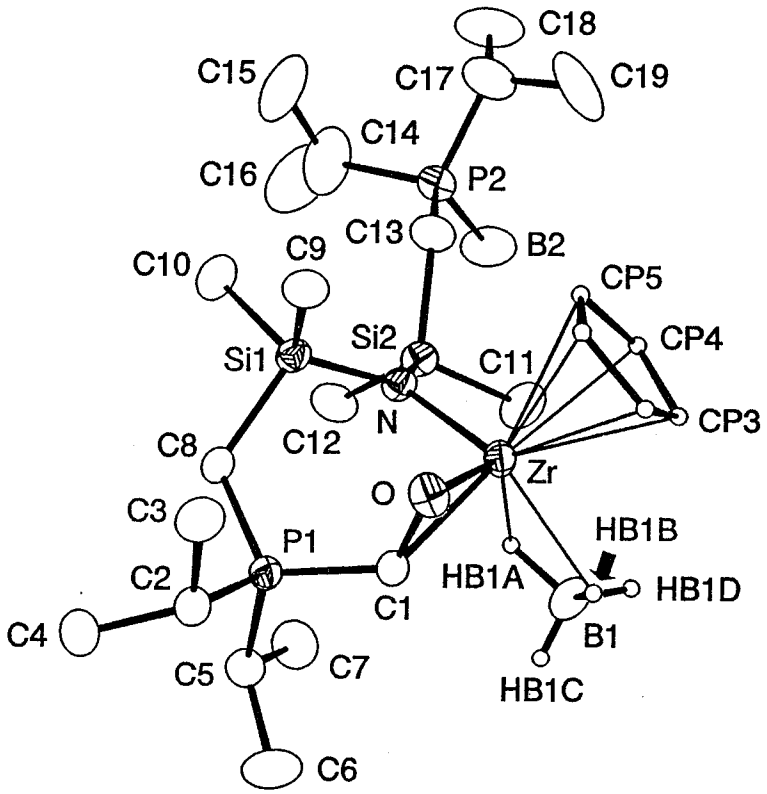

After anisotropic refinement of all non-hydrogen atoms, methyl, formyl, and borane hydrogen atoms were located and fixed via inspection of a difference Fourier map, temperature factors being based upon the atom to which they are bonded. Borate hydrogen atoms were located and refined. Methylene and sp^2 hydrogen atoms were fixed in calculated positions ($d_{C\text{-}H}$=1.08) with temperature factors being based upon the carbon to which they are bonded. All crystallographic calculations were conducted with the PC version of the NRCVAX program package locally implemented on an IBM compatible 80486 computer.

X-ray Crystallographic Analysis of $Zr(\eta^5\text{-}C_5H_5)(\eta^2\text{-}BH_4)(\eta^2\text{-}CHO)\{[N(SiMe_2CH_2PPr^i_2)\text{-}[SiMe_2CH_2(Pr^i_2P{\bullet}BH_3)]]\}$, 4.23 continued

Atomic Parameters x,y,z and B_{iso}

	x	y	z	B_{iso}
Zr	0.59612(4)	0.85878(5)	0.138626(16)	3.334(20)
P1	0.68673(9)	1.11441(11)	0.06067 (4)	2.98 (5)
P2	0.86911(10)	0.92905(15)	0.35646 (5)	3.90 (6)
Si1	0.69846(10)	1.16080(13)	0.17736 (4)	3.33 (6)
Si2	0.80563(11)	0.91100(14)	0.23448 (5)	3.66 (6)
O	0.52305(22)	0.9919 (3)	0.08702 (11)	3.94 (15)
N	0.7087 (3)	0.9827 (3)	0.18801 (12)	3.19 (18)
CP1	0.4318 (5)	0.8835 (6)	0.1695 (3)	8.6 (5)
CP2	0.4185 (4)	0.7701 (8)	0.14117 (22)	7.9 (4)
CP3	0.4837 (7)	0.6694 (6)	0.1645 (3)	12.0 (6)
CP4	0.5338 (5)	0.7264 (9)	0.2075 (3)	12.2 (6)
CP5	0.5037 (6)	0.8542 (9)	0.21052 (23)	11.3 (5)
C1	0.6127 (3)	0.9665 (4)	0.06808 (15)	3.21 (21)
C2	0.6108 (4)	1.2365 (4)	0.01540 (15)	3.49 (22)
C3	0.5224 (4)	1.2977 (5)	0.03501 (18)	4.43 (24)
C4	0.6778 (4)	1.3520 (5)	-0.00019 (19)	5.1 (3)
C5	0.7936 (4)	1.0547 (5)	0.03513 (18)	4.07 (24)
C6	0.7575 (5)	0.9896 (7)	-0.01698 (20)	6.7 (3)
C7	0.8637 (4)	0.9551 (6)	0.07098 (22)	6.0 (3)
C8	0.7387 (3)	1.2072 (4)	0.11764 (16)	3.32 (21)
C9	0.5652 (4)	1.2287 (5)	0.17330 (18)	4.7 (3)
C10	0.7844 (4)	1.2739 (5)	0.22539 (18)	5.6 (3)
C11	0.8093 (4)	0.7158 (5)	0.23357 (20)	5.9 (3)
C12	0.9364 (4)	0.9669 (6)	0.22802 (19)	5.4 (3)
C13	0.7767 (4)	0.9597 (5)	0.29700 (16)	4.39 (25)
C14	0.9470 (5)	1.0882 (7)	0.3665 (3)	9.6 (5)
C15	0.8917 (6)	1.2176 (7)	0.3771 (3)	10.0 (5)
C16	1.0457 (7)	1.0849 (11)	0.3820 (5)	19.5 (9)
C17	0.7898 (4)	0.9284 (7)	0.40251 (19)	6.3 (3)
C18	0.8558 (6)	0.9172 (8)	0.45659 (21)	9.3 (5)
C19	0.7094 (5)	0.8175 (8)	0.3927 (3)	10.0 (5)
B1	0.6696 (5)	0.6441 (6)	0.10097 (24)	5.5 (4)
B2	0.9545 (6)	0.7647 (8)	0.3621 (3)	7.0 (4)

B_{iso} is the Mean of the Principal Axes of the Thermal Ellipsoid

Hydrogen Parameters x,y,z and B

	x	y	z	B
HB1A	0.718 (3)	0.731 (4)	0.1292 (13)	3.9 (9)
HB1B	0.577 (3)	0.671 (5)	0.0846 (17)	7.0 (13)
HB1C	0.703 (4)	0.646 (5)	0.0734 (19)	9.2 (16)
HB1D	0.678 (3)	0.540 (4)	0.1207 (14)	5.3 (11)
HB2A	1.006	0.749	0.401	7.9
HB2B	0.903	0.666	0.354	7.9
HB2C	1.001	0.770	0.332	7.9

Interatomic Distances (Å) and Angles (°)

Distances

Zr-O	1.987(3)	Si1-C10	1.878(5)
Zr-N	2.135(3)	Si2-N	1.733(4)
Zr-Cp1	2.534(6)	Si2-C11	1.871(5)
Zr-Cp2	2.527(5)	Si2-C12	1.868(5)
Zr-Cp3	2.555(6)	Si2-C13	1.906(5)
Zr-Cp4	2.573(6)	O-C1	1.429(5)
Zr-Cp5	2.560(6)	Cp1-Cp2	1.325(10)
Zr-C1	2.254(4)	Cp1-Cp5	1.330(11)
Zr-B1	2.594(6)	Cp2-Cp3	1.355(11)
P1-C1	1.765(4)	Cp3-Cp4	1.332(13)
P1-C2	1.832(4)	Cp4-Cp5	1.297(13)
P1-C5	1.818(5)	C2-C3	1.520(7)
P1-C8	1.795(4)	C2-C4	1.543(7)
P2-C13	1.828(5)	C5-C6	1.535(7)
P2-C14	1.828(7)	C5-C7	1.525(7)
P2-C17	1.827(5)	C14-C15	1.504(10)
P2-B2	1.927(7)	C14-C16	1.283(11)
Si1-N	1.731(4)	C17-C18	1.546(8)
Si1-C8	1.896(4)	C17-C19	1.487(9)
Si1-C9	1.868(5)		

Zr-Cent	2.2855(9)
Zr-HB1A	2.09(4)
Zr-HB1B	2.31(4)

Angles

O-Zr-N	104.63(13)	Zr-O-C1	80.78(21)
O-Zr-C1	38.73(14)	Zr-N-Si1	115.11(17)
N-Zr-C1	95.70(14)	Zr-N-Si2	122.76(18)
C1-P1-C2	110.90(21)	Si1-N-Si2	122.11(20)
C1-P1-C5	107.41(21)	Cp2-Cp1-Cp5	107.3(6)
C1-P1-C8	114.15(20)	Cp1-Cp2-Cp3	108.8(6)
C2-P1-C5	107.18(21)	Cp2-Cp3-Cp4	105.2(6)
C2-P1-C8	108.51(20)	Cp3-Cp4-Cp5	110.2(6)
C5-P1-C8	108.43(22)	Cp1-Cp5-Cp4	108.5(7)
C13-P2-C14	103.9(3)	Zr-C1-P1	129.48(22)
C13-P2-C17	104.17(23)	Zr-C1-O	60.49(19)
C13-P2-B2	117.7(3)	P1-C1-O	116.1(3)
C14-P2-C17	107.2(3)	P1-C2-C3	110.8(3)
C14-P2-B2	111.5(3)	P1-C2-C4	112.6(3)
C17-P2-B2	111.4(3)	C3-C2-C4	111.5(4)
N-Si1-C8	110.55(18)	P1-C5-C6	112.7(3)
N-Si1-C9	112.93(20)	P1-C5-C7	111.3(3)
N-Si1-C10	116.00(20)	C6-C5-C7	111.2(4)
C8-Si1-C9	108.77(21)	P1-C8-Si1	120.78(23)
C8-Si1-C10	103.08(22)	P2-C13-Si2	122.3(3)
C9-Si1-C10	104.81(24)	P2-C14-C15	115.5(5)
N-Si2-C11	113.80(21)	P2-C14-C16	122.0(7)
N-Si2-C12	111.47(21)	C15-C14-C16	117.7(7)
N-Si2-C13	107.30(19)	P2-C17-C18	112.2(4)
C11-Si2-C12	104.9(3)	P2-C17-C19	112.5(5)
C11-Si2-C13	105.55(24)	C18-C17-C19	110.4(5)
C12-Si2-C13	113.78(23)		

O-Zr-Cent	105.68(9)	HB1B-Zr-Cent	94.1(11)
N-Zr-Cent	110.30(9)	Zr-C1-H1	115.2(3)
C1-Zr-Cent	141.84(12)	P1-C1-H1	110.0(3)
HB1A-Zr-Cent	121.6(10)	O-C1-H1	116.6(4)